Final Report

for

US Geological Survey Award No. G10AP00047

Subsurface Investigation and Analysis of Bridges in Costa Rica Damaged by Lateral Spreading to Evaluate and Improve Design Procedures for Kinematic Loading of Piles

by

Kyle M. Rollins and Kevin W. Franke

368 CB, Civil & Environmental Engineering Dept.
Brigham Young University
Provo, UT 84602

Performance Period: March, 1, 2010-Feb 28, 2011

Author Contact Information:

Kyle Rollins: email: rollinsk@byu.edu, phone: 801 422-6334, fax: 801 422-0159
Kevin Franke: email: kwfranke@gmail.com, phone: 801 904-4097, fax: 801-904-4100

ABSTRACT

The M7.6 earthquake that struck the Limon province of Costa Rica on April 22, 1991 killed 53 people, injured another 193 people, and disrupted an estimated 30-percent of the highway pavement and railways in the region due to fissures, scarps, and soil settlements resulting from liquefaction. Significant lateral spreading was observed at bridge sites throughout the eastern part of Costa Rica near Limon, and the observed structural damage ranged from moderate to severe. This study identified five such bridges where liquefaction-induced damage was either observed following the earthquake or is still visible to this day. A geotechnical investigation was performed at each of these five bridges in an attempt to back-analyze the soil conditions leading to the liquefaction and lateral spreading observed during the 1991 earthquake, and each of the five resulting case histories was developed and is summarized in this report.

Modern analysis techniques for evaluating liquefaction triggering, lateral spreading displacements and kinematic pile response are summarized and evaluated against applicable Costa Rican case histories. In addition, a new performance-based kinematic pile response procedure based on the probabilistic framework developed by the Pacific Earthquake Engineering Research Center (PEER) is presented. The procedure incorporates existing analysis methodologies familiar to most practicing geotechnical professionals including empirical computation of lateral spreading displacement and p-y soil spring methods for computing kinematic pile response. The performance-based pile response procedure is demonstrated on the applicable Costa Rican case histories, and deterministic procedures are evaluated against the probabilistic results where appropriate.

The proposed objectives of this study were to (1) collect data and develop five new lateral spreading case histories from the 1991 Limon earthquake; (2) evaluate existing deterministic methods for computing lateral spreading displacements and kinematic pile response; and (3) apply principles of performance-based design to develop a new performance-based procedure for evaluating lateral spreading displacements and kinematic pile response. All of these objectives were successfully achieved, and the results, observations and conclusions are summarized in the following report.

ACKNOWLEDGEMENTS

This research was supported by the U.S. Geological Survey (USGS), Department of the Interior, under USGS award number G10AP00047 and this support is gratefully acknowledged. The views and conclusions contained in this document are those of the authors and should not be interpreted as necessarily representing the official policies, either expressed or implied, of the U.S. Government.

We express gratitude to the Costa Rican Ministry of Transportation for allowing access to the bridge sites and for providing bridge plan and soil test data. We thank Insuma S.A. Geotechnical Consultants of San Jose, Costa Rica who performed the drilling, Standard Penetration (SPT) testing, and soil testing for each bridge site and David Anderson, Head Technician in the BYU Civil & Environmental Engineering Department who conducted the site surveys using high resolution GPS equipment. We also express appreciation to Daniel Avila from the Utah Department of Transportation who conducted energy throughput measurements for the SPT testing and to Les Youd who served as a consultant on the study and reviewed the testing and analysis procedures at key points during the process. Finally, we express our appreciation to Norm Jones who helped develop the Monte Carlo macro used in conjunction with LPILE in this study.

We express our gratitude to Kleinfelder Group, Inc. and URS Corporation who provided analysis software and spreadsheets for use in this study.

TABLE OF CONTENTS

LIST OF TABLES

LIST OF FIGURES

1 Introduction

Lateral spreading is a seismic hazard associated with soil liquefaction in which permanent deformations are developed within a soil profile. Lateral spreading has historically been one of the largest causes of earthquake-related damage to infrastructure. One of the infrastructure components most at risk from lateral spreading is that of deep foundations. Although deterministic methods have been developed for evaluating pile displacements within lateral spreads, performance-based engineering is increasingly becoming adopted in earthquake engineering practice. Therefore, it would be beneficial for practicing engineers to have a performance-based methodology for predicting pile performance during a lateral spreading event.

This report presents the findings of a study to develop such a performance-based methodology and to validate it against a number of lateral spreading case histories. This study utilizes the probabilistic performance-based framework developed by the Pacific Earthquake Engineering Research (PEER) Center to develop a robust and flexible procedure to compute probabilistic estimates of kinematic pile response for a given single pile or pile group. The procedure incorporates performance-based empirical lateral spreading and liquefaction triggering procedures with Beam-on-Winkler Foundation methods to develop the probabilistic pile response estimates.

As part of this study, an investigation was performed at five bridge sites in Costa Rica where damage was observed following the M7.6 earthquake that occurred in the Limon Province of Costa Rica on April 22, 1991. The purpose of the investigation was to evaluate the subsurface soil conditions at these bridges and to subsequently develop lateral spreading case histories for use in this study and in future earthquake engineering research. Both deterministic and probabilistic pile response analyses were subsequently performed, where possible, for each of these bridge sites, and the computed results were compared against the observed performance of the bridges and their foundations.

The goal of this study is to develop a relatively simple procedure which will allow engineers and owners to make probabilistic estimates of the performance of deep foundation systems when exposed to kinematic lateral spreading displacements corresponding to desired return period(s) (i.e. given level(s) of risk). In addition, the study introduces several new lateral spreading case histories which may shed additional light on the phenomenon of lateral spreading and provide researchers with the ability to validate and calibrate models for predicting pile performance during lateral spreading.

2 Liquefaction and Lateral Spreading

2.1 Introduction

Lateral spreading is a term commonly used to describe the permanent deformation of the ground resulting from soil liquefaction due to earthquake shaking. Its effects on infrastructure and critical lifelines can be devastating. Soil deformations can range from millimeters to several meters, with the greatest displacements usually occurring near free-faces at the margins of rivers and oceans. Bridges spanning bodies of water with underlying soils prone to liquefaction, as well as pile foundations placed through liquefiable layers are especially at risk for sustaining damage due to lateral spreading. Lateral spreading has been a major contributor to earthquake-related damage and costs throughout the world. Historically, it was partly responsible for the shearing of water lines that prevented firefighters from battling the ravaging fires following the 1906 San Francisco Earthquake. Port and coastal facilities near the Prince William Sound were severely damaged, and roads and bridges for hundreds of square kilometers were moderately to severely disrupted as a result of the 1964 M_w = 9.2 earthquake there. During that same year, parts of Niigata, Japan that were built over reclaimed river channels spread over 8 meters during a M_w = 7.5 quake. More recently, lateral spreads during the 1989 Loma Prieta earthquake (M_w = 7.0) caused significant displacements along the entire 150 to 300 meter wide spit at Moss Landing by Monterey Bay that nearly resulted in the collapse of the $6 million Moss Landing Marine Laboratory that was under construction at the time. Lateral spreads during the 1995 Hyogoken-Nanbu earthquake in Japan left the port facilities of the city of Kobe severely damaged. Quay walls had displaced several meters, cranes were toppled, and rails were misaligned. The disaster left thousands of citizens unemployed and/or homeless and ultimately had a huge effect on the local and regional economy because port business went elsewhere and much of it has never returned. Finally, lateral spreading demolished port facilities in Port-au-Prince, Haiti following the deadly earthquake there in January of 2010. Due to this damage, delivery of humanitarian relief from other countries was significantly slowed.

The occurrence of lateral spreading is conditional on the triggering of liquefaction, which is a phenomenon involving the rapid increase of pore water pressures in contractive soils most often due to dynamic loading and the associated decrease of soil shear strength. This chapter will review the basic mechanics of liquefaction and lateral spreading. In addition, several of the simplified empirical procedures currently used in engineering practice to design for these phenomena will be presented and briefly discussed.

2.2 Liquefaction

Liquefaction involves the reduction of stiffness and strength of saturated, cohesionless soils caused by monotonic, transient, or repeated disturbance of saturated cohesionless soils under undrained conditions (Kramer, 1996). Liquefaction occurs in two general forms: *flow liquefaction* and *cyclic mobility.* While both types of liquefaction will be discussed at length later in this chapter, flow liquefaction occurs fairly rarely, but the dramatic and sudden loss of strength it produces can potentially be very dangerous. Much more common is cyclic mobility, which tends to produce far less dramatic displacements, but can be extremely damaging to structures just the same.

The phenomena of liquefaction became the topic of focused research following the occurrence of two significant earthquakes in 1964. The first occurred on Good Friday near the Prince William Sound in Alaska (M_w = 9.2). Liquefaction caused by that earthquake damaged roads and lifelines, as well as the foundations of several structures located in Anchorage, approximately 120 km northwest of the epicenter. The second occurred three months later in Niigata, Japan (M_S = 7.5), where soil liquefaction caused similar lifeline damage, as well as the destruction of several structures which failed due to post-liquefaction settlement and bearing capacity failure. Since that time, geotechnical engineers have learned much about the phenomena of liquefaction and how to approach it. Kramer (1996) provides some systematic and logical steps that should be considered in the evaluation of liquefaction hazard – *liquefaction susceptibility, liquefaction initiation,* and *liquefaction effects* (i.e. lateral spreading).

2.3 Liquefaction Susceptibility

Not all soils are susceptible to liquefaction. When evaluating liquefaction hazard, it is important to know what criteria are required for the occurrence of liquefaction to even be possible. Kramer (1996) divides susceptibility criteria into four general categories: *historical, geologic, compositional,* and *state.*

Historical criteria recognize that if a soil has liquefied before, there is a strong probability that it will liquefy again as long as the soil and groundwater conditions remain relatively unchanged (Youd, 1984). By noting similarities in soil and groundwater characteristics at such sites, researchers can then take that knowledge and look for other sites possibly prone to liquefaction. Sites that contain prehistoric evidence of the occurrence of liquefaction (termed *Paleoliquefaction*) have been used in such studies for over 15 years (Obermeier and Pond, 1999).

Geologic criteria are based on the fact that the nature of soil's environment may determine whether or not it is susceptible to liquefaction. The environment in which a soil was deposited, hydrological conditions in that environment, and the age of the soil deposit all help contribute to liquefaction susceptibility (Youd and Hoose, 1977). Alluvial, fluvial, and aeolian deposits have a high potential for liquefaction when saturated due to the loose configuration in which they were deposited. Saturated man-made soil deposits are also prone to liquefaction unless properly compacted. Finally, liquefaction probability tends to increase as groundwater levels are near the ground surface. Most liquefaction seems to occur within 15 meters of the ground surface (Kramer, 1996).

Compositional criteria state that the soil itself may determine whether or not it is susceptible to liquefaction. In general, it is recognized that soils need to be cohesionless and saturated in order to liquefy. Also, liquefaction susceptibility increases with increasing soil-grain uniformity, and decreases with increasing fines content and soil-grain angularity. Initially, it was believed that only sands were prone to liquefaction. However, liquefaction in gravels and even course silts has been witnessed in the field and replicated in the laboratory (Chen, et al., 2009; Ishihara, 1984, 1985; Coulter and Migliaccio, 1966; Wong et al., 1975). Additionally, much debate has occurred during the last ten years in industry regarding the liquefaction susceptibility of fine-grained silts and clays. To evaluate liquefaction susceptibility of fine-grained soils, Youd, et al. (2001) recommended adherence to the 'Chinese criteria,' which is a simple set of criteria based on Atterberg limits, water content, and clay content. However, Bray and Sancio (2006) published observed case histories from recent earthquakes in Turkey that seemed to suggest that low-plasticity clays could potentially liquefy, and thus presented a set of susceptibility criteria that was significantly more conservative than the Chinese criteria. Idriss and Boulanger (2008) later acknowledged that some low-plasticity clays could experience behavior similar to liquefaction, calling it "cyclic softening." However, they were much more adamant in defining the difference between "sand-like behavior" and "clay-like behavior." As a result of these recent publications, most engineering professionals now disregard the Chinese criteria for evaluating the liquefaction susceptibility of fine-grained soils, having labeled it as "potentially unconservative." However, Youd, et al. (2009) point out that liquefaction in clay-like materials often does not result in the same secondary hazards usually associated with liquefaction in sand-like materials, using lateral spreading as a particular example.

State criteria infer that the actual "state" (i.e. density and initial stress conditions) of the soil may determine whether or not it is susceptible to liquefaction, and if so, which type of liquefaction.

2.4 Liquefaction Initiation

Because a certain soil meets the criterion for liquefaction susceptibility does not necessarily mean that liquefaction is certain to occur. A chain of events must take place in order to initiate liquefaction, and even the occurrence of those events does not necessarily mean that catastrophic soil failure will happen. Prediction of the types of deformations that would occur upon the initiation of liquefaction greatly depends on understanding the state of the soil when liquefaction is triggered (Kramer 1996).

2.4.1 Flow Liquefaction and Estimating Steady State Strength

Research has shown that undrained loading of a soil specimen can reveal the existence of a virtual line in *p'-q* space that defines the general behavior of the soil once liquefaction initiates. This surface is called the *Flow Liquefaction Surface* (FLS). If the effective stress path of the soil specimen that is being disturbed either monotonically or cyclically reaches the FLS, flow liquefaction is initiated. Kramer (1996) points out that initiating flow liquefaction is only the first of two requirements needed for the occurrence of a flow slide, often recognized as the most devastating and dangerous hazard of liquefaction. The other requirement involves the presence of driving stresses which continue to push the soil to its steady state strength. Driving stresses are static shear stresses that already exist in the soil prior to liquefaction and are caused by gravity. Thus, the initiation of a flow slide is simply a demonstration that the soil in its liquefied state does not have sufficient shear strength to maintain its structure.

Figure 2-1 shows the FLS and the initial states in p'-q space where a liquefiable soil has the potential of initiating flow liquefaction if loading is sufficient to move the effective stress path to the FLS.

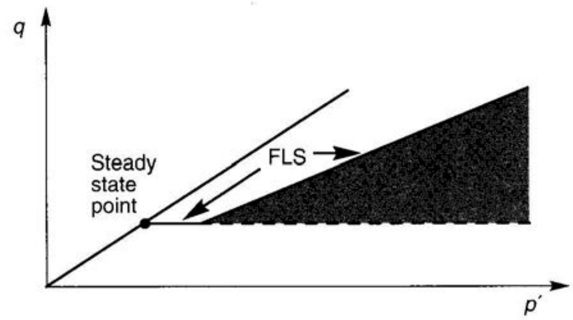

Figure 2-1: Zone susceptible to flow liquefaction shown in *p'-q* space (shown as shaded; after Kramer, 1996)

All that is needed is an undrained soil disturbance strong enough to push the effective stress path of the soil to the FLS. Kramer and Seed (1988) note that if large static stresses already exist in a particular element of soil under drained conditions, very little excess pore pressure may be needed to initiate flow liquefaction.

The critical key when considering flow liquefaction hazard is to obtain an accurate estimate of the liquefiable soil's steady state strength. Unfortunately, for being such a critical aspect to evaluating flow liquefaction potential, obtaining an accurate estimate of the steady state strength of a soil is extremely difficult to do in practice. Engineers today generally rely on in situ and normalized strength techniques to estimate a soil's steady state strength.

In situ strength measurement was first proposed by Seed (1986), and was later updated by Seed and Harder (1990). The idea of the approach is to correlate SPT or CPT resistance with the apparent shear strength back-calculated from observed flow slides. This back-calculated strength is termed the *residual strength.* The Seed and Harder (1990) approach remains a very popular approach among geotechnical engineers today and it still constitutes the "state of practice" in many seismic-prone regions for computing residual strengths. The method requires that the soil either have 10% or less fines content, or that the measured SPT resistance be corrected for fines. According to Youd et al. (2001), the clean sand corrected SPT blowcount, $N_{1,60,CS}$, can be computed using Equation (2-1) in conjunction with Table 2-1 below.

$$N_{1,60,CS} = \alpha + \beta\left(N_{1,60}\right) \qquad (2\text{-}1)$$

Table 2-1: Correction factors for computing clean sand corrected SPT blowcount

Fines content, FC	α	β
$FC \leq 5\%$	0	1.0
$5\% < FC < 35\%$	$\exp[1.76 - 190/FC^2]$	$0.99 + FC^{1.5}/1000$
$FC \geq 35\%$	5.0	1.2

Once the value of $N_{1,60,CS}$ is obtained, the residual shear strength can be estimated from Figure 2-2 for clean-sand blowcounts less than 16 blows/foot.

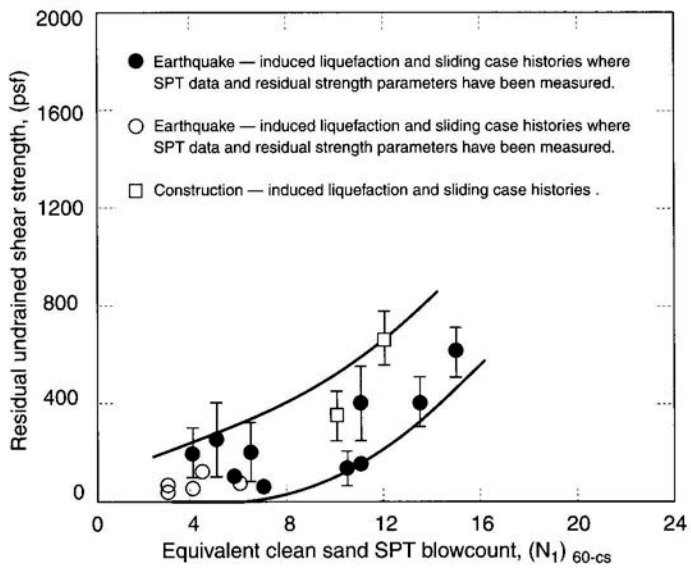

Figure 2-2: Relationship between residual shear strength and clean-sand SPT resistance (after Seed and Harder, 1990)

Normalized strength techniques are based on the idea that if the consolidation curve and the steady state line for a given liquefiable soil are parallel, then the steady state strength should be proportional to the consolidation stress (Kramer, 1996). The application of this technique, however, is complicated by the fact that liquefiable soils do not portray unique consolidation characteristics, which are largely a function of the state of the soil and can vary significantly even within the same soil deposit. In addition, the residual strength back-calculated from field case histories may be strongly influenced by the presence of water interlayers which are not replicated from standard laboratory tests. However, if a specimen of soil can be prepared to resemble the in-situ conditions (i.e. void ratio, density, effective confining pressures) and tested in undrained shear, then the resulting *residual strength ratio*, or S_r / σ_{vo}', is theorized to closely represent field conditions (Vasquez-Herrera, et al., 1990; Baziar, et al., 1992; Ishihara, 1993).

Several researchers (e.g., Olson and Stark, 2002; Idriss and Boulanger, 2007) have performed such tests and utilized field data to back-calculate residual strength ratios from multiple case histories where flow liquefaction has occurred in the past. Ledezma and Bray (2010) used many of these models to develop a mean estimate of the residual shear strength ratio, (μ_{Su}/σ'_{vc}) which is given as

$$\mu_{s_u/\sigma'_{vc}} \approx \exp\left(\frac{\mu_{N_{1,60,CS}}}{8} - 3.5\right) \times \left[1 + \frac{\left(0.3\mu_{N_{1,60,CS}}\right)^2}{158}\right] \tag{2-2}$$

where $\mu_{N_{1,60,CS}}$ is the mean estimate of clean-sand SPT blowcount. Ledezma and Bray (2010) report that the estimated standard deviation of the residual shear strength ratio, $\sigma_{s_u/\sigma'_{vc}}$ is approximately equal to $0.4\mu_{s_u/\sigma'_{vc}}$. It is important to apply good engineering judgment when using methods involving residual strength ratios, bearing in mind that they provide only an approximation of the steady state strength of liquefied soil. In addition, many engineers call into question the validity of residual strength ratios at shallow depths, citing that the computed residual strengths seem extraordinarily low and unrealistic. No published references and or research supporting this claim could be identified; however, such a concern is valid and could warrant further research and investigation.

2.4.2 Cyclic Mobility

When initial stress conditions exist such that static shear stresses in a liquefiable soil element are less than the steady state strength, S_{su} of the soil, as shown in Figure 2-3, then the soil is considered safe from flow liquefaction. However the soil is still susceptible to cyclic mobility. *Cyclic mobility* is the gradual strain and loss of strength that occurs in a soil due to incremental buildup of pore water pressures induced by cyclic loading under undrained conditions. Lateral spreading is generally recognized as an effect of cyclic mobility.

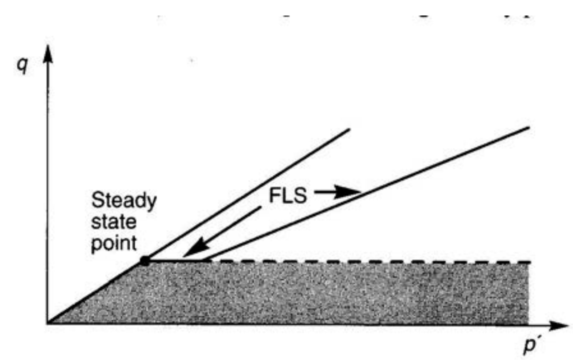

Figure 2-3: Zone susceptible to cyclic mobility as shown in p'-q space (shown as shaded; after Kramer, 1996)

2.4.3 Evaluation of Initiation of Liquefaction

Now that much of the basic mechanics behind the occurrence of liquefaction has been discussed, actual methods used in engineering practice today to estimate a particular site's vulnerability to liquefaction will be considered.

The cyclic stress approach is used by the majority of practicing professionals to predict whether or not liquefaction will initiate at a given site assuming some level of earthquake loading. The final product of this approach is typically a factor of safety which is calculated by dividing the soil's resistance to liquefaction initiation by the demand (loading) induced in the soil. A factor of safety equal to or less than unity would infer that liquefaction was likely to initiate if loaded at the level of shaking considered in the analysis. The resistance to liquefaction for a given soil is often quantified by using the cyclic shear stress required to initiate liquefaction at a given level of loading, $\tau_{cyc,L}$, or by normalizing that parameter with the effective overburden pressure, σ_{vo}', to obtain the *cyclic resistance ratio, CRR* (sometimes denoted as CSR_L). The demand for liquefaction placed on the soil is often quantified by using the equivalent cyclic shear stress induced by an earthquake, τ_{cyc}, or by normalizing that parameter with σ_{vo}' to obtain the *cyclic stress ratio, CSR*. Therefore, the equation for the factor of safety against liquefaction can be expressed as

$$FS_L = \frac{\tau_{cyc,L}}{\tau_{cyc}} = \frac{CRR}{CSR} = \frac{CSR_L}{CSR} \tag{2-3}$$

The shear stress required to trigger liquefaction used to be estimated from cyclic uniform harmonic tests performed in the laboratory. However, many researchers discovered that it was very difficult to replicate a soil's in situ stress state in a laboratory. As a result, most professionals today favor using in situ procedures. These procedures involve performing in-situ tests at sites where liquefaction was known to have occurred in order to characterize the liquefaction resistance in terms of the various in-situ parameters. While various procedures have been developed and published for cone penetration tests (CPT), shear wave velocity, and dilatometer index, the most commonly-used procedure today arguably involves the standard penetration test (SPT).

The SPT resistance correlates fairly well with liquefaction resistance because the same factors that cause the resistance to liquefaction to increase (e.g., density, overconsolidation, non-uniformity, angularity, fines content) also increase the SPT resistance. Beginning with the charts created by Seed and Idriss (1971) which plotted the *CSR* versus SPT resistance for several sites known to have liquefied and several sites known not to have liquefied during earthquakes of M_w = 7.5, many researchers have since been creating similar approaches for both deterministic and probabilistic scenarios. Of these many approaches, three appear to have become widely accepted among the engineering community today, though they tend to differ significantly from one another in various aspects: Youd et al. (2001), Cetin et al. (2004), and Idriss & Boulanger (2008). Since about 2006, there has been quite a large amount of disagreement and confusion regarding which of these methods should be applied in engineering practice. In particular, the arguments between the Idriss & Boulanger supporters and the Cetin et al. supporters have become quite significant. The basis of these arguments transcends the scope of this research, however, and defense of a particular approach will not be attempted in this report. However, a performance-based procedure for liquefaction triggering has already been developed and published by Kramer and Mayfield (2007) which incorporates the Cetin et al. (2004)

probabilistic model for liquefaction triggering. Since the performance-based pile response procedure developed as part of this study will incorporate the Kramer and Mayfield (2007) liquefaction model, only the Cetin et al. (2004) procedure will be summarized in this report. However, until greater consensus is reached by the professional community on this issue, it is recommended that all three simplified methods for evaluating liquefaction triggering be performed and that sound engineering judgment be applied in interpreting the results. Such an approach was applied to the deterministic case histories in this study and will be explained further in Chapter 6 of this report.

In order to compute the factor of safety against liquefaction for a given soil layer, the cyclic resistance ratio for that layer must be computed. Traditionally, the *CRR* was obtained from charts prepared from hundreds of case histories where liquefaction was either known to have occurred or to have not occurred. Cetin et al. (2004) utilized Bayesian statistical analysis with these case histories and developed a relatively simple equation for computing *CRR*, which is given as

$$CRR = \exp\left[\frac{\left(N_{1,60}\cdot\left(1+0.004\cdot FC\right)-29.53\cdot\ln\left(M_w\right)-3.70\cdot\ln\left(\frac{\sigma_v'}{P_a}\right)+0.05\cdot FC+16.85+2.70\cdot\Phi^{-1}\left(P_L\right)\right)}{13.32}\right] \qquad (2\text{-}4)$$

where $N_{1,60}$ is the SPT blowcount corrected for hammer energy and overburden, FC is the fines content in percent ($5 \le FC \le 35$), M_w is the moment magnitude of the design earthquake, σ_v' is the effective vertical stress at the depth of interest, P_a is atmospheric pressure ($= 1 \text{ atm} \approx 100 \text{ kPa} \approx 1 \text{ tsf}$) and has units consistent with the effective vertical stress, P_L is the probability of liquefaction in decimals (common to use 15% or 0.15), and $\Phi^{-1}\left(P_L\right)$ is the inverse of the standard cumulative normal distribution (i.e. mean = 0, standard deviation = 1). Figure 2-4 shows a plot of these CRR curves for both (a) probabilistic liquefaction evaluation, and (b) deterministic liquefaction evaluation (i.e. P_L is assumed to be 15%).

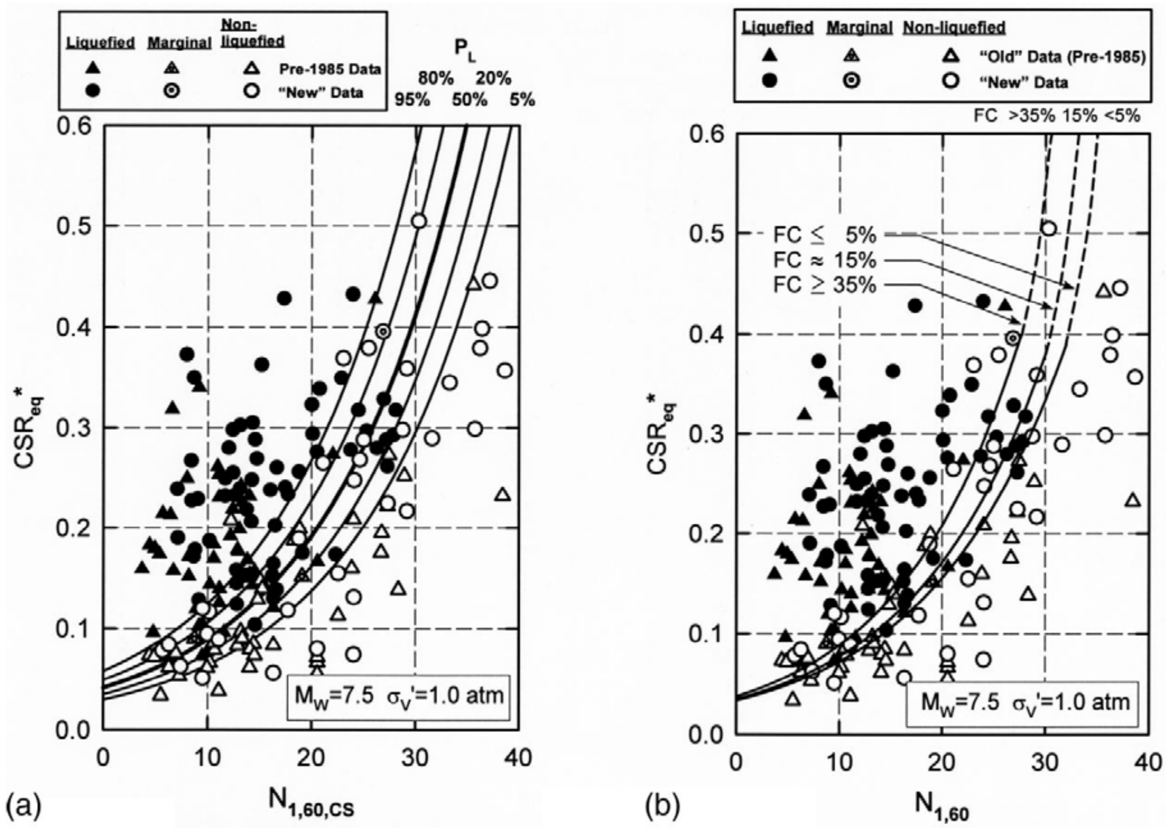

Figure 2-4: (a) Probabilistic SPT-based CRR correlation for *Mw* = 7.5 and σ'_v = 1 atm, and (b) Deterministic SPT-based CRR correlation for *Mw* = 7.5 and σ'_v = 1 atm (after Cetin et al., 2004)

The most commonly used method for calculating the *CSR* in current practice is the simplified procedure for estimating τ_{cyc} (Seed and Idriss, 1971). This procedure was developed for correlating cyclic shear stresses observed during harmonic uniform cyclic loading in the laboratory with cyclic shear stresses in the field. By comparing several lab test results and earthquake ground-motion recordings, it was hypothesized that $\tau_{cyc} \approx 0.65\tau_{\max}$. Using this conversion, Seed and Idriss (1971) estimated the uniform cyclic shear stress amplitude for level or gently sloping sites as

$$\tau_{cyc} = 0.65 \frac{a_{\max}}{g} \sigma_v r_d \qquad (2\text{-}5)$$

where $a_{\max}$ is the peak ground surface acceleration (typically estimated from a separate seismic hazard analysis, which will be explained in Chapter 5), g is the acceleration of gravity, σ_v is the total vertical stress at the depth of interest, and r_d is a depth stress reduction factor. The relationship for r_d developed by Cetin et al. (2004) is based on Bayesian statistical updating, and is given as

$$r_d = \frac{\left[1 + \frac{-23.013 - 2.949 \cdot a_{\max} + 0.999 \cdot M_w + 0.0525 \cdot V_{s,12}^*}{16.258 + 0.201 \cdot e^{0.341\left(-d + 0.0785 \cdot V_{s,12}^* + 7.586\right)}}\right]}{\left[1 + \frac{-23.013 - 2.949 \cdot a_{\max} + 0.999 \cdot M_w + 0.0525 \cdot V_{s,12}^*}{16.258 + 0.201 \cdot e^{0.341\left(0.0785 \cdot V_{s,12}^* + 7.586\right)}}\right]} \pm \sigma_{\varepsilon_{r_d}} \quad \left(d < 20m\right) \tag{2-6}$$

$$r_d = \frac{\left[1 + \frac{-23.013 - 2.949 \cdot a_{\max} + 0.999 \cdot M_w + 0.0525 \cdot V_{s,12}^*}{16.258 + 0.201 \cdot e^{0.341\left(-20 + 0.0785 \cdot V_{s,12}^* + 7.586\right)}}\right]}{\left[1 + \frac{-23.013 - 2.949 \cdot a_{\max} + 0.999 \cdot M_w + 0.0525 \cdot V_{s,12}^*}{16.258 + 0.201 \cdot e^{0.341\left(0.0785 \cdot V_{s,12}^* + 7.586\right)}}\right]} - 0.0046\left(d - 20\right) \pm \sigma_{\varepsilon_{r_d}} \quad \left(d \ge 20m\right) \tag{2-7}$$

where d is the depth in meters, M_w is the moment magnitude of the design earthquake, $a_{\max}$ is the horizontal peak ground acceleration in units of gravity, and $V_{s,12}^*$ is the average shear wave velocity in the upper 12 meters (~40 feet) of soil in meters/second. The parameter $\sigma_{\varepsilon_{r_d}}$ is the standard deviation of the stress reduction factor and is given as

$$\sigma_{\varepsilon_{r_d}} = d^{0.85} \cdot \left(0.0198\right) \qquad \left(d < 12m\right) \tag{2-8}$$

$$\sigma_{\varepsilon_{r_d}} = 12^{0.85} \cdot \left(0.0198\right) \qquad \left(d \ge 12m\right) \tag{2-9}$$

Two factors known to affect the CSR must be accounted for in order to use the simplified procedure to estimate FS_L. First, because the Seed and Idriss (1971) procedure was based on earthquakes with a known magnitude of M_w = 7.5, a Duration Weighting Factor (DWF), also known as the Magnitude Weighting Factor (MWF), must be applied for earthquakes of different magnitudes in order to obtain a CSR value valid to use with $CRR_{M_w=7.5}$ obtained from plots like that in Figure 2-4. The DWF as recommended by Cetin et al. (2004) can be approximated as

$$DWF \approx e^{\left(-0.3353 \cdot M_w + 2.5281\right)} \qquad \left(5.5 \le M_w \le 8.5\right) \tag{2-10}$$

The second factor that should be accounted for when computing the CSR in accordance with the Cetin et al. (2004) procedure is the effective overburden stress. Cyclically loaded laboratory test data indicate that liquefaction resistance increases with increasing confining stress. The rate of increase, however, is nonlinear (Youd et al., 2001). Therefore, an overburden correction factor, K_σ, is used to account for this phenomenon. Both Cetin et al. (2004) and Youd et al. (2001) recommend that K_σ be computed as

$$K_\sigma = \left(\sigma_v' / p_a\right)^{f-1} \tag{2-11}$$

where p_a is in the same units as the effective overburden pressure, σ_v'; and *f* is a function of relative density and is equal to 0.8 for loose soils, 0.7 for medium-dense soils, and 0.6 for dense soils. Cetin et al. (2004) state that this relationship is valid for effective overburden pressures greater than about 0.3 atmospheres.

Thus correcting the *CSR* for both magnitude (i.e. duration) and overburden stress, the corrected cyclic stress ratio can now be computed as

$$CSR_{eq,M_w=7.5,1\text{ atm}} = CSR_{eq}^{*} = \frac{CSR_{eq}}{DWF \cdot K_\sigma} = \frac{\tau_{cyc}}{\sigma'_{vo}\left(DWF \cdot K_\sigma\right)} = 0.65\left(\frac{\sigma_{vo}}{\sigma'_{vo}}\right)\cdot\left(\frac{a_{\max}}{g}\right)\cdot\frac{r_d}{\left(DWF \cdot K_\sigma\right)} \quad (2\text{-}12)$$

Using Equations (2-4) and (2-12), the factor of safety against liquefaction can be computed as

$$FS_L = \frac{CRR}{CSR_{eq}^{*}} \quad (2\text{-}13)$$

By plotting the variation of *CRR* and CSR_{eq}^{*} with depth as shown in Figure 2-5, the factor of safety against liquefaction triggering can conveniently be visualized over a cross section of the soil profile of interest.

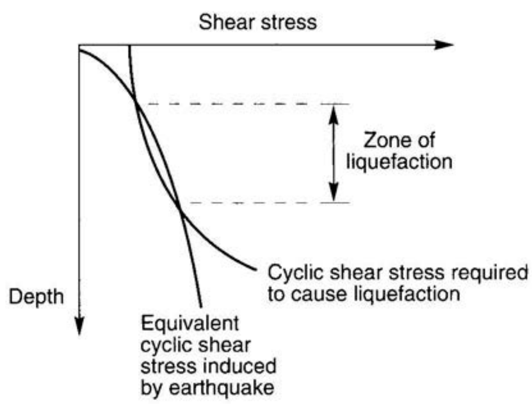

Figure 2-5: Example of plotting *CSR* versus *CRR* with depth (after Kramer, 1996)

2.5 Lateral Spreading Displacement

If a soil is susceptible to liquefaction, and the state of soil and loading parameters are such that liquefaction initiates, then it becomes important to consider what the possible effects of the occurrence of liquefaction would be. One of the most significant and costly hazards associated with liquefaction is lateral spreading displacement.

Lateral spreading refers to the downslope movement of liquefied soil due to the presence of small existing static shear stresses in the soil and cyclic earthquake loading. Lateral spreading can occur on gently sloping ground or near a free-face, and can be a major engineering concern because critical and expensive infrastructure is often located in these areas.

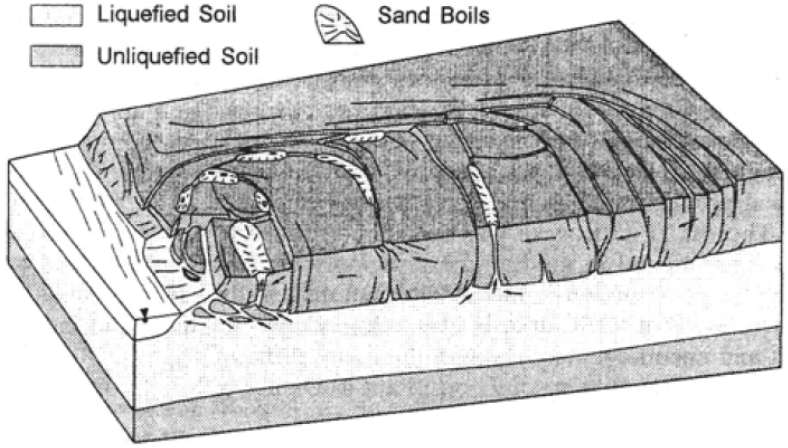

Figure 2-6: Sketch demonstrating the phenomenon of lateral spreading (after Varnes, 1978)

Figure 2-7: Lateral spreading at the port in Port-au-Prince, Haiti following the 2010 earthquake (courtesy of EERI)

2.5.1 Experimental Studies of Lateral Spread

In order to better understand the phenomena of lateral spreading and the mechanics behind it, researchers have performed several types of laboratory experiments. These experiments have included shake table studies (Miyajima et al., 1991; Sasaki et al., 1991;), centrifuge studies (Balakrishnan et al., 1997; Toboada-Urtuzuastegui and Dobry, 1998; Boulanger et al., 2003; and Malvick et al., 2006), undrained torsional tests (Yasuda et al., 1994; Shamoto et al., 1997), and undrained triaxial tests (Nakese et al., 1997). These studies have led researchers to understand that lateral spreading can occur in liquefied soil that is located in sloping ground or level ground adjacent to a free-face. The deformations due to cyclic mobility in a lateral spread occur only while transient loading is taking place. However, the development of a water film between an impermeable non-liquefied soil crust and the liquefied soil could potentially allow for significant deformations following transient loading. The magnitude of the permanent lateral spreading deformation appears to strongly dependent on the initial density of the liquefiable soil and its previous strain history. Experimental studies of lateral spreading also suggest that the magnitude of lateral deformations increases with the thickness of the liquefiable layer, the ground slope angle, and duration of shaking. Furthermore, since the studies suggest that low frequency and high acceleration loading decreases the time to liquefaction initiation, such ground motion characteristics could also cause increased lateral deformations. Ground motion directivity also appears to be significant in that ground deformations increase when the direction of horizontal loading is parallel with the slope or perpendicular to the free face.

When lateral spreading occurs, there appears to be a region in the liquefied soil where the excess pore pressure ratio is close or equal to unity. With continued strain, this zone begins to stiffen and decrease in pore pressure due to dilation. Pore pressures continue to decrease as straining continues, but increase to achieve equilibrium when straining ceases.

2.5.2 Methods for Predicting Lateral Spreading Displacements

In order to predict the permanent deformations resulting from the occurrence of lateral spreading during earthquake loading, researchers have developed several methods of analyses. These different methods of analyses can be categorized into two general types: *Analytical Methods* and *Empirical Methods*.

Analytical methods are those that are developed from our current understanding of soil mechanics and science. They generally are closed-form mathematical models. There are several different types of analytical models developed for predicting permanent displacements resulting from lateral spreading. Analytical methods include the Numerical Model (e.g., Gu et al., 1994; Yang, 2000; Yang et al., 2003; and Arduino et al., 2006), the Elastic Beam Model (e.g., Hamada et al., 1978; Towhata et al., 1992; and Yasuda et al., 1991), and the Newmark Sliding Block Model (e.g., Toboada et al., 1996; Bray and Travasarou, 2007; Olson and Johnson, 2008; and Saygili and Rathje, 2008). While it is recognized that analytical methods are widely used in engineering practice, this study will focus on the use of empirical methods in the development of a performance-based kinematic pile response procedure. This focus on empirical methods is in no way intended to discredit or diminish the appropriateness and/or effectiveness of analytical methods. However, empirical methods are widely used in engineering practice today due to their relative simplicity and the fact that they do not require earthquake time histories to perform. Therefore, this study sought to employ empirical methods in the development of a performance-based kinematic pile response procedure.

Empirical multi-linear regression (MLR) methods involve the use of lateral spreading case histories in order to develop statistical relationships between lateral deformations and some measurable soil parameters (e.g. SPT or CPT resistance, ground slope, M_w, R, etc.). The analyses often do not involve any consideration of soil mechanics, but are solely based on linear regression and choosing soil parameters such that some prediction error is minimized. The assumption behind such an approach is that the soil parameters selected in order to minimize error in linear regression should also be governing parameters in the complex soil mechanics. Though this assumption may not always true, empirical methods have been used with databases of lateral spreading case histories to develop models for prediction of deformations that have proven to be fairly accurate, often predicting values within a factor of two from the observed displacement.

The development of an empirical MLR model must include clearly stated conditions and assumptions for the lateral spreading case histories that will be considered by the analysis. Use of inconsistent data during model calibration can not only result in increased error calculated during linear regression, but can also result in the application of the final predictive model in locations and conditions where its use should not be warranted. Nearly all predictive models include a range of input parameter values for which the application of the models would be appropriate.

While many empirical models have been developed and published over the years, this study will incorporate three of these models. These models were selected based on their apparent popularity among practicing engineers, their relatively higher value of correlation coefficient, and/on their ability to easily fit within a probabilistic framework for incorporation into the performance-based model. These empirical models include Youd et al. (2002), Bardet et al. (2002), and Baska (2002).

2.5.3 Youd et al. (2002) Procedure

Youd et al. (2002) presented revisions of the original Bartlett and Youd (1992, 1995) empirical equations developed for predicting lateral spreading displacements. The original procedure incorporated 448 displacement values compiled from 7 different earthquakes that occurred either in Japan or the western United States. The database of displacements was divided into two general categories: free-face displacements and ground-slope displacements. Standard linear regression was used to determine the combination of variables that maximized the regression coefficient. Youd et al. (2002) made the following updates to the original procedure: erroneous displacement values were corrected; cases that were determined not to be lateral spreading were removed; additional case histories from the earthquakes at Borah Peak, Loma Prieta, Northridge, and Kobe were added to the database; the mean grain size parameter was weighted so that it would not affect the resulting displacements as significantly; a cap was placed on the fines content; and a term to accommodate near-fault conditions was added. The Youd et al. procedure is arguably the most widely used and accepted procedure for predicting lateral spreading displacements in engineering practice today.

The Youd et al. (2002) procedure, like the earlier Bartlett and Youd procedure, requires the user to characterize the site geometry as either “Free-Face” or “Ground Slope.” Figure 2-8 below uses a simplified geometry to demonstrate this site geometry characterization.

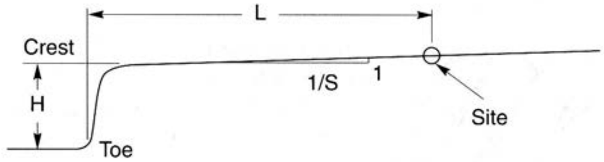

Figure 2-8: Determination of site geometry for empirical MLR equation

Once the site geometry is classified, the estimated permanent lateral spreading displacement can be computed respectively for the free-face case or the ground slope case as

$$\log D_{H-FF} = b_o + b_{off} + b_1 M + b_2 \log R^* + b_3 R + b_4 \log W + b_6 \log T_{15} + b_7 \log\left(100 - F_{15}\right) + b_8 \log\left(D50_{15} + 0.1\right) \quad (2\text{-}14)$$

$$\log D_{H-GS} = b_o + b_1 M + b_2 \log R^* + b_3 R + b_5 \log S + b_6 \log T_{15} + b_7 \log\left(100 - F_{15}\right) + b_8 \log\left(D50_{15} + 0.1\right) \quad (2\text{-}15)$$

where M is the earthquake moment magnitude, R is the source-to-site distance in kilometers, W is the free-face ratio in percent, S is the ground slope gradient in percent, T_{15} is the cumulative thickness of all saturated soil layers with $\left(N_1\right)_{60}$ values less than 15 blows/foot, F_{15} is the average fines content in percent from all saturated soil layers with $\left(N_1\right)_{60}$ values less than 15 blows/foot, and $D50_{15}$ is the average mean grain size diameter from all saturated soil layers with $\left(N_1\right)_{60}$ values less than 15 blows/foot. R^* is defined as the modified source-to-site distance in kilometers, and is computed as

$$R^* = R + 10^{(0.89M - 5.64)} \quad (2\text{-}16)$$

Regression coefficients for use in Equations (2-14) and (2-15) are given below in Table 2-2.

Table 2-2: Regression coefficients for the Youd et al. (2002) MLR model

b_o	b_{off}	b_1	b_2	b_3	b_4	b_5	b_6	b_7	b_8
-16.213	-0.5	1.532	-1.406	-0.012	0.592	0.338	0.54	3.413	-0.795

Upon computing the lateral spreading displacement from either Equations (2-14) or (2-15), it is important to check the model input parameters against the recommended model bounds in order to verify that the user is not extrapolating with the model. Youd et al. (2002) provided such bounds based on the limits in their database, and they are presented below in Table 2-3 and Figure 2-9. Note that the term Z_T is defined as the depth, in meters, from the ground surface to the top of the liquefiable layer

Table 2-3: Recommended range of parameters for the Youd et al. (2002) procedure

Variable	Description	Range
M	Moment magnitude of earthquake	6.0 to 8.0
R (km)	Source-to-site distance from the site to the epicenter of the earthquake	0.2 to 100 km
W (%)	Free face ratio (height of free face/distance from the free face to the point of displacement in percent)	1 to 20 percent
S (%)	Ground slope in percent	0.1 to 6 percent
T_{15} (m)	Cumulative thickness in meters of saturated soil with an SPT resistance less than 15	1 to 15 m
Z_T (m)	Depth in meters from ground surface to top of liquefied layer	1 to 10 m

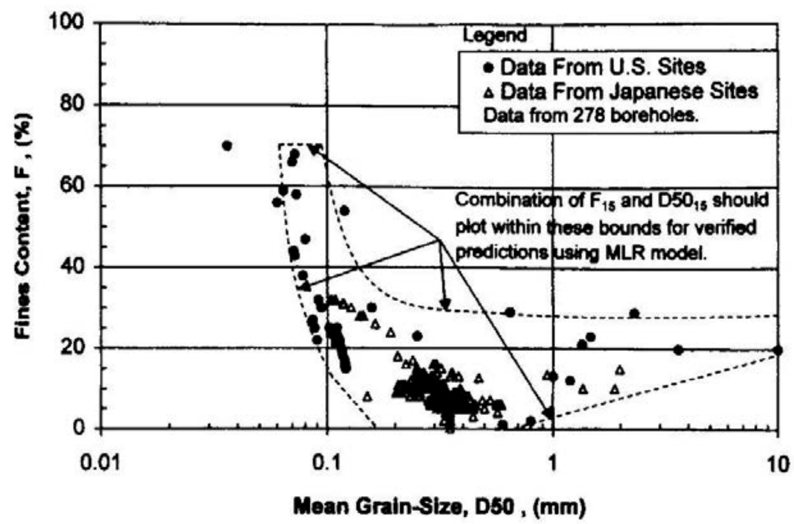

Figure 2-9: Compiled grain-size data with ranges of F_{15} and $D50_{15}$ for use with the Youd et al. (2002) procedure (after Youd et al., 2002)

2.5.4 Bardet et al. (2002) Procedure

Bardet et al. (2002) developed a four-parameter empirical MLR model for estimating displacements due to lateral spreading. The model was developed for use over large areas or regions, and was intended for the prediction of large-scale lateral displacements that could significantly damage or destroy lifeline networks. The Bardet et al. (2002) procedure was termed FFGS4 (Free-Face, Ground-Slope, # of parameters) and is divided into two data sets: complete data for all ranges of displacement amplitude (Data Set A), and data limited to displacement amplitudes smaller than 2 meters (Data Set B). However, because the linear regression analysis provided a nearly identical regression coefficient for both amplitudes of displacement, the coefficients for from Data Set B will not be further discussed in this dissertation. An attractive feature of the FFGS4 procedure for engineers is that it allows them to make displacement predictions without the often difficult challenge of measuring or estimating the average fines content and mean grain size for various layers of soil across a possibly large area. With that being said, the regression coefficient for the four-parameter procedure is only 64.25%, as opposed to 83.6% for the six-parameter Youd et al. (2002) procedure. Therefore the accuracy of the predictions is obviously a function of the number of significant parameters included in the empirical model.

The Bardet et al. (2002) procedure, like the Youd et al. (2002) procedure, requires the user to characterize the site geometry as either "Free-Face" or "Ground Slope" as described in Figure 2-8. Once the site geometry is classified, the estimated permanent lateral spreading displacement can be computed respectively for the free-face case or the ground slope case as

$$\log\left(D_{H-FF} + 0.01\right) = b_o + b_{off} + b_1 M + b_2 \log R + b_3 R + b_4 \log W + b_6 \log T_{15} \qquad (2\text{-}17)$$

$$\log\left(D_{H-GS} + 0.01\right) = b_o + b_1 M + b_2 \log R + b_3 R + b_5 \log S + b_6 \log T_{15} \qquad (2\text{-}18)$$

where M is the earthquake moment magnitude, R is the source-to-site distance in kilometers, W is the free-face ratio in percent, S is the ground slope gradient in percent, and T_{15} is the cumulative thickness of all saturated soil layers with $\left(N_1\right)_{60}$ values less than 15 blows/foot. Regression coefficients for use in Equations (2-17) and (2-18) are given below in Table 2-4.

Table 2-4: Regression coefficients for the Bardet et al. (2002) FFGS4 model

b_o	b_{off}	b_1	b_2	b_3	b_4	b_5	b_6
-6.815	-0.465	1.017	-0.278	-0.026	0.497	0.454	0.558

Recommended bounds for the FFGS4 model parameters are given below in Table 2-5.

Table 2-5: Recommended range of parameters for the Bardet et al. (2002) FFGS4 model

Variable	Description	Range
D (m)	Displacement in meters calculated by procedure	0 to 10.15 m
M	Moment magnitude of earthquake	6.4 to 9.2
R (km)	Source-to-site distance from the site to the epicenter of the earthquake	0.2 to 100 km
W (%)	Free face ratio (height of free face/distance to the free face from the point of displacement in percent)	1.64 to 55.68 percent
S (%)	Ground slope in percent	0.05 to 5.9 percent
T_{15} (m)	Cumulative thickness in meters of saturated soil with an SPT resistance less than 15	1 to 15 m

2.5.5 Baska (2002) Procedure

Baska (2002) and Kramer et al. (2007) developed an empirical procedure for estimation of lateral spreading displacement that is consistent with the known mechanics of liquefiable soil and with observed case histories of liquefaction in the field. Baska developed a constitutive model that accounts for the many of the important characteristics of liquefiable soils, and implemented it within a nonlinear one-dimensional site response analysis program to compute seismically-induced strains (i.e. lateral spreads). The site response program was then used to develop a "numerical database" of lateral spreads – using thousands of combinations of slope geometries, material properties, and time histories, which was then used to determine the basic form of an empirical displacement estimation relationship. That form of the relationship was then calibrated against available field case history data using standard multiple regression techniques. The result is an empirical predictive model that is consistent with the mechanical behavior of liquefiable soil and with available field data.

Unlike the Youd et al. (2002) and the Bardet et al. (2002) procedures, the Baska (2002) procedure does not utilize the T_{15} parameter to characterize the thickness of the soils susceptible to lateral spreading. Rather, the model computes the cumulative effective thickness of the laterally spreading soils, T^*, which can be computed respectively for the ground slope case or the free-face case as

$$T_{\mathrm{gs}}^* = 2.586\sum_{\mathrm{i=1}}^{\mathrm{n}} t_{\mathrm{i}} \cdot \exp\left[-0.05\cdot\left(N_{1,60-cs}\right)_i - 0.04\cdot z_i\right] \Big/ \left[1+\left(PI_i/5.5\right)^8\right] \tag{2-19}$$

$$T_{ff}^{*} = 5.474\sum_{\mathrm{i}=1}^{\mathrm{n}} t_{\mathrm{i}} \cdot \exp\left[-0.08 \cdot \left(N_{1,60-cs}\right)_i - 0.10 \cdot z_i\right] \Big/ \left[1 + \left(PI_i/5.5\right)^8\right] \tag{2-20}$$

where n is the number of sublayers in the soil profile, t_i is the thickness in meters of sublayer *i* (recommended to be no larger than 1.5 meters), $\left(N_{1,60-cs}\right)_i$ is the corrected clean sand-equivalent SPT blowcount for sublayer *i*, z_i is the depth in meters of the midpoint of sublayer *i*, and PI_i is the plasticity index for sublayer *i* (if applicable).

After computing the effective thickness of the laterally spreading soil for either the free-face or ground slope case, the median permanent lateral spreading displacement can be computed as

$$\hat{D}_H = \begin{cases} 0 & \text{for } \overline{\sqrt{D_H}} \le 0 \\ \left(\overline{\sqrt{D_H}}\right)^2 & \text{for } \overline{\sqrt{D_H}} > 0 \end{cases} \tag{2-21}$$

$$\overline{\sqrt{D_H}} = \frac{\beta_1 + \beta_2 T_{gs}^{*} + \beta_3 T_{ff}^{*} + 1.231M - 1.151\log R^{*} - 0.01R + \beta_4\sqrt{S} + \beta_5 \log W}{1 + 0.0223\left(\beta_2/T_{gs}^{*}\right)^2 + 0.0125\left(\beta_3/T_{ff}^{*}\right)^2} \tag{2-22}$$

$$R^{*} = R + 10^{(0.89M - 5.64)} \tag{2-23}$$

where *M* is the earthquake moment magnitude, *R* is the source-to-site distance in kilometers to the epicenter of the earthquake, *S* is the ground slope gradient in percent, and *W* is the free-face ratio in percent. Regression coefficients for the Baska (2002) model are provided below in Table 2-6.

Table 2-6: Regression coefficients for Baska (2002) model

Model	β_1	β_2	β_3	β_4	β_5
Ground Slope	-7.207	0.067	0	0.544	0
Free Face	-7.518	0	0.086	0	1.007

Recommended bounds for the model parameters are provided in Table 2-7.

Table 2-7: Recommended range of parameters for Baska (2002) model

Variable	Description	Range
$\left(N_{1,60-cs}\right)_i$	Corrected clean sand-equivalent SPT blowcount for sublayer computed using Equation (2-1) and Table 2-1	unlimited
z_{i}	Depth to the midpoint of sublayer in meters	unlimited
t_{i}	Sublayer thickness in meters	≤ 1 m
T^*	Equivalent thickness of saturated cohesionless soils (clay content ≤ 15 percent) in meters	0 to 20 m
M	Moment magnitude of the earthquake.	6.0 to 8.0
R	Source-to-site distance from the site to the epicenter of the earthquake	0 to 100 km
W	Free face ratio (height of free face/distance to the free face from the point of displacement) in percent	≤ 20 percent
S	Ground slope in percent	0 to 6 percent

2.6 Incorporation of Uncertainty in the Estimation of Lateral Spreading Displacements

Deterministic procedures for lateral spreading displacements can be very convenient tool for providing quick estimates of lateral spreading displacements. However, these procedures were derived from data that is often very scattered at best, and do not account for uncertainty in the estimated value. For this reason, many researchers and professional engineers prefer to use a statistical-based approach which allows them to consider the variability in lateral spreading data and give a level of confidence with their estimation.

While Youd et al. (2002) did not formally define the uncertainty of their MLR empirical lateral spreading model, they did indicate that approximately 90% of the predicted displacements from the MLR database fell within factor of two of the actual displacement. However, Bartlett (2009) indicated that the residual mean square, s^2 for the 2002 updated MLR model is equal to 0.0408. While it is technically correct to quantify uncertainty for the MLR model by using the Student's *t*-distribution in conjunction with the residual mean square and the model's covariance matrix, several simplifying assumptions can reasonably be made in order to streamline the process. First, because there is essentially no difference in the computed statistical probability density between the Student's *t*-distribution and the Normal distribution for degrees of freedom greater than about 100, and because the Youd et al. (2002) model has almost 450 degrees of freedom, one could reasonably use the Normal distribution instead of the Student's *t*-distribution in order to approximate the probability density for the MLR model. In addition, because the covariance matrix produced from the Youd et al. (2002) MLR model contains individual covariance values that are relatively low, thus suggesting that the parameters are essentially behaving independently from one another, one could reasonably neglect its incorporation in the evaluation of uncertainty. While these assumptions will add some bias to the estimated standard error of the model, this bias is not considered to be significant in a practical sense, and will result in an overall simplification of the evaluation of uncertainty with the MLR model for the user. Therefore, the standard deviation for log of displacement from the Youd et al. (2002) MLR model can be approximated as $\sigma_{\log D_{H-ff,gs}} \approx \sqrt{0.0408} \approx 0.2020$.

Unlike Youd et al. (2002), Bardet et al. (2002) reported the residual mean square, s^2 for the FFGS4 model as 0.0840, as well as provided the model's covariance matrix. However, since the model has over 450 degrees of freedom, and no individual value in the covariance matrix is greater than 5%, it is reasonable to simplify the uncertainty characterization of the FFGS4 model by approximating the standard deviation of the log of displacement as $\sigma_{\log(D+0.01)} \approx \sqrt{0.0840} \approx 0.2898$, which can be used with a Normal distribution. Such a simplification in the uncertainty characterization generally introduces bias of about $\pm 3\%$ or less into the estimate of the uncertainty, which would be considered negligible by most standards. However, for situations where such bias would not be acceptable, then it would be necessary to incorporate the residual mean square with the Student's *t*-distribution and the covariance matrix in order to compute a more accurate estimate of the model uncertainty.

Baska (2002) reports the model uncertainty as $\sigma_{\sqrt{D}} = 0.28$, which can be used with a Normal distribution. Finally, because the Baska (2002) model calculates the square root of the lateral spreading displacement, the model allows the possibility of zero displacement to be calculated. However, using such a model also allows negative square root displacement values to be calculated. Such cases indicate either lower loading or greater resistance than that associated with zero displacement and are therefore interpreted as corresponding to zero displacement.

Assuming the simplifying assumptions regarding model uncertainty which were previously discussed are incorporated, the *probability density function* (PDF) for Youd et al. (2002), Bardet et al. (2002), and Baska (2002) empirical models can be approximated by using a Normal (or Gaussian) distribution, which is given by the following equation:

$$f_X(x) = \frac{1}{\sqrt{2\pi}\sigma_x} e^{-\left(\frac{1}{2}\left(\frac{x-\bar{x}}{\sigma_x}\right)^2\right)} \tag{2-24}$$

where $\bar{x}$ is the mean value and σ_x is the standard deviation of the distribution. By plotting this function, one obtains the familiar bell curve. The probability that a random occurrence of x (represented as X) is less than or equal to a known value of x is equal to the sum of the area under the PDF from $-\infty$ to the known value of x. This probability could be cumulatively summed against x to produce the *cumulative density function* (CDF) and can be represented in equation form as

$$F_X(x) = P[X \le x] = \int_{-\infty}^{x} f_X(x)\,dx \tag{2-25}$$

Equation (2-25) can be approximated numerically by using a closed-form representation of the CDF developed by Abramowitz and Stegun (1965). This approximation can be written as

$$F_X(x) \approx 1 - f_X(x)\left[a_1 t + a_2 t^2 + a_3 t^3\right] \tag{2-26}$$

where $a_1 = 0.4361836$, $a_2 = -0.1201676$, $a_3 = 0.9372980$, and $t = 1/(1+0.33267x)$.

Because the Baska (2002) model calculates the square root of the lateral spreading displacement, the model allows the possibility of zero displacement to be calculated. However, using such a model also allows negative square root displacement values to be calculated. Such cases indicate either lower loading or greater resistance than that associated with zero displacement and are therefore interpreted as corresponding to zero displacement.

Bray and Travasarou (2007) faced a similar situation with their Newmark-type model that predicted seismic slope displacements, and treated it u sing a mixed discrete-continuous probability distribution. This type of distribution can be seen in Figure 2-10. The probabilities of all the square roots of displacements equal to or less than zero are summed to represent a discrete probability, $\tilde{p}$, of zero displacement. The remaining square roots of displacement that have values greater than zero are represented using a continuous function. The sum of the area under the continuous portion of the curve is equal to $1-\tilde{p}$ so that the sum of the area under both the discrete and continuous portions is equal to unity.

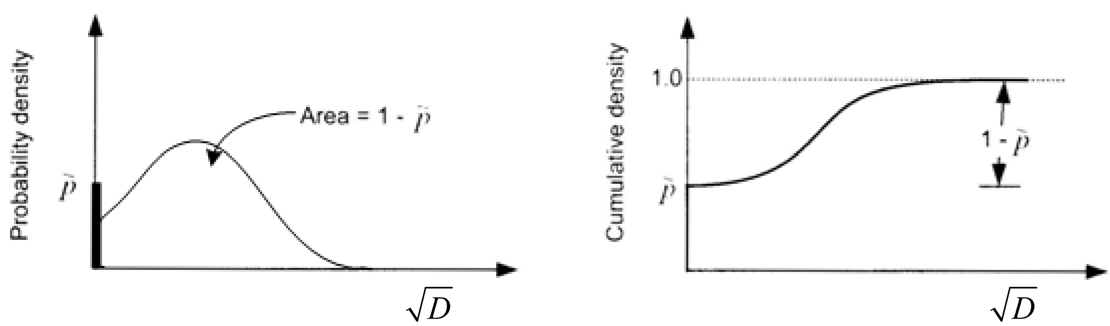

Figure 2-10: Mixed discrete-continuous probability and cumulative density functions

The discrete portion of the PDF, $\tilde{p}$ can be calculated from the CDF by inserting the *Z*-value that corresponds to zero displacement.

$$P\left[D=0 \middle| M,R,S,T^*_{gs,ff}\right] = \tilde{p} = F_Z(z_0) = F_Z\left(\frac{0-\sqrt{D}}{\sigma_{\sqrt{D}}}\right) = F_Z\left(\frac{-\sqrt{D}}{0.28}\right) \qquad (2\text{-}27)$$

2.7 Estimating Lateral Spreading Displacement versus Depth

Although all empirical procedures for estimating lateral spreading displacements provide an estimate of the total cumulative displacement at the ground surface, most neglect lateral displacement prediction with depth. Knowledge of the horizontal strain versus depth is essential for accurately predicting the pile response to kinematic loading from lateral soil deformations. In particular, accurate estimation of the strain profile through the non-liquefied soil crust can be crucial to the pile response analysis since many researchers have shown that the non-liquefied soil crust typically governs the pile response during kinematic loading (Abdoun et al., 1997; Tokimatsu and Asaka, 1998; Singh, 2002; Boulanger et al., 2003).

However, despite the critical nature of accurately estimating the horizontal strain profile in performing a pile response analysis, lack of both empirical data and knowledge of the mechanics governing lateral spreading have forced researchers to develop many simplified assumptions for distributing the predicted surficial lateral spreading displacement down through the rest of the soil profile. These assumptions typically involve distributing the lateral spreading displacement through the liquefied soil layer and assuming that the non-liquefied soil crust moves as a coherent block. While such an assumption appears to be an over-simplification of the problem based on the few actual lateral spreading strain profiles that researchers have observerd (e.g., Holzer and Youd, 2007), this approach appears to produce reasonable pile response results. Previous researchers have recommended linear displacement distributions (Juirnarongrit and Ashford, 2006), quarter-cosine displacement distributions (Cubrinovski and Ishihara, 2004), and half-cosine displacement distributions (Finn and Thavaraj, 2001). One drawback that all of these approaches appear to have in common, however, is that they typically assume that the soil mass behaves as a homogeneous liquefied soil layer, with the exception of the non-liquefied soil crust. Such an assumption erroneously neglects the possible existence of intermediate non-liquefiable soil layers within the liquefied soil mass. Valsamis et al. (2007) developed a model based on many numerical simulations of lateral spreads for estimating displacement versus depth distributions for multi-layered soil systems. Valsamis et al. evaluated one-layer, two-layer, and four-layer liquefied systems, as shown in Figure 2-11.

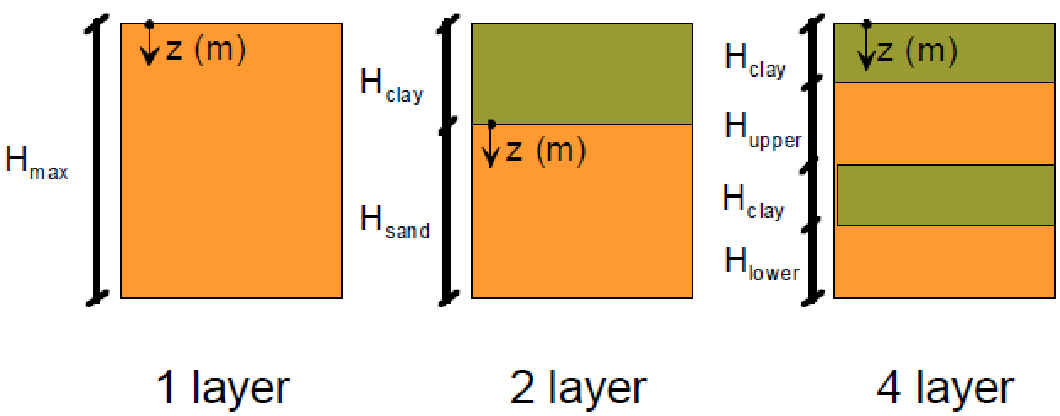

Figure 2-11: Types of soil profiles evaluated numerically by Valsamis et al. (after Valsamis et al., 2007)

For a one-layer system (i.e. homogenous liquefied soil), Valsamis et al. (2007) recommend that a sinusoidal displacement distribution be used. For both two-layer systems and four-layer systems, Valsamis et al. recommended that a linear displacement distribution be used. However, investigation of available inclinometer data from actual lateral spreads from the field such as the Wildlife array (Holzer and Youd, 2007; shown in Figure 2-12) and Moss Landing (Boulanger et al., 1997; shown in Figure 2-13) suggest that sinusoidal displacement distributions are appropriate for even multi-layered systems. Therefore, sinusoidal displacement distributions will be incorporated in this study.

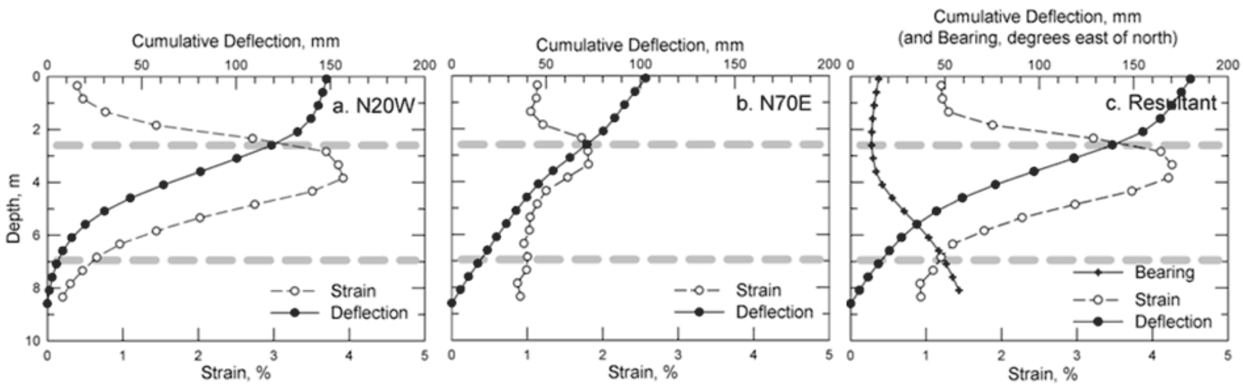

Figure 2-12: Deflection and strain profiles at the Wildlife array (after Holzer and Youd, 2007)

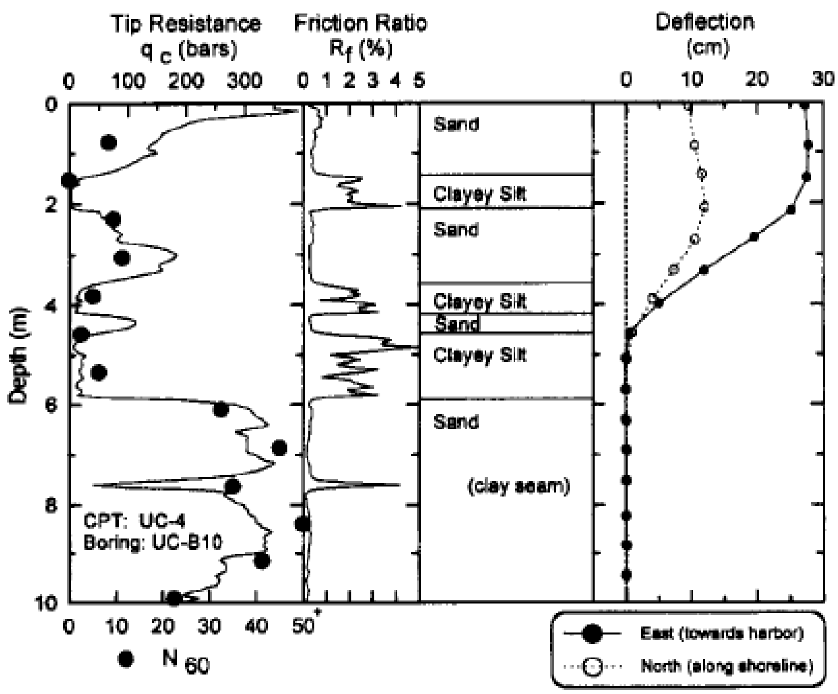

Figure 2-13: Select deflection profile from Moss Landing lateral spread (after Boulanger et al., 1997)

To compute the relative displacements at any relative depth within a given zone of liquefied soil, the sinusoidal displacement distribution can be developed using a half-cosine distribution as

$$D(z) = D_{bottom} + \cos\left(\pi \cdot \frac{z}{H}\right)\left(\frac{D_{top}}{2}\right) + \left(\frac{D_{top}}{2}\right) \tag{2-28}$$

where D_{bottom} is the total lateral displacement at the bottom of the liquefied sublayer (equals zero at the bottom of the deepest liquefied layer), z is the relative depth within the liquefied sublayer from the top of the sublayer, H is the total thickness of the liquefied sublayer, and D_{top} is the total lateral displacement at the top of the liquefied sublayer (equals the total predicted lateral spreading displacement at the ground surface).

For a four-layer system, as shown in Figure 2-11, Valsamis et al. (2007) suggest that the relative maximum displacements at the top of the upper and lower liquefiable layers can respectively be estimated as

$$D_{top,upper} = (1-m)D_{total} \tag{2-29}$$

$$D_{top,lower} = (m)D_{total} \tag{2-30}$$

$$m = \frac{1}{1+0.60\left(H_{upper}/H_{lower}\right)} \tag{2-31}$$

where m is the proportion of the total displacement assigned to the lower liquefied layer, D_{total} is the total predicted lateral spreading displacement at the ground surface, and H_{upper} and H_{lower} are the total thicknesses of the upper and lower liquefiable layers, respectively.

Unfortunately, no displacement distribution recommendations are made regarding layered liquefied systems larger than four total layers. Due to a lack of knowledge for such systems, it is reasonable at this time to assume that the total displacement distribution assigned to a given liquefiable layer is proportional to the ratio of the thickness of the liquefiable layer to the cumulative thickness of all the liquefiable layers.

2.8 Depth Limitations when Developing Lateral Spreading Displacement Profiles

Observations from both the field and the laboratory suggest that lateral spreading is a phenomenon that occurs at depths relatively near the ground surface. Intuitively, this makes sense because it is well known that shear stresses resulting from the presence of a free face or some slope gradient at the ground surface tend to decrease with depth, and lateral spreading is known to be a function of shear stress. Therefore, it would make sense that lateral spreading hazard generally decreases with depth. The question is: "What is the depth at which lateral spreading displacements can be neglected?"

Youd et al. (2002) indicated that their data showed no lateral spreading when the top of the liquefied soil layer (i.e. the top of the first soil layer to be included in the computation of T_{15}) was at a depth greater than 10 meters (approximately 33 feet) below the native ground surface. In addition, Youd (2009) indicated in a personal communication that, based on his experience and observations, lateral spreading generally does not occur at depths greater than about 13.7 meters (45 feet) below the native ground surface for ground slope cases, and at depths greater than about two-times the free face height below the native ground surface (one free face height below the slope toe) for free face cases. Therefore, this study will adopt the simplified recommendations made by Youd (2009) in developing depth limitations for lateral spreading displacement profiles.

3 Review of Kinematic Pile Response Analysis

3.1 Introduction

Since the mid-to-late 1990s, engineers and researchers have developed methodologies to analyze the response of pile and shaft foundation systems to seismically-induced loading from lateral soil movement, or *kinematic loading*. These methodologies were developed in response to severe damage observed to pile/shaft foundations following large earthquakes such as 1964 Niigata, Japan; 1964 Prince William Sound, Alaska; 1989 Loma Prieta, California; 1994 Northridge, California; and 1995 Kobe, Japan. In particular, the massive 1995 earthquake in Kobe, Japan appeared to spark a firestorm of research interest in the topic of kinematic pile response analysis, and many of the modern methods that are utilized in industry today to analyze the kinematic response of piles came about due to this research.

This chapter will briefly present some of the basic background behind the topic of kinematic pile response analysis, and a simplified procedure to perform kinematic pile response analysis will be presented. While many studies have demonstrated the potential importance of considering inertial loading from the superstructure in the analysis of the foundation (e.g., Yoshida and Hamada, 1990; Abdoun et al., 1996; Tokimatsu and Asaka, 1998; Fujii et al., 1998; Adachi et al., 1998; Singh, 2002; Boulanger et al., 2007), such considerations are beyond the scope of this study. Therefore, only kinematic loading due to lateral spreading displacements will be considered in this study.

3.2 Computing Kinematic Pile Response

Many methodologies have been developed by researchers over the years to analyze and predict the soil-pile interaction effect resulting from a given lateral spreading event. These methodologies vary greatly in their approach and complexity, ranging from a simplistic generalization of lateral pressures using limit equilibrium methods (e.g., Ledezma and Bray, 2010; He et al., 2009; Gonzalez et al. 2005; Cubrinovski and Ishihara, 2004; Dobry et al. 2003; Haigh 2002; Haigh and Madabushi 2002; JRA, 2002) to advanced numerical models (e.g., Cheng and Jeremic, 2009; Lam et al., 2009; Arduino et al., 2006; Yang et al. 2003; Finn and Thavaraj, 2001; Li and Dafalius 2000).

Representation of lateral soil resistance using p-y soil springs in a Beam-on-Winkler Foundation (BWF) method is a popular method among practicing engineers to evaluate both the inertial and the kinematic pile response in liquefied and/or laterally spreading soil. As noted by Juirnarongrit and Ashford (2006), this method is often preferred over more simplistic limit equilibrium methods due to its ability to predict pile displacements. Juirnarongrit and Ashford (2006) also note that it is often preferred over more complex methodologies such as 3D numerical models due to the advanced nature of numerical modeling in general and the inherent dependency on a reliable constitutive model. Therefore, despite its relative simplicity, the BWF method has repeatedly been demonstrated to provide reasonable representation of the observed inertial and kinematic response of single piles and pile groups in both the laboratory and in the field (Wilson et al., 2000; Tokimatsu et al., 2001; Ashford and Rollins, 2002; Boulanger et al., 2003; Tokimatsu and Suzuki, 2004; Brandenberg, 2005; Rollins et al. 2005; Weaver et al. 2005; Juirnarongrit and Ashford 2006; Brandenberg et al. 2007).

3.3 P-Y Analysis Methodology

Juirnarongrit and Ashford (2006) note that BWF procedures are most commonly used by engineers today to evaluate inertial loading of a pile. However, they point out that BWF procedures can also reliably compute the kinematic response of pile loading as well. Reese et al. (2000) originally demonstrated a BWF p-y procedure to analyze the kinematic loading of a pile, and their approach is well-summarized in Juirnarongrit and Ashford (2006). This approach is demonstrated in Figure 3-1 below.

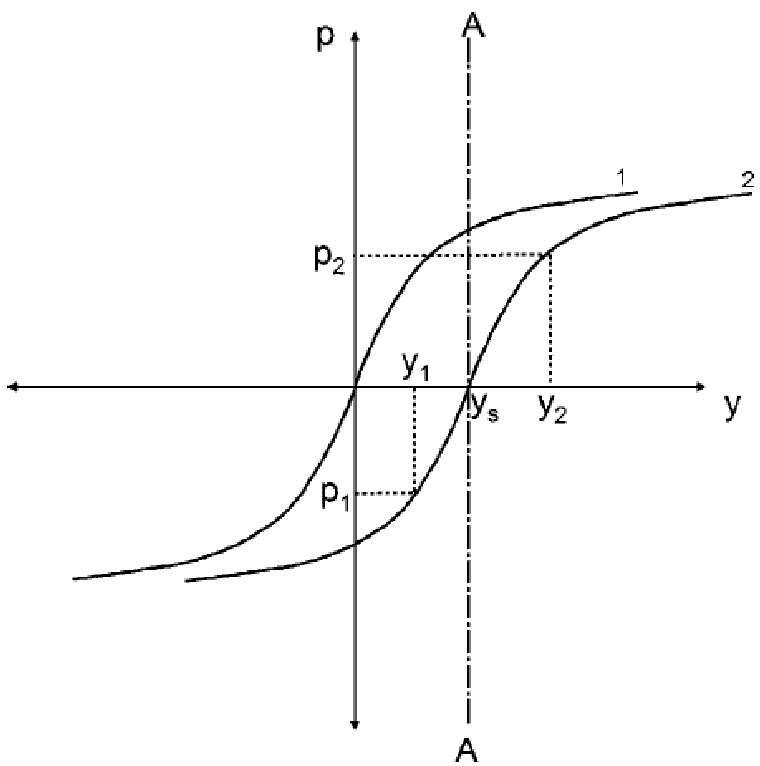

Figure 3-1: Depiction of procuedure for using p-y curves to account for the kinematic loading of piles (after Juirnarongrit and Ashford, 2006; modified from Reese et al., 2000)

If the soil mass surrounding the pile is stationary, then the p-y curve for the soil is symmetrical about the *p*-axis, as shown for curve 1 in Figure 3-1. The pile response for this case can be determined by solving the following differential equation:

$$EI\frac{d^4 y_p}{dz^4} - py_p = 0 \tag{3-1}$$

where EI is the pile stiffness, p is the soil reaction per unit length of pile, y_p is the pile displacement, and z is the depth.

However, if the soil mass moves relative to the pile, then the soil resistance curve (curve 2) is offset by the soil movement. Therefore, if the pile movement, y_p, is less than the soil movement, y_s, then the soil applies a driving force (p_1) to the pile. However, if the pile movement is greater than the soil movement, then the soil provides a resistance force (p_2) to the pile. Thus, to predict the response of the pile to kinematic loading using a p-y analysis, the free-field soil movement can be applied as boundary conditions to the Winkler soil springs in the BWF model, as demonstrated in Figure 3-2 .

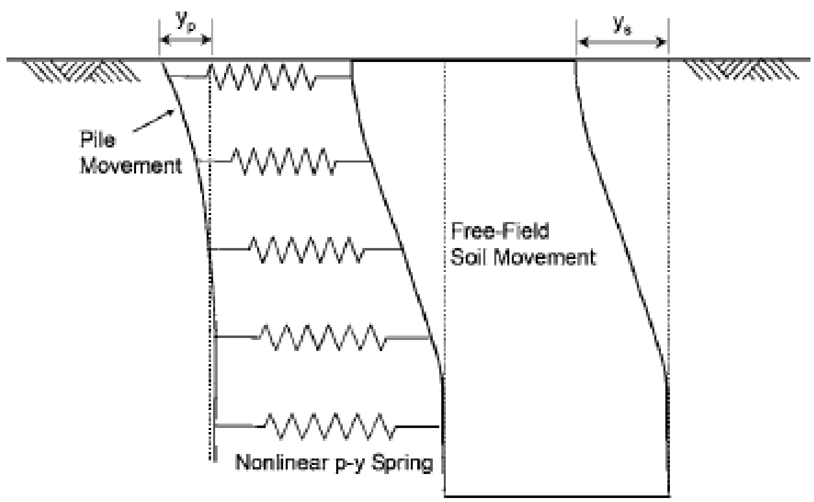

Figure 3-2: p-y analysis model for kinematic loading (after Juirnarongrit and Ashford, 2006)

The pile response for the p-y soil springs shown in Figure 3-2 can then be computed by solving the following differential equation:

$$EI\frac{d^4 y_p}{dz^4} - p\left(y_p - y_s\right) = 0 \tag{3-2}$$

Juirnarongrit and Ashford (2006) note that Equation (3-2) can be solved using either finite difference or finite element methods. The popular lateral pile response computer software

LPILE Plus 5.0 (Ensoft, 2004) uses the finite difference technique to solve the differential equation. All pile response analyses in this study were modeled using this software.

3.4 P-Y Development for Soil Layering

Since BWF analysis incorporates soil spring models, often called p-y curves, some discussion regarding selection of these models is merited. For a soil layer at a given site, p-y curves can be developed from site-specific lateral load pile tests (e.g., Hales, 2003; Bowles, 2005) by measuring strains in the pile and integrating curvature and slope to obtain pile deflections, *y*, while also differentiating bending moment and shear force to obtain the distributed soil load or pressure, *p*. This site-specific approach is diagramed in Figure 3-3.

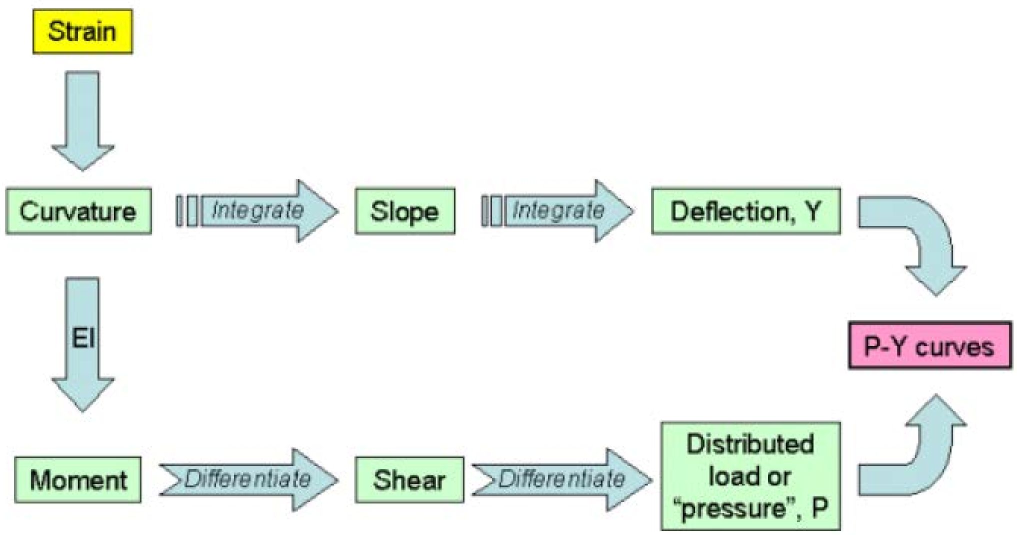

Figure 3-3: Process for computing site-specific p-y curves from measurement of pile strain (after Hales, 2003)

Due to the relatively high cost and complex logistics of performing and analyzing site-specific lateral pile load tests, most engineers in practice today choose to use published p-y curve models for various generalized soil types rather than develop site-specific p-y curves. Such curves include Matlock (1970) for soft clay, Reese et al. (1974) for sand, and Reese et al. (1975) for stiff clay beneath the water table. Published p-y curves typically require the user to characterize the soil with properties such as friction angle, undrained strength, confining stress, and p-y modulus. These curves can generally provide a reasonable approximation of the p-y behavior of most soils as long as the user accurately characterizes the properties of the soil.

Although there is relatively little discord among researchers and engineers regarding p-y behavior of typical soils such as sands and clays, there is considerable uncertainty and disagreement regarding the p-y behavior of liquefied soil. The reason for this uncertainty is due to the complex behavior of liquefied soil and our inability to predict that behavior under variable conditions. Commonly-used procedures today for modeling p-y behavior of liquefied soil include residual strength-based methods (Wang and Reese, 1998), methods incorporating dilative behavior (Rollins et al., 2005), and methods based on load reduction factors known as "p-multipliers" (Brandenberg et al., 2007). Although an argument can be made regarding which procedure should be incorporated in this study, the p-multiplier approach presented by Brandenberg et al. (2007) was selected to be used in this study since it has been repeatedly shown to reasonably represent the load-displacement behavior of piles subjected to very large soil strains. However, other p-y models may be substituted into the procedure presented in this study at the discretion of the geotechnical engineer if deemed appropriate. As new p-y approaches for representing liquefied soil are developed in the future, they should be compatible with this procedure and may replace the Brandenberg et al. p-multiplier approach if desired.

The Brandenberg et al. (2007) model correlates p-multipliers with $N_{1,60-CS}$. These p-multipliers range from 0.0 to approximately 0.5. According to the Brandenberg et al. procedure, the p-y behavior for a non-liquefied sand can be computed using a modified form of the API (1993) p-y model for sand. According to the modified API (1993) procedure, the governing ultimate soil resistance of the sand must be computed as

$$p_u = \min \begin{cases} p_{u1} \\ p_{u2} \end{cases} \tag{3-3}$$

where

$$p_{u1} = \left(c_1 x + c_2 b\right) \gamma' x \tag{3-4}$$

$$p_{u2} = c_3 b \gamma' x \tag{3-5}$$

$$c_1 = \frac{k_0 \tan\phi \sin\beta}{\tan\left(\beta-\phi\right)\cos\alpha} + \frac{\tan^2\beta \tan\alpha}{\tan\left(\beta-\phi\right)} + k_0 \tan\beta\left(\tan\phi\sin\beta - \tan\alpha\right) \tag{3-6}$$

$$c_2 = \frac{\tan\beta}{\tan\left(\beta-\phi\right)} - \tan^2\left(45-\frac{\phi}{2}\right) \tag{3-7}$$

$$c_3 = k_0 \tan\phi \tan^4\beta + \tan^2\left(45-\frac{\phi}{2}\right) \tag{3-8}$$

and γ' is the buoyant unit weight, b is the width or diameter of the pile/shaft, x is the depth below the ground surface, ϕ is the soil friction angle, and $\beta = 45 + \frac{\phi}{2}$. According to Boulanger et al. (2003), k_0 and α are typically assumed to be equal to 0.4 and $\phi/2$, respectively. Once the value of p_u is computed, the soil resistance per unit length of pile for non-liquefied sand can be computed as

$$p = A\left(p_u\right)\tanh\left(\frac{k^* x}{A p_u} y\right) \tag{3-9}$$

where $A = 3 - 0.8\left(x/b\right) \geq 0.9$ for static loading, y is the relative movement between the soil and the pile/shaft, and k^* is the modified subgrade modulus corrected for overburden pressure. According to Boulanger et al. (2003), the modified subgrade modulus can be computed as

$$k^* = \sqrt{\frac{\sigma'_{ref}}{\sigma'_v}}k \tag{3-10}$$

where k is the initial subgrade modulus recommended by the API (1993) criteria for sand, σ'_v is the vertical effective stress at the depth x, and σ'_{ref} is the reference stress at which k is calibrated (recommended to be 50 kPa or 7.25 psi by Boulanger et al., 2003). Finally, with the computation of the non-liquefied soil resistance p, the liquefied soil resistance can be computed as

$$p_{liq} = \left(m_p\right) p \tag{3-11}$$

where m_p is the p-multiplier and can be estimated from the shaded region shown in Figure 3-4.

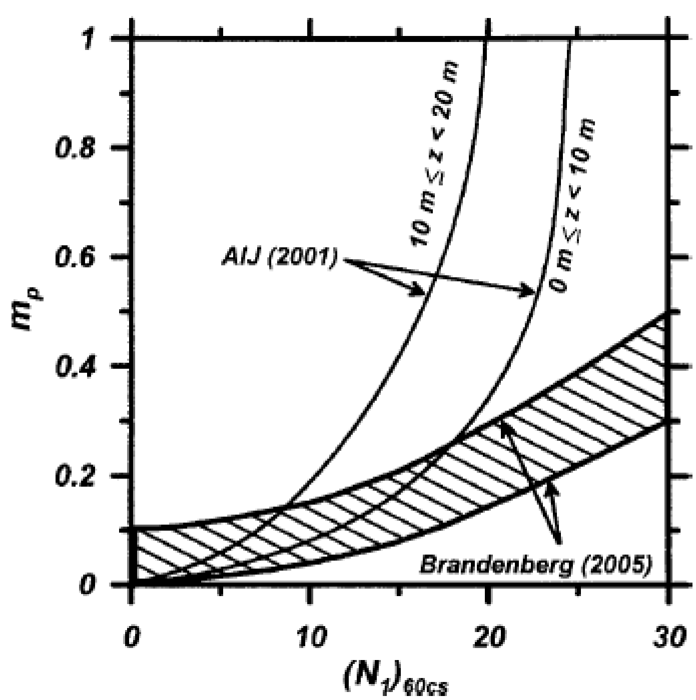

Figure 3-4: Recommended p-multipliers to compute p-y behavior of liquefied sand (after Brandenberg et al., 2007)

3.5 Equivalent Single Pile for Kinematic Group Response

Juirnarongrit and Ashford (2006) presented a simplified procedure to compute the average kinematic response of a pile group using p-y soil springs and the BWF method of analysis. The procedure was based heavily on the work of Mokwa (1999) and Mokwa and Duncan (2003), and develops an equivalent "single" pile to represent the average soil-pile response behavior of the group and the pile cap. However, Juirnarongrit and Ashford (2006) warn that since this procedure uses a simplified pseudo-static push over analysis to solve what in reality can be a very complex problem, caution should be applied when interpreting the analysis results. Furthermore, they recommend that for the design of important and/or critical structures, additional analysis such as numerical modeling should be used to validate the procedure's results. The procedure is not able to account for battering of piles; but the engineering standard of practice in most areas appears to neglect the battering of piles in the kinematic analysis in order to be conservative. If it is desired to know the pile response of a particular row of piles, or if complexities such as pile batter or non-typical foundation geometries are desired to be accounted for, then a more sophisticated approach such as a numerical model should be employed by the analyst.

3.5.1 Development of the Equivalent Single Pile

Mokwa (1999) suggested that a pile group could be converted to an equivalent single pile by computing the flexural stiffness of a single pile, multiplying that stiffness by the number of total piles in the group, and then reducing the p-y soil springs in the model to account for the pile group (i.e. pile shadowing) effect. Therefore, the soil spring resistance in the equivalent single pile model can be computed as

$$p = \sum_{i=1}^{N} p_i \left(f_m \right)_i \tag{3-12}$$

where p_i is the soil spring resistance computed for a single pile, $\left(f_m \right)_i$ is the group reduction p-multiplier for the row containing the given pile *i,* and *N* is the total number of piles in the group. Several studies have been performed to estimate the group reduction p-multiplier including Brown and Reese (1985), Morrison and Reese (1986), McVay et al. (1994, 1995), Rollins et al. (1998), Ashford and Rollins (2002), and Rollins et al. (2006). For this project, the Rollins et al. (2006) procedure will be incorporated for estimating group reduction p-multipliers. According to the Rollins et al. procedure, the group reduction multiplier for a given row in a pile group can be computed as

$$\left.\begin{array}{l} f_m = 0.26\ln\left(S/D\right) + 0.5 \le 1.0 \\ f_m = 0.52\ln\left(S/D\right) \le 1.0 \\ f_m = 0.60\ln\left(S/D\right) - 0.25 \le 1.0 \end{array}\right\} \left\{\begin{array}{l} \text{Leading Row of Piles} \\ \text{Second Row of Piles} \\ \text{Third and Higher Rows of Piles} \end{array}\right\} \tag{3-13}$$

where *S* is the uniform center-to-center spacing between the piles, and *D* is the diameter of the piles.

Figure 3-5 demonstrates the equivalent single pile procedure for a simplified four-pile group geometry. Recommendations regarding the rotational soil spring for the pile cap shown in Figure 3-5 will be summarized in the following section.

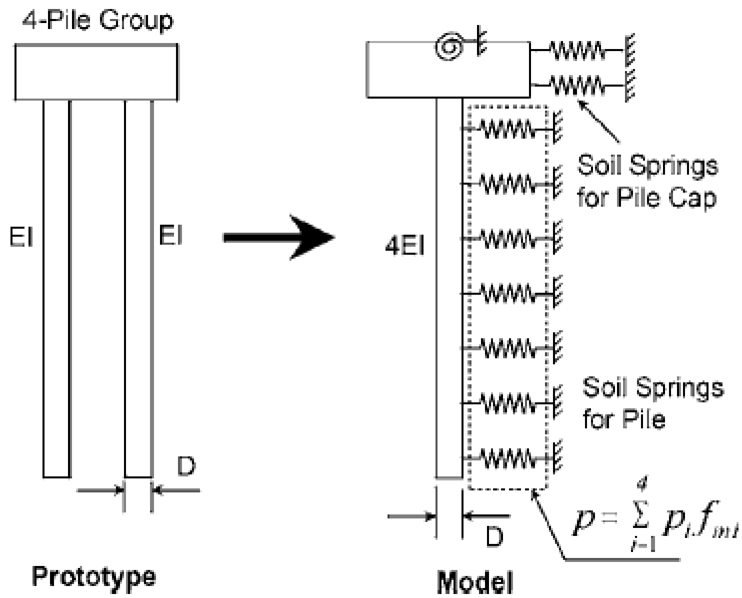

Figure 3-5: Equivalent "single" pile for a simplified four-pile group (after Juirnarongrit and Ashford, 2006)

3.5.2 Resistance of the Pile Cap and Development of the Rotational Soil Spring

The phenomenon of lateral spreading has often been observed to cause a rotation in the cap of the pile groups. This rotation is due to the tendency of the back row of piles in the group (i.e. the pile fronting the lateral spreading displacements) to be pulled down, while concurrently the leading row of piles are pulled up. Mokwa (1999) and Mokwa and Duncan (2003) theorized that a rotational stiffness coefficient could be developed to describe this observed behavior. According to their work, the rotational stiffness of the pile group can be estimated as

$$k_{m\theta} = \frac{M}{\theta} \tag{3-14}$$

where M is the restraining moment from the piles that resists rotation, and θ is the angular rotation of the pile head. Juirnarongrit and Ashford (2006) state that the value of $k_{m\theta}$ can be determined from the ultimate restraining moment M_{ult} and the ultimate angular rotation θ_{ult} if a linear relationship is assumed between M and θ up to the ultimate restraining moment. This assumption is demonstrated in Figure 3-6.

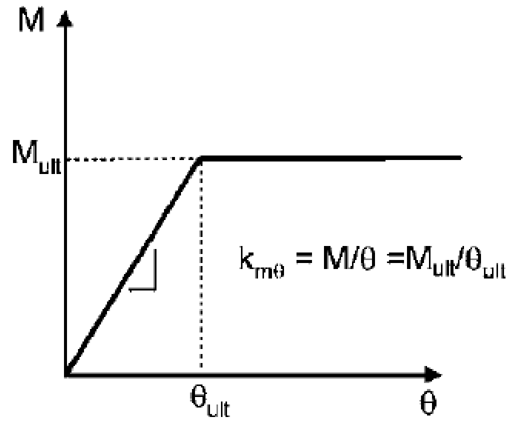

Figure 3-6: Linear relationship assumption between M and θ for the rotational stiffness (after Juirnarongrit and Ashford, 2006)

Thus, the ultimate resisting moment from a pile group can be computed as

$$M_{ult} = \sum_{i=1}^{N} \left[(Q_s)_i + (Q_p)_i \right] X_i \tag{3-15}$$

where $(Q_s)_i$ is the skin friction resistance for pile *i*, $(Q_p)_i$ is the end bearing resistance for pile *i*, X_i is the moment arm for pile *i*, and *N* is the number of piles in the pile group. Note that for upward-moving piles, $(Q_p)_i$ is equal to zero. Juirnarongrit and Ashford (2006) recommend computing skin friction resistance using the α method for cohesive soils and the β method for non-liquefied cohesionless soils. It is recommended that skin friction be neglected in liquefied soil. Commonly-used procedures for computing (Q_s) and (Q_p) for a single pile and/or pile groups are presented in any basic foundation design textbook such as Das (2004) or Coduto (2001) and will not be explained in any further detail in this report.

Calculation of X_i in the computation of M_{ult} depends on the chosen point in the system about which the moments are summed. Juirnarongrit and Ashford (2006) note that for pile groups with three rows or less, it is convenient to sum the moments about the back row of piles (i.e., the pile being pulled down). By doing so, the end-bearing resistance of the downward-moving piles can be neglected because their moment arm is equal to zero. Figure 3-7 demonstrates this concept for a simplified two-row pile group.

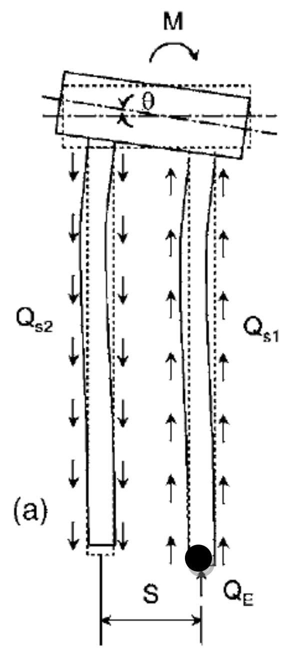

Figure 3-7: Summing the moments about downward-moving piles (adapted from Juirnarongrit and Ashford, 2006)

Based on Mokwa's approach (Mokwa, 1999), the ultimate angular rotation of the pile cap depends on whether the piles are free to move downward if loaded (i.e. frictional piles), or if they are fixed at their ends (i.e. end-bearing piles). This concept is demonstrated in Figure 3-8.

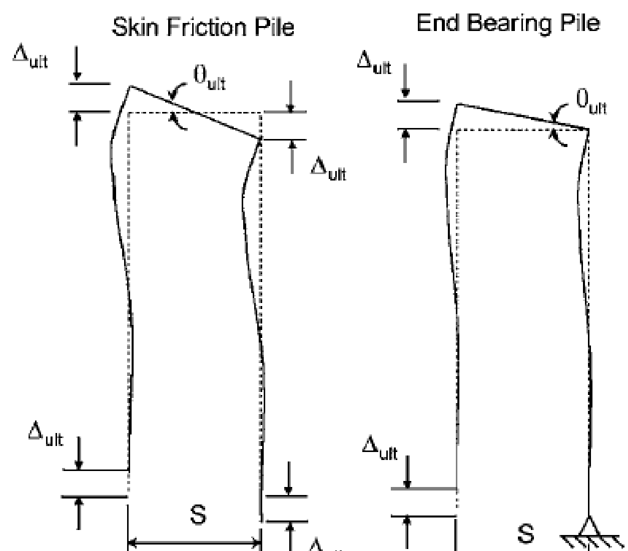

Figure 3-8: Ultimate angular rotation of the pile cap for both the frictional pile group and the end-bearing pile group (after Juirnarongrit and Ashford, 2006; originally adapted from Mokwa and Duncan, 2003)

For the frictional piles, rotation is assumed to occur about the center of the pile cap. Therefore, the ultimate angular rotation of the pile cap is given by Juirnarongrit and Ashford to be

$$\theta_{ult} = \tan^{-1}\left(\frac{2\Delta_{ult}}{S}\right) \tag{3-16}$$

where S is the pile spacing and Δ_{ult} is the relative displacement between the soil and pile required to fully mobilize skin friction along the pile shaft.

For the end-bearing piles, rotation is assumed to occur about the back row of piles in the pile group. Therefore, the ultimate angular rotation of the pile cap is given as

$$\theta_{ult} = \tan^{-1}\left(\frac{\Delta_{ult}}{S}\right) \tag{3-17}$$

For the purpose of estimating Δ_{ult}, Das (2004) suggested that skin friction along a pile shaft would be fully mobilized when the relative displacement between the pile and the soil was between 5 to 8 millimeters (mm) irrespective of pile diameter and length. Juirnarongrit and Ashford (2006) recommend using a value of 8 mm (0.315 inches or 0.026 feet) for Δ_{ult} based on the results of their study. This study will follow the recommendations made by Juirnarongrit and Ashford.

3.6 Additional Discussion Regarding Kinematic Loading and the Pile Cap

Most lateral spreading case histories have shown that the interaction between the pile cap and the non-liquefied soil crust plays a very significant role in the ultimate kinematic response of a given pile group. Under static conditions, soil movement against the pile cap can be represented as a passive pressure distribution against the face of the pile cap. Past research into passive pressures on pile caps under static conditions has shown that full passive pressures are generally developed with relative soil-cap displacements of 1% to 6% of the pile cap height, depending on the type of soil surrounding the pile cap (Duncan and Mokwa, 2001; Rollins and Sparks, 2002). However, relatively recent research with centrifuge testing (Boulanger et al., 2003; Brandenberg et al., 2005) has shown that for conditions where the passive failure surface extends into the liquefied zone, the largest passive resistance from the non-liquefied soil crust against the pile cap is achieved at relative displacements ranging from 40% to 100% of the pile cap height. For such conditions, Brandenberg et al. (2005) proposed a relationship to account for this apparent "softening" effect of the non-liquefied crust as

$$\frac{F_{crust}}{F_{crust,ult}} = \left[\left(\frac{y}{C\cdot H}\right)^{-0.33} + \left(\frac{16\cdot y}{C\cdot H}\right)^{-1}\right]^{-1} \le 1 \tag{3-18}$$

where $F_{crust}/F_{crust,ult}$ is the ratio of the "softened" soil resistance divided by the ultimate predicted soil resistance of the non-liquefied soil crust, y is the relative displacement between the soil and the pile, H is the height of the pile cap (in units consistent with y), and C is an empirical curve-fitting constant that controls the curvature of the relationship and ranges between 0.2 to 0.8 for liquefied soil conditions. Equation (3-18) is demonstrated graphically in Figure 3-9. Brandenberg et al. (2007b) expanded on the findings of Brandenberg et al. (2005) to develop a more comprehensive but complex iterative process for estimating the apparent softening p-y effect in kinematic loading due to soil liquefaction. However, due to its complexity this procedure will not be described in detail in this report.

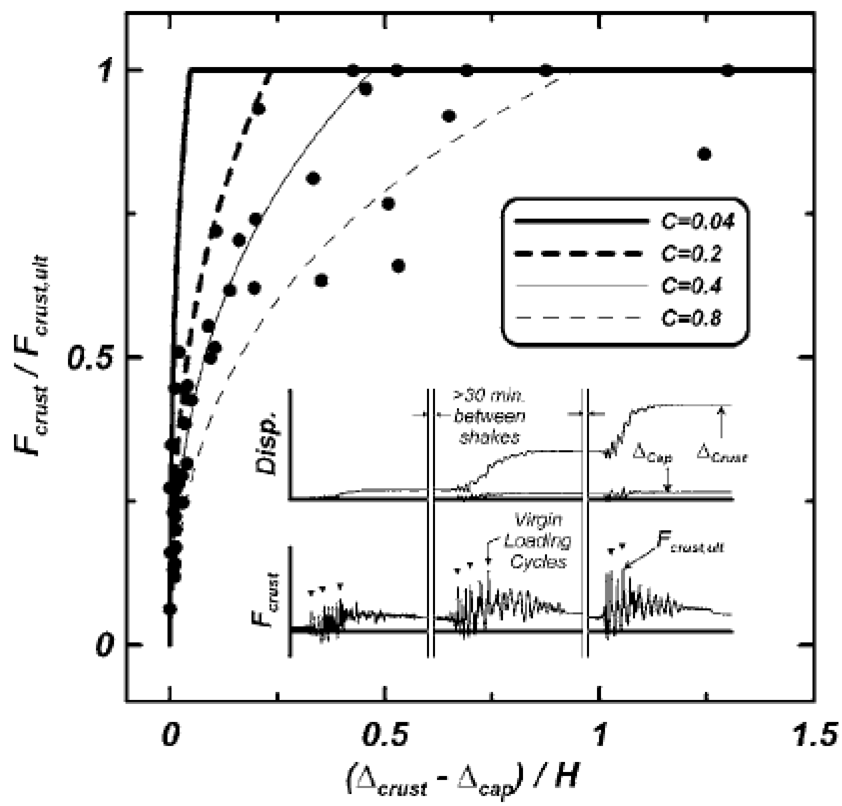

Figure 3-9: Normalized load-displacement curves for non-liquefied crust over liquefied soil from centrifuge study (after Brandenberg et al., 2005)

A final additional consideration that could significantly alter the soil-pile cap interaction is friction along the sides and base of the pile cap. From their centrifuge studies, Boulanger et al. (2003) and Brandenberg et al. (2005) reported that up to 50% of the total kinematic lateral force exerted on their model pile cap was produced from side and base friction from the soil flowing around the cap. In theory, it would take a relatively small amount of differential displacement between the pile cap and the laterally spreading soil to mobilize skin friction on the pile cap. However, some researchers and consultants hesitate to account for such friction by arguing that liquefaction-induced soil settlements have often been observed to create a gap between the bottom of the pile cap and the soil. These professionals also point out the possibility that soil beneath the pile cap could become trapped between piles rather than slide along the base of the pile cap. Finally, these researchers and consultants argue that the shallow depth at which most pile caps are located often negates the effects of friction acting on the pile cap due to relatively low confining pressures. Therefore, while it is acknowledged that cases may exist in practice where skin friction could potentially have a significant effect on t he predicted kinematic response analysis of the pile group (especially for caps that are geometrically very long in the direction of the lateral spreading displacements), such consideration was neglected for pile groups in this study due to the relatively narrow pile caps associated with the case histories in this research, and because such consideration was not recommended in the procedure presented by Juirnarongrit and Ashford (2006).

4 Performance-Based Earthquake Engineering Design

4.1 Introduction

Ever since earthquakes have destroyed man-made buildings, society has turned to engineers to find solutions to make its structures more resilient against earthquake-induced damage. Especially during the 20^{th} century, engineers began making design breakthroughs in helping their structures become more resistant to earthquake damage. The 1920's and 1930's saw the first specific earthquake provisions in building codes in Japan and the United States. These codes were improved upon as engineers and seismologists began understanding increasingly more about the geologic make-up of the earth, plate tectonics, earthquake characteristics, structural response, and soil/structure interaction. In the latter half of the century, research on local site effects, the phenomenon of liquefaction, and probabilistic applications in determining design specifications led to even better earthquake-resistant designs.

As part of this on-going effort to improve seismic design codes, several institutions and researchers are currently studying the idea of Performance-Based Earthquake Engineering (PBEE). PBEE is a revolutionary concept in earthquake resistant design which would ideally help the owner and engineer jointly decide on a design based on the desired structural performance under common and severe earthquake loading. Such a concept would be a significant step toward the application of the current state of knowledge of earthquake engineering in earthquake-resistant design, and it would begin moving engineers and owners away from conventional empirically and deterministically-based decisions.

This chapter will briefly present the basic ideas and philosophies of PBEE, review the concepts of Probabilistic Seismic Hazard Analyses, describe the information available from the USGS National Seismic Mapping Program website, and introduce the Pacific Earthquake Engineering Research Center's recommended framework for PBEE. Finally, published performance-based models related to liquefaction and estimation of lateral spreading displacements will also be summarized.

4.2 Basic Philosophy of PBEE

Since the early 1980s, many researchers have analyzed the effects of significant earthquakes and have concluded seismic risks in urban areas are increasing and are far from socio-economically acceptable levels. These researchers believe that the key to correcting this problem is to develop more reliable seismic standards and code provisions than those currently available, and to implement these codes in the engineering of new structures and upgrading of older structures (Bertero and Bertero, 2004). This belief led to the development of PBEE, which was first formally proposed by SEAOC Vision 2000 Committee in 1995 in its report entitled "Performance-Based Seismic Engineering of Buildings" (Bertero and Bertero, 2004).

Since that time, researchers have been working to further develop the idea of PBEE, simple but reliable procedures for its practical application, and guidelines by which it could be implemented in building codes. As a result, PBEE is continuously evolving into a well-structured framework that implies design, evaluation, construction, monitoring the function and maintenance of engineered facilities whose performance under common and extreme loads responds to the diverse needs and objectives of owners, users, and society (Krawinkler and Miranda, 2004). However, there are still many legal and professional barriers that will need to be overcome in order to prove PBEE as a safe, simple, and reliable methodology to be applied in the field of Earthquake Engineering.

PBEE is founded on the idea that uncertainty in engineering design can be quantified and used in predicting performance such that engineers and owners together can make intelligent and informed trade-offs based on l ife-cycle considerations rather than construction costs alone (Krawinkler and Miranda, 2004). For example, if an owner would like a building to be fully operational immediately following a major earthquake, then engineers could design the building to a higher performance level than that considered for a building in which the owner simply desired a level of performance that provided life-safety. Owners therefore would have options for maximizing the return of their investment by designing for greater levels of performance for their buildings beyond the minimum life-safety requirements imposed by society if they so desired (Krawinkler and Miranda, 2004). PBEE could also be very beneficial in that minimum levels of performance beyond life-safety could be mandated for critical structures such as hospitals, storage facilities for hazardous waste, or nuclear facilities.

In order to predict the likely performance of a structure subjected to a wide range of earthquake loading scenarios, engineers must consider the entire range of possible earthquake hazards and their corresponding uncertainties as opposed to focusing on a single scenario earthquake. This means that design procedures that are more firmly rooted in the realistic prediction of structural behavior exposed to a realistic distribution of possible earthquake loads must be developed in such a way that they are practical to apply and relatively simple to interpret. In addition, engineers must begin to move away from purely empirical procedures (Krawinkler and Miranda, 2004). This may involve developing new procedures that consider the entire seismic hazard spectrum, or modifying deterministic empirical procedures so that they can be implemented in a performance-based engineering framework.

The implication of PBEE is that damage to a building from earthquake loading is acceptable as long as it does not exceed the level of damage prohibited by society and it proves the most economic solution (Krawinkler and Miranda, 2004). In order to make such an implication work, engineers must not only have procedures that can realistically predict the building response under a given level of earthquake loading, but must also have procedures which can predict the earthquake loading itself. Through the 1970's and 1980's, most engineers developed design ground motions by using observation-based and empirical approaches that are generally considered simplistic by today's standards. Uncertainty in the estimation of these ground motions was typically accounted for by applying heavy doses of conservatism. However, since PBEE involves moving engineers away from these simplistic and conservative procedures, a seismic hazard analysis that objectively considers the entire seismic hazard spectrum and quantifies the uncertainties involved in the hazard analysis must be incorporated instead. Such a seismic hazard analysis was already being applied by many engineers well before the advent of PBEE. It is called Probabilistic Seismic Hazard Analysis.

4.3 Seismic Hazard Analysis

A key element of seismic design is the ability to quantify the level of demand placed on a structure or foundation. This quantification can be expressed in terms of a *design ground motion*, which can be characterized by *design ground motion parameters* (Kramer, 1996). The computation of design ground motion parameters is called a *seismic hazard analysis*. During the advent of earthquake engineering, little was understood regarding the estimation of earthquake ground motions. However, a substantial amount of data has been collected in the form of earthquake recordings during the past century, and researchers have used this data to develop empirical predictive relationships to estimate earthquake ground motions. While these predictive relationships were initially quite simplistic, most have evolved into very complex equations developed from advanced statistical regression methods. These ground motion predictive relationships are commonly referred to as *attenuation relationships* because the amplitude of the predicted ground motion tends to attenuate with increasing source-to-site distance.

4.3.1 Estimating Earthquake Ground Motions using Attenuation Relationships

Site-specific ground motions can be influenced by the style of faulting, magnitude of the earthquake, and local soil or rock condition. The attenuation relationships used to estimate ground motion from an earthquake source need to consider these effects.

Many attenuation relationships have been developed, particularly during the last 20 years, to estimate the variation of peak ground surface acceleration with earthquake magnitude and distance from the site to the source of an earthquake. Recently, under a Pacific Earthquake Engineering Research (PEER) Center project entitled "Next Generation Attenuation of Ground Motions (NGA)," five separate research teams developed new attenuation relationships for shallow crustal earthquakes in Western North America from a common dataset of ground motions by applying whatever limitations and statistical transformations of the data they felt necessary. These relationships are Abrahamson and Silva (2008), Boore and Atkinson (2008), Campbell and Bozorgnia (2008), Chiou and Youngs (2008), and Idriss (2008).

The NGA predictive relationships were developed from statistical analyses of recorded worldwide earthquakes, including the records from the 1989 Loma Prieta earthquake, the 1992 Landers earthquake, the 1994 Northridge earthquake, the 1995 Kobe earthquake, and more recent important earthquakes that were not included in previous attenuation relationships developed during the 1990's (e.g., 1999 Kocaeli, Turkey earthquake and the 1999 Chi-Chi, Taiwan earthquake). The attenuation relationships provide geometric mean values of horizontal ground motions associated with one set of parameters: magnitude, distance, site soil conditions, and mechanism of faulting. The uncertainty in the predicted ground motion is taken into consideration by including a standard error in the probabilistic analysis. Though the NGA attenuation relationships were developed specifically for the western United States, they theoretically can be applied to other areas in the world with moderate to high seismicity and crustal faulting regimes because they also include many ground motions from other high seismicity regions in the world such as Japan and Turkey. Because the various NGA attenuation relationships are very complex equations, they are simply referred to and are not presented in detail in this dissertation. For deterministic liquefaction analyses performed in this study, an NGA calculation spreadsheet, developed and made available by PEER (Al Atik, 2009), was used to estimate the ground motions from the scenario earthquake event. In addition, for the seismic hazard analyses performed as part of this study, all but the Idriss (2008) NGA attenuation models were used and averaged with equal weights. The reason that the Idriss (2008) model was not used is because it is only applicable to rock sites.

Attenuation relationships have also been developed to predict ground motions from other faulting regimes such as subduction zones and inter-continental seismic zones. Because the case histories evaluated in this study included significant earthquake hazard contributions from subduction zone sources, including both *interface* sources (i.e. slip and resulting crustal uplift along the interface between a crustal tectonic plate and an oceanic tectonic plate) and *intraplate* sources (i.e. very deep events resulting from the bending and breaking of the subducted oceanic crust located in a region known as the Benioff zone), attenuation relationships that accounted for these two types of events were selected for use in this study. These relationships include Youngs et al. (1997), Atkinson and Boore (2003), and Zhao et al. (2006). To compute the weighted-average ground motions from the subduction zone sources in this study, equal weights were applied to these attenuation relationships.

Using ground motion predictive equations to estimate an earthquake ground motion for use in design can be a significant challenge because the amount of uncertainty associated with all of the potential earthquake sources, their associated recurrence rates, their size, and the significance of their effect on the site of interest can be great, indeed. To objectively account for all of these uncertainties, seismologists and engineers have utilized Total Probability Theory to compute probabilistic estimates of ground motions. This type of analysis is known as *Probabilistic Seismic Hazard Analysis* or PSHA.

4.3.2 Probabilistic Seismic Hazard Analysis

To provide a more complete picture of the seismic hazard, a PSHA uses rational principles of mathematics and probability theory to identify, quantify, and combine the uncertainties involved with earthquake prediction. The theory of PSHA has been developed and presented by many researchers over the years (e.g., Cornell, 1968; Cornell, 1971; Merz and Cornell, 1973; McGuire, 2004). The uncertainties that are evaluated and quantified in a PSHA typically include *uncertainty in earthquake location, uncertainty in earthquake size, uncertainty in the attenuation relationship(s),* and *temporal uncertainty.*

4.3.2.1 Uncertainty in Earthquake Location

Spatial uncertainty is an important aspect to consider in a seismic hazard analysis. The distance between site and earthquake source can contribute greatly to the intensity of shaking felt at a site. Spatial uncertainty is related to the geometry of the earthquake source zones considered in the PSHA. To understand this idea, one must know that there are four basic source geometries: *point sources, linear sources, areal sources,* and *volumetric sources.* Point sources can be a single geographical location which can act as an earthquake source, such as a volcano or a small earthquake. Linear sources are generally well-defined faults where the focal depth along the fault can generally be assumed to be approximately constant. Areal sources generally characterize areas with dense faulting schemes and well-defined faulting planes where an earthquake could occur in many possible locations. Volumetric sources usually characterize areas where the earthquake mechanism is poorly defined or where the faulting network is so dense and complicated that it is difficult to distinguish individual faults. Examples of several of these sources and their corresponding PDFs are presented in Figure 4-1.

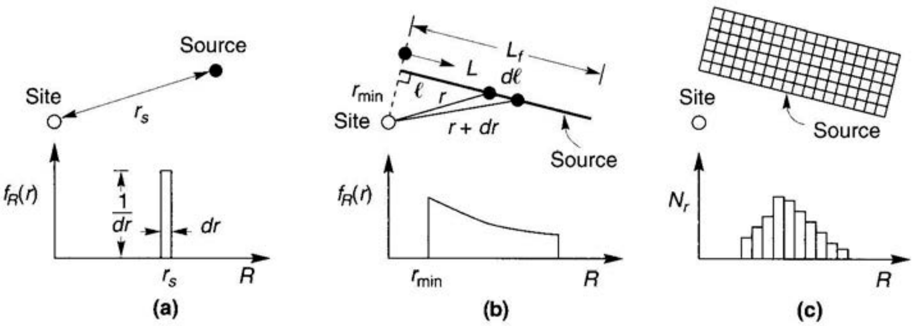

Figure 4-1: Example probability density functions for source-to-site distance for a (a) point source, (b) line source, and (c) area source (after Kramer, 1996)

4.3.2.2 Uncertainty in Earthquake Size

To consider the uncertainty in earthquake size, scientists have developed various relationships called *recurrence laws* that describe the mean annual frequency of a given earthquake magnitude. Though a wide variety of recurrence laws have been developed over the years, two particular recurrence laws that have found wide acceptance among practicing engineers and scientists today, namely: the *Gutenberg-Richter recurrence law* and the *Characteristic Earthquake recurrence law*.

1) The Gutenberg-Richter recurrence law was originally developed by Gutenberg and Richter (1944) from data gathered from Southern California earthquakes over a period of many years. The recurrence law can be written as

$$\log \lambda_m = a - bm \tag{4-1}$$

where λ_m is the *mean annual rate of exceedance* of magnitude *m,* 10^a is the mean yearly number of earthquakes of magnitude greater than or equal to zero, and *b* describes the relative likelihood of large and small earthquakes. The reciprocal of λ_m is called the *return period* of an earthquake exceeding magnitude *m*, and is often symbolized as T_R. Equation (4-1) above can also be written as

$$\lambda_m = 10^{a-bm} = \mathrm{e}^{\alpha - \beta m} \tag{4-2}$$

where $\alpha = 2.303a$ and $\beta = 2.303b$. Figure 4-2(a) shows the graphical meaning of the parameters *a* and *b*. Finally, McGuire and Arabasz (1990) demonstrated that a bounded modification of the Gutenberg-Richter recurrence law works well in a PSHA to account for both a minimum (i.e. threshold) and a maximum magnitude.

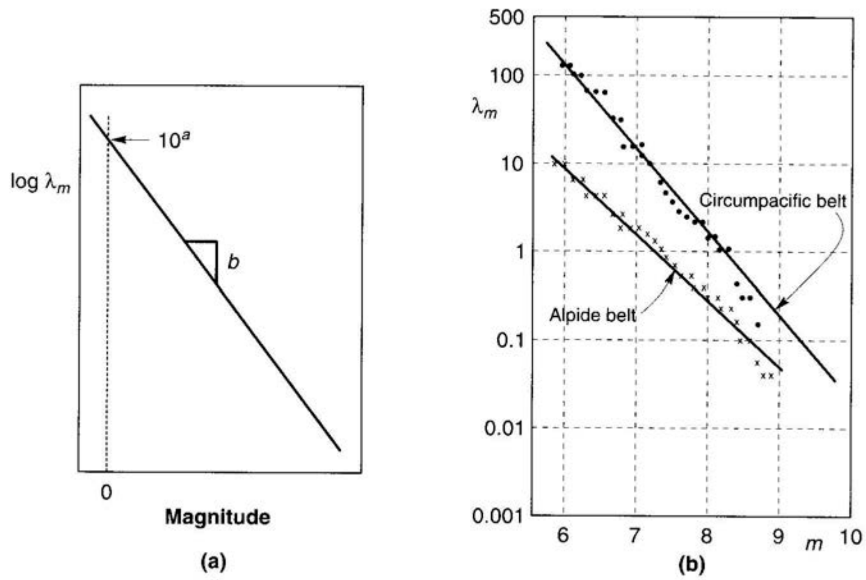

Figure 4-2: (a) Graphical meaning of the parameters a and b used in the Gutenberg-Richter recurrence law; (b) Gutenberg-Richter recurrence law applied to two tectonic belts (after Kramer, 1996)

2) Characteristic Earthquake recurrence laws were developed from paleoseismic studies that suggest that individual points on faults and fault segments tend to move by approximately the same distance in each earthquake. This repetitive earthquake is called the *characteristic earthquake* and considered to be fault-specific. This theory is supported by geologic evidence that suggests that the characteristic earthquake occurs more frequently along a given fault than would be predicted by extrapolation of the Gutenberg-Richter law (Kramer, 1996). The result is a more complex recurrence law which combines the use of seismicity data to predict the recurrence of lower magnitude earthquakes and geologic data to predict the recurrence of higher magnitude earthquakes. Youngs and Coppersmith (1985) developed such a model, combining an exponential magnitude distribution at lower magnitudes with a uniform distribution near the characteristic earthquake. This model is demonstrated in Figure 4-3. Wesnousky (1994) has suggested that the Characteristic Earthquake recurrence model is likely more appropriate for well-defined faults than the Gutenberg-Richter recurrence model.

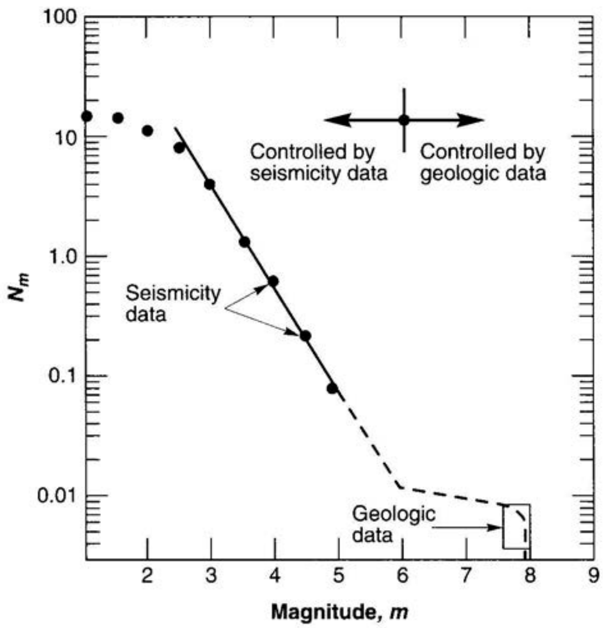

Figure 4-3: Inconsistency of mean annual rate of exceedance as determined from seismicity data and geologic data (after Youngs and Coppersmith, 1985)

4.3.2.3 Uncertainty in the Attenuation Relationships

Because ground motion attenuation relationships are empirically regressed, they have scatter associated with their data. Though least-squares regression is often employed to minimize this scatter, some scatter inherently will remain. This scatter results from randomness in the mechanics of rupture and from variability and heterogeneity of the source, travel path, and site conditions (Kramer, 1996). Typically, the standard deviation from each attenuation relationship is incorporated into the PSHA to account for the uncertainty in ground motion computation.

4.3.2.4 Temporal Uncertainty

The ability to account for temporal uncertainty is an important aspect of a probabilistic seismic hazard analysis and is closely related to uncertainty in earthquake size. Because studies of seismicity data have revealed little evidence of temporal patterns in earthquake recurrence, scientists have long assumed that the occurrence of earthquakes is a random process, therefore enabling them to apply simple probabilistic models such as the Poisson probability model to their analyses.

The Poisson probability model can be written as follows:

$$P\left[N=n\right]=\frac{\left(\lambda t\right)^{n}\,\mathrm{e}^{-\lambda t}}{n!} \tag{4-3}$$

where the random variable N is the number of occurrences of a particular event during a time period of interest, n is the test number of occurrences, t is the time period of interest, and λ is the average rate of occurrence of the event. However, engineers often desire to know the probability that one *or more* significant events will occur during a given time period. By obtaining a mean annual rate of exceedance, λ_m, from a recurrence law and combining it with the Poisson model, the probability of occurrence of at least one event in a period of t years can be expressed as

$$P\left[N \geq 1\right] = 1 - \mathrm{e}^{-\lambda_m t} \tag{4-4}$$

4.3.2.5 Steps for Performing a PSHA

The steps for performing a PSHA are similar to the steps for performing a DSHA, but they numerically account for all possible combinations of magnitude and distance, as well as their corresponding uncertainties. Reiter (1990) described the procedure as a four-step process, which is shown schematically in Figure 4-4:

1) *Identify and c haracterize the earthquake sources.* This includes characterizing the probability distribution of potential rupture within each of the sources. A uniform probability distribution of potential rupture is often assumed (i.e. the probability of rupture is the same for every specific point in the source).
2) *Characterize the seismicity or temporal distribution of earthquake recurrence by using a recurrence relationship.* Choose a r ecurrence law that is applicable to all of the earthquake sources and determine the specific relationship for each source.
3) *Determine the ground motion produced at the site for all possible combinations of earthquake size and location within a s ource by using a pr edictive relationship.* The predictive relationship used in a PSHA often comes in the form of an attenuation relationship.
4) *Combine the uncertainties in earthquake location, earthquake size, and ground motion parameter prediction.* This step involves the creation of a *seismic hazard curve*, which is a useful function that plots some ground motion parameter against the mean annual rate of exceedance for that parameter and will be reviewed in the following section. By utilizing Equation (4-4), seismic hazard curves can be incorporated effectively with the Poisson model to account for temporal uncertainty and to determine the probability that a ground motion parameter will be exceeded during a particular time period. Such information could potentially be very valuable to decision-makers, owners, and engineers.

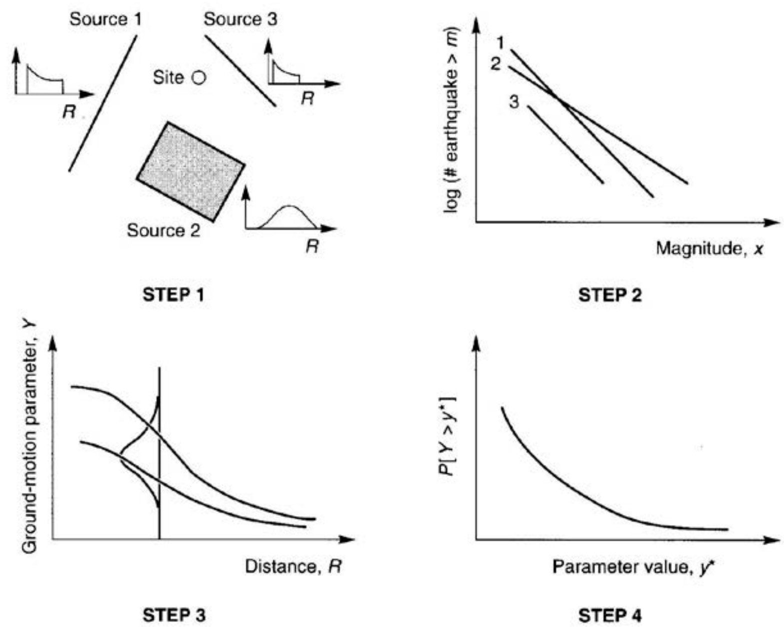

Figure 4-4: Schematic diagram of the steps involved in completing a PSHA for a given site (after Kramer, 1996)

4.3.2.6 Developing a Seismic Hazard Curve

Combining the uncertainties in earthquake location, earthquake size, and ground motion parameter prediction in a PSHA involves the creation of a seismic hazard curve. A seismic hazard curve is a function that relates a certain ground motion parameter to its mean annual rate of exceedance. Such curves can be calculated for each individual earthquake source in a PSHA and then be summed to provide one curve that considers the effects of all possible combinations of magnitude and distance, together with their corresponding uncertainties, from each earthquake source.

By applying the total probability theorem, the average annual rate of exceeding any ground motion parameter of interest $y*$ can be expressed as

$$\lambda_{y*} = \sum_{i=1}^{N_S} \nu_i \int\int P\left[Y > y* \mid m,\ r\right] f_{M_i}\left(m\right) f_{R_i}\left(r\right)\ dm\ dr \qquad (4\text{-}5)$$

$$\nu_i = \mathrm{e}^{\alpha_i - \beta_i m_0} \qquad (4\text{-}6)$$

where $f_M\left(m\right)$ and $f_R\left(r\right)$ are the probability density functions for magnitude and distance, N_s is the number of potential earthquake sources, ν_i is the total average rate of threshold magnitude exceedance, and $\alpha = 2.303a$ and $\beta = 2.303b$.

A single point on a seismic hazard curve is created when λ_{y*} is computed. In order to develop the entire curve, the process must be repeated for different values of $y*$. Once the desired number of values of λ_{y*} has been computed, then the points can be connected with a line and the seismic hazard curve is complete. A seismic hazard curve can be versatile for designers because it can be combined with the Poisson model shown in Equation (4-4) to return the probability that some ground motion parameter is exceeded in a given time period.

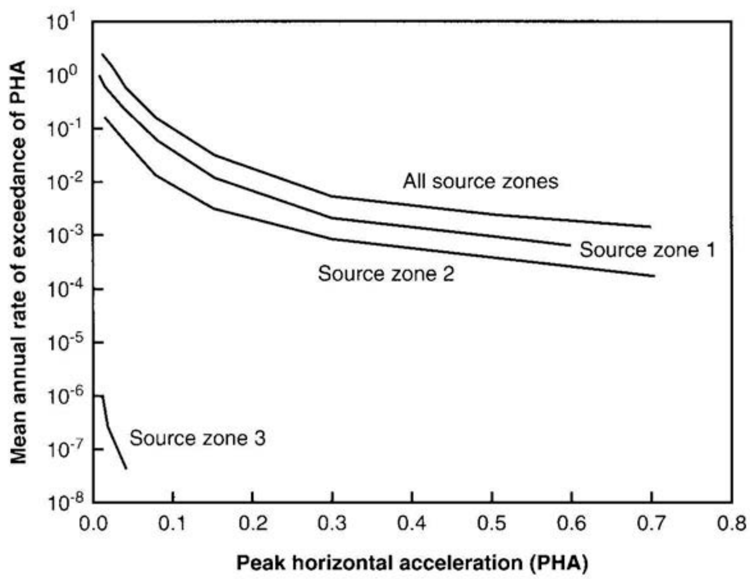

Figure 4-5: Example of seismic hazard curves for the peak horizontal acceleration (PHA) computed for a given site with three separate seismic sources (after Kramer, 1996)

4.4 Introduction to PEER PBEE Framework

It has been established that PBEE provides a methodology that considers the contributions from *all hazard levels* and incorporates them into a performance evaluation. Such an approach may be preferable over a deterministic design approach, which usually considers a single ground motion hazard level (i.e. a single return period) in earthquake engineering design. In order to consider the probabilistic contributions from all return periods, PBEE must be performed in a probabilistic framework. By doing so, PBEE can ultimately compute the risk associated with earthquake hazard at a given site, which can be expressed in terms of economic loss, fatalities, or other form of loss measurement. The Pacific Earthquake Engineering Research Center (PEER) has developed such a framework (Cornell and Krawinkler, 2000; Krawinkler, 2002; Deierlein et al., 2003). By utilizing PBEE within the PEER probabilistic framework, risk can effectively be computed as a function of ground shaking through the use of several intermediate variables, which will be defined in the following section.

4.4.1 PEER PBEE Framework Variable Definitions

The variables that compose the PBEE probabilistic framework developed by PEER are defined as:

1) *Intensity Measure, IM* – This variable characterizes the ground motion or the seismic loading. The mean annual rate of exceedance of the *IM*, λ_{IM}, is used in PBEE and must be calculated by means of a PSHA utilizing *IM* as the ground motion parameter of interest.
2) *Engineering Demand Parameter, EDP* – This variable shows the effects of the *IM* on the response of a system of interest.
3) *Damage Measure, DM* – This variable shows the physical effect of the *EDP* on damage to the system of interest. It describes the damage and consequences of damage to a structure or to a component of the structural, nonstructural, or content system (Krawinkler and Miranda, 2004).
4) *Decision Variable, DV* – This variable is the quantifiable value on which ultimate performance assessment is based, and can be thought of as the risk associated with the *DM*.

4.4.2 PEER PBEE Framework Equation

The framework equation developed by PEER to house PBEE is based on the same probabilistic principles that are used in a PSHA calculation. The fundamental equation for this framework can be given (using *EDP* and *IM* in this case) as

$$\lambda_{edp} = \int P\left[EDP > edp \mid IM\right] d\lambda_{IM} \tag{4-7}$$

where $P\left[a \mid b\right]$ describes the conditional probability of a given b. Equation (4-7) returns the single value on the seismic hazard curve corresponding to a value of *edp*. Also note that Equation (4-7) can be applied to any of the PEER PBEE parameters as long as a proper chain of relations is established (i.e. *IM* → *EDP* → *DM* → *DV*). In other words, one cannot calculate λ_{DM} directly from the *IM* since *DM* is dependent on the *EDP*.

Equation (4-7) can be rewritten using a numerical approximation as

$$\lambda_{edp} \approx \sum_{i=1}^{N_i} P\left[EDP > edp \mid IM = im_i\right] \Delta\lambda_{IM} \tag{4-8}$$

where $P\left[EDP > edp \mid IM = im_i\right]$ can be obtained from a complementary CDF that relates $P\left[EDP > edp\right]$ to the *IM*. This type of CDF is called a *fragility curve*. An example of a fragility curve can be seen in Figure 4-6. Equation (4-8) is demonstrated visually in Figure 4-7.

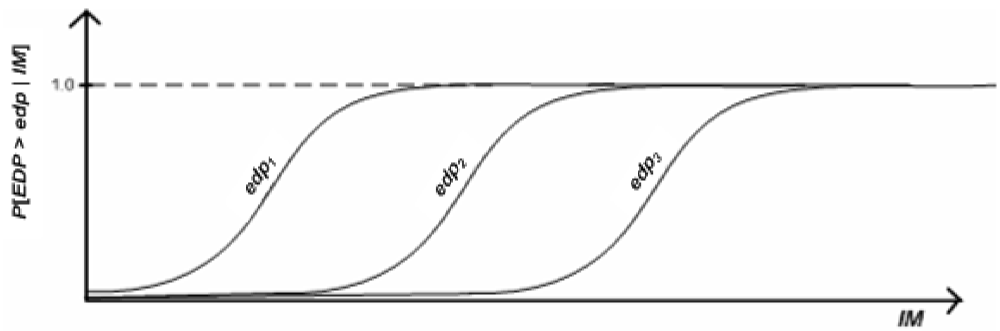

Figure 4-6: Example for fragility curves for some *EDP* given some *IM*

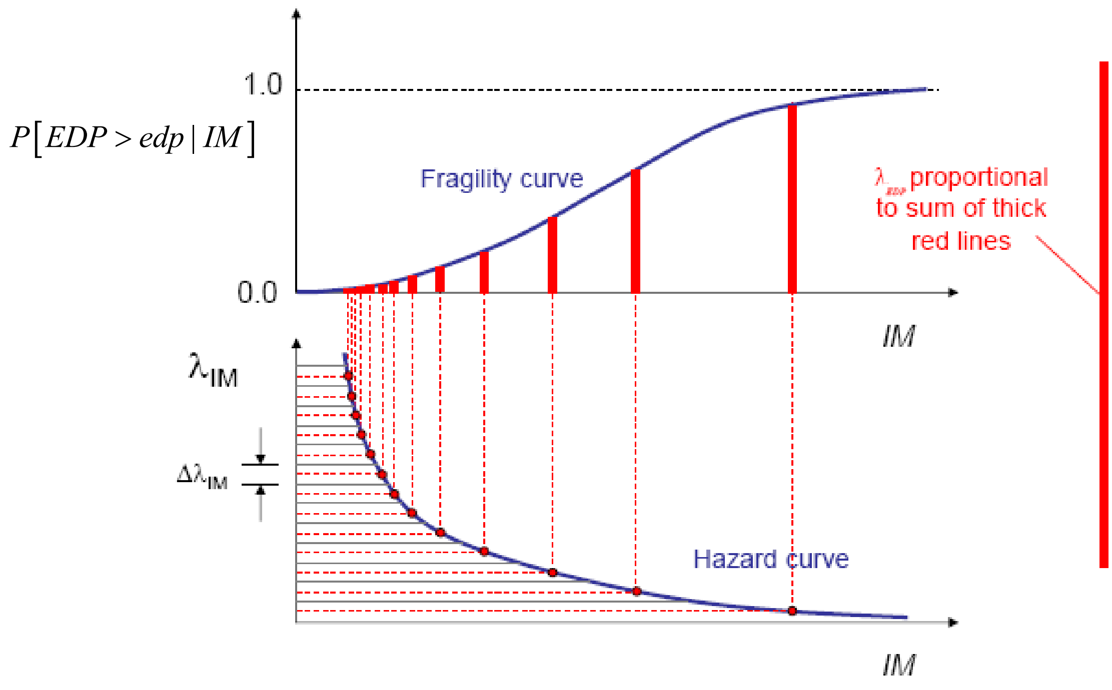

Figure 4-7: Visual representation of Equation (4-8) (courtesy of Steven Kramer, from a NEES presentation in 2005)

It is possible to consider all of the PEER PBEE parameters in a single equation to obtain the seismic hazard curve for the *DV* by utilizing the seismic hazard curve for the *IM*. This mathematical equation has become well-known in the earthquake engineering community as "PEER's triple integral." The equation is given as

$$\lambda_{DV} = \iiint P[DV \mid DM]\ dP[DM \mid EDP]\ dP[EDP \mid IM]\ d\lambda_{IM} \tag{4-9}$$

The final product of Equation (4-9) is the mean annual rate of exceedance of the *DV*, λ_{DV}. This implies that one could incorporate λ_{DV} with a temporal uncertainty model (i.e. the

Poisson model) to obtain the probability that some value, DV,* will be exceeded during a given time period. Such information could be extremely valuable to decision-makers and spare the challenge of attempting to base decisions on subjective interpretations of the *IM* or the *EDP* alone.

One of the advantages to the PEER PBEE framework is that it compartmentalizes the various aspects of system response that ultimately contribute to overall seismic performance. Because the framework is organized into these compartments, it makes it possible for researchers to develop individual components for the framework that can be incorporated with components developed by other researchers. The goal of this study is to therefore develop a component for the framework that characterizes the kinematic pile response due to lateral spreading as a *DM*. While the current study does not include the development of a *DV* related to kinematic pile response, the procedure presented in this study will be able to be incorporated into future research for the development of such relationships.

5 Performance-Based Kinematic Pile Response

5.1 Assumptions of the Procedure

The performance-based procedure presented in this chapter is developed for the analysis of lateral spreading in the native soil, which is sometimes referred to as *regional* lateral spreading. While it is recognized that seismic slope displacements are closely related to the phenomenon of lateral spreading and that both are capable of inflicting significant damage to foundations due to kinematic loading, the methodologies applied by engineers to estimate displacements/deformations from each can be quite different, and it is therefore justifiable that the mechanisms be evaluated separately. With that assumption being stated, the performance-based procedure presented in this chapter is sufficiently robust to be applicable to the evaluation of seismic slope displacements as well as to the evaluation of lateral spreading displacements. However, the development of a procedure to estimate performance-based seismic slope displacements for use in the performance-based kinematic pile response procedure is beyond the scope of this study, and only a procedure for the performance-based computation of lateral spreading displacements are presented herein.

The procedure developed in this study assumes that kinematic loading due to lateral spreading is the primary cause of loading to the foundations. While it is possible to include the addition of other externally-applied loads in the kinematic analysis including inertial loads, drag loads from the free-field soil displacements, and structural bracing loads from the superstructure, no recommendations regarding the evaluation and quantification of the uncertainty of such loads is provided in this study. Therefore, the addition of such loads requires structure-specific evaluation. Such assumptions are not intended to minimize or de-emphasize the effects that these externally-applied forces can have on the performance of a given foundation system. Rather, they are intended to simplify the procedure and remain consistent with many of the deterministic practices that are commonly applied in industry today. Ultimately, it is left to the user to apply sound engineering judgment in evaluating whether or not to include the effects of externally-applied forces in the performance-based kinematic pile response procedure presented in this study.

The performance-based procedure developed in this study is applicable only to sites where lateral spreading displacements can reasonably be predicted. Conditions where liquefaction flow failure is likely to occur are not valid to be modeled with the procedure presented herein. A simple evaluation of the potential likelihood of a flow failure occurring given the triggering of liquefaction in one or more soil layers can be easily be performed using a post-seismic 2D limit equilibrium slope stability analysis. If the limit equilibrium stability analysis yields a factor of safety equal to unity or less, then it can be assumed that liquefaction flow failure is likely to occur given liquefaction triggering of the soil, and significantly large soil deformations are likely to result. As stated previously, no reliable methodology currently exists for accurately predicting the deformations resulting from a liquefaction flow failure.

5.2 Soil Site Characterization

Evaluation of the soils at the site of interest is a critical component of the performance-based kinematic pile response analysis. Since the procedure recommended in this study involves regional lateral spreading, it is necessary to identify continuous liquefiable layers upon which non-liquefiable soil may displace laterally due to earthquake ground motion. Ideally, the site characterization would be comprised of several SPT borings and CPT soundings in order to establish the possibility of soil layer continuity. In the event that significant soil continuity does not exist at the site, then it is not likely that regional lateral spreading will occur at the site and the performance-based kinematic pile response procedure is considered to be complete. However, other potential hazards to the foundation may still need to be considered such as seismic slope displacements, inertial loading and other soil-structure-interaction effects due to the seismic response of the superstructure, and kinematic loading on the piles due to wave passage effects and soil impedance. The elaboration on such hazards, however, is beyond the scope of the current study.

Once all of the soil samples are obtained from the borings, certain laboratory tests should be assigned to various representative samples in order to estimate soil properties that are potentially necessary in the analysis of liquefaction triggering and lateral spreading. These tests include sieve analyses and/or -#200 washes to evaluate fines content and grain size distributions, Atterberg limits on fine-grained soil samples to measure liquid limits and soil plasticity, and water content measurements.

5.3 Characterization of Site Geometry/Topography

Characterization of site geometry is a critical part of performing any lateral spreading analysis. If using empirical MLR lateral spreading procedures to estimate displacements, it is typically necessary to characterize the site as having either a “free-face” geometry or a “ground-slope” geometry. A free-face geometry is generally recognized as a distinct break in the slope or the topography. A simple graphical representation of a free-face is shown in Figure 2-8. Examples of conditions which are typically considered free-face geometries include river channels, quay walls, and man-made excavations. A ground-slope geometry is generally recognized as the average regional slope gradient across the site of interest. History has demonstrated that even very shallow gradients can be susceptible to lateral spreading displacements.

5.4 Characterization of Site Seismicity

A critical component of the performance-based kinematic pile response procedure is the characterization of seismicity and liquefaction potential at the site. Evaluation of the seismicity for the performance-based procedure consists of estimating the seismic hazard curve for the Peak Ground Acceleration. Evaluation of the PGA ground motion parameter can be performed by either a 1) site-specific PSHA, or 2) reliance on seismic hazard results developed as part of the National Seismic Hazard Mapping Project (NSHMP) of the United States Geological Survey (USGS Earthquake Hazard Program, 2010). Note that the latter option can only be performed for sites located within the boundaries of the United States. Either option requires that the seismic hazard curve for the PGA be defined and corresponding deaggregation results be tabulated. In order to adequately define the seismic hazard curve for most performance-based engineering applications, PGA values and corresponding deaggregations should be developed for at least seven return periods: 108 years (50% probability of exceedance in 50 years), 225 years (20% probability of exceedance in 50 years), 475 years (10% probability of exceedance in 50 years), 975 years (5% probability of exceedance in 50 years), 2475 years (2% probability of exceedance in 50 years), 4975 years (1% probability of exceedance in 50 years), and 100,000 years (<<1% probability of exceedance in 50 years). Intermediate values on the seismic hazard curve can generally be log-linearly interpolated from these results with relatively small amounts of error.

Probabilistic ground motions for this study were computed in a site-specific PSHA using the popular commercially available software EZ-FRISK (Risk Engineering, 2010).

5.4.1 Liquefaction Triggering Analysis

Part of the characterization of the seismicity of the site in the proposed performance-based procedure for the analysis of kinematic pile response is the liquefaction triggering analysis. Deterministic procedures for estimating liquefaction triggering using the Cetin et al. (2004) procedure with a given set of values for magnitude, PGA, average shear wave velocity, and soil SPT blowcounts was presented in Chapter 2. However, values of PGA and magnitude are not considered constant parameters in a performance-based analysis. As such, the performance-based procedure developed by Kramer and Mayfield (2007) for the evaluation of liquefaction triggering is recommended for use in this procedure. According to this procedure, the annual rate of non-exceedance for factor of safety against liquefaction can be computed as

$$\Lambda_{FS_L^*} = \sum_{j=1}^{N_M} \sum_{i=1}^{N_{a_{\max}}} P\left[FS_L < FS_L^* \mid a_{\max_i}, m_j\right]\left(\Delta\lambda_{a_{\max_i}, m_j}\right) \tag{5-1}$$

where N_M and $N_{a_{\max}}$ are the number of magnitude and peak acceleration increments into which the "hazard space" is subdivided; $P\left[FS_L < FS_L^* \mid a_{\max_i}, m_j\right]$ is the probability of non-exceedance of the factor of safety against liquefaction FS_L^* computed according to Cetin et al. (2004) and given peak ground acceleration $a_{\max_i}$ and magnitude m_j; and $\Delta\lambda_{a_{\max_i}, m_j}$ is the incremental mean annual rate of exceedance from the seismic hazard curve of peak ground acceleration $a_{\max_i}$ corresponding to magnitude m_j.

5.5 Development of the *IM* for the Performance-Based Procedure

Kramer et al. (2007) noted that empirical MLR models for lateral spreading are generally comprised of parameters that deal with either 1) site conditions (e.g., liquefiable layer thickness, gradient or free-face ratio, etc.) or 2) seismic loading (e.g., earthquake magnitude and source-to-site distance). Thus, a given empirical lateral spreading model can generally be re-written as

$$\text{Displacement} = \mathscr{L} + \mathscr{S} + \varepsilon \tag{5-2}$$

where $\mathscr{L}$ represents all of the parameters and their corresponding regression coefficients associated with earthquake loading, $\mathscr{S}$ represents all of the parameters and their corresponding regression coefficients associated with site conditions, and ε represents the model uncertainty.

Every empirical lateral spreading model that fits within the framework defined by Kramer et al. (2007) will therefore have unique values of $\mathscr{L}$ and $\mathscr{S}$. For the three empirical lateral spreading models incorporated in this study, the value of $\mathscr{L}$ for each model can be given as

$$\mathscr{L}_{Youd} = 1.532M - 1.406\log\left(R + 10^{(0.89M - 5.64)}\right) - 0.012R \tag{5-3}$$

$$\mathscr{L}_{Bar\,\mathrm{det}} = 1.017M - 0.278\log R - 0.026R \tag{5-4}$$

$$\mathscr{L}_{Baska} = 1.231M - 1.151\log\left(R + 10^{(0.89M - 5.64)}\right) - 0.01R \tag{5-5}$$

for the Youd et al. (2002), Bardet et al. (2002), and Baska (2002) models, respectively. A plot of the $\mathscr{L}$ parameter for the Youd et al. (2002) model is demonstrated in Figure 5-1, thus showing how the parameter is a function of both earthquake magnitude and distance.

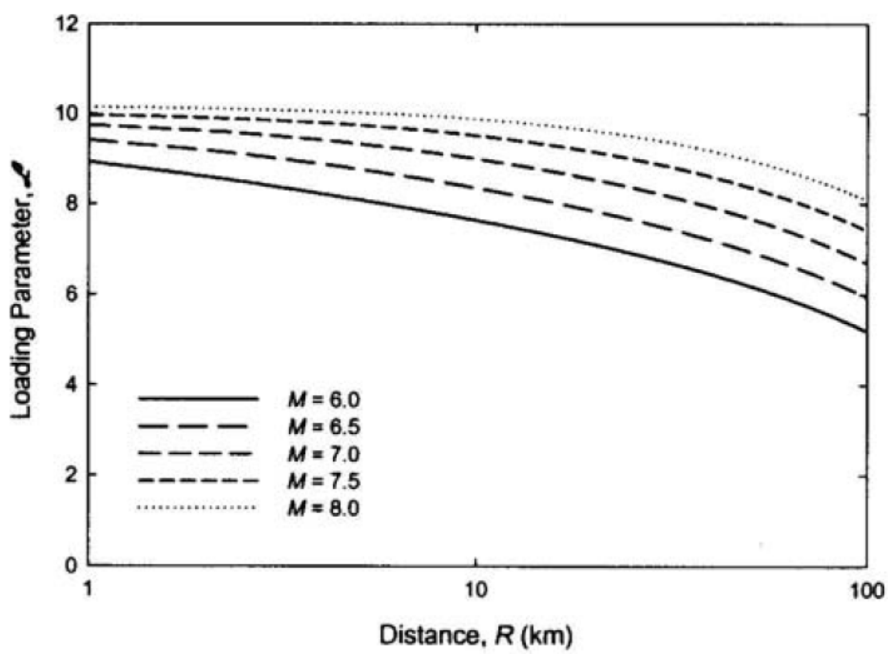

Figure 5-1: $\mathscr{L}$ parameter for the Youd et al. (2002) model

As pointed out by Kramer et al. (2007), the $\mathscr{L}$ parameter for a given empirical lateral spreading resembles an attenuation relationship. As such, it is possible to use the parameter in a PSHA to develop probabilistic estimates of $\mathscr{L}$. Since $\mathscr{L}$ represents the earthquake loading in a given empirical lateral spreading model, it can be designated as the *IM* in a performance-based analysis according to the methodology presented by Kramer et al. (2007) and Franke (2005).

Development of the seismic hazard curve for a given $\mathscr{L}$ parameter requires that a PSHA be performed using seismic hazard analysis software capable of incorporating user-defined attenuation relationships. The analyses performed in this study used the seismic hazard analysis software EZ-FRISK (Risk Engineering, 2010) to develop the seismic hazard curves for the various $\mathscr{L}$ parameters.

Therefore, development of the *IM* for the performance-based kinematic pile response procedure involves developing seismic hazard curves and deaggregation plots for $\mathscr{L}_{Youd}$, $\mathscr{L}_{Bardet}$, and $\mathscr{L}_{Baska}$. It is recommended that at least seven return periods be used to define each seismic hazard curve: 108 years, 225 years, 475 years, 975 years, 2475 years, 4975 years, and 100,000 years.

5.6 Development of Fragility Curves for the *EDP*

Kramer et al. (2007) point out that when re-writing a given empirical lateral spreading model to match the format shown in Equation (5-2), the site term $\mathscr{S}$ is treated as a constant value for each site. Like $\mathscr{L}$, the site parameter $\mathscr{S}$ also varies between empirical lateral spreading models. In addition, the parameter also depends on whether the site is characterized as a free-face geometry or a ground slope geometry. For the three models used in this study, the values of the $\mathscr{S}$ parameter are given as

$$\begin{aligned}\left[\mathscr{S}_{Youd}\right]_{free-face} = & -16.713 + 0.592\log\left(W\right) + 0.54\log\left(T_{15}\right) + \\ & 3.414\log\left(100 - F_{15}\right) - 0.795\log\left(D50_{15} + 0.1\right)\end{aligned} \tag{5-6}$$

$$\begin{aligned}\left[\mathscr{S}_{Youd}\right]_{ground-slope} = & -16.213 + 0.338\log\left(S\right) + 0.54\log\left(T_{15}\right) + \\ & 3.414\log\left(100 - F_{15}\right) - 0.795\log\left(D50_{15} + 0.1\right)\end{aligned} \tag{5-7}$$

$$\left[\mathscr{S}_{Bar\det}\right]_{free-face} = -7.28 + 0.497\log\left(W\right) + 0.558\log\left(T_{15}\right) \tag{5-8}$$

$$\left[\mathscr{S}_{Bar\det}\right]_{ground-slope} = -6.815 + 0.454\log\left(S\right) + 0.558\log\left(T_{15}\right) \tag{5-9}$$

$$\left[\mathscr{S}_{Baska}\right]_{free-face} = -7.518 + 0.086\left(T_{ff}^{*}\right) + 1.007\log\left(W\right) \tag{5-10}$$

$$\left[\mathscr{S}_{Baska}\right]_{ground-slope} = -7.207 + 0.067\left(T_{gs}^{*}\right) + 0.544\sqrt{S} \tag{5-11}$$

for the Youd et al. (2002), Bardet et al. (2002), and Baska (2002) models, respectively. While the validity of assuming a constant value of $\mathscr{S}$ for a given site may be argued, such an assumption greatly simplifies the performance-based computation. In addition, variability in the $\mathscr{S}$ parameter is indirectly accounted for in the uncertainty parameter ε for each model. Like $\mathscr{S}$ and $\mathscr{L}$, the uncertainty parameter ε varies between empirical lateral spreading models and is defined as the estimated standard deviation for each empirical lateral spreading model. Therefore, the values of the uncertainty parameter ε for the three models used in this study are given as

$$\varepsilon_{Youd} = \sigma_{\log D_{H-ff,gs}} \cdot \Phi^{-1}\left[P\right] \approx 0.2020 \cdot \Phi^{-1}\left[P\right] \tag{5-12}$$

$$\varepsilon_{Bar\det} = \sigma_{\log\left(D_{H-ff,gs}+0.01\right)} \cdot \Phi^{-1}\left[P\right] \approx 0.2898 \cdot \Phi^{-1}\left[P\right] \tag{5-13}$$

$$\varepsilon_{Baska} = \sigma_{\overline{\sqrt{D_H}}} \cdot \Phi^{-1}\left[P\right] = 0.28 \cdot \Phi^{-1}\left[P\right] \tag{5-14}$$

for the Youd et al. (2002), Bardet et al. (2002), and Baska (2002) models, respectively. $\Phi^{-1}\left[P\right]$ is defined as the inverse standard cumulative distribution function for a given probability of exceedance P.

Therefore, the final re-written form for each of the three empirical models used in this study following the procedure presented by Kramer et al. (2007) are

$$\log D_{H-ff,gs} = \mathscr{L}_{Youd} + \left[\mathscr{S}_{Youd}\right]_{free-face,ground-slope} + \varepsilon_{Youd} \tag{5-15}$$

$$\log\left(D_{H-ff,gs} + 0.01\right) = \mathscr{L}_{Bar\det} + \left[\mathscr{S}_{Bar\det}\right]_{free-face,ground-slope} + \varepsilon_{Bar\det} \tag{5-16}$$

$$\overline{\sqrt{D_H}} = \frac{\mathscr{L}_{Baska} + \left[\mathscr{S}_{Baska}\right]_{free-face,ground-slope}}{1 + 0.0223\left(\beta_2 / T_{gs}^*\right)^2 + 0.0125\left(\beta_3 / T_{ff}^*\right)^2} + \varepsilon_{Baska} \tag{5-17}$$

for the Youd et al. (2002), Bardet et al. (2002), and Baska (2002) models, respectively. Note that the Baska (2002) model is more complicated than the other two models simply due to the fact that the empirical model incorporates a denominator.

By designating the Displacement term in Equation (5-2) (i.e. $\log\left(D_{H-ff,gs}\right)$, $\log\left(D_{H-ff,gs}+0.01\right)$, or $\overline{\sqrt{D_H}}$) as the Engineering Demand Parameter, fragility curves must be developed for all possible values of the Displacement term as a function of $\mathscr{L}$. This can be performed for each empirical model presented in Equations (5-15) through (5-17) by considering the estimated standard deviation for each model given a set of $\mathscr{L}$ and $\mathscr{S}$. With the empirical models written with the $\mathscr{L}$ and $\mathscr{S}$ format, the Displacement term essentially becomes a linear function of $\mathscr{L}$ with a y-intercept directly proportional or equal to $\mathscr{S}$. For a given level of lateral spreading displacement d, the probability of exceeding that displacement can be computed for various values of $\mathscr{L}$ (i.e. $\mathscr{L}_i$) and assuming a constant value of $\mathscr{S}$. By plotting these probabilities of exceedance against the $\mathscr{L}$ parameter, the fragility curve corresponding to the displacement d is developed. This process is demonstrated graphically with the Baska (2002) model in Figure 5-2. Because this curve only represents the probability of exceeding one given displacement d, multiple curves must developed to represent the fragilities for all possible values of d.

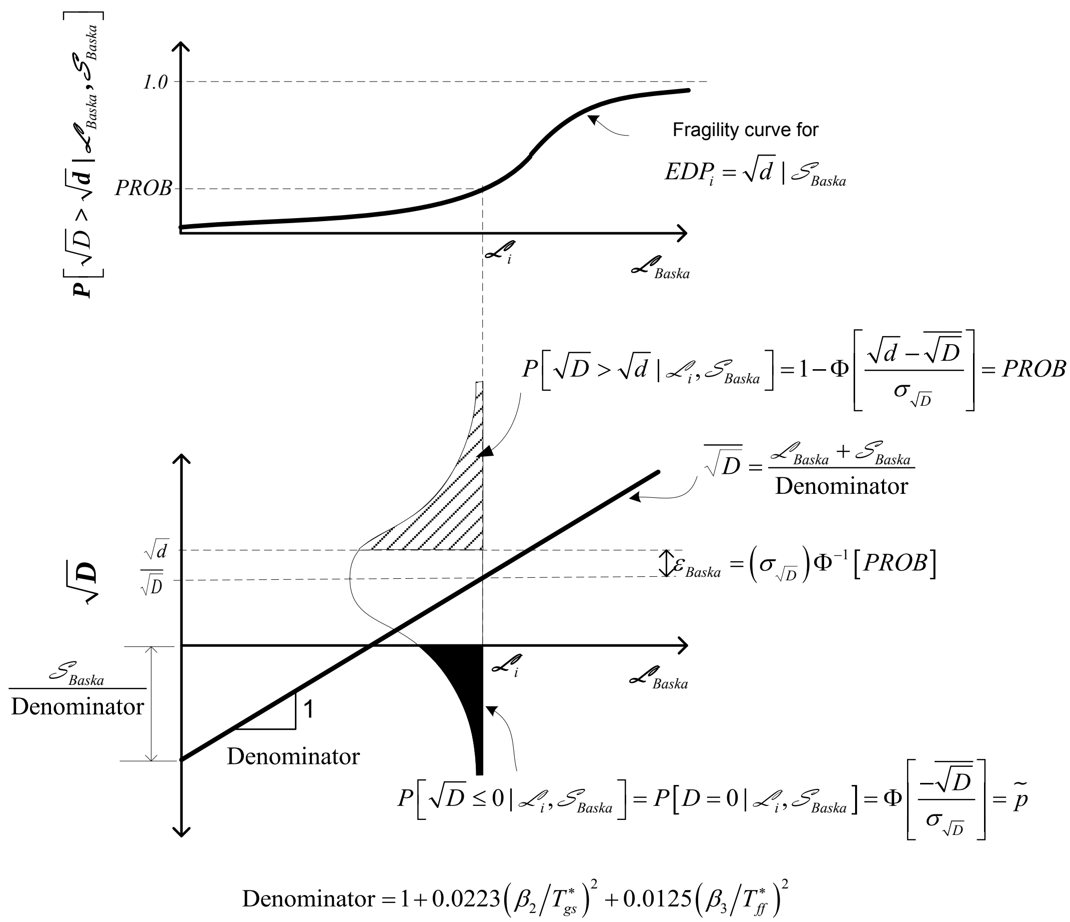

Figure 5-2: Computing the fragility curve for EDP_i = Sqrt(d) for the Baska (2002) empirical model. Modified from Franke (2005).

5.7 Development of the *EDP* for the Performance-based Procedure

The process to develop a seismic hazard curve for lateral spreading displacement at the ground surface is described at length in both Kramer et al. (2007) and Franke (2005) and involves convolving the fragility curves for the Displacement term with the seismic hazard curve for the $\mathscr{L}$. Once the fragility curves for the Displacement term are developed for each empirical lateral spreading model, they can be convolved with each corresponding seismic hazard curve for the loading parameter $\mathscr{L}$ by utilizing the PEER PBEE framework as shown in Equation (4-7) to develop the seismic hazard curve for lateral spreading displacement at the ground surface for each of the empirical models. Therefore, for a given empirical lateral spreading model and assuming that the hazard curve for $\mathscr{L}$, the fragility curve for a given lateral displacement *d*, and the site-specific value of $\mathscr{S}$ have already been developed, then the steps to developing point $\left(\lambda_d, d\right)$ on the seismic hazard curve for lateral spreading displacement at the ground surface can be developed by convolving the fragility curve for $d|\mathscr{S}$ with the hazard curve for $\mathscr{L}$ as in the manner demonstrated in Figure 4-7. Since there are three separate empirical lateral spreading models incorporated in this study, the final seismic hazard curve for lateral spreading displacement at the ground surface will be computed as average of the three individual lateral spreading seismic hazard curves.

Following development of the total estimated lateral spreading displacement at the ground surface, the displacement profile versus depth can be developed by applying the recommendations made by Valsamis et al. (2007) and depth limitation recommendations made by Youd (2009) as summarized in Chapter 2. Liquefaction layering for the Valsamis et al. (2007) procedure can be determined from the results of the performance-based liquefaction triggering analysis following the Kramer and Mayfield (2007) procedure. Therefore, each lateral spreading value on the hazard curve can be coupled with the factor of safety against liquefaction profile corresponding to the same mean annual rate of exceedance in order to develop the lateral displacement profile with depth. In the instance where no liquefaction is computed at a given mean annual rate of liquefaction, soil displacements can be distributed through the layers with the lowest factors of safety.

Thus, the *EDP* does not necessarily represent a single lateral displacement at a given depth. Rather, the *EDP* is actually defined as the collection of all lateral spreading displacements across all depths, or the lateral spreading displacement profile. As such, the lateral spreading displacement hazard curve can be plotted for a given depth in a soil profile, but no single hazard curve represents the entire lateral spreading displacement profile. In order to adequately characterize the engineering demand, lateral spreading displacement profiles should be developed for at least seven return periods: 108 years, 225 years, 475 years, 975 years, 2475 years, 4975 years, and 100,000 years. Lateral spreading displacement profiles corresponding to most other return periods of interest can be log-linearly interpolated from these seven profiles.

5.8 Development of Fragility Curves for the *DM*

With the seismic hazard curves comprising the lateral spreading displacement profiles (i.e. the *EDP*) defined, the seismic hazard curve for the kinematic pile response (i.e. the *DM*) can be developed if a series of fragility curves relating the *EDP* and the *DM* are computed. This study incorporates the simplified p-y soil spring analysis procedure published by Juirnarongrit and Ashford (2006) for computing the average kinematic pile response of a pile group as summarized in Chapter 3. Development of fragility curves using this methodology requires that the uncertainty in the soil-pile interaction be computed in the simplified p-y soil spring analysis. However, no published method for computing uncertainty in kinematic pile response directly from the p-y soil springs could be located for use in this study. Ideally, fragility curves could be computed directly in a probabilistic framework if the incorporated p-y soil spring models provided a formal definition of their model uncertainties. Unfortunately, published p-y soil spring models do not typically provide any indication or definition of their uncertainty. It is therefore currently impossible to directly compute fragility functions for the kinematic pile response using p-y methods. However, it is possible to employ a Monte Carlo simulation approach randomizing the various input parameters utilized by the p-y soil spring models in order to estimate the uncertainty in the soil-pile interaction given a certain level of kinematic loading.

A method often employed by engineers to compute soil-pile response using p-y soil springs is the popular commercial software LPILE (Ensoft, 2004). Unfortunately, LPILE does not directly allow the user to operate in batch mode, thus complicating the process of performing a Monte Carlo simulation. However, development of a separate computer code or macro that manually operates LPILE in an iterative fashion will allow a user to perform Monte Carlo simulations with the software.

Use of a Monte Carlo simulation to estimate uncertainty in kinematic pile response given a certain level of free-field soil movement requires estimation of the uncertainty of the various input parameters used in the computation of p-y soils springs for each soil layer in the model. In the absence of many soil samples from which these input parameters could be directly measured and their uncertainties computed, one could rely on pub lished values of typical ranges of uncertainties for various soil parameters (e.g. Harr, 1984; Kulhawy, 1992; Lacasse and Nadim, 1997; Duncan, 2000). Table 5-1 shows a series of published coefficients of variation for various soil parameters based on the recommendations of Duncan (2000). These coefficients of variation can be used with a normal distribution to estimate the standard deviation of interest given an estimate of the mean.

Table 5-1: Coefficients of variation for commonly-used soil input parameters for many p-y soil spring models (after Duncan, 2000)

Property or in-situ test result	Coefficient of variation, S/x
Unit weight (γ)	3-7%
Buoyant unit weight (γ_b)	0-10%
Effective stress friction angle (ϕ')	2-13%
Undrained shear strength (S_u)	13-40%
SPT blow count (N)	15-45%

Therefore, given the lateral spreading displacement profile corresponding to a given mean annual rate of exceedance or return period, the resulting mean kinematic pile response and its variance can be estimated at each node in the LPILE model by performing a Monte Carlo simulation. Pile response can be defined as pile displacements, shear forces in the pile, bending moments in the pile, and/or curvature of the pile. Figure 5-3 demonstrates a mean pile response and its standard deviation as computed in LPILE with a Monte Carlo simulation.

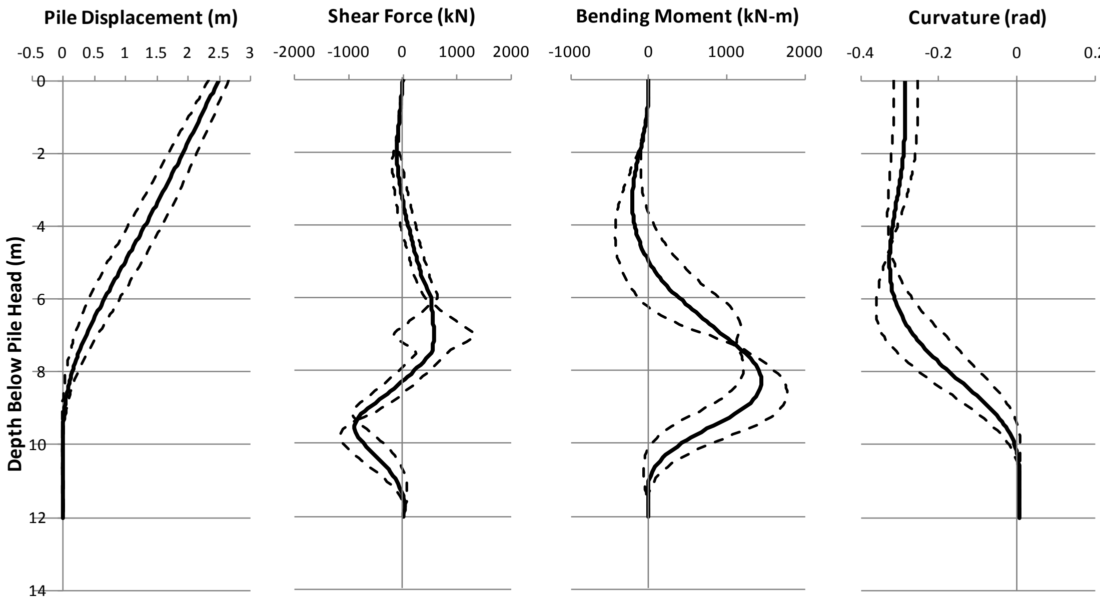

Figure 5-3: Example of mean pile response with +/- 1 standard deviation computed from a Monte Carlo simulation in LPILE

A numerical challenge in dealing with probabilities of exceedance in pile response is that many of the response values may be positive or negative depending on the direction of the displacements, bending moment, and curvature, or the type (i.e. tension or compression) of the shear force. For negative values of pile response, the probability of interest is not that of exceedance, but rather that of non-exceedance. However, computation of probabilities can be greatly simplified if considering only the absolute value of the pile response. In doing so, the directional component of the pile response is lost, but amplitude of the response value is retained.

Since the Monte Carlo simulation utilizing p-y analysis methods provides mean pile response and its estimated standard deviation at each node in the model, fragility curves must be developed for every node in the model in order to characterize the uncertainty in the pile response across the entire pile. Thus, for a given node in the model, the fragility curve as a function of lateral spreading displacement profile EDP can be computed as

$$P\left[DM > \left|DM^*\right| \mid EDP\right] = 1 - \Phi\left(\frac{\left|DM^*\right| - \overline{DM} \mid EDP}{S_{DM|EDP}}\right) \tag{5-18}$$

where DM is the pile response at the node of interest, $\left|DM^*\right|$ is the absolute value of the pile response value corresponding to the fragility curve, EDP is the given lateral spreading displacement profile, $\overline{DM} \mid EDP$ is the mean computed pile response at the node of interest from the Monte Carlo simulation given the lateral spreading displacement profile, $S_{DM|EDP}$ is the computed standard deviation of the pile response at the node of interest from the Monte Carlo simulation, and Φ is the standard cumulative density function. Equation (5-18) is specific only to the pile response value $\left|DM^*\right|$, and a family of fragility curves for all possible values of $\left|DM^*\right|$ must be developed in order adequately characterize the uncertainty in the performance-based pile response analysis. Finally, development of families of fragility curves must be repeated for all nodes in the p-y pile response model.

Because performing a Monte Carlo simulation with a p-y soil spring analysis in LPILE can require a significant effort, Monte Carlo simulations need only be performed with the seven lateral spreading displacement profiles developed to define the *EDP* (i.e. at return periods of 108, 225, 475, 975, 2475, 4975, and 100,000 years). With mean pile responses and standard deviations computed at each of these seven return periods, the probability of exceeding $\left|DM^*\right|$ given an *EDP* corresponding to a different return period can be computed by interpolating mean pile response values and standard deviations for use in Equation (5-18).

5.9 Development of the *DM* for the Performance-based Procedure

With fragility curves developed for the pile response and a series of lateral spreading displacement profiles defined across multiple return periods (i.e. the *EDP*), performance-based estimates of the pile response can now be computed using the probabilistic framework developed by PEER. The base equation for this computation is similar to Equation (4-7) and is given as

$$\lambda_{\left|DM^*\right|} = \int P\left[DM > \left|DM^*\right| \mid EDP\right]\left(d\lambda_{EDP}\right) \tag{5-19}$$

Equation (5-19) must be performed for all possible values of $\left|DM^*\right|$ at all nodes in the pile response model in order to develop the pile response hazard curve at each node along the pile. With these hazard curves, it is possible to develop the pile response profile for a return period of interest by identifying and plotting the pile response value on each hazard curve corresponding to that return period. This idea is demonstrated visually in Figure 5-4, which shows a seismic hazard curve for lateral pile displacements at the pile head. The bubbles shown in Figure 5-4 are intended to represent the idea that similar hazard curves exist at other depths along the pile, and that those curves can be used to develop pile response profile plots corresponding to a given mean annual rate of exceedance or return period.

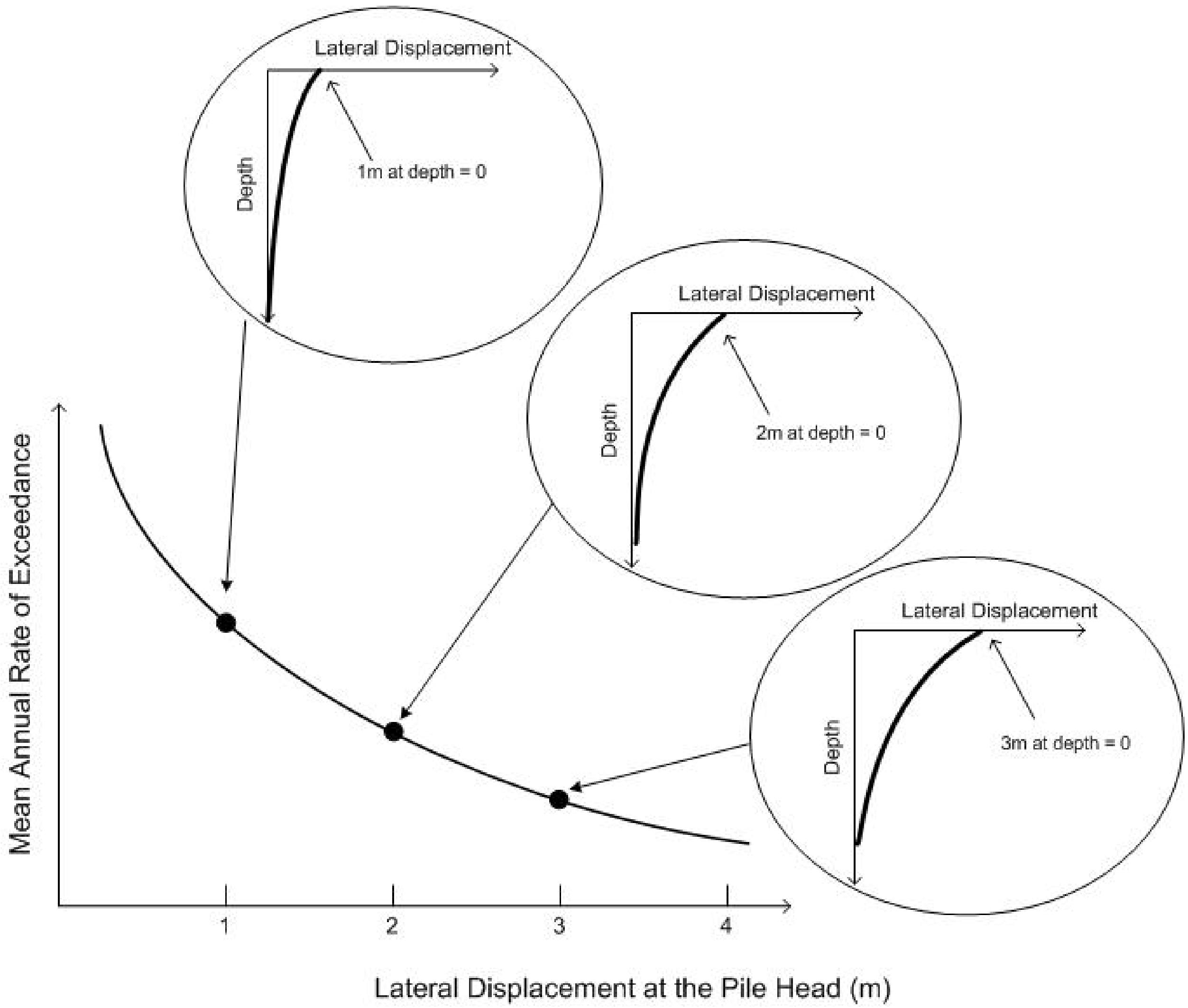

Figure 5-4: Example of seismic hazard curve for pile displacement at the pile head

6 Development and Analysis of Costa Rica Case Histories

6.1 1991 Limon Earthquake

At 15:57pm local time on April 22, 1991, a large (magnitude 7.5) earthquake struck the Limon Province of Costa Rica near the Caribbean Sea. The earthquake killed 53 people, injured another 193 people, and disrupted an estimated 30-percent of the highway pavement and railways in the region due to fissures, scarps, and soil settlements resulting from liquefaction. (EERI, 1991). While the Limon Province is dominated by a broad plain that gently slopes from the Cordillera de Talamanaca to the Caribbean Sea and is dissected by several large and small river valleys that generally broaden as they approach the coast, most of the observed liquefaction appeared to occur in the alluvial and fluvial deposits underlying river floodplains or in deltaic, lagoonal or estuarine deposits that underlie the coastal lowlands. (EERI, 1991; Youd, 1993).

Santana (1992) reported a maximum Modified Mercalli Intensity (MMI) equal to IX in Matina, which is just north of Highway 32 near the Caribbean Sea. Accelerograms were recovered from 14 of the 19 permanent stations deployed by the Earthquake Engineering Laboratory of the University of Costa Rica (Santana, 1991). The closest strong-motion station was located in San Isidro approximately 73 km southwest of the epicenter and located on hard ground. The San Isidro station registered a maximum acceleration of 0.20g horizontal and 0.17g vertical (Santana et al., 1991). The maximum free-field acceleration was recorded in Cartago, which is located on soft ground approximately 94 km to the northwest of the epicenter. The recorded peak horizontal ground acceleration at Cartago was approximately 0.27g. The recorded ground motions indicate that strong shaking (>0.05g) occurred for approximately 26.2 seconds. The USGS records the approximate latitudinal and longitudinal coordinates of the epicenter as 9.67° North 83.07° West, and a focal depth of approximately 12.9 kilometers. A shakemap produced by the USGS (2008) is shown in Figure 6-1.

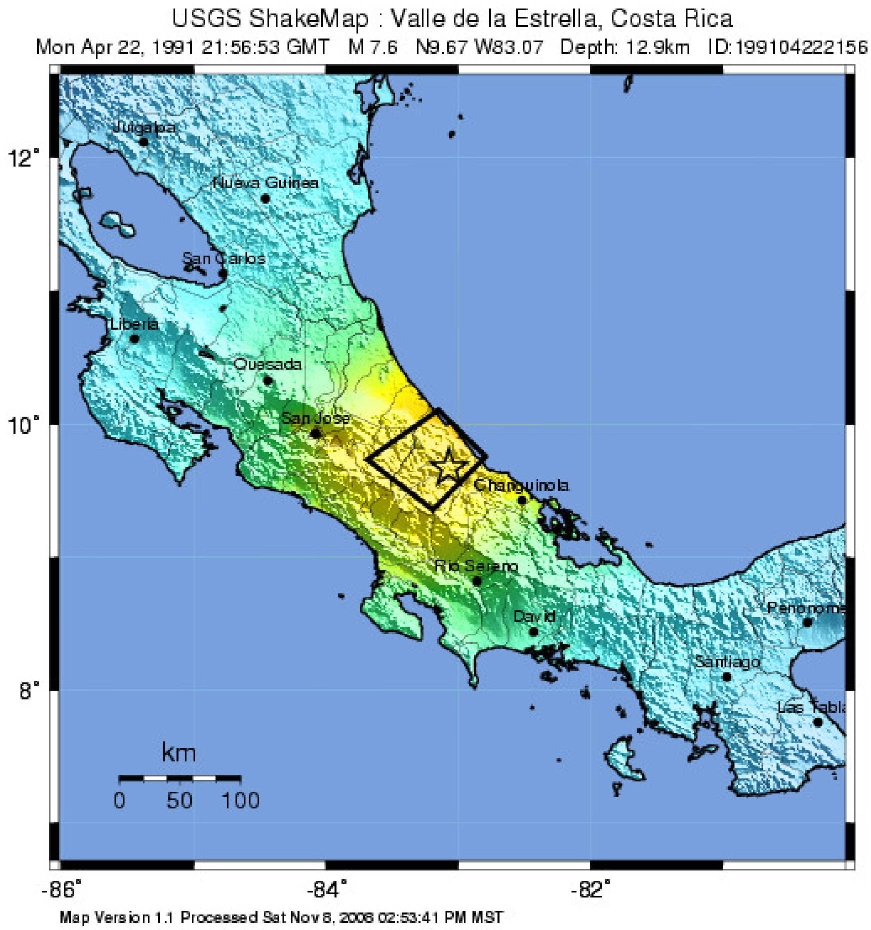

PERCEIVED SHAKING	Not felt	Weak	Light	Moderate	Strong	Very strong	Severe	Violent	Extreme
POTENTIAL DAMAGE	none	none	none	Very light	Light	Moderate	Moderate/Heavy	Heavy	Very Heavy
PEAK ACC.(%g)	<.17	.17-1.4	1.4-3.9	3.9-9.2	9.2-18	18-34	34-65	65-124	>124
PEAK VEL.(cm/s)	<0.1	0.1-1.1	1.1-3.4	3.4-8.1	8.1-16	16-31	31-60	60-116	>116
INSTRUMENTAL INTENSITY	I	II-III	IV	V	VI	VII	VIII	IX	X+

Figure 6-1: Shakemap for the April 22, 1991 Costa Rica earthquake (after USGS, 2008)

A total of nine bridges in the epicentral region were severely damaged or collapsed as a result of the April 22, 1991 earthquake (Santana, 1992). Minor damage was reported for most other bridges in the region. The damage to these bridges occurred due to both inertial loading effects during the ground shaking and kinematic loading effects on the foundations due to liquefaction-induced ground displacements. This study identified five of these bridges that sustained damage ranging from severe to minor, and that post-earthquake reconnaissance efforts could identify and measure elements of the seismic bridge performance. The location of these bridges relative to the approximate epicenter of the April 22, 1991 earthquake is shown in Figure 6-2.

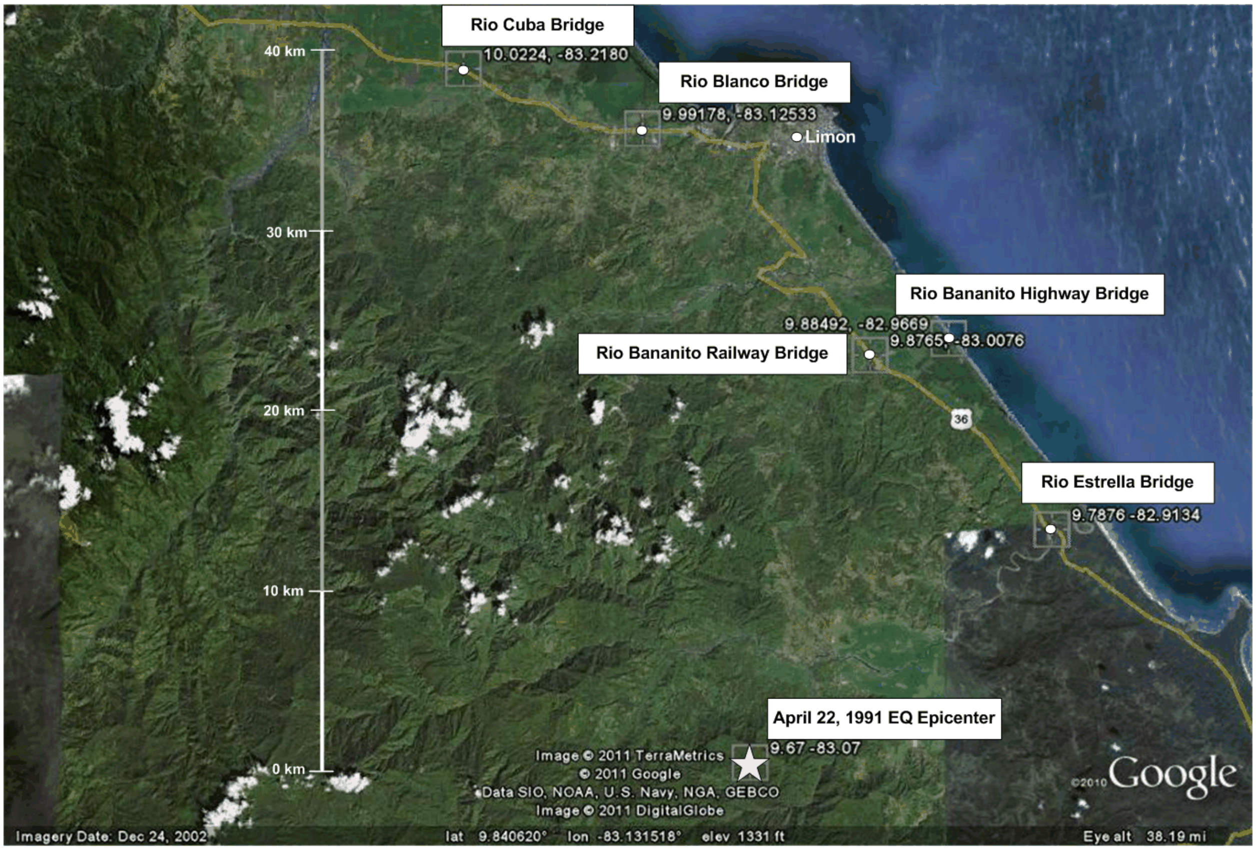

Figure 6-2: Bridge location map (image courtesy of Google Earth ™ 2011)

6.2 Site Investigation

Our site investigation for this study consisted of a preliminary site-reconnaissance and a subsurface investigation performed at the five identified bridge locations. The preliminary site-reconnaissance was performed in April 2009 with the intent of (1) identifying bridges that were capable of being analyzed for kinematic pile response nearly 20 years after the earthquake event, (2) establishing ties with and support from key research institutions and governmental agencies within Costa Rica, and (3) identifying a reputable engineering subconsultant who could perform the geotechnical investigation. All of these objectives were successfully achieved during the preliminary site-reconnaissance. Five bridges were identified where sufficient bridge performance information and/or free-field soil deformations were either collected during the reconnaissance efforts immediately following the 1991 earthquake event or was still visible during our reconnaissance. Critical support was established from the Costa Rica Ministerio de Transporte, which provided original blueprints and some soil boring information for the five identified bridges. In addition, contacts were established with various engineering researchers at the Universidad de Costa Rica. Finally, a reputable engineering subconsultant was identified to perform soil borings at the five identified bridges.

Our subsurface investigation was performed during April 2010 by Insuma S.A. Geotechnical Consultants. A total of seven borings ranging in depth from 14 meters to 20 meters were performed at the five identified bridges using a tripod-mounted Standard Penetration Test

(SPT) performed in accordance with ASTM D-1586. Representative soil samples were obtaining during SPT tests using a standard split-spoon sampler. Diagrams of the SPT procedure and the hammer/sampling equipment used are shown in Figure 6-3 and Figure 6-4, respectively.

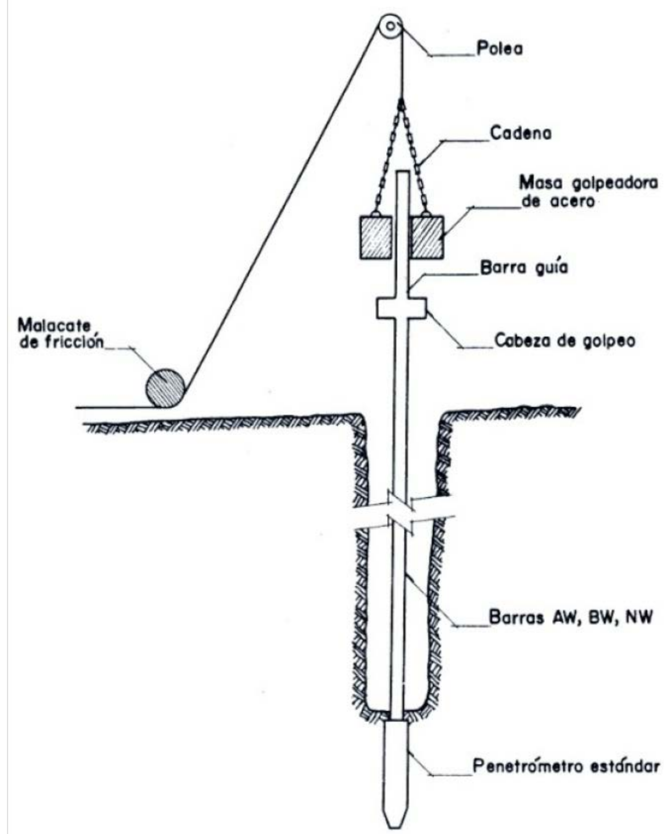

Figure 6-3: Sketch of the standard penetration method (ASTM D-1586)

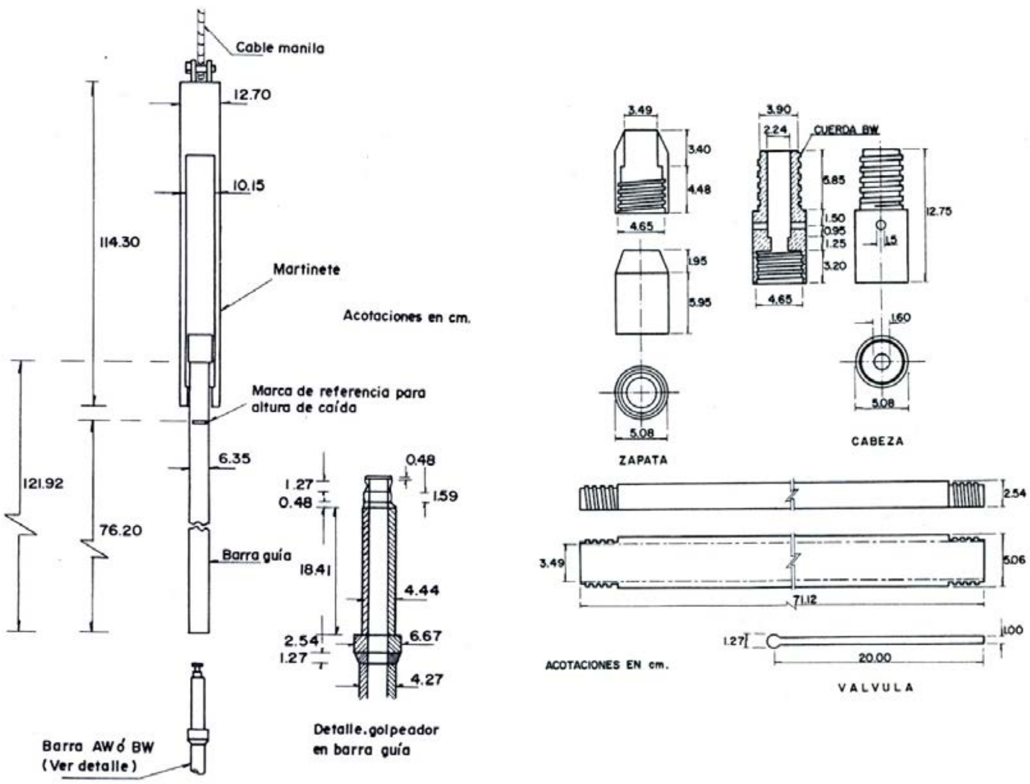

Figure 6-4: Details for the 64 kg (140 lb) hammer and split-spoon sampler used in the field investigation

To correct the recorded SPT blowcounts from the field for hammer energy efficiency, the efficiency of the cathead/falling-weight hammer was measured using electronic equipment provided by the Utah Department of Transportation. Hammer efficiency was measured multiple times, and an average efficiency ratio of approximately 87-percent was computed. This value is within the range of reasonable efficiency ratio values reported by Kovacs et al. (1983) for cathead and rope SPT systems.

Continuous SPT sampling was employed in all seven of the borings that were performed. Retrieved soil samples were returned to the Insuma laboratories for additional evaluation and testing. Laboratory tests performed in this study included particle size analysis, fines measurement using a -200 sieve wash, measurement of natural moisture content, and plasticity evaluation on fine-grained samples using the Atterberg limits. These tests were not performed on every retrieved soil sample, but were performed at a frequency of one set of tests every 1.5 – 1.75 meters and/or whenever a different type of soil was detected. The boring logs and laboratory test results are found in the Geotechnical Study report prepared by Insuma S.A. Geotechnical Consultants dated July, 2010, which is included as Appendix A of this report.

6.3 Rio Cuba Bridge

The bridge over the Rio Cuba is a three-span reinforced concrete bridge supporting two lanes of traffic. Each span is approximately 22 meters in length and composed of simply-supported reinforced concrete girders, and the total span of the bridge is nearly 69 meters. The bridge is located along National Route 32 just south of the town of Maravilla. The latitude/longitude coordinates of the bridge are approximately 10.02237° North 83.217967° West.

According to bridge plans provided by the Costa Rican Ministry of Transportation, the bridge is founded on a series of 14-inch square reinforced concrete piles. The abutments are supported by two rows of piles (8 piles in the front row, 7 piles in the second row, and 15 piles in total) that are approximately 14 meters in length and spaced at 4.1 diameters in the transverse direction and 2.5 diameters in the longitudinal direction. The approximate dimensions of the pile cap at each abutment is 10.36 meters (transverse) x 1.90 meters (longitudinal) x 2.50 meters (vertical). The two bents are each founded on two 3.60-meter x 4.50 meter pile caps. Each of these pile caps is supported by 20 piles 14-inch x 14-inch (five rows of four piles) that are 10 meters in length and spaced at 2.5 diameters in both the transverse and longitudinal directions. The abutments and the bents are skewed at an angle of 30 degrees to the transverse orientation of the bridge. Finally, the front row of piles at each abutment and bent location are battered at approximately 5V:1H. However, any batter in the piles was neglected in the pile response analysis because the Juirnarongrit and Ashford (2006) pile response procedure does not specify how to account for pile batter in a few of the piles in the group.

6.3.1 Surface Conditions and Bridge Geometry

The Rio Cuba is a relatively small river bounded on both sides by a gently sloping floodplain and extensive vegetation. According to elevations shown on the blueprints that were provided by the Costa Rican Ministry of Transporation, the river itself ranges in elevation from about 6.80 meters at the bottom of the river channel to approximately 10.8 meters at the river bank near the bridge abutments. Results from our own survey of the site using Global Positioning System (GPS) equipment provided by the Utah Department of Transportation indicate that the current elevation of the river bank at the bridge is approximately 10.25 meters. According to the bridge blueprints, the roadway elevation across the bridge varied from 14.87 meters at the west abutment to 14.71 meters at the east abutment. From the blueprints, it also appears that the approach embankment was originally constructed at a 2H:1V slope. The elevation of the water in the Rio Cuba was approximately 8.1 meters at the time of our investigation.

Because the bridge is surrounded by banana plantations, it is possible that significant modification to the ground surface has been performed throughout the years. While we may assume that the site geometry at the time of the 1991 earthquake was the same as was measured during our site survey, it is impossible for us to know with certainty. However, there appears to be relatively good agreement between the elevations shown on the blueprints and the elevations that we measured during our own site survey. Therefore, we have relied on the results from our own site survey to develop the generalized site geometry used in our analysis, relying on the elevations shown in the blueprints to fill in the gaps as necessary where important topographic information may not have been measured during our survey.

A sketch of the plan and profile views of the Rio Cuba Bridge as they are shown on the plans provided by the Costa Rican Ministry of Transportation are presented in Figure 6-5.

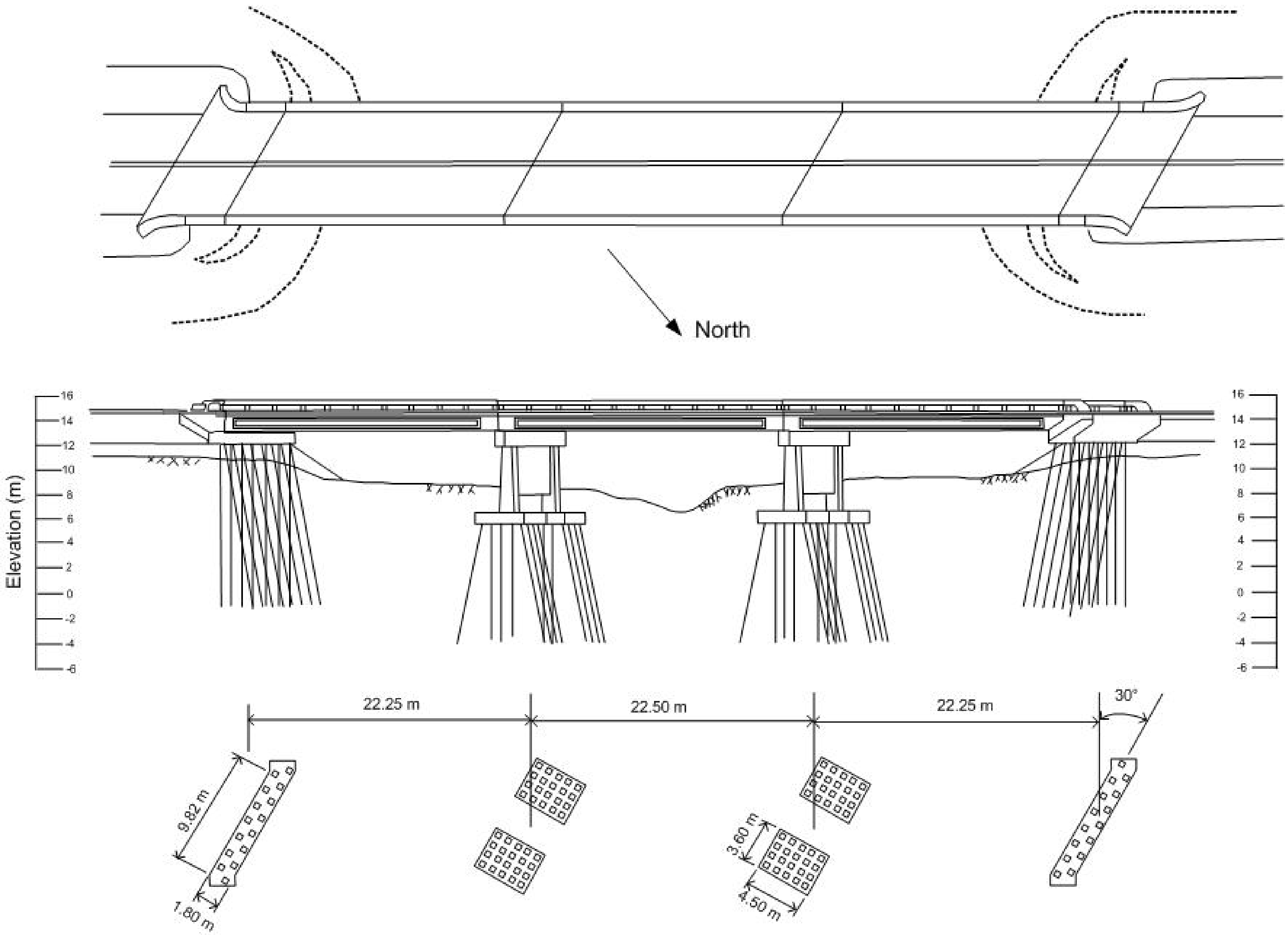

Figure 6-5: Simplified sketch of the plan and profile views of the Rio Cuba Bridge as shown on the bridge plans provided by the Costa Rican Ministry of Transportation

6.3.2 Subsurface Conditions

Insuma S.A. Geotechnical Consultants performed a single boring immediately adjacent to the embankment fill at the eastern abutment of the bridge. The boring extended to a depth of approximately 15 meters. The soils encountered in the boring were reported to consist primarily of alluvial deposits alternating between clays, silts, and sands. The clays encountered appeared to have high plasticity while the silts encountered appeared to have either low or no plasticity. The sands encountered appeared to be fine-grained and varied in fines content from clean to silty. Groundwater was encountered in the boring at an approximate depth of 2.1 meters, which corresponds to an approximate elevation of 8.1 meters. To be conservative and to account for the fact that ground water levels can fluctuate, groundwater was modeled at a depth of 1.80 meters (EL 7.80 meters) in the liquefaction and lateral spreading analysis. A simple diagram of the soils encountered in the boring performed is shown in Figure 6-6 below. Further details regarding the boring at the Rio Cuba Bridge and the corresponding laboratory test results can be found in the Insuma Geotechnical Report included as Appendix A of this report.

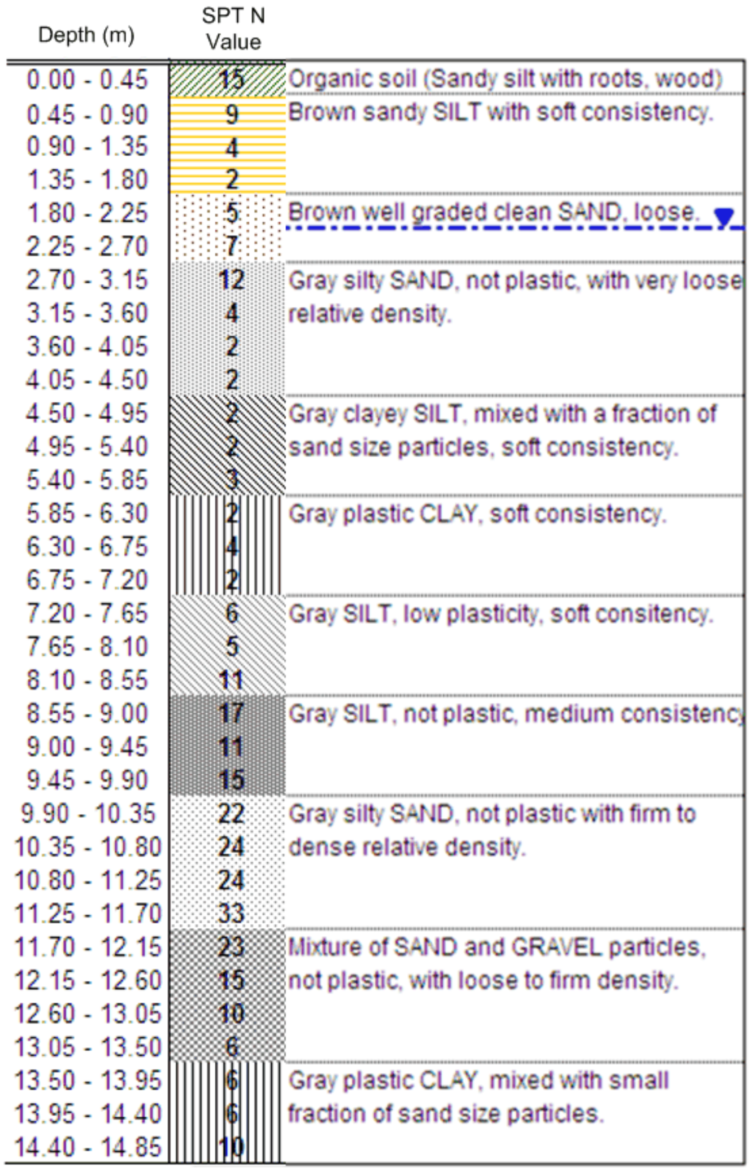

Figure 6-6: Boring P-1 performed at the Rio Cuba Bridge

The information from boring P-1 was used to develop a generalized soil profile for the east abutment of the Rio Cuba Bridge. Empirical correlations with SPT blowcounts were averaged to estimate the friction angle of granular soils and non-plastic silts. These correlations include Peck et al. (1974), Hatanaka and Uchida (1996), and Bowles (1977). Relative density of granular soils was estimated using the empirical correlation presented by Kulhawy and Mayne (1990). Corrected soil modulus estimates K^* of the granular soils for use with the API (1993) p-y relationship were estimated using the recommendations presented by Boulanger et al. (2003). Undrained strength of cohesive plastic soils was averaged from empirical correlations including Hara et al. (1971), Kulhawy and Mayne (1990), and Skempton (1957). Assumptions regarding the unit weight of the native soil as well as the strength properties of the embankment fill were made. Groundwater is modeled at an elevation of 7.8 meters (i.e. a depth of 6.3 meters from the top of the embankment fill). Table 6-1 summarizes our generalized model of the soil profile at the east abutment of the Rio Cuba Bridge.

Table 6-1: Generalized soil profile for the east abutment at the Rio Cuba Bridge

Top Depth (m)	Top Elevation (m)	Thickness (m)	USCS Soil Class	Friction Angle (deg)	Moist Unit Weight (kN/m3)	Undrained Strength (kPa)	Relative Density (%)	Corrected Soil Modulus (kN/m3)	Liquefied p-multiplier
0	14.7	4.5	SM (Fill)	35	18.5	---	62	24,800	NA
4.5	10.2	1.84	ML	---	17.3	25.0	---	---	NA
6.34	8.36	0.92	SW	33	18.1	---	48	11,000	0.14
7.26	7.44	1.84	SM	32	18.1	---	39	7,100	0.09
9.1	5.6	1.38	ML	---	18.1	16.8	---	---	NA
10.48	4.22	1.38	CH	---	18.8	22.1	---	---	NA
11.86	2.84	1.38	ML	---	18.8	38.8	---	---	NA
13.24	1.46	1.38	ML	36	18.1	---	59	15,130	NA
14.62	0.08	1.84	SM	39	18.1	---	77	24,050	NA
16.46	-1.76	1.84	GP	34	18.1	---	53	11,100	0.17
18.3	-3.6	1.38	CH	38	18.8	45.3	---	---	NA

6.3.3 Ground Motions and Liquefaction

The Rio Cuba Bridge is located approximately 41 kilometers northwest from the epicenter of the April 22, 1991 e arthquake. Assuming an average V_{s30} value of 270 m/s, the average computed median spectral acceleration along with median $\pm 1\sigma$ from the four selected NGA models are shown in Figure 6-7. The median computed PGA and spectral accelerations corresponding to 0.2-second and 1.0-second are approximately 0.150g, 0.313g, and 0.204g.

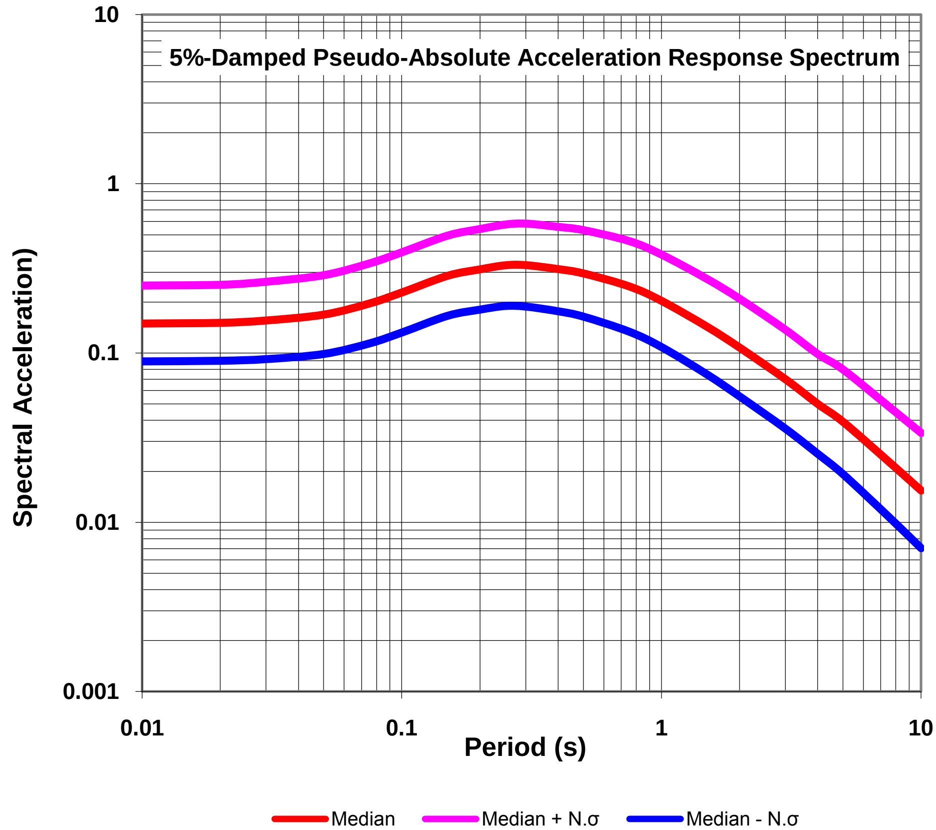

Figure 6-7: Computed deterministic response spectra for the Rio Cuba Bridge from the 1991 earthquake. N = 1

Using the average deterministic ground motions from the NGA equations, the deterministic liquefaction triggering was evaluated at the Rio Cuba Bridge for the M7.6 1991 Limon earthquake using the SPT blowcounts from Boring P-1. The results of the deterministic liquefaction triggering analysis are shown in Figure 6-8. This evaluation included consideration of the Cetin et al. (2004), Idriss and Boulanger (2008), and Youd et al. (2001) simplified procedures. In general, good agreement was observed between the three procedures, suggesting that liquefaction triggered from depths of 3.2 meters to 4.6 meters (EL 7.0m to EL 5.6m) and from depths of 12.5 meters to 13.8 meters (EL -2.3m to EL -3.6m).

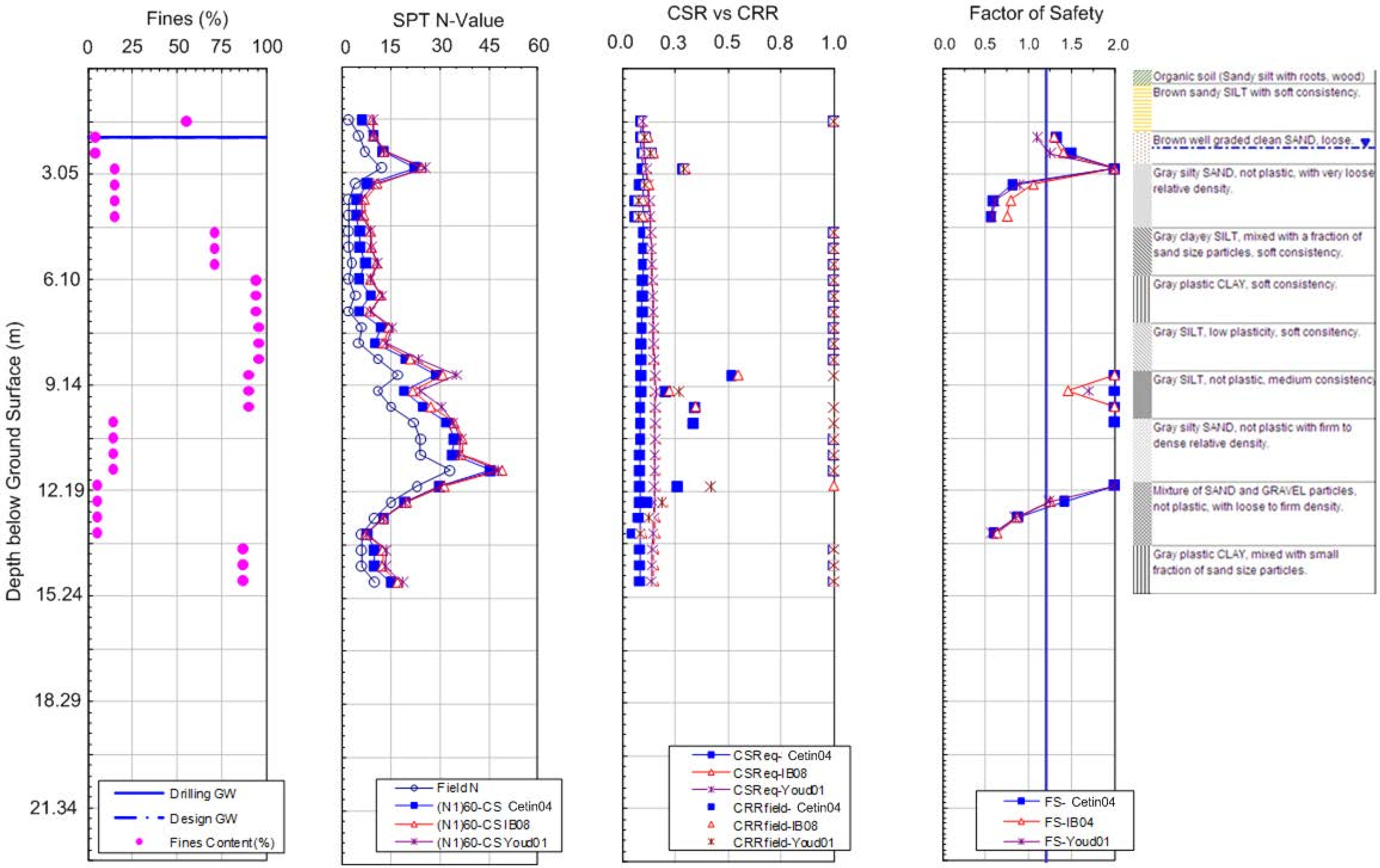

Figure 6-8: Deterministic liquefaction triggering results for the M7.6 1991 Limon earthquake at the Rio Cuba Bridge

The results of our PSHA using EZ-FRISK software suggest that the seismicity at the bridge is moderate to high. The seismic hazard curve for the PGA is shown below in Figure 6-9.

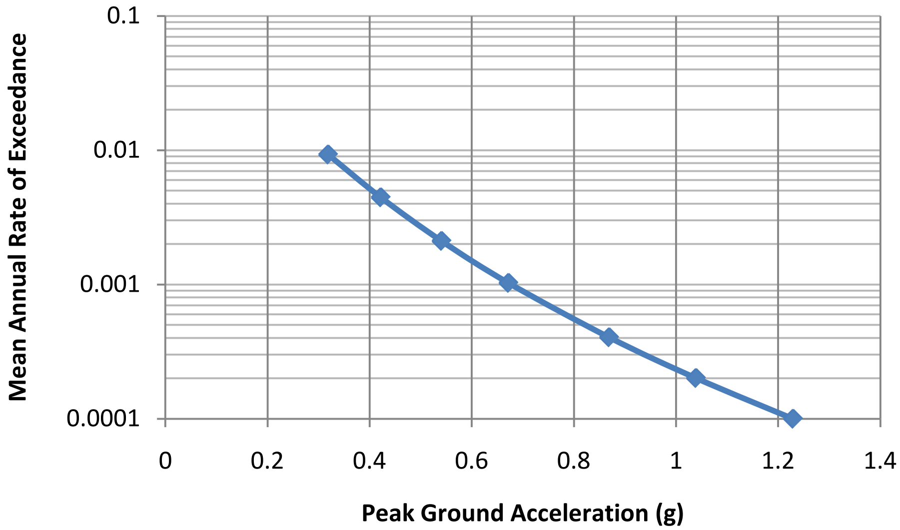

Figure 6-9: Computed seismic hazard curve for the PGA at the Rio Cuba Bridge

The magnitude/distance deaggregations for the PGA are shown in Figure 6-10. These deaggregations are used in conjunction with the seismic hazard curve for the PGA shown in Figure 6-9 to perform the performance-based liquefaction triggering analysis according to the Kramer and Mayfield (2007) procedure. The performance-based factors of safety against liquefaction for various return periods are shown in Figure 6-11. These factors of safety were computed using the SPT blowcount information from Insuma boring P-1 at the Rio Cuba Bridge. A factor of safety less than or equal to 1.2 was assumed to be liquefiable for this study. Note that for fine-grained soil layers not considered susceptible to liquefaction due to plasticity, a generic factor of safety against liquefaction equal to 2.0 w as assigned regardless of return period. A maximum factor of safety equal to 4.0 w as assigned to layers with very high resistance to liquefaction triggering. Figure 6-11 shows that for most return periods, liquefaction triggers from depths of about 3.22 meters to 4.60 meters (EL. 6.98m to 5.60m) and from depths of about 12.88 meters to 13.80 meters (EL. -2.68m to -3.6m) below the native ground surface.

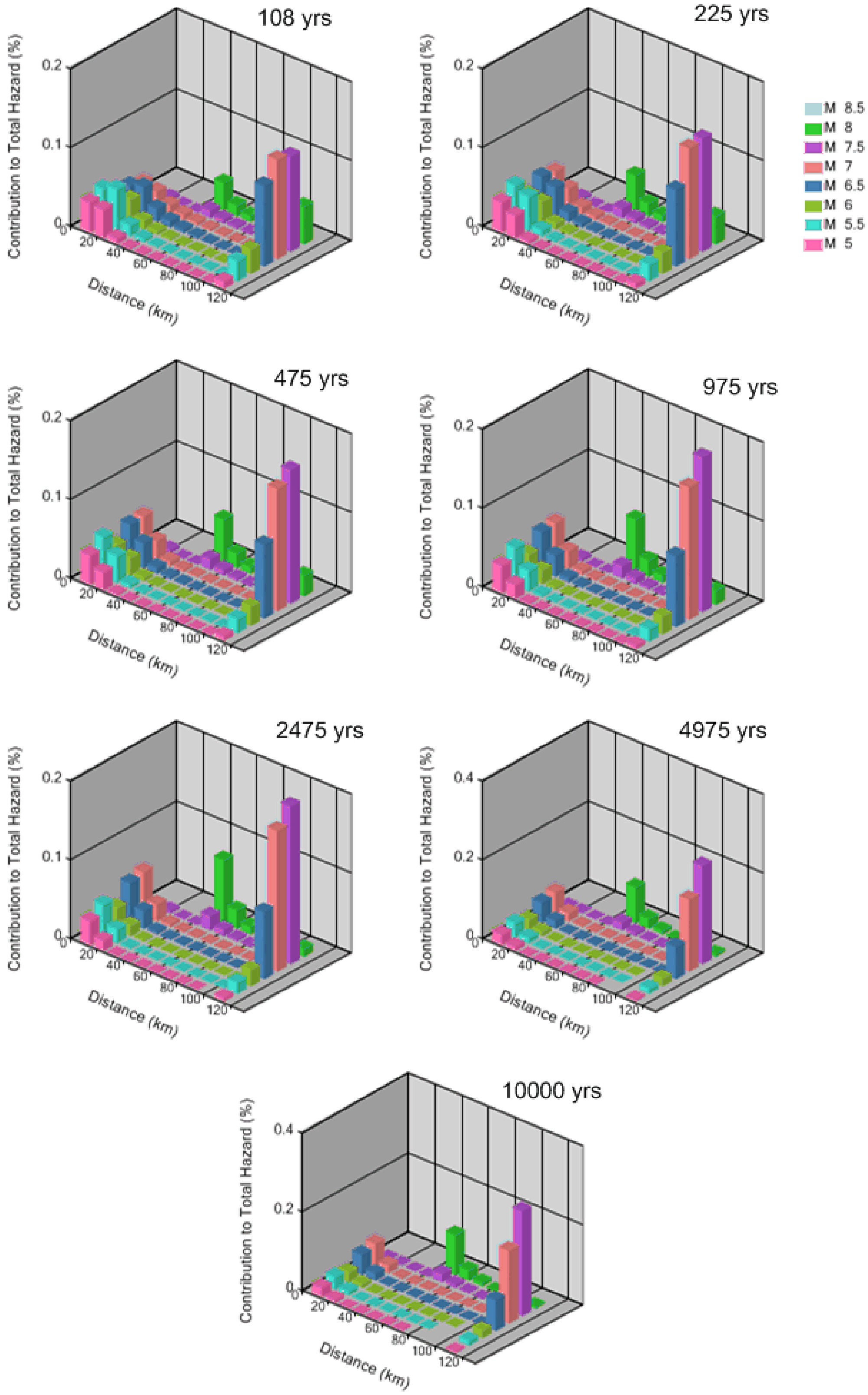

Figure 6-10: Magnitude/distance deaggregations for the PGA at the Rio Cuba Bridge

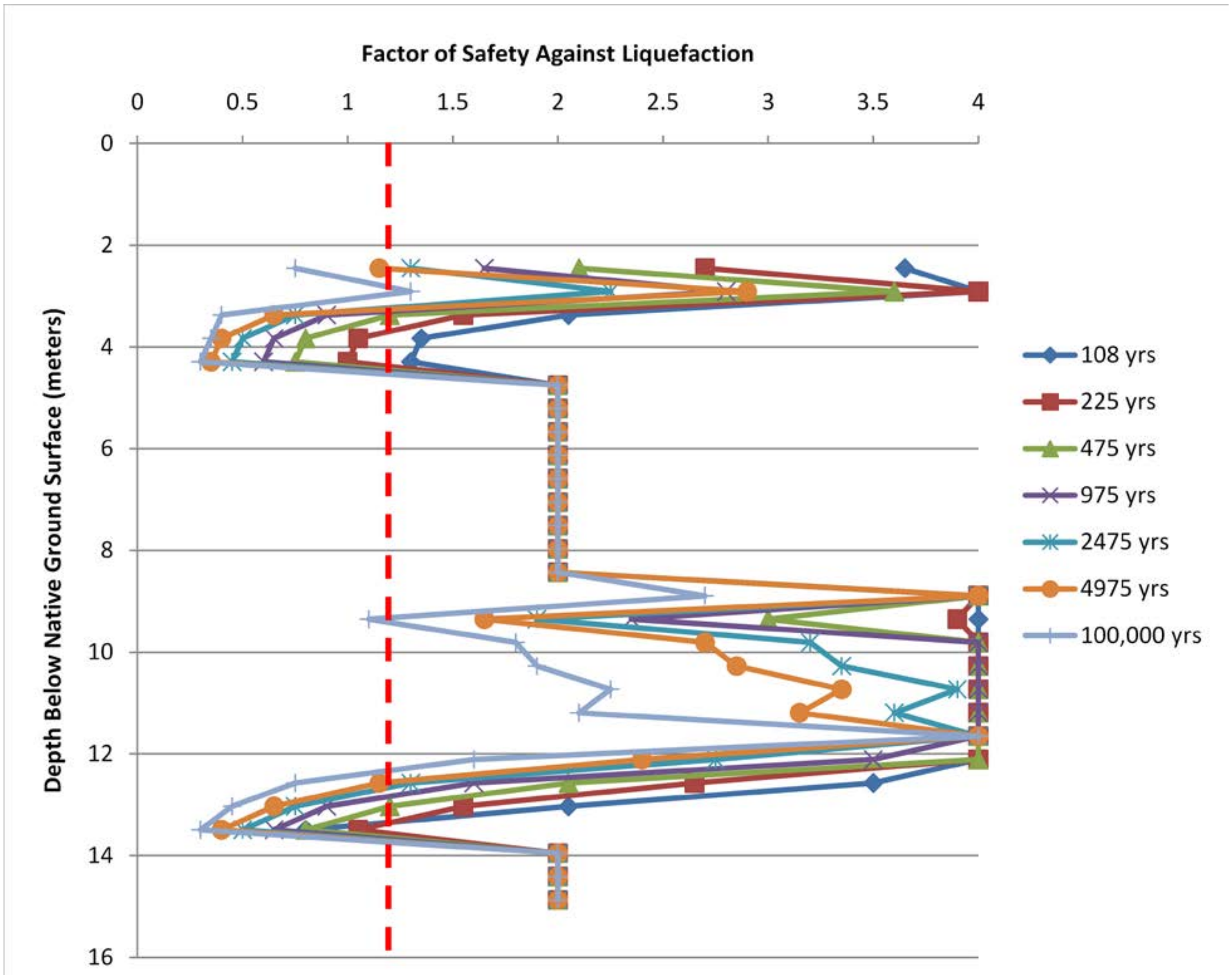

Figure 6-11: Performance-based liquefaction triggering results for the Rio Cuba Bridge

6.3.4 Lateral Spreading

Observed evidence of lateral spreading at the Rio Cuba Bridge following the 1991 earthquake is quite minimal. No tension cracks or sand boils were reported at the bridge in any of the reconnaissance reports published immediately following the earthquake. However, damage to the bridge structure itself was observed and recorded both in the original reconnaissance reports and our own reconnaissance in 2009. While little to no lateral displacement was observed at the pavement elevation, a rotation of the pile cap/abutment of up to approximately 8.5 degrees was observed at the west abutment. Slight cracking and spalling of the front row of piles was observed, and the rebar in the piles is slightly exposed as a result. The rotation of the pile cap suggests that free-field soil and/or slope displacements occurred, but the bridge deck behaved as a reinforcing strut and prevented any significant lateral deformation of the abutment to occur.

Empirical evaluation of the free-field soil displacements due to lateral spreading was performed using the Youd et al. (2002), Bardet et al. (2002), and Baska (2002) models. Our analysis assumed an earthquake magnitude of 7.6, a source-to-site distance of 41 kilometers, a free-face ratio of 12-percent, and a free-face height of 1.8 meters. The mean grain size diameter for each soil sublayer in the analysis was estimated from the Insuma sieve results. The median computed lateral spreading displacement value and the 95th-percentile confidence interval for each of the three empirical models is shown in Figure 6-12. The average computed median displacement from the three models is approximately 0.27 meter.

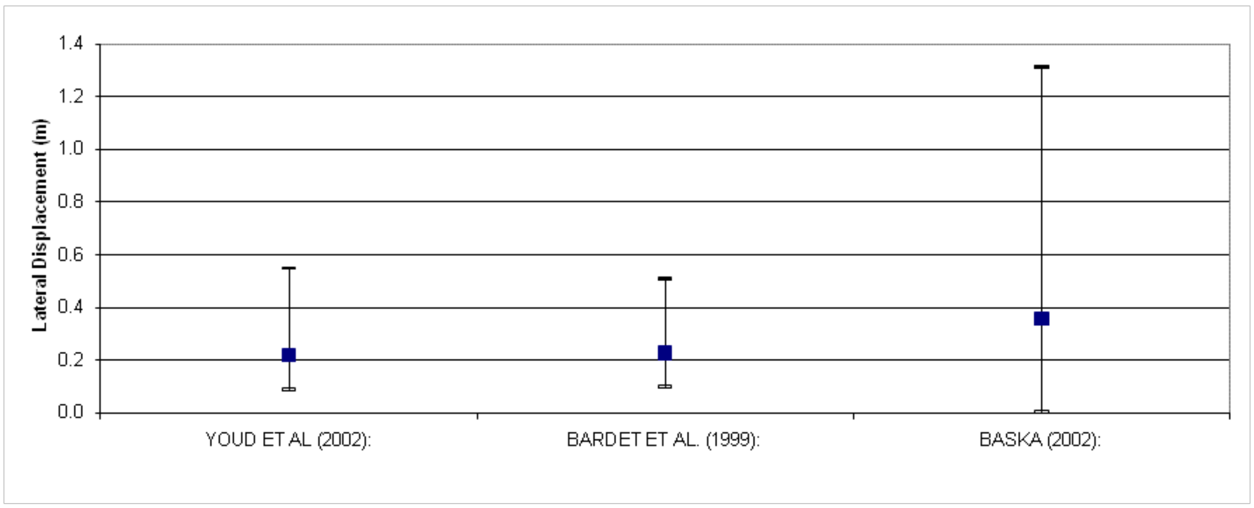

Figure 6-12: Deterministic median and 95-percentile evaluations of lateral spreading displacement using select empirical models for the Rio Cuba Bridge

The estimated lateral spreading displacement profile for the M7.6 1991 Limon earthquake was computed according to the procedure presented in Sections 2.7 and 2.8 of this report. This displacement profile is shown in Figure 6-13.

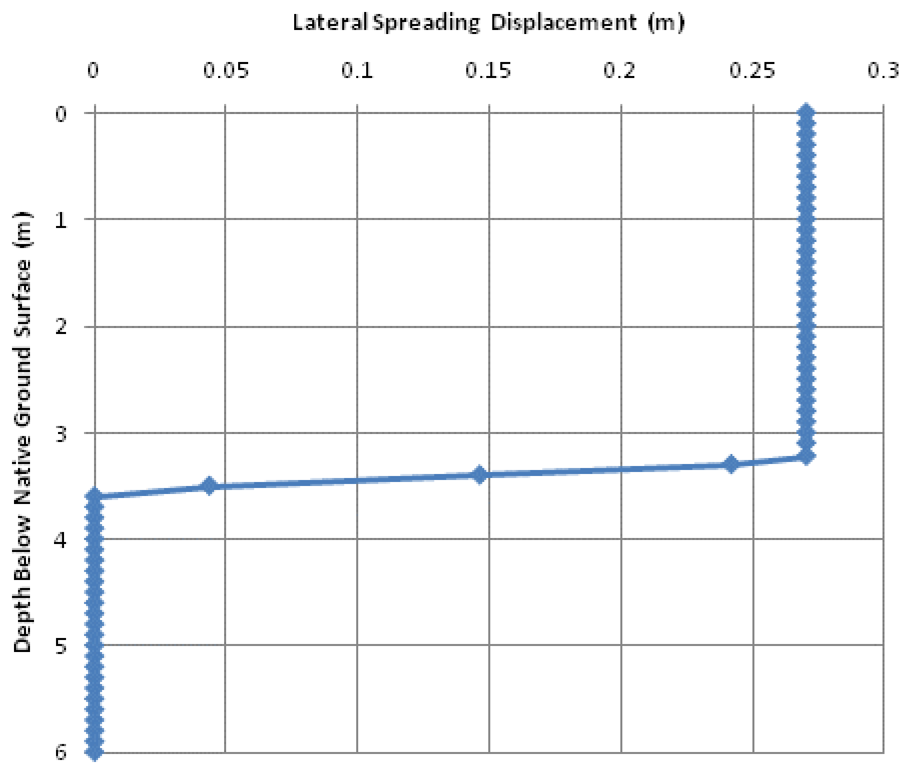

Figure 6-13: Computed lateral spreading displacement profile at the Rio Cuba Bridge for the M7.6 1991 Limon earthquake

In the performance-based framework, values of $\mathscr{L}$ and $\mathscr{S}$ were computed at the Rio Cuba Bridge for each of the three empirical models. These values are shown in Table 6-2.

Table 6-2: $\mathscr{L}$ and $\mathscr{S}$ parameters for the performance-based lateral spreading analysis at the Rio Cuba Bridge

	$\mathscr{L}$ parameter							$\mathscr{S}$ parameter
	108yrs	225yrs	475yrs	975yrs	2475yrs	4975yrs	100000yrs	
Youd et al. (2002)	8.421	8.948	9.327	9.566	9.774	9.854	9.936	-9.367
Bardet et al. (2002)	6.018	6.483	6.854	7.119	7.363	7.467	7.700	-6.933
Baska (2002)	6.725	7.154	7.455	7.652	7.817	7.893	7.950	-6.351

Using the values of $\mathscr{L}$ and $\mathscr{S}$ with the performance-based procedure for computing the lateral spreading displacement as described in Sections 5.6 and 5.7, performance-based estimates of lateral spreading deformation are computed and shown in Figure 6-14.

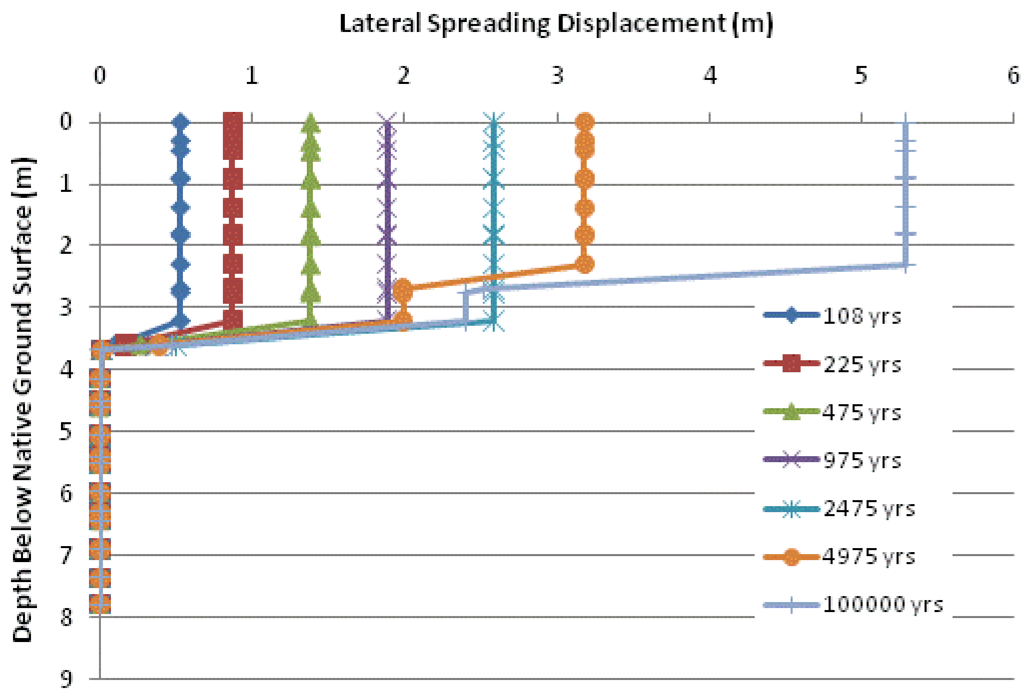

Figure 6-14: Performance-based lateral spreading displacement profiles for the Rio Cuba Bridge

6.3.5 Deterministic Pile Response Analysis

With lateral spreading displacement profiles, an analysis of the pile response at the east abutment of the Rio Cuba Bridge can be performed using the procedure summarized in Chapter 3 of this report. However, several assumptions must be made in order to attempt to replicate the pile response that was observed to occur at the Rio Cuba Bridge following the Limon earthquake.

Because the bridge deck did not fall from its supports as a result of the earthquake, the kinematic response of the piles at the abutments was likely significantly affected by the presence of the bridge deck. The presence of the deck would likely act as a supporting strut, thus limiting the amount of lateral deformation at the ground surface. However, brittle foundations such as the reinforced concrete piles supporting the Rio Cuba Bridge would likely not be able to resist very large shear loads and bending moments, and would therefore be susceptible to large deformations and rotation beneath the bridge deck. Such a phenomenon was observed during the initial reconnaissance as part of this study in which pile cap rotations were still visible and were measured at approximately 9 degrees from vertical. However, had the bridge deck not been in place, it is likely that the piles would have deformed in conjunction with the free-field soil deformations, resulting in greater horizontal displacements and less rotation at the abutments.

Currently, no simplified methodology could be identified in the literature review for predicting when a bridge deck will fall off its supports and no longer act as a reinforcing strut. Such a phenomenon is obviously complex and is dependent on many potential variables including ground motions, foundation stiffness, bridge orientation in relation to the ground motions, bridge/abutment type, connections at the supports, and magnitude of the free-field soil deformations. All of these variables result in significant uncertainty in dealing with the problem. This uncertainty is emphasized by the fact that many other bridges in the Limon earthquake with similar spans, abutment types, foundation stiffness, etc. lost their bridge decks during earthquake shaking and therefore did not have the benefit of a strut load in resisting kinematic loading. Development of a solution to this problem is beyond the scope of this study, but could be a valuable focus for future research. This study only attempted to replicate the pile response that was observed following the Limon earthquake.

To account for the presence of the bridge deck, a lateral resisting load was applied to the head of the pile cap in the LPILE analysis. The load was taken as the lesser of the load required to maintain zero displacement at the head of the pile cap and the limiting passive load computed from the log-spiral passive pressure from pushing the pile cap and bridge abutment into the approach embankment. The limiting passive load was computed to be approximately 5700 kN for the entire bridge abutment.

Since reinforcing details for the piles were not shown on the bridge plans provided to us by the Costa Rican Ministry of Transportation, assumptions had to be made regarding the amount and size of rebar in the piles in order to compute their flexural stiffness (i.e. EI). A study was made into many of the available reinforced concrete design standards in practice during 1968 when the bridge was constructed, and it was found that most piles in use at the time only incorporated four vertical steel bars for reinforcement. It was assumed that #4 bars were used in the piles. The resulting composite initial flexural stiffness of the piles was computed to be approximately 41,200 kN-m^2. A nonlinear pile response analysis was also performed in LPILE with a single reinforced concrete pile to estimate the yielding moment of the pile. The yield moment for the modeled pile was computed to be approximately 22.8 kN-m.

Applying the lateral spreading deformations shown in Figure 6-13 to the equivalent single pile, the LPILE deterministic pile response from the 1991 Limon earthquake is shown in Figure 6-15. It was observed that rotational stiffness in the pile cap could reasonably be neglected, likely due to the relatively flexible piles and the close pile-to-pile spacing in the orientation of the lateral spread. Therefore, the equivalent single pile was modeled with a free-head condition with an applied lateral load representing the bridge deck.

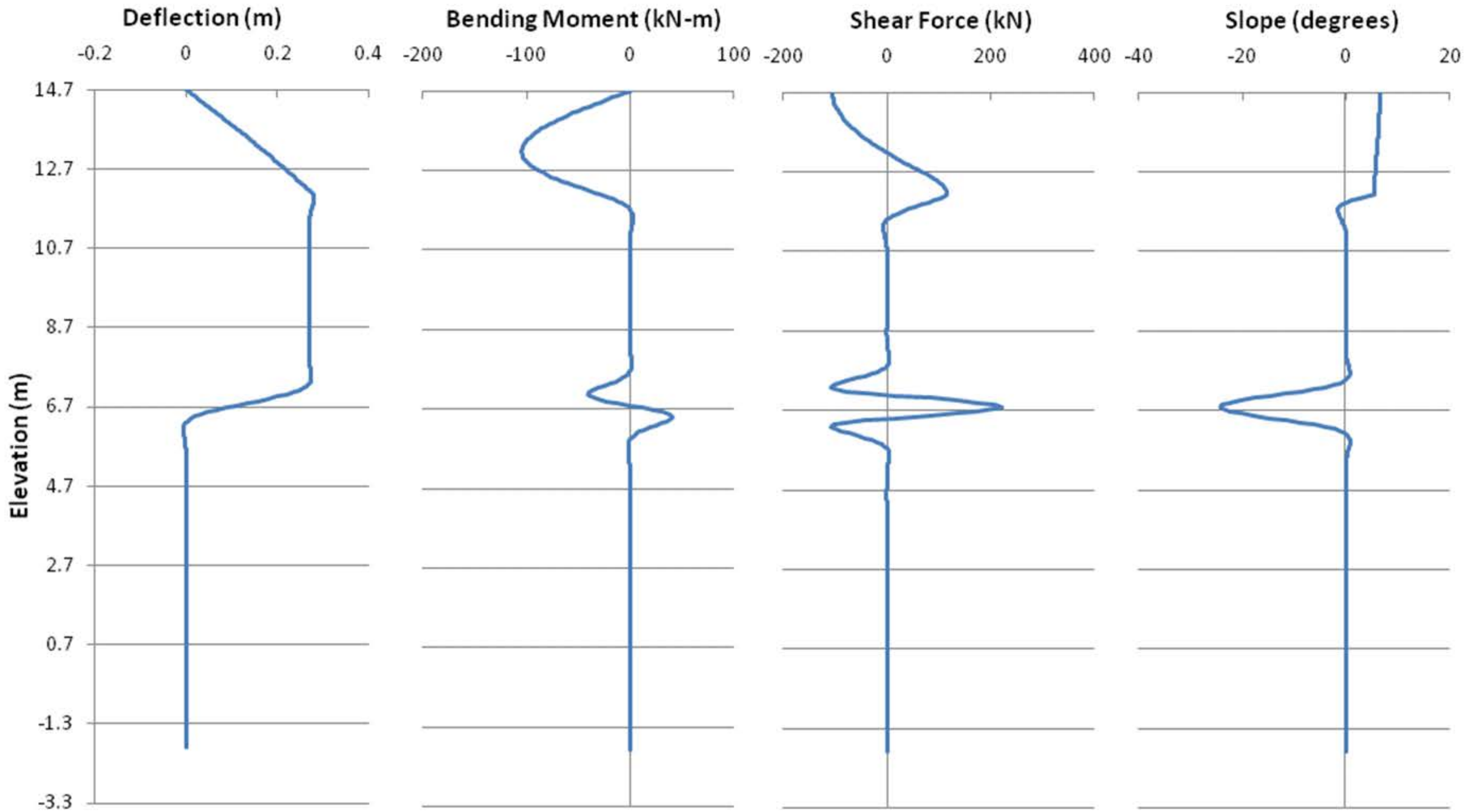

Figure 6-15: Deterministic computed pile response for the Rio Cuba Bridge east abutment from the 1991 Limon earthquake

In general, the deterministic analysis reasonably replicated the response of the bridge foundation to the earthquake. Using the average lateral spreading displacement computed from the empirical models, a rotation of approximately 6.5 degrees was computed for the pile cap. Back-analysis showed that a lateral displacement of approximately 0.35 meter would have produced a pile cap rotation of 8.5 degrees.

6.3.6 Performance-Based Pile Response

The performance-based procedure for computing kinematic pile response presented in this report was applied to the Rio Cuba Bridge. However, the question of how to properly account for the strut load provided by the bridge deck in a performance-based framework is significant and requires some discussion. The results from the deterministic pile response analysis at the Rio Cuba Bridge demonstrate that the bridge deck played a critical role in the observed performance of the bridge foundations during the kinematic loading of the 1991 Limon earthquake. Had the bridge deck fallen from its supports, the kinematic loading would likely have overwhelmed the foundations, and much larger horizontal deformations would have been observed at the abutment. However, the presence of the bridge deck limited lateral deformations, but caused the foundation and pile cap to rotate beneath the bridge deck.

In a p robabilistic framework where earthquake loading and lateral spreading displacements are considered from across a wide range of return periods, two critical questions arise when attempting to account for the possible bracing effects of a bridge deck:

1. At what return period of ground motion/displacement does the bridge deck fall off its supports?
2. How can you adjust the strut load in the probabilistic framework in order to account for the possible variability in the p-y behavior of the soil?

The first question is difficult, if not impossible to answer with simplified analysis techniques. The issue of bridge collapse can be very complex, and is dependent on a large number of variables including the intensity, frequency, and duration of the ground motion; the orientation of the bridge deck; the magnitude of ground displacement at the abutment(s); and the bridge/support type. To simply attempt to correlate bridge collapse with the magnitude of lateral spreading displacement potentially introduces significant error into the analysis. For example, evaluation of the 1991 Limon earthquake shows at least one bridge (Rio Estrella Highway Bridge) which collapsed with very little to no deformations of the foundation and at least one bridge (Rio Bananito Railway Bridge) whose foundation experienced significant deformations but did not collapse. Therefore, any attempt to estimate the return period at which a bridge deck would collapse would likely be better suited for a more sophisticated analysis such as a dynamic numerical model that could account for both soil-structure interaction and dynamic response of the superstructure itself.

The second question deals more with the limitations of the simplified analysis methodology employed in this study. An important aspect of the performance-based evaluation of kinematic pile response is the consideration of variability in the soil-pile interaction. This study employed a basic Monte Carlo approach in LPILE to estimate the variance of the pile response at various depths along the equivalent single pile. However, addition of a strut load at the head of the equivalent single pile significantly affects the computed pile response. Ideally, the strut load should be modified for each permutation in the Monte Carlo simulation such that the resulting lateral displacement at the pile head is approximately zero. However, there is no means to program LPILE to automatically alter the applied load such that zero deformation at the pile head is maintained during the parameter randomization of the Monte Carlo simulation. Maintaining a constant strut load in the Monte Carlo simulation is one possible solution to the problem; however, the computed variance in the pile response would be unrealistically high because a constant strut load could either provide too much or too little resistance to kinematic loading for a given permutation. Such unrealistically high variances were observed during preliminary Monte Carlo simulations with a constant strut load at the Rio Cuba Bridge, resulting in computed coefficients of variation exceeding 300%.

It is apparent that the simplified procedures for computing mean kinematic pile response and estimating its variance as presented in Section 5.8 of this report are not well-suited for considering additional complex structural phenomenon such as the potential bracing effect from a bridge deck. Such complexity would be better modeled using more sophisticated numerical methods capable of accounting for more of the uncertainty associated with the phenomenon. However, the performance-based framework for computing the pile response (i.e. damage measure) as described in Section 5.9 of this report would still be applicable to a more sophisticated approach and be capable of incorporating the results from that approach to develop hazard curves for the kinematic pile response.

For the sake of demonstration, two analyses were performed at the Rio Cuba Bridge. The first analysis neglected the presence of a reinforcing bridge deck, thus assuming that the kinematic loading is being resisted solely by the lateral stiffness of the piles themselves. The assumption of no b ridge deck is routinely used in engineering practice today because it is considered to be conservative. However, such an assumption inherently defeats the idea of performance-based design because true performance is not necessarily being considered. The second analysis assumed that a constant reinforcing strut load was present at each return period of lateral spreading displacement. A constant coefficient of variation equal to 50% was assumed and applied across the entire pile to represent the variability in the kinematic pile response. This approach was used rather than performing a Monte Carlo simulation in order to maintain more realistic values of the variance. However, we recognize that such an approach should not be applied in actual engineering design; rather, the variance in the kinematic pile response should be estimated using more sophisticated methods such as a Monte Carlo simulation coupled with a dynamic numerical model. The results from these two analyses are shown in Figure 6-16 and Figure 6-17.

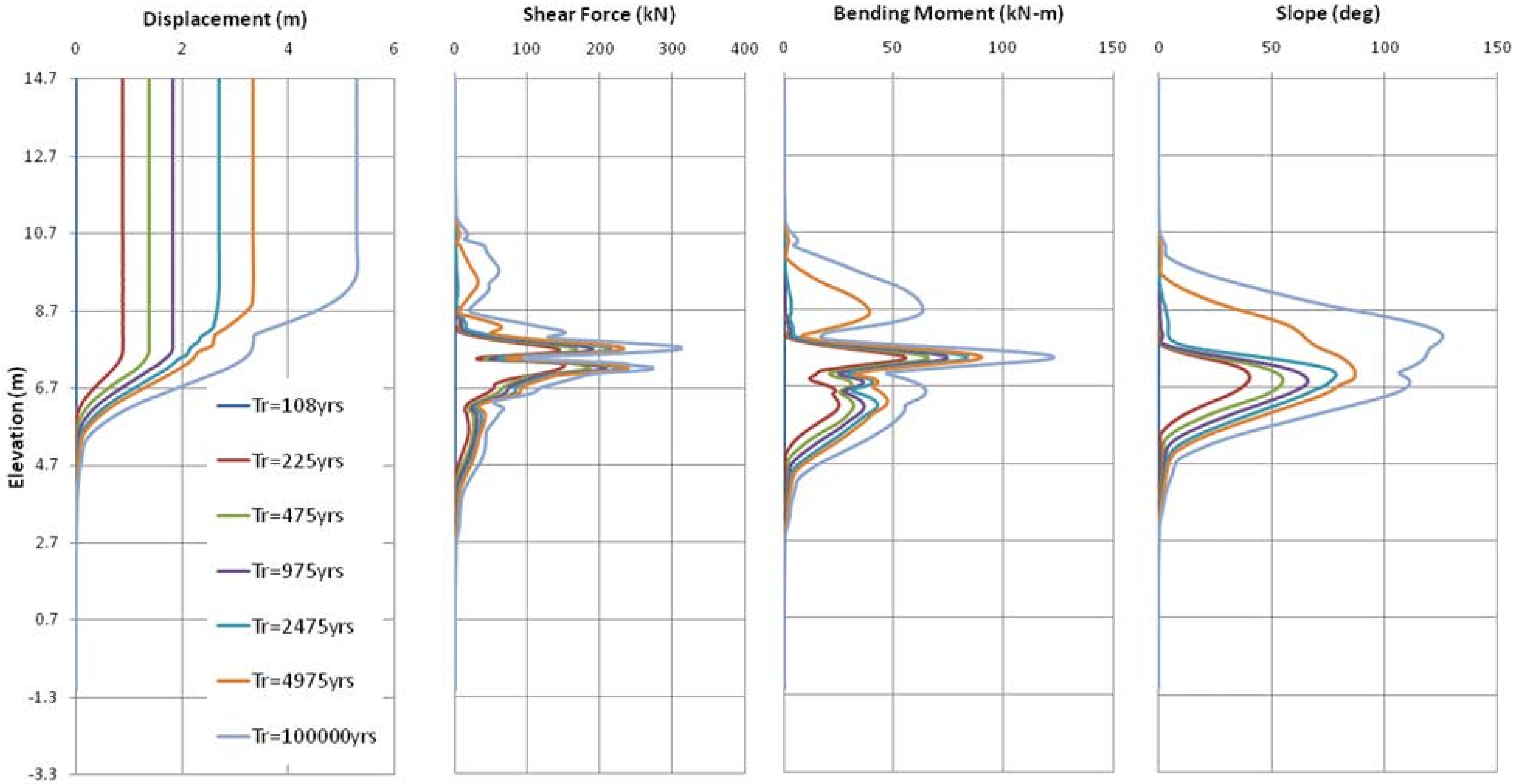

Figure 6-16: Performance-based pile response results for an average single pile assuming no bridge deck at the Rio Cuba Bridge

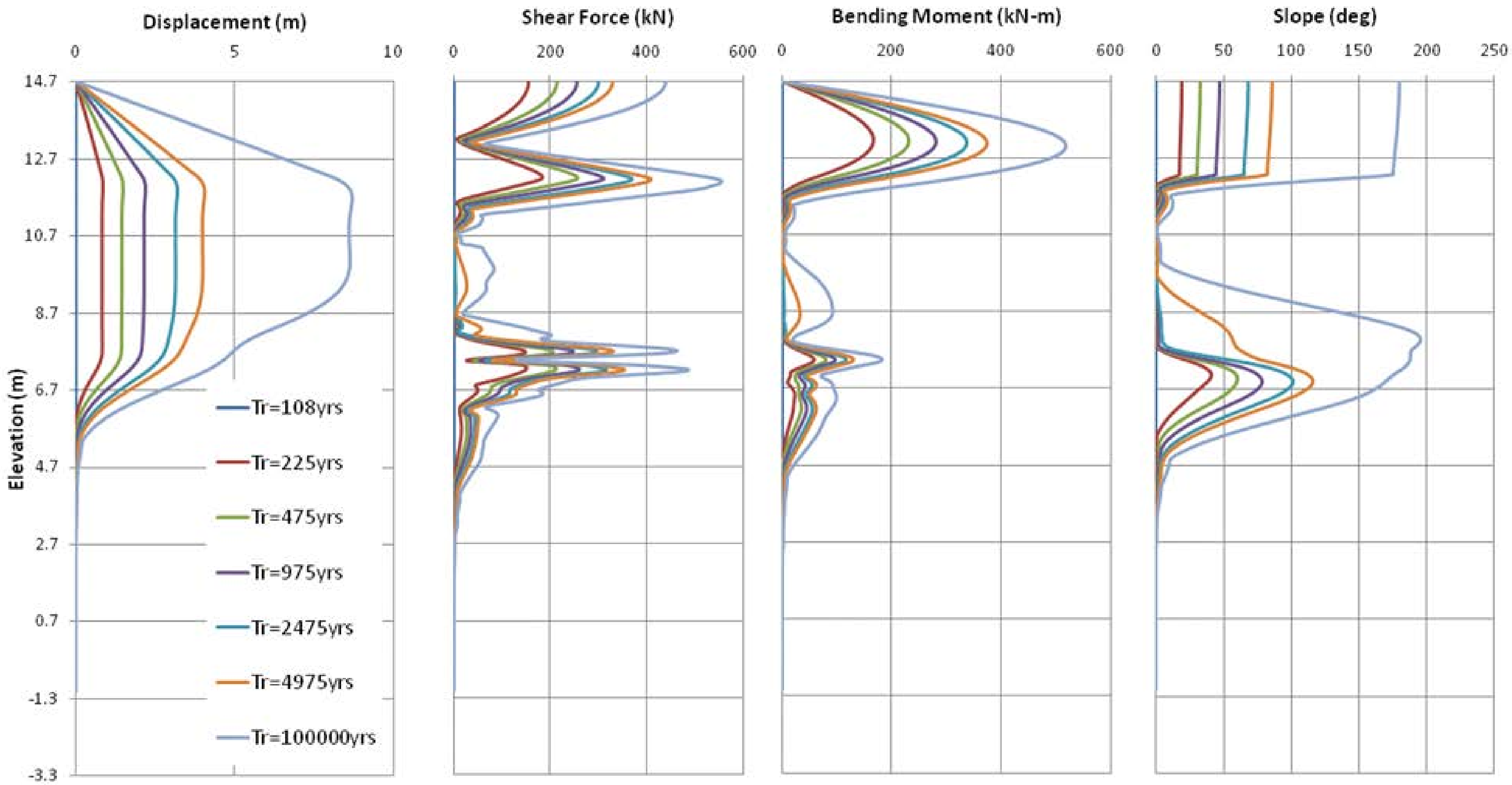

Figure 6-17: Performance-based pile response results for an average single pile assuming a bridge deck and coefficient of variation of 50% at the Rio Cuba Bridge

6.3.7 Discussion of Results

Thoughtful review and study of Figure 6-16 and Figure 6-17 reveal a few important observations that deserve discussion. First, the drastically different results from the two performance-based analyses demonstrate the significance that the bridge deck can have in computing the kinematic pile response of a bridge foundation. As performance-based pile response analysis methods become more sophisticated, significant attention should be paid to the estimated dynamic behavior of the bridge deck because it can dramatically affect the performance of the piles in resisting kinematic loading.

The pile response analysis results shown in Figure 6-16, which represent the assumption of no br idge deck, demonstrate that two rows of reinforced concrete piles are generally insufficient to resist any significant amount of kinematic loading. No deformations were computed for a return period of 108 years; however, significant deformations and pile yielding (i.e. bending moments greater than 22.7 kN-m) were computed at return period of 225 years. These results suggest that the piles were unable to resist even small ground deformations. In addition, the pile deformation profiles are remarkably similar at each return period to the computed free-field ground deformations shown in Figure 6-14, suggesting that the piles essentially experience the same deformations as the surrounding soils. Ledezma and Bray (2008, 2010) note that such behavior is likely typical of most bridge foundations if the reinforcing effect of the bridge deck is neglected.

The pile response results shown in Figure 6-17 demonstrate the significance that the estimated variance in the soil-pile interaction can have in a performance-based pile response analysis. Using a uniform coefficient of variation of 50% for the pile response produced very large and unrealistic computed probabilistic estimates of the kinematic pile response at return periods greater than about 4,975 years. Therefore, reasonable care should be provided whenever possible to obtain realistic estimates of the variance in the soil-pile interaction when computing performance-based kinematic pile response.

Finally, when comparing the measured pile cap rotation of 8.5 de grees following the Limon earthquake with the computed performance-based pile response results shown in Figure 6-17, a rotation of 8.5 degrees corresponds with an approximate return period of 130 years (i.e. 32% probability of exceedance in 50 years). Therefore, according to the performance-based analysis, the east abutment of the Rio Cuba Bridge has one-in-three chance in experiencing a pile cap rotation of at least 8.5 degrees in any given 50 year timeframe if the bridge deck stays in place and the coefficient of variation in the soil-pile interaction is approximately 50%.

6.4 Rio Blanco Bridge

The bridge over the Rio Blanco is a three-span reinforced concrete bridge supporting two lanes of traffic. The two outside spans are approximately 17 m eters in length and the interior span is approximately 22 meters in length. Each span is composed of reinforced concrete girders, and the total span of the bridge is shown to be approximately 59 meters. The bridge is located along National Route 32 just east of the town of Liverpool. The latitude/longitude coordinates of the bridge are approximately 9.9918° North 83.1253° West.

According to bridge plans provided by the Costa Rican Ministry of Transportation and dated September 1967, the bridge is founded on a series of 14-inch square reinforced concrete piles. The abutments are supported by two rows of piles (6 piles in the front row, 7 piles in the second row, and 13 piles in total) that are approximately 15 meters in length and spaced at 5-6 diameters in the transverse direction and 3 diameters in the longitudinal direction. The approximate dimensions of the pile cap at each abutment is 12.3 meters (transverse) x 1.90 meters (longitudinal) x 2.50 meters (vertical). The two bents are each founded on two 4-meter x 5-meter pile caps. Each of these pile caps is supported by 20 14-inch x 14-inch piles (five rows of four piles) that are 11 meters in length and spaced at 2.8 diameters in both the transverse and longitudinal directions. The abutments and the bents are skewed at an angle of 35 degrees to the transverse orientation of the bridge.

6.4.1 Surface Conditions and Bridge Geometry

The Rio Blanco is a relatively small river bounded on both sides by a gently sloping floodplain and extensive vegetation. According to elevations shown on the blueprints that were provided by the Costa Rican Ministry of Transportation and are dated September 1967, the river channel itself ranges in elevation from about -0.75 meter at the bottom of the river channel to approximately 4.75 meters at the river bank near the eastern bridge abutment. Due to a malfunction with the GPS equipment, updated elevations at the bridge were not able to be measured during our site reconnaissance. According to the bridge blueprints, the roadway elevation across the bridge varies from 9.52 meters at the east abutment to 9.54 meters at the west abutment. From the blueprints, it also appears that the approach embankment was originally constructed at a 1.5H:1V slope. The elevation of the water in the Rio Blanco was estimated to be approximately 2.2 meters at the time of our investigation.

A sketch of the plan and profile views of the Rio Blanco Bridge as they are shown on the plans provided by the Costa Rican Ministry of Transportation is presented in Figure 6-18.

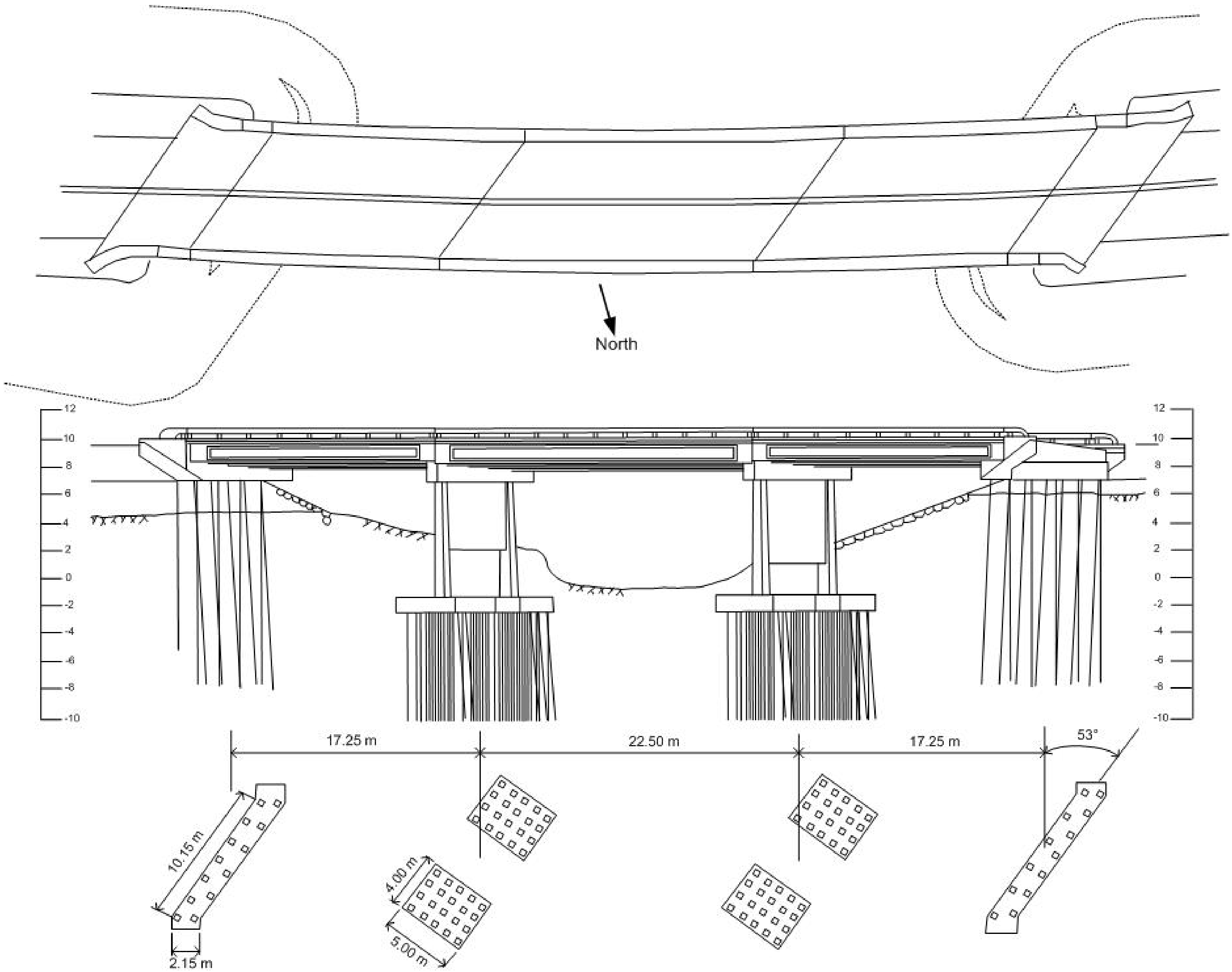

Figure 6-18: Simplified sketch of the plan and profile views of the Rio Blanco Bridge as shown on the bridge plans provided by the Costa Rica Ministry of Transportation

6.4.2 Subsurface Conditions

Insuma S.A. Geotechnical Consultants performed a single boring immediately adjacent to embankment fill at the eastern abutment of the bridge. The boring extended to a depth of approximately 15 meters. The soils encountered in the boring were reported to consist primarily of alluvial deposits alternating between clays, silts, and sands. The clays encountered appeared to have high plasticity while the silts encountered appeared to have either low or no plasticity. The sands encountered appeared to be fine-grained and varied in fines content from clean to silty/clayey. Groundwater was encountered in the boring at an approximate depth of 4.8 meters, which corresponds to an estimated elevation of approximately 2.2 meters. A simple diagram of the soils encountered in the boring performed is shown in Figure 6-19 below. Further details regarding the boring at the Rio Blanco Bridge and the corresponding laboratory test results can be found in the Insuma Geotechnical Report included as Appendix A of this report.

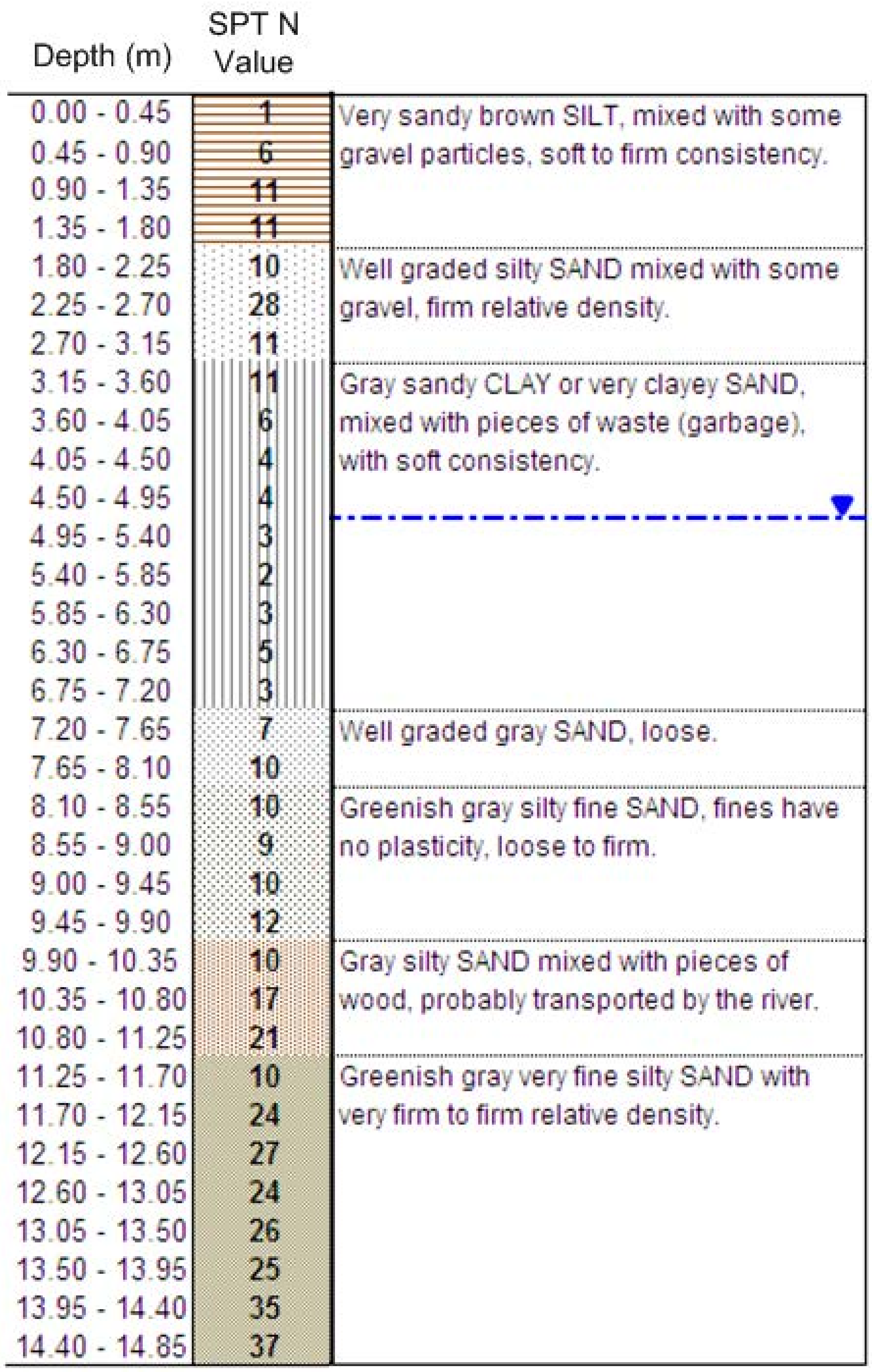

Figure 6-19: Boring P-1 performed at the Rio Blanco Bridge

The information from boring P-1 was used to develop a generalized soil profile for the east abutment of the Rio Blanco Bridge. Empirical correlations with SPT blowcounts were averaged to estimate the friction angle of granular soils and non-plastic silts. These correlations include Peck et al. (1974), Hatanaka and Uchida (1996), and Bowles (1977). Relative density of granular soils was estimated using the empirical correlation presented by Kulhawy and Mayne (1990). Corrected soil modulus estimates K^* of the granular soils for use with the API (1993) p-y relationship were estimated using the recommendations presented by Boulanger et al. (2003). Undrained strength of cohesive plastic soils was averaged from empirical correlations including Hara et al. (1971), Kulhawy and Mayne (1990), and Skempton (1957). Assumptions regarding the unit weight of the native soil as well as the strength properties of the embankment fill were made. Groundwater is modeled at an elevation of 2.2 meters (i.e. an estimated depth of 7.32 meters from the top of the embankment). Table 6-3 summarizes our generalized model of the soil profile at the east abutment of the Rio Blanco Bridge.

Table 6-3: Generalized soil profile for the east abutment at the Rio Blanco Bridge

Top Depth (m)	Top Elevation (m)	Thickness (m)	USCS Soil Class	Friction Angle (deg)	Moist Unit Weight (kN/m3)	Undrained Strength (kPa)	Relative Density (%)	Corrected Soil Modulus (kN/m3)	Liquefied p-multiplier
0	9.52	2.52	SM (Fill)	35	18.5	---	62	24,800	NA
2.52	7.00	1.80	ML (Fill)	---	18.1	38.0	---	---	NA
4.32	5.20	1.35	SW(Fill)	36	18.1	---	63	24,160	NA
5.67	3.85	1.65	CH	---	18.5	24.0	---	---	NA
7.32	2.20	2.40	CH	---	8.7	24.0	---	---	NA
9.72	-0.20	3.15	SW/SM	33	8.3	---	45	10,000	0.12
12.87	-3.35	4.50	SM/ML	38	8.5	---	71	19,300	NA

6.4.3 Ground Motions and Liquefaction

The Rio Blanco Bridge is located approximately 34 kilometers northwest from the epicenter of the April 22, 1991 earthquake. Assuming an average V_{s30} value of 270 m/s, the average computed median spectral accelerations and median ±1σ from the four selected NGA models are shown in Figure 6-20. The median computed PGA and spectral accelerations corresponding to 0.2-second and 1.0-second are approximately 0.168g, 0.351g, and 0.227g.

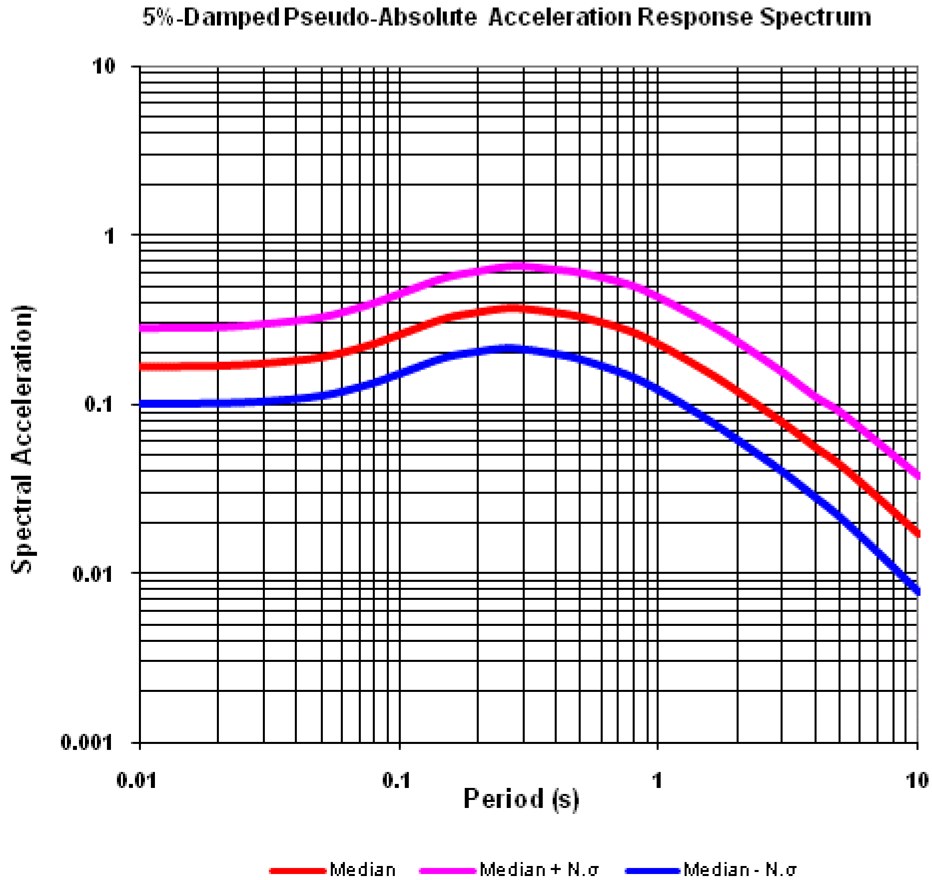

Figure 6-20: Computed deterministic response spectra for the Rio Blanco Bridge from the 1991 earthquake. N = 1

Using the average deterministic ground motions from the NGA equations, the deterministic liquefaction triggering was evaluated at the Rio Blanco Bridge for the M7.6 1991 Limon earthquake using the SPT blowcounts from Boring P-1. The results of the deterministic liquefaction triggering analysis are shown in Figure 6-21. This evaluation included consideration of the Cetin et al. (2004), Idriss and Boulanger (2008), and Youd et al. (2001) simplified procedures. In general, good agreement was observed between the three procedures. Assuming that the top of the boring is at an approximate elevation of 7.0 meters, the results of the analysis suggest that liquefaction triggered from depths of approximately 7.2 meters to 10.4 meters below the ground surface (EL -0.2m to EL -3.4m).

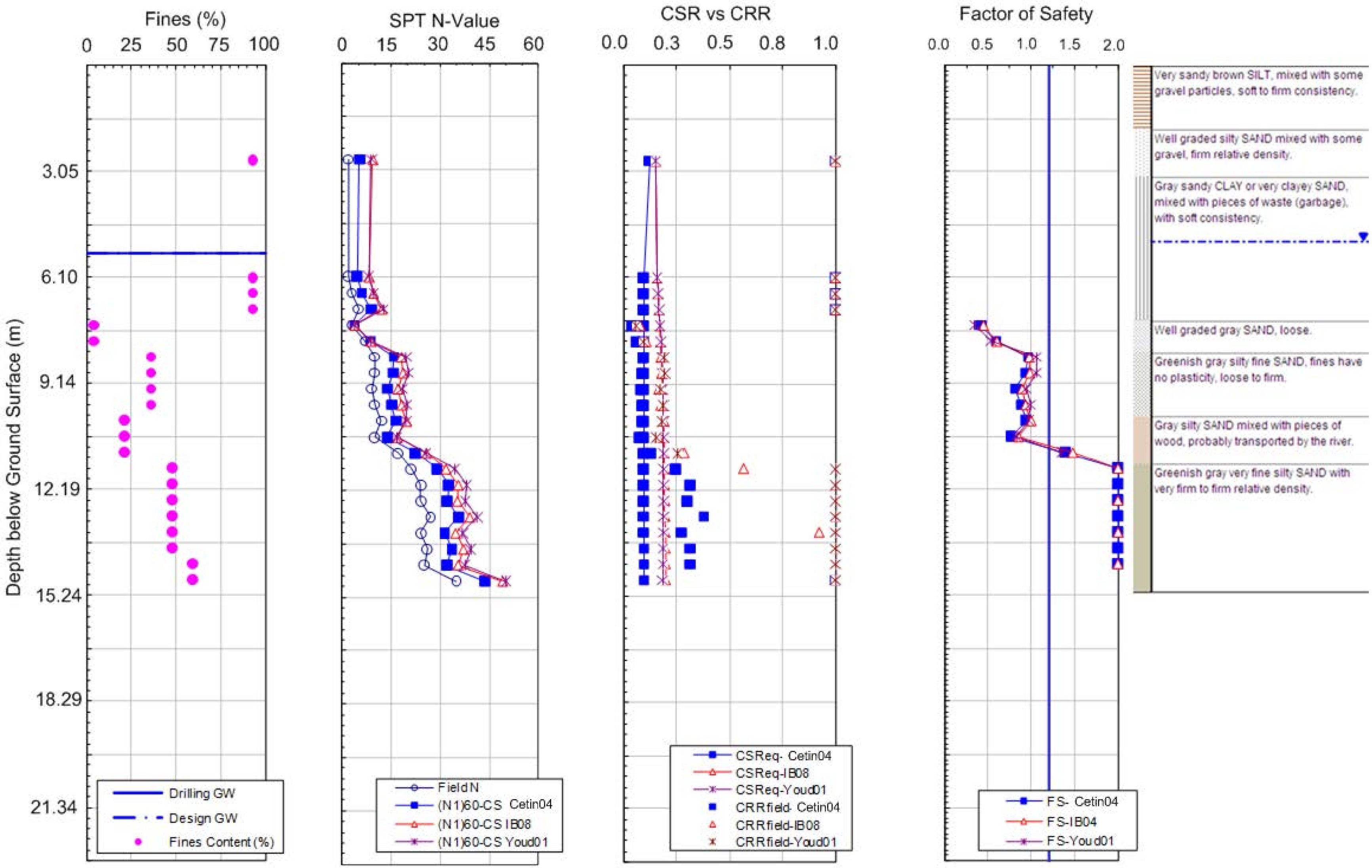

Figure 6-21: Deterministic liquefaction triggering results for the M7.6 1991 Limon earthquake at the Rio Blanco Bridge

The results of our PSHA using EZ-FRISK software suggest that the seismicity at the bridge is moderate to high. The seismic hazard curve for the PGA is shown below in Figure 6-22.

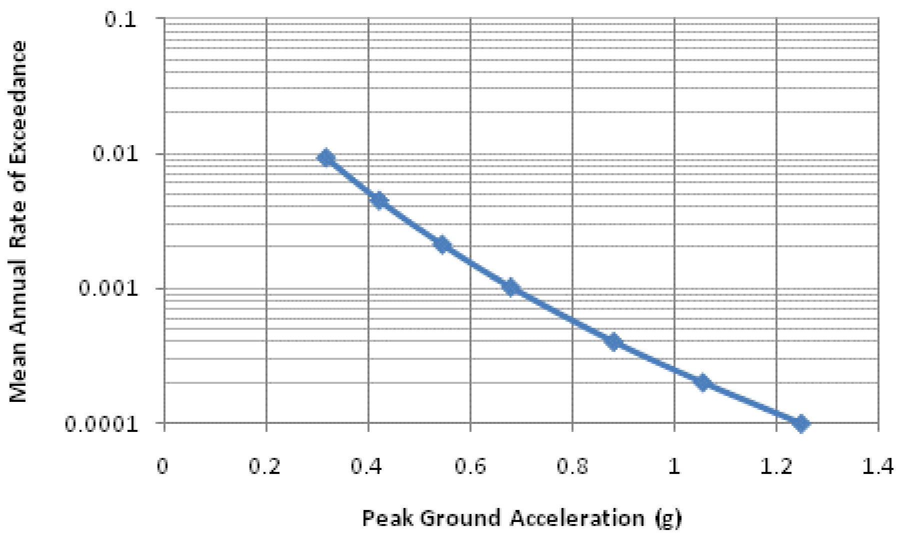

Figure 6-22: Computed seismic hazard curve for the PGA at the Rio Blanco Bridge

The magnitude/distance deaggregations as estimated by EZ-FRISK for the PGA are shown in Figure 6-23. These magnitude deaggregations are used in conjunction with the seismic hazard curve for the PGA shown in Figure 6-22 to perform the performance-based liquefaction triggering analysis according to the Kramer and Mayfield (2007) procedure. The performance-based factors of safety against liquefaction for various return periods are shown in Figure 6-24. These factors of safety were computed using the SPT blowcount information from Insuma boring P-1 at the Rio Blanco Bridge. A factor of safety less than or equal to 1.2 was assumed to be liquefiable for this study. Note that for fine-grained soil layers not considered susceptible to liquefaction due to plasticity, a generic factor of safety against liquefaction equal to 2.0 was assigned regardless of return period. A maximum factor of safety equal to 4.0 was assigned to layers with very high resistance to liquefaction triggering. In general, Figure 6-24 shows that for return periods greater than about 475 years, liquefaction triggers from depths of about 7.20 meters to 10.35 meters (EL. -0.2m to -3.35m) below the ground surface.

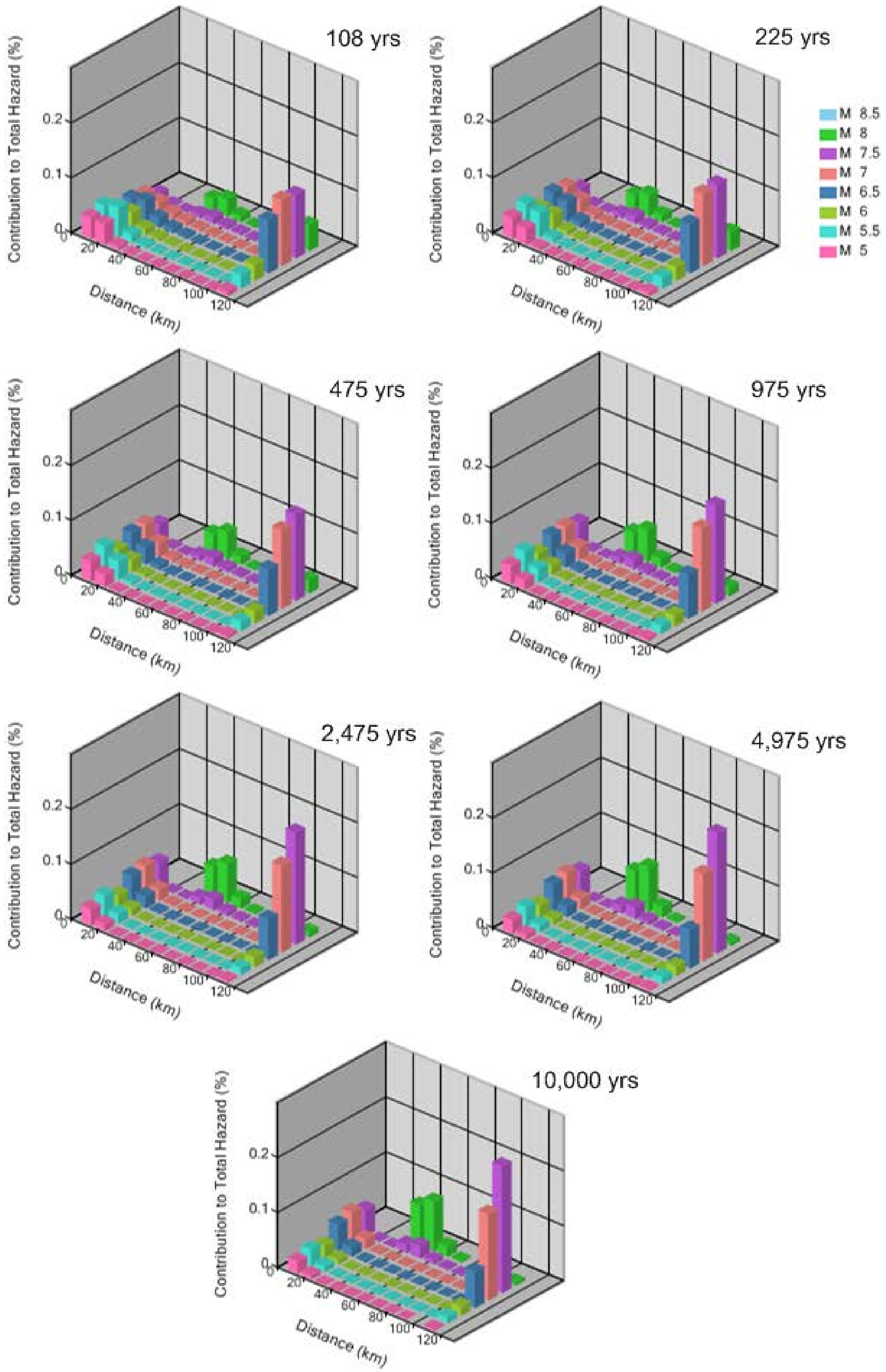

Figure 6-23: Magnitude/distance deaggregations for the PGA at the Rio Blanco Bridge

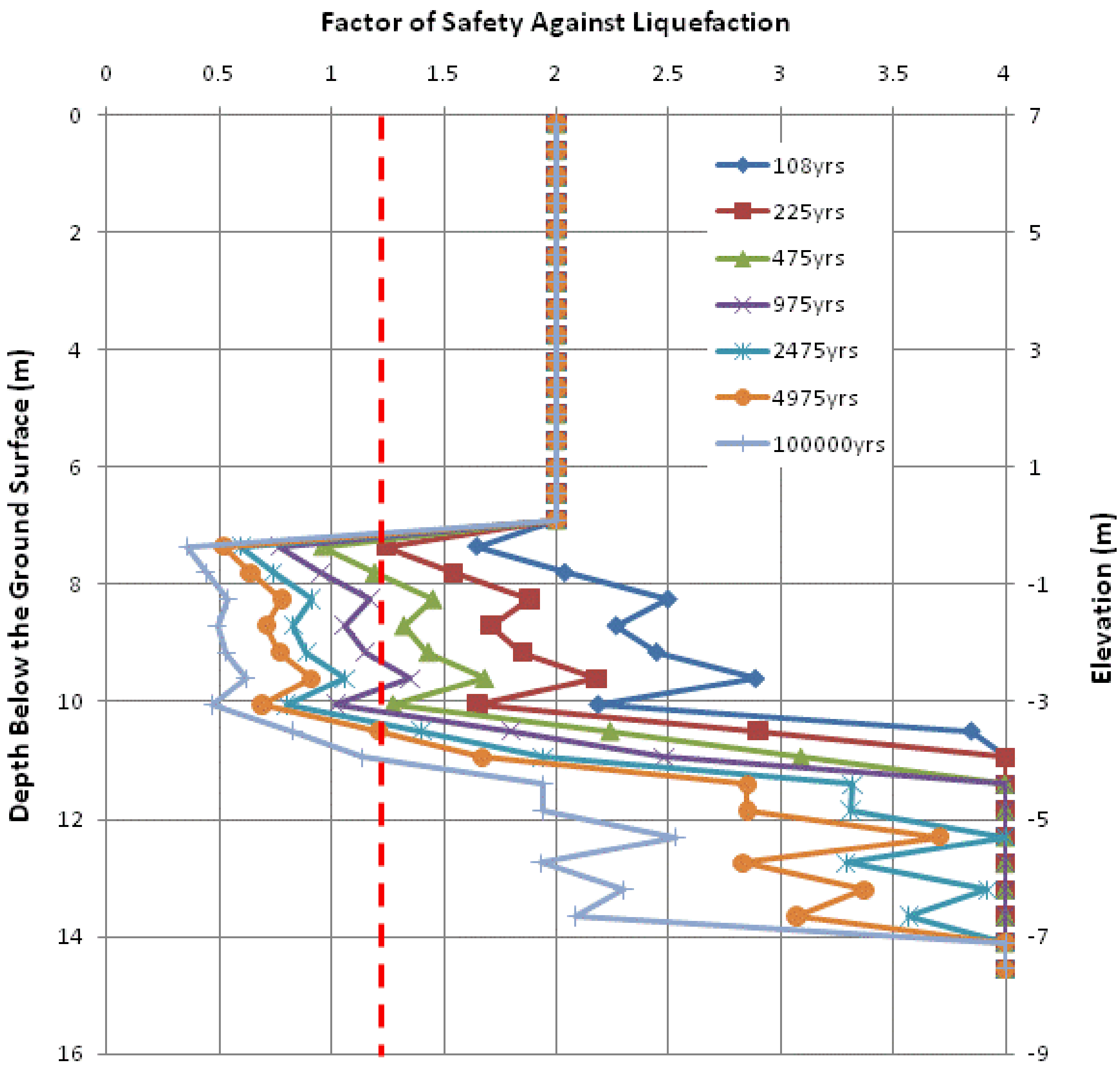

Figure 6-24: Performance-based liquefaction triggering results for the Rio Blanco Bridge

6.4.4 Lateral Spreading

Observed evidence of lateral spreading at the Rio Blanco Bridge following the 1991 earthquake is quite minimal. No tension cracks or sand boils were reported at the bridge in any of the reconnaissance reports published immediately following the earthquake. However, damage to the bridge structure itself was observed and recorded both in the original reconnaissance reports and our own reconnaissance in 2009. While little to no lateral displacement was observed at the pavement elevation, a rotation of the pile cap/abutment of up to approximately 8.5 degrees was observed at the west abutment. Slight cracking and spalling of the front row of piles was observed, and the rebar in the piles is slightly exposed as a result. The rotation of the pile cap suggests that free-field soil and/or slope displacements occurred, but the bridge deck behaved as a reinforcing strut and prevented any significant lateral deformation of the abutment to occur.

Empirical evaluation of the free-field soil displacements due to lateral spreading was performed using the Youd et al. (2002), Bardet et al. (2002), and Baska (2002) models. Our analysis assumed an earthquake magnitude of 7.6, a source-to-site distance of 34 kilometers, a free-face ratio of 20-percent, and a free-face height of 5.5 meters. The mean grain size diameter for each soil sublayer in the analysis was estimated from the Insuma sieve results. The median computed lateral spreading displacement value and the 95th-percentile confidence interval for each of the three empirical models is shown in Figure 6-25. The average computed median displacement from the three models is approximately 0.99 meter.

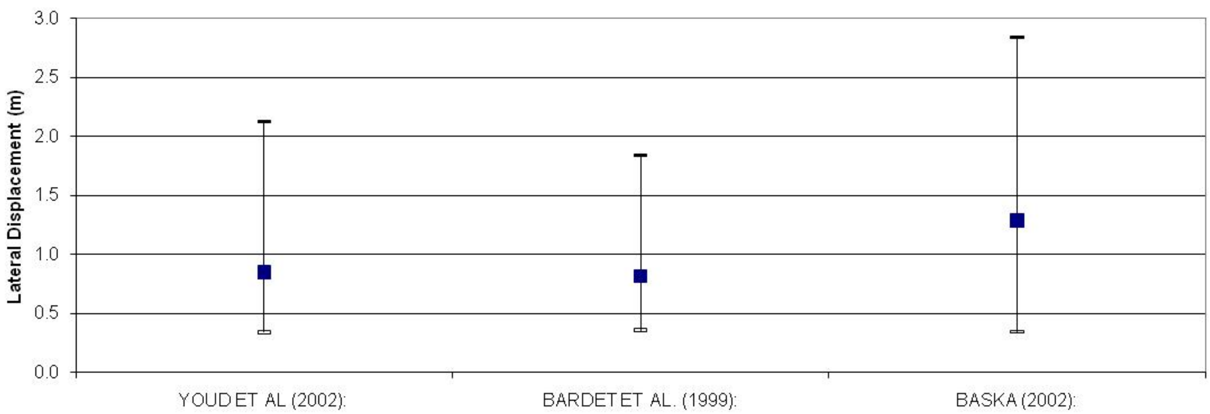

Figure 6-25: Deterministic median and 95-percentile evaluations of lateral spreading displacement using select empirical models for the Rio Blanco Bridge

The estimated lateral spreading displacement profile for the M7.6 1991 Limon earthquake was computed according to the procedure presented in Sections 2.7 and 2.8 of this report. This displacement profile is shown in Figure 6-26.

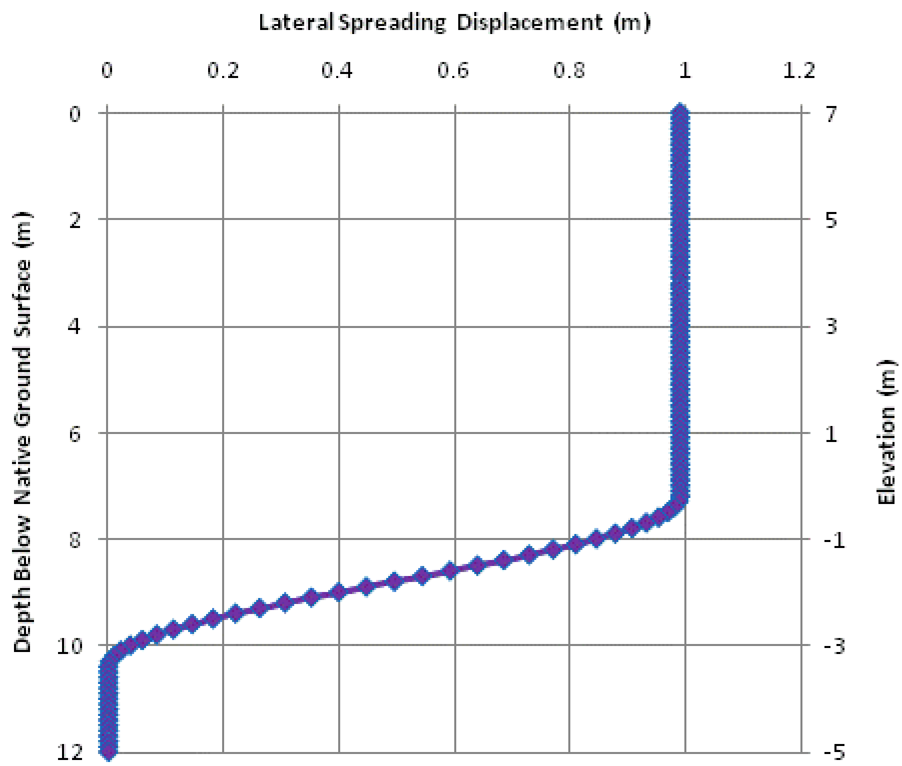

Figure 6-26: Computed lateral spreading displacement profile at the Rio Blanco Bridge for the M7.6 1991 Limon earthquake

In the performance-based framework, values of $\mathscr{L}$ and $\mathscr{S}$ were computed at the Rio Blanco Bridge for each of the three empirical models. These values are shown in Table 6-4.

Table 6-4: $\mathscr{L}$ and $\mathscr{S}$ parameters for the performance-based lateral spreading analysis at the Rio Blanco Bridge

	$\mathscr{L}$ parameter							$\mathscr{S}$ parameter
	108yrs	225yrs	475yrs	975yrs	2475yrs	4975yrs	100000yrs	
Youd et al. (2002)	8.402	8.976	9.393	9.741	9.941	10.040	10.200	-8.948
Bardet et al. (2002)	6.007	6.503	6.930	7.323	7.663	7.873	8.300	-6.319
Baska (2002)	6.712	7.172	7.515	7.793	7.962	8.036	8.160	-5.952

Using the values of $\mathscr{L}$ and $\mathscr{S}$ with the performance-based procedure for computing the lateral spreading displacement as described in Sections 5.6 and 5.7, performance-based estimates of lateral spreading deformation are computed and shown in Figure 6-27.

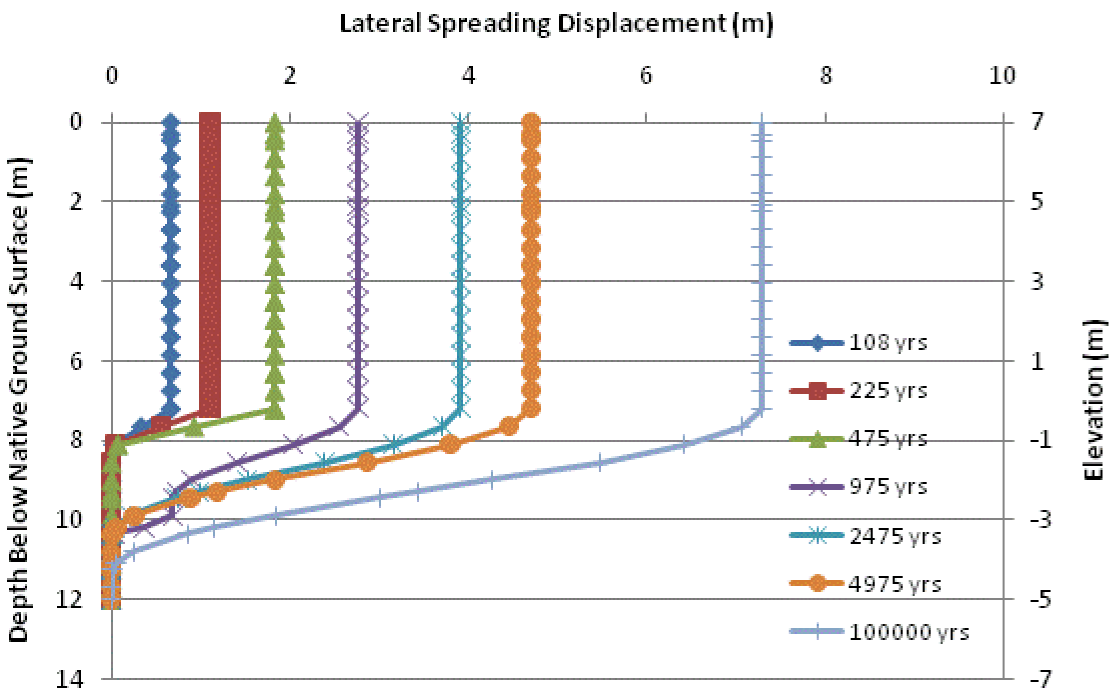

Figure 6-27: Performance-based lateral spreading displacement profiles for the Rio Blanco Bridge

6.4.5 Deterministic Pile Response Analysis

With lateral spreading displacement profiles, an analysis of the pile response at the east abutment of the Rio Blanco Bridge can be performed using the same procedure used to analyze the Rio Cuba Bridge as explained in Section 6.3. To account for the presence of the bridge deck, a lateral resisting load was applied to the head of the pile cap in the LPILE analysis. The load was taken as the lesser of the load required to maintain zero displacement at the head of the pile cap and the limiting passive load computed from the log-spiral passive pressure from pushing the pile cap and bridge abutment into the approach embankment. The limiting passive load was computed to be approximately 6,400 kN for the entire bridge abutment.

Since reinforcing details for the piles were not shown on the bridge plans provided to us by the Costa Rican Ministry of Transportation, assumptions had to be made regarding the amount and size of rebar in the piles in order to compute their flexural stiffness (i.e. EI). A study was made into many of the available reinforced concrete design standards in practice during 1968, and it was observed that most piles in use at the time only incorporated four vertical steel bars for reinforcement. It was assumed that #4 bars were used in the piles. The resulting composite initial flexural stiffness of the piles was computed to be approximately 41,200 kN-m^2. A nonlinear pile response analysis was also performed in LPILE with a s ingle reinforced concrete pile to estimate the yielding moment of the pile. The yield moment for the modeled pile was computed to be approximately 22.8 kN-m.

Applying the lateral spreading deformation shown in Figure 6-25 to the equivalent single pile, the LPILE deterministic pile response from the 1991 Limon earthquake is shown in Figure 6-28. It was observed that rotational stiffness in the pile cap could reasonably be neglected, likely due to the relatively flexible piles and the close pile-to-pile spacing in the orientation of the lateral spread. Therefore, the equivalent single pile was modeled with a free-head condition with an applied lateral load representing the bridge deck.

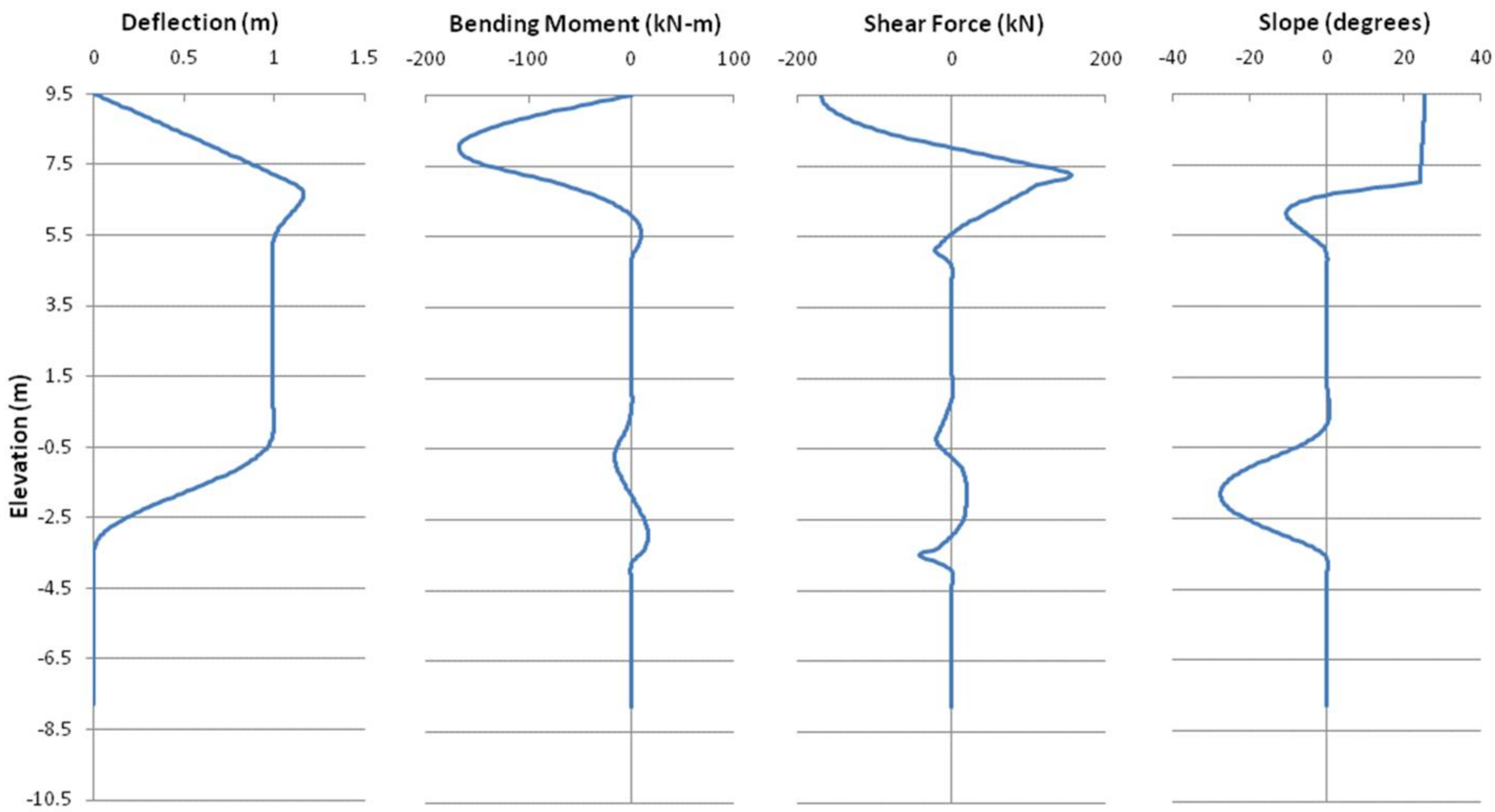

Figure 6-28: Deterministic computed pile response for the Rio Blanco Bridge east abutment from the 1991 Limon earthquake

6.4.6 Performance-Based Pile Response

As with the Rio Cuba Bridge, two analyses were performed at the Rio Blanco Bridge. These analyses are intended to represent the bounding conditions for the kinematic loading. The first analysis neglected the presence of a reinforcing bridge deck, thus assuming that the kinematic loading is being resisted solely by the lateral stiffness of the piles themselves. The assumption of no b ridge deck is routinely used in engineering practice today because it is considered to be conservative. However, such an assumption inherently defeats the idea of performance-based design because true performance is not necessarily being considered. The second analysis assumed that a constant reinforcing strut load was present at each return period of lateral spreading displacement. A constant coefficient of variation equal to 50% was assumed and applied across the entire pile to represent the variability in the kinematic pile response. This approach was used rather than performing a Monte Carlo simulation in order to maintain more realistic values of the variance. However, we recognize that such an approach should not be applied in actual engineering design; rather, the variance in the kinematic pile response should be estimated using more sophisticated methods such as a Monte Carlo simulation coupled with a dynamic numerical model. The results from these two analyses are shown in Figure 6-29 and Figure 6-30.

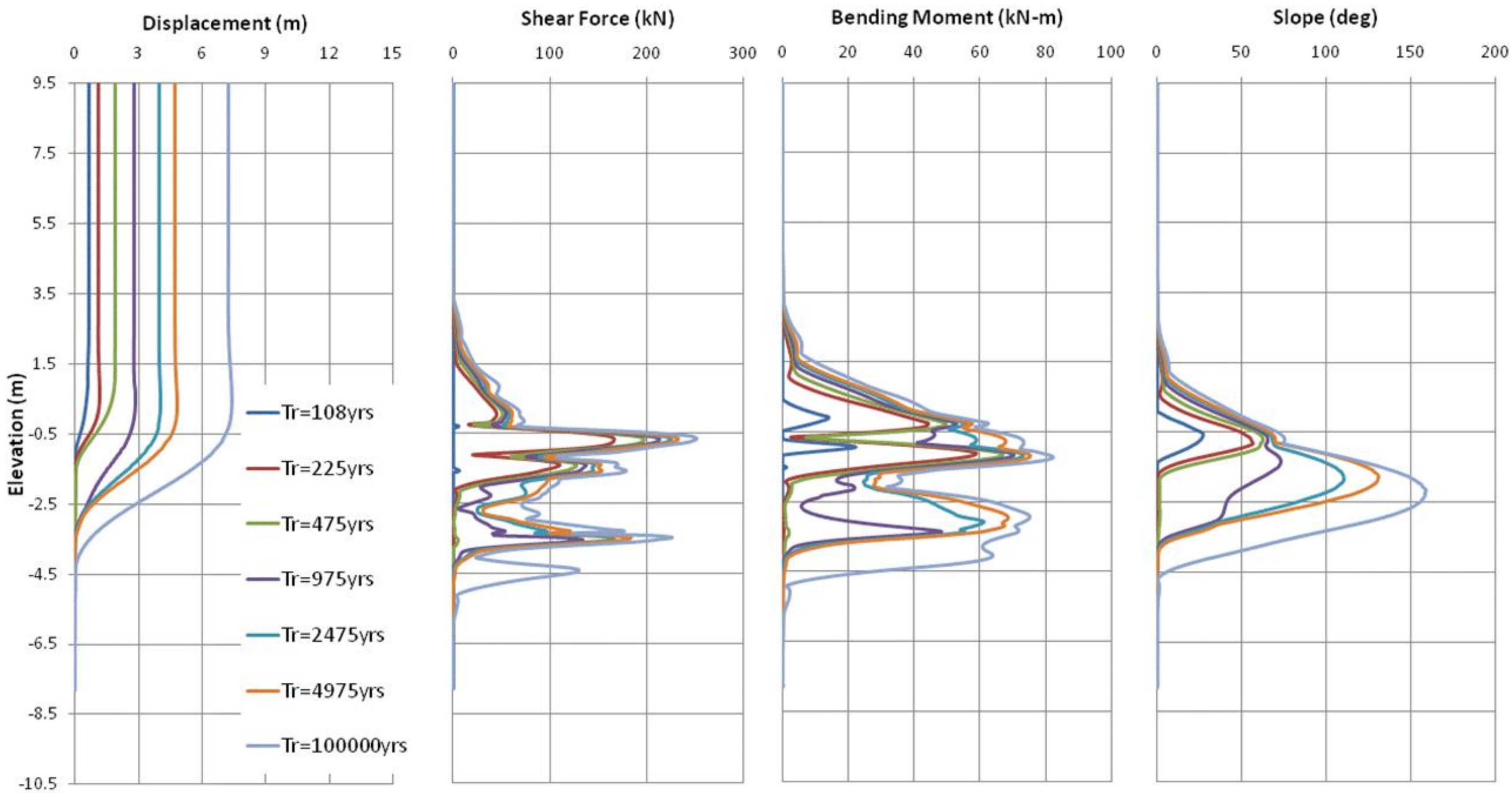

Figure 6-29: Performance-based pile response results for an average single pile assuming no bridge deck at the Rio Blanco Bridge

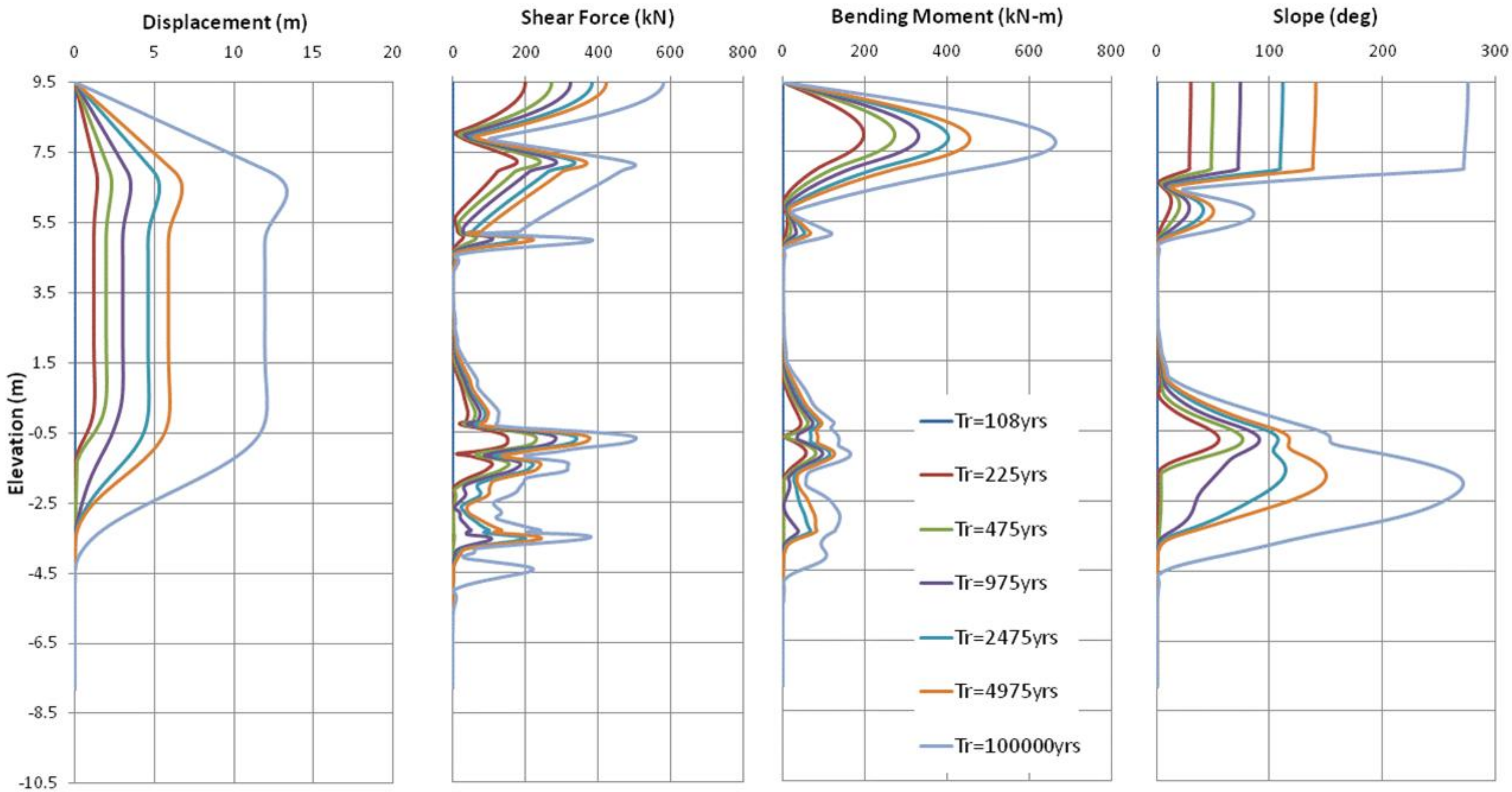

Figure 6-30: Performance-based pile response results for an average single pile assuming a bridge deck and coefficient of variation of 50% at the Rio Blanco Bridge

6.4.7 Discussion of Results

The deterministic pile response analysis results shown in Figure 6-28 suggest that a pile cap rotation of approximately 25 degrees would occur with a lateral spreading displacement of approximately 1 meter at the abutment if the bridge deck remained in place. Measurement of the actual pile cap rotation at the east abutment of the Rio Blanco Bridge showed an approximate rotation of 10 to 11.5 degrees. This rotation would be achieved in the pile response analysis with a lateral spreading displacement of approximately 0.45 meter. Such a displacement is within a factor of 2 of the computed median lateral spreading displacements from the three empirical models used in this study. The displacement is also located within the 95th- percentile bounds for all three models.

The pile response analysis results shown in Figure 6-29, which represent the assumption of no bridge deck, demonstrate that two rows of reinforced concrete piles are generally insufficient to resist any significant amount of kinematic loading. Relatively small deformations were computed for a return period of 108 years; however, significant deformations and pile yielding (i.e. bending moments greater than 22.7 kN-m) were computed at return period of 225 years and greater. These results suggest that the piles were unable to resist even small ground deformations. In addition, the pile deformation profiles are remarkably similar at each return period to the computed free-field ground deformations shown in Figure 6-27, suggesting that the piles essentially experience the same deformations as the surrounding soils. Ledezma and Bray (2008, 2010) note that such behavior is likely typical of most bridge foundations if the reinforcing effect of the bridge deck is neglected.

The pile response results shown in Figure 6-30 demonstrate the significance that the estimated variance in the soil-pile interaction can have in a performance-based pile response analysis. Using a uniform coefficient of variation of 50% for the pile response produced very large and unrealistic computed probabilistic estimates of the kinematic pile response at return periods greater than about 4,975 years. Therefore, reasonable care should be provided whenever possible to obtain realistic estimates of the variance in the soil-pile interaction when computing performance-based kinematic pile response.

Finally, when comparing the measured pile cap rotation of 10-11.5 degrees following the Limon earthquake with the computed performance-based pile response results shown in Figure 6-30, a rotation of 11.5 degrees corresponds with an approximate return period of 165 years (i.e. 26% probability of exceedance in 50 years). Therefore, according to the performance-based analysis, the east abutment of the Rio Blanco Bridge has an approximate one-in-four chance of experiencing a pile cap rotation of at least 11.5 degrees in any given 50 year timeframe if the bridge deck stays in place and the coefficient of variation in the soil-pile interaction is approximately 50%.

6.5 Rio Bananito Highway Bridge

The highway bridge over the Rio Bananito is a two-span reinforced concrete bridge supporting two lanes of traffic. According to bridge plans provided by the Costa Rican Ministry of Transportation and dated January 1971, the southern span is approximately 28.4 meters in length and the northern span is approximately 25.4 meters in length. The total length of the bridge is shown to be approximately 55.3 meters. The bridge is located along National Route 36 just west of the Bananito Beach. The latitude/longitude coordinates of the bridge are approximately 9.8849° North 82.9669° West.

According to bridge plans provided by the Costa Rican Ministry of Transportation, the bridge is founded on a series of 14-inch square reinforced concrete piles. The north abutment is supported by two rows of piles (3 piles in the front row, 3 piles in the second row, and 6 piles in total) that are approximately 15.2 meters in length and spaced at 5 diameters in the transverse direction and 2 diameters in the longitudinal direction. The south abutment is supported by two rows of piles (4 piles in the front row, 5 piles in the second row, and 9 piles in total) that are approximately 15.2 meters in length and spaced at 2.5-3 diameters in the transverse direction and 2 diameters in the longitudinal direction. The approximate dimensions of the pile cap and abutment wall at each abutment is 5.66 meters (transverse) x 1.80 meters (longitudinal) x 2.50 meters (vertical). The bent is founded on a 1.64-meter x 5.4-meter pile cap that is supported by ten 14-inch x 14-inch piles (two rows of five piles) that are 11 meters in length and spaced at 2.7 pile diameters in the transverse direction and 2.9 pile diameters in the longitudinal direction. The abutments and the bent are skewed at an angle of 30 degrees to the transverse orientation of the bridge.

6.5.1 Surface Conditions and Bridge Geometry

The Rio Bananito is a moderately-sized river bounded on both sides by a gently sloping floodplain and extensive vegetation. According to elevations shown on the bridge plans provided by the Costa Rican Ministry of Transportation, the river channel itself ranges in elevation from about -3.0 meters at the bottom of the river channel to approximately 0.5 meter at the river bank near both the north and south abutments. According to the bridge plans, the roadway elevation across the bridge is approximately 4.50 meters. From the bridge plans, it also appears that the berm at the spillslope and the approach embankment were originally constructed at a 1.5H:1V slope. The elevation of the water in the Rio Bananito was estimated to be approximately 0.0 meters at the time of our investigation.

A sketch of the Rio Bananito Highway Bridge as originally presented by Priestley et al. (1991) is shown in Figure 6-31.

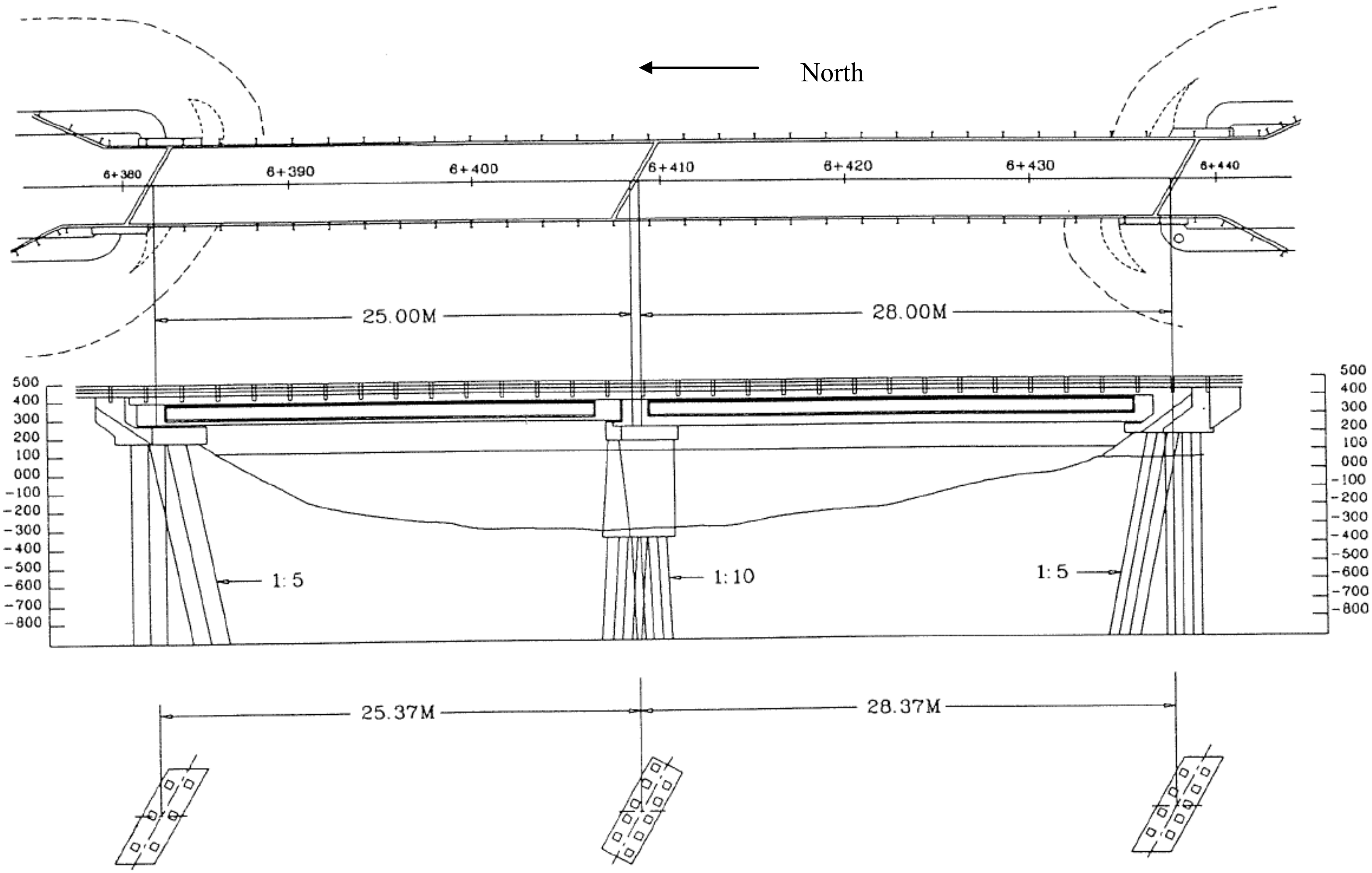

Figure 6-31: Simplified sketch of the plan and profile views of the Rio Bananito Highway Bridge (after Priestley et al, 1991; McGuire, 1994)

6.5.2 Subsurface Conditions

Insuma S.A. Geotechnical Consultants performed two borings in the vicinity of the southern abutment. Boring P-1 was performed immediately adjacent to the southern abutment and was extended to a depth of approximately 20.25 meters below the ground surface. Boring P-2 was performed about 20 meters to the south of Boring P-1 and was extended to a depth of 20.25 meters. The soils encountered in the borings were reported to consist primarily of varying amounts of surficial embankment fill and alluvial silt and sand deposits. The silts encountered appeared to have low to no plasticity and would be expected to demonstrate sand-like behavior when loaded cyclically. The sands encountered appeared to be fine-grained and varied in fines content from about 9-percent to 50-percent. Groundwater was encountered in the borings at an approximate depth of 2.0 meters in Boring P-1 and 2.6 meters in Boring P-2, which correspond to estimated elevations of 0.0 meter and 1.64 meters, respectively. Simple diagrams of the soils encountered in the borings performed are shown in Figure 6-32 and Figure 6-33 below. Further details regarding the borings at the Rio Bananito Highway Bridge and the corresponding laboratory test results can be found in the Insuma Geotechnical Report included as Appendix A of this report.

Depth (m)	SPT N Value	
0.00 - 0.45	4	Brown SAND mixed with organic matter (roots).
0.45 - 0.90	2	
0.90 - 1.35	3	Poorly graded gray silty SAND, not plastic fines, loose relative density.
1.35 - 1.80	10	
1.80 - 2.25	5	
2.25 - 2.70	2	
2.70 - 3.15	1	Fine gray SILT, not plastic, mixed with a fraction of sand size particles, very loose. Presence of wood detected.
3.15 - 3.60	1	
3.60 - 4.05	2	
4.05 - 4.50	3	
4.50 - 4.95	1	
4.95 - 5.40	3	Gray, very silty SAND and/or sandy SILT, fines are not plastic, very loose to loose relative density.
5.40 - 5.85	4	
5.85 - 6.30	4	
6.30 - 6.75	12	
6.75 - 7.20	*	
7.20 - 7.65	*	
7.65 - 8.10	23	Fine gray SILT, not plastic, mixed with a fraction of sand size particles, firm.
8.10 - 8.55	18	
8.55 - 9.00	14	
9.00 - 9.45	12	Very fine gray silty SAND, fines are not plastic, firm relative density.
9.45 - 9.90	24	
9.90 - 10.35	15	
10.35 - 10.80	28	Greenish gray very sandy SILT and/or very silty SAND, fines are not plastic, very firm relative density.
10.80 - 11.25	9	
11.25 - 11.70	20	
11.70 - 12.15	22	
12.15 - 12.60	25	
12.60 - 13.05	12	Very fine gray silty SAND, with green spots, fines are not plastic, relative density varies between firm and very firm.
13.05 - 13.50	21	
13.50 - 13.95	13	
13.95 - 14.40	11	
14.40 - 14.85	22	
14.85 - 15.30	10	
15.30 - 15.75	24	
15.75 - 16.20	20	
16.20 - 16.65	14	
16.65 - 17.10	21	
17.10 - 17.55	18	
17.55 - 18.00	19	
18.00 - 18.45	13	
18.45 - 18.90	13	
18.90 - 19.35	14	
19.35 - 19.80	15	
19.80 - 20.25	15	

Figure 6-32: Boring P-1 performed at the Rio Bananito Highway Bridge

Depth (m)	SPT N Value	
0.00 - 0.45	36	Brown poorly graded GRAVEL, mixed with some sand and silt, dense.
0.45 - 0.90	39	
0.90 - 1.35	43	
1.35 - 1.80	35	
1.80 - 2.25	21	Very fine gray SAND, poorly graded, mixed with a fraction of silt size particles, fines are not plastic, loose relative density.
2.25 - 2.70	28	
2.70 - 3.15	17	
3.15 - 3.60	8	
3.60 - 4.05	8	
4.05 - 4.50	7	
4.50 - 4.95	6	Fine gray SILT, not plastic, mixed with fraction of sand size particles, loose to firm
4.95 - 5.40	6	
5.40 - 5.85	12	
5.85 - 6.30	28	Very fine gray silty SAND, fines are not plastic, firm to very firm relative density, some seashells are observed.
6.30 - 6.75	16	
6.75 - 7.20	24	
7.20 - 7.65	23	
7.65 - 8.10	19	
8.10 - 8.55	25	
8.55 - 9.00	22	
9.00 - 9.45	13	
9.45 - 9.90	21	
9.90 - 10.35	23	
10.35 - 10.80	31	Very fine greenish gray silty SAND, fines are not plastic, some seashells observed, relative density beween firm and dense.
10.80 - 11.25	23	
11.25 - 11.70	23	
11.70 - 12.15	18	
12.15 - 12.60	11	
12.60 - 13.05	19	
13.05 - 13.50	23	
13.50 - 13.95	30	
13.95 - 14.40	22	
14.40 - 14.85	24	Greenish gray very sandy SILT, fines are not plastic, firm to dense relative density.
14.85 - 15.30	32	
15.30 - 15.75	18	
15.75 - 16.20	23	
16.20 - 16.65	23	
16.65 - 17.10	17	
17.10 - 17.55	26	
17.55 - 18.00	14	
18.00 - 18.45	16	
18.45 - 18.90	16	
18.90 - 19.35	18	
19.35 - 19.80	22	
19.80 - 20.25	20	

Figure 6-33: Boring P-2 performed at the Rio Bananito Highway Bridge

In addition to the borings performed in 2010 by Insuma S.A. Geotechnical Consultants, the Costa Rican Ministry of Transportation provided us with boring logs performed when the bridge was initially being designed. According to the bridge plans for the Rio Bananito Highway Bridge, Boring T-2 was performed at the southern abutment. No detailed surveying information regarding this borings was available, so we estimated that the ground surface elevation at Boring T-2 was approximately 0.6 m eter. Groundwater was encountered in Boring T-2 at an approximate depth of 0.6 meter, which corresponds to an approximate elevation of 0.0 meter. A tabular summary of our interpretation of Boring T-2 is provided in Table 6-5.

Table 6-5: Tabular summary of Boring T-2 at the Rio Bananito Highway Bridge

Depth (m)	SPT N Value	Estimated Fines Content (%)	Liquid Limit (%)	Plasticity Index (%)	USCS Soil Class
0.15	0	80	28	17	Silt with Sand (ML)
0.61	0	80	28	17	
1.07	0	80	28	17	
1.52	0	80	28	17	
1.98	0	80	28	17	
2.44	0	80	28	17	
2.90	0	80	28	17	
3.35	4	80	28	17	
3.81	4	80	28	17	
4.27	4	80	28	17	
4.72	2	25	---	---	Silty Sand (SM)
5.18	2	25	---	---	
5.64	8	25	---	---	
6.10	20	25	---	---	
6.55	20	25	---	---	
7.01	20	25	---	---	
7.47	12	25	---	---	
7.92	12	25	---	---	
8.38	13	25	---	---	
8.84	17	25	---	---	
9.30	30	25	---	---	
9.75	8	25	---	---	
10.21	13	25	---	---	
10.67	15	50	---	---	Silty Sand (SM) / Sandy Silt (ML)
11.13	13	50	---	---	
11.58	25	50	---	---	
12.04	15	50	---	---	
12.50	15	50	---	---	
12.95	20	50	---	---	
13.41	15	50	---	---	
13.87	20	50	---	---	
14.33	20	50	---	---	
14.78	18	50	---	---	
15.24	18	50	---	---	
15.70	30	50	---	---	
16.15	14	50	---	---	
16.61	6	50	---	---	
17.07	6	50	---	---	
17.53	8	50	---	---	
17.98	3	50	---	---	

For the analysis at the southern abutment at the Rio Bananito Highway Bridge, an averaged profile of the SPT blowcounts and fines content was developed. Since Boring P-2 appears to have more embankment fill and denser surficial sands, only Borings P-1 and T-2 were averaged to an approximate elevation of -5.0 meters since it is assumed that these borings better represent the soil profile at the abutment itself. A plot of the averaged SPT values used for the analysis of the Rio Bananito Highway Bridge is shown in Figure 6-34.

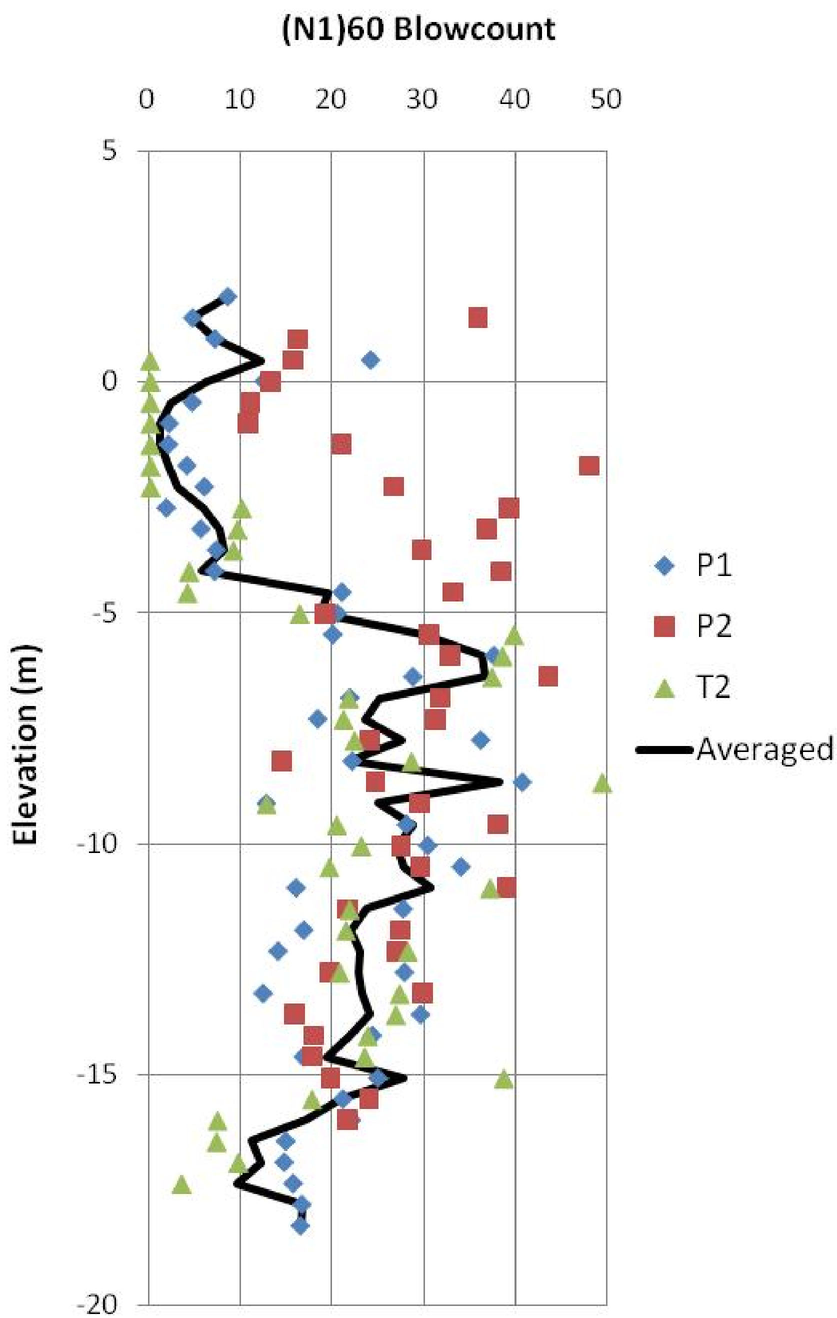

Figure 6-34: Averaged SPT blowcounts for the southern abutment at the Rio Bananito Highway Bridge

The information from Borings P-1, P-2, and T-2 was used to develop a generalized soil profile for the southern abutment of the Rio Bananito Highway Bridge. Empirical correlations with SPT blowcounts were averaged to estimate the friction angle of granular soils and non-plastic silts. These correlations include Peck et al. (1974), Hatanaka and Uchida (1996), and Bowles (1977). Relative density of granular soils was estimated using the empirical correlation presented by Kulhawy and Mayne (1990). Corrected soil modulus estimates K^* of the granular soils for use with the API (1993) p-y relationship were estimated using the recommendations presented by Boulanger et al. (2003). Undrained strength of cohesive plastic soils was averaged from empirical correlations including Hara et al. (1971), Kulhawy and Mayne (1990), and Skempton (1957). Assumptions regarding the unit weight of the native soil as well as the strength properties of the embankment fill were made. Groundwater is modeled at an elevation of 0.0 meter (i.e. an estimated depth of 4.50 meters from the top of the embankment). Table 6-6 summarizes our generalized model of the soil profile at the south abutment of the Rio Bananito Highway Bridge.

Table 6-6: Generalized soil profile for the south abutment at the Rio Bananito Highway Bridge

Top Depth (m)	Top Elevation (m)	Thickness (m)	USCS Soil Class	Friction Angle (deg)	Moist Unit Weight (kN/m3)	Undrained Strength (kPa)	Relative Density (%)	Corrected Soil Modulus (kN/m3)	Liquefied p-multiplier
0	4.50	4.00	SM (Fill)	35	18.5	---	62	24,800	NA
4.00	0.50	0.50	ML	31	18.06	---	40	9,900	NA
4.50	0.00	3.20	ML	31	8.25	---	40	9,900	0.1
7.70	-3.20	0.90	SM	31	8.25	---	40	8,400	0.1
8.60	-4.10	4.40	SM	36	9.04	---	68	18,600	NA
13.00	-8.50	6.30	SM	38	9.04	---	76	18,900	NA
19.30	-14.40	3.60	SM	33	8.44	---	50	7,900	0.16

6.5.3 Ground Motions and Liquefaction

The Rio Bananito Highway Bridge is located approximately 25 kilometers north from the epicenter of the April 22, 1991 e arthquake. Assuming an average V_{s30} value of 270 m /s, the average computed median spectral accelerations and median±1σ spectral accelerations from the four selected NGA models are shown in Figure 6-35. The median computed PGA and spectral accelerations corresponding to 0.2-second and 1.0-second are approximately 0.213g, 0.445g, and 0.290g.

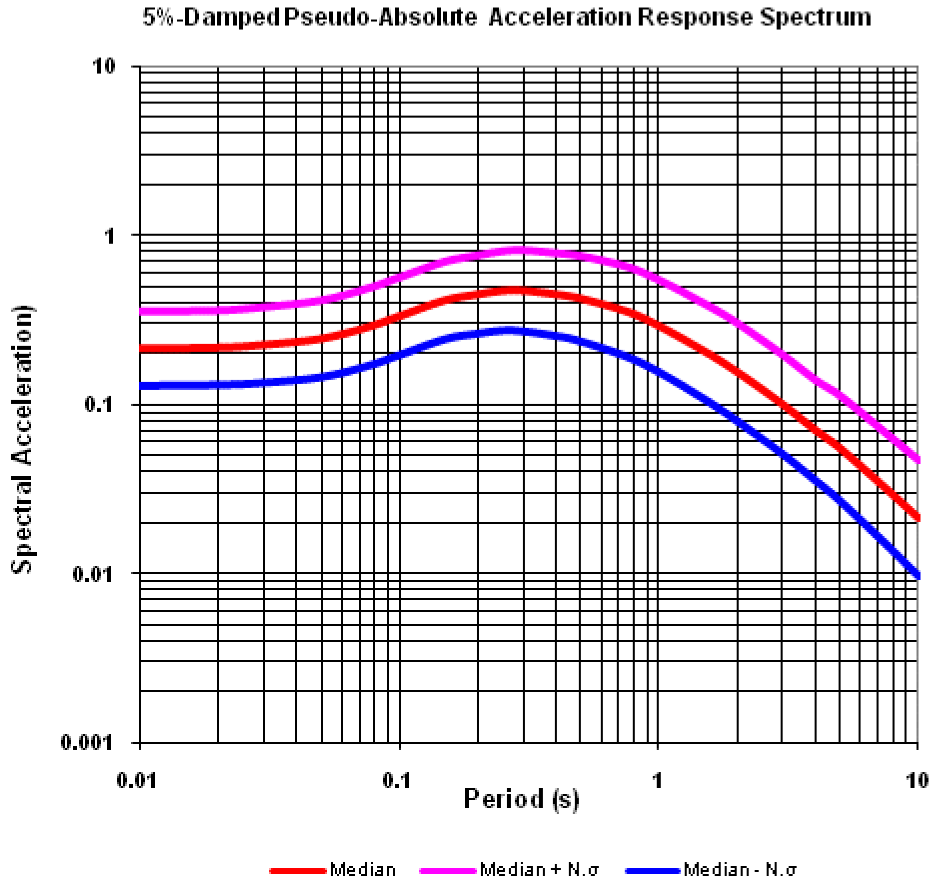

Figure 6-35: Computed deterministic response spectra for the Rio Bananito Highway Bridge from the 1991 earthquake. N = 1

Using the average deterministic ground motions from the NGA equations, the deterministic liquefaction triggering was evaluated at the Rio Bananito Highway Bridge for the M7.6 1991 Limon earthquake using the SPT blowcounts from both borings P-1 and P-2. The results of the deterministic liquefaction triggering analysis are shown in Figure 6-36 and Figure 6-37. This evaluation included consideration of the Cetin et al. (2004), Idriss and Boulanger (2008), and Youd et al. (2001) simplified procedures. In general, good agreement was observed between the three procedures. The results of the analysis at boring P-1 suggest that liquefaction triggered from depths of approximately 2.0 meters to 6.4 meters below the ground surface (EL 0.0m to EL -4.4m). In addition, thin layers of sand are shown to liquefy at about 1.5-meter intervals from depths of about 9.1 meters to 18.3 meters (EL -7.1m to EL -16.3m). The results of the analysis at boring P-2 suggest that liquefaction triggered from depths of approximately 2.6 meters to 5.5 meters below the ground surface (EL 1.6m to EL -1.2m). Though there is a small discrepancy in the elevations of the principle liquefiable layer between borings P-1 and P-2, it is clear that there is a continuous liquefiable layer near the ground surface that likely governed the observed soil deformations following the 1991 Limon earthquake.

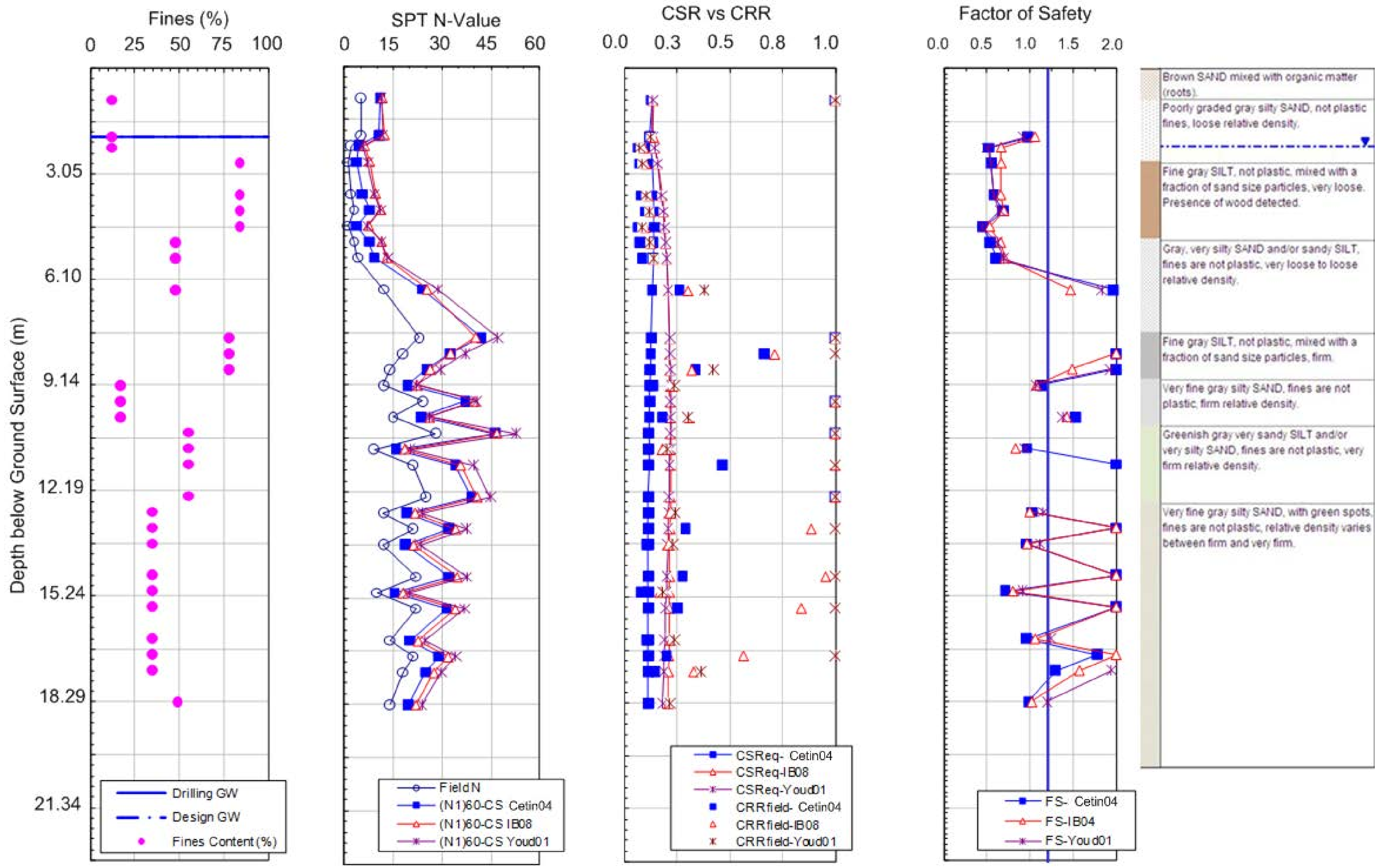

Figure 6-36: Deterministic liquefaction triggering results from Boring P-1 for the M7.6 1991 Limon earthquake at the Rio Bananito Highway Bridge

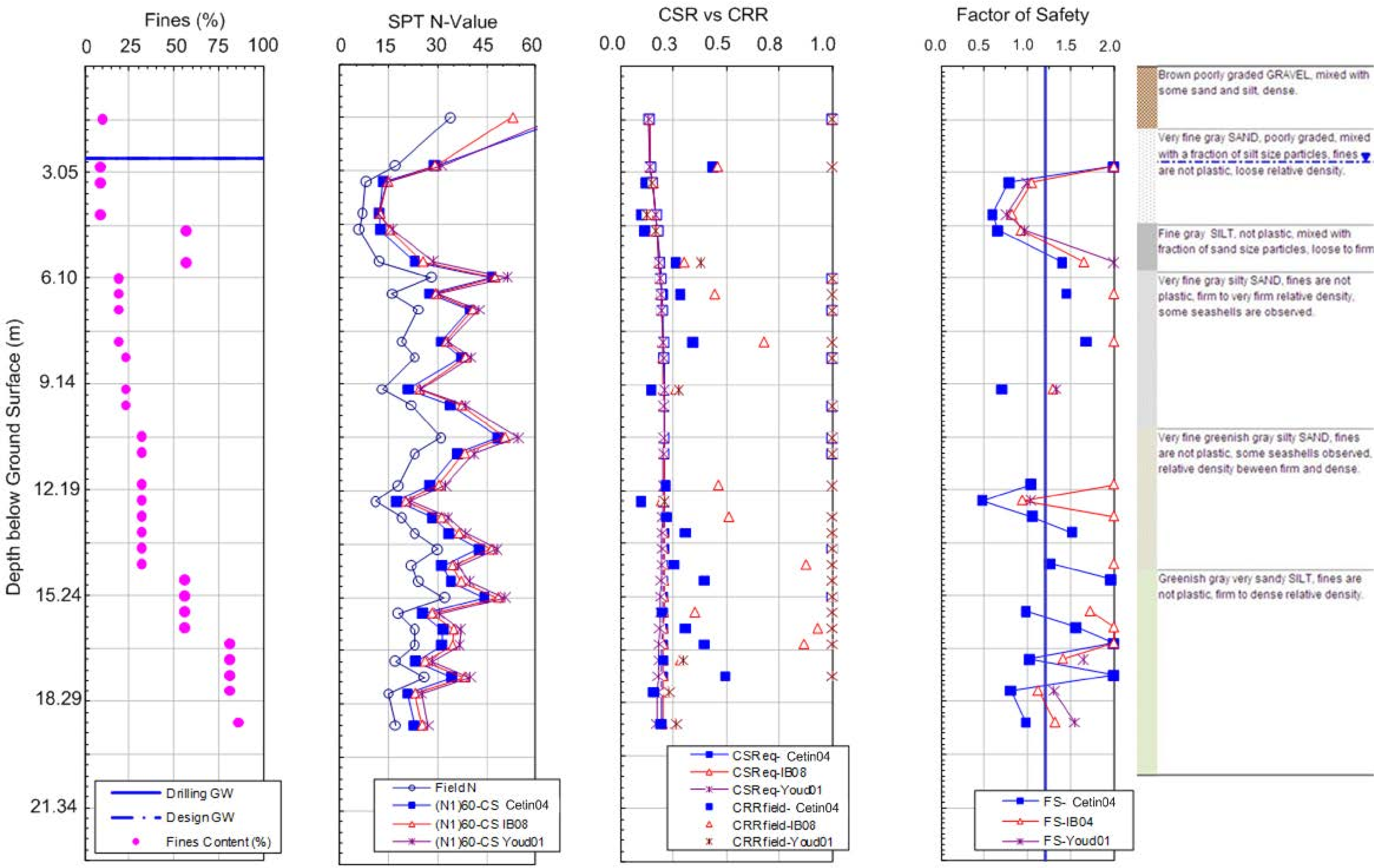

Figure 6-37: Deterministic liquefaction triggering results from Boring P-2 for the M7.6 1991 Limon earthquake at the Rio Bananito Highway Bridge

The results of our PSHA using EZ-FRISK software suggest that the seismicity at the bridge is moderate to high. The seismic hazard curve for the PGA is shown below in Figure 6-38.

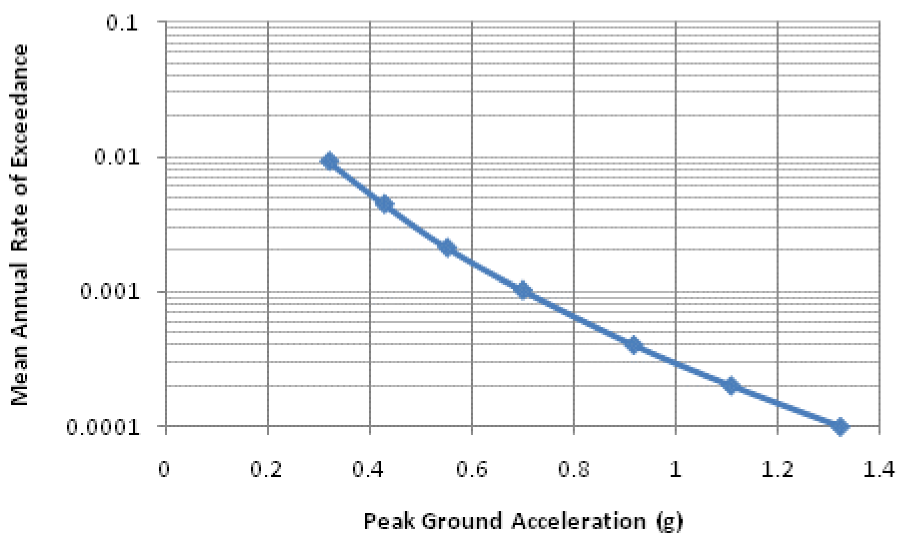

Figure 6-38: Computed seismic hazard curve for the PGA at the Rio Bananito Highway Bridge

6.5.4 Lateral Spreading

Significant ground deformations were observed at both abutments of the Rio Bananito Highway Bridge following the 1991 Limon earthquake. McGuire (1994) documented much of the observed liquefaction deformations and resulting damage to the bridge. Ground deformations, sand boils, and fissures parallel to the river were documented on both sides of the river. Fissure widths were reported to range from 0.35 meter to 1.54 meters.

No settlement, translation, or rotation was observed at the center pier of the bridge. However, both bridge spans fell off their supports on the central pier and were thrown in the direction of the skew. Both bridge abutments experienced significant deformations. The north abutment was rotated 10 degrees from vertical, fracturing five of the six piles immediately below the pile cap. The south abutment was rotated approximately 14-15 degrees from vertical. Horizontal translations at the abutment were estimated to range from 3.42 meters to 3.89 meters towards the river, and settlements on the order of 1.52 meters were measured. The rotations of the abutments indicate that the bridge spans acted as a strut load limiting the horizontal deformations at the abutments prior to the spans falling into the river. Once the spans fell into the river, eyewitness reports indicated that the abutments immediately displaced towards the river.

This study focuses solely on the southern abutment of the Rio Bananito Highway Bridge. McGuire (1994) documented that significant horizontal and vertical soil deformations were observed within a distance of approximately 43 meters south of the southern abutment, where a stark "boundary" consisting of a 2.0-meter high scarp was observed. Almost no evidence of liquefaction-related damage at the ground surface was observed south of this scarp. North of this scarp, horizontal soil deformations in the free-field were measured and estimated to be approximately 5.13 meters. The difference in soil deformations between those measured in the free-field and those measured behind the abutment is likely due to the reinforcing strut load provided by the bridge deck prior to it falling into the river.

The relatively large amount of both horizontal and vertical deformations observed near the southern abutment of the Rio Bananito Railway Bridge leads us to suspect that liquefaction flow failure may have occurred rather than lateral spreading. This hypothesis was investigated using a simple two-dimensional limit equilibrium post-liquefaction slope stability analysis. This analysis only considered the stability of the native soil slopes and neglected the presence of the approach embankment. A factor of safety less than 1.0 would suggest that the native soils would flow upon the initiation of liquefaction. The results of this analysis are shown in Figure 6-39. Residual strengths for the liquefied soil were estimated from the mean normalized residual strength ratio relationship as recommended by Ledezma and Bray (2010).

The post-liquefaction factor of safety was computed to be 0.77, which is significantly less than 1.0. Therefore, the lateral soil deformations observed at the southern abutment of the Rio Bananito Highway Bridge were likely caused by liquefaction flow failure and not lateral spreading. Such a finding would have significant impact on design if the bridge were being evaluated for seismic stability using modern design standards. While engineers currently have many methodologies for estimating lateral spreading displacements, few reliable and practical methodologies currently exist for engineers to estimate displacements due to liquefaction flow failures. Therefore, if liquefaction flow failure is determined to pose a significant threat of occurring, the standard of practice in most locations currently requires that liquefaction mitigation techniques be implemented to prevent liquefaction from triggering. Such mitigation usually involves the installation of soil ground improvement and the implementation of stabilization alternatives such as a berm.

Because it is likely that liquefaction flow failure caused the ground deformations and resulting damage to the bridge at the southern abutment, the Rio Bananito Highway Bridge was not analyzed in the performance-based lateral spreading framework presented in this report. However, a deterministic pile response analysis was performed to attempt to replicate the damage that was observed at the southern abutment following the 1991 Limon earthquake.

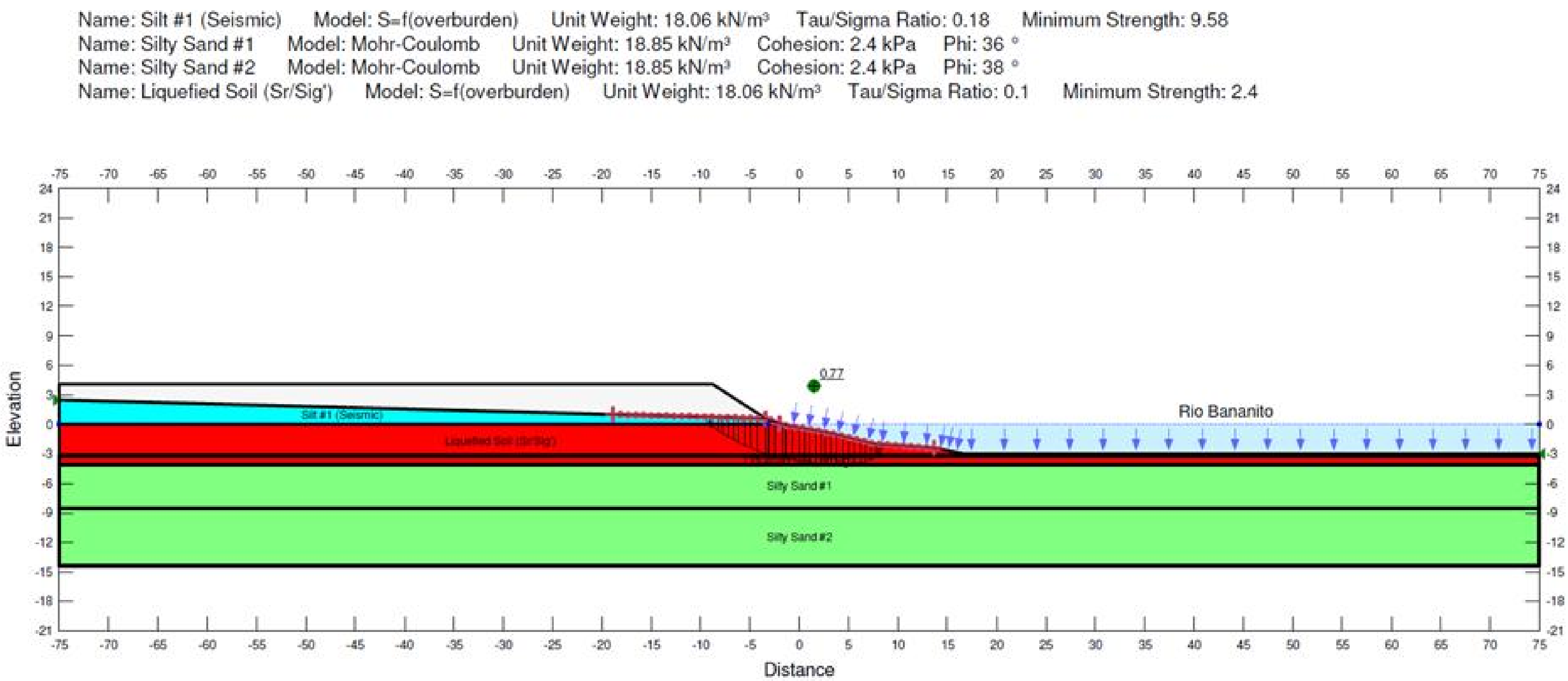

Figure 6-39: Post-liquefaction slope stability analysis at the southern bank of the Rio Bananito River

6.5.5 Deterministic Pile Response Analysis

To evaluate the deterministic pile response at the southern abutment of the Rio Bananito Highway Bridge, a two-stage analysis was performed. The first stage of the analysis evaluated the initial deformation of the soil in which the bridge deck stayed in place and behaved as a reinforcing strut load. The second stage of the analysis evaluated the final deformation of the soil after the bridge deck fell off its supports.

In the first stage of the analysis, the magnitude of lateral deformations which occurred to cause the pile cap to rotate 14-15 degrees was unknown. Therefore, an iterative procedure was performed in LPILE in which the magnitude of soil deformation was modified incrementally until a pile cap rotation of 14-15 degrees was achieved. The zone of lateral soil deformation was limited to Elevations 0.0 meters to -4.1 meters and was distributed with depth in accordance with the procedure described in Section 2.7 of this report. A reinforcing strut was included in the analysis in the same manner as was described in Section 6.3.5. It was found that a pile cap rotation of 14.5 degrees was obtained when a soil displacement of 0.6 meter was applied to the modeled system. The deterministic pile response results from the first stage are shown in Figure 6-40.

In the second stage of the analysis, a total of 3.89 meters of soil movement were added to the soil movements from the first stage (i.e. 0.6 meter). No additional strut loads were added to account for the bridge deck falling into the river. Therefore, a total of 4.49 meters of soil movement were applied to the model. The deterministic pile response results from the second stage are shown in Figure 6-41. The computed horizontal displacement at the top of the pile cap at the end of the second stage of analysis was 3.89 meters, and the pile cap rotation was 14.5 degrees. These results match the measured pile response at the southern abutment following the 1991 Limon earthquake.

While the results of this deterministic analysis are simplified in that they do not account for the vertical deformations that occurred at the bridge abutment, assuming that the flow failure displacements behave similarly to lateral spreading displacements, and are based on back-calculated soil deformations, they demonstrate that modern p-y pile response analysis methodologies can reasonably model the kinematic pile response of even moderately complex systems given adequate information regarding the system itself.

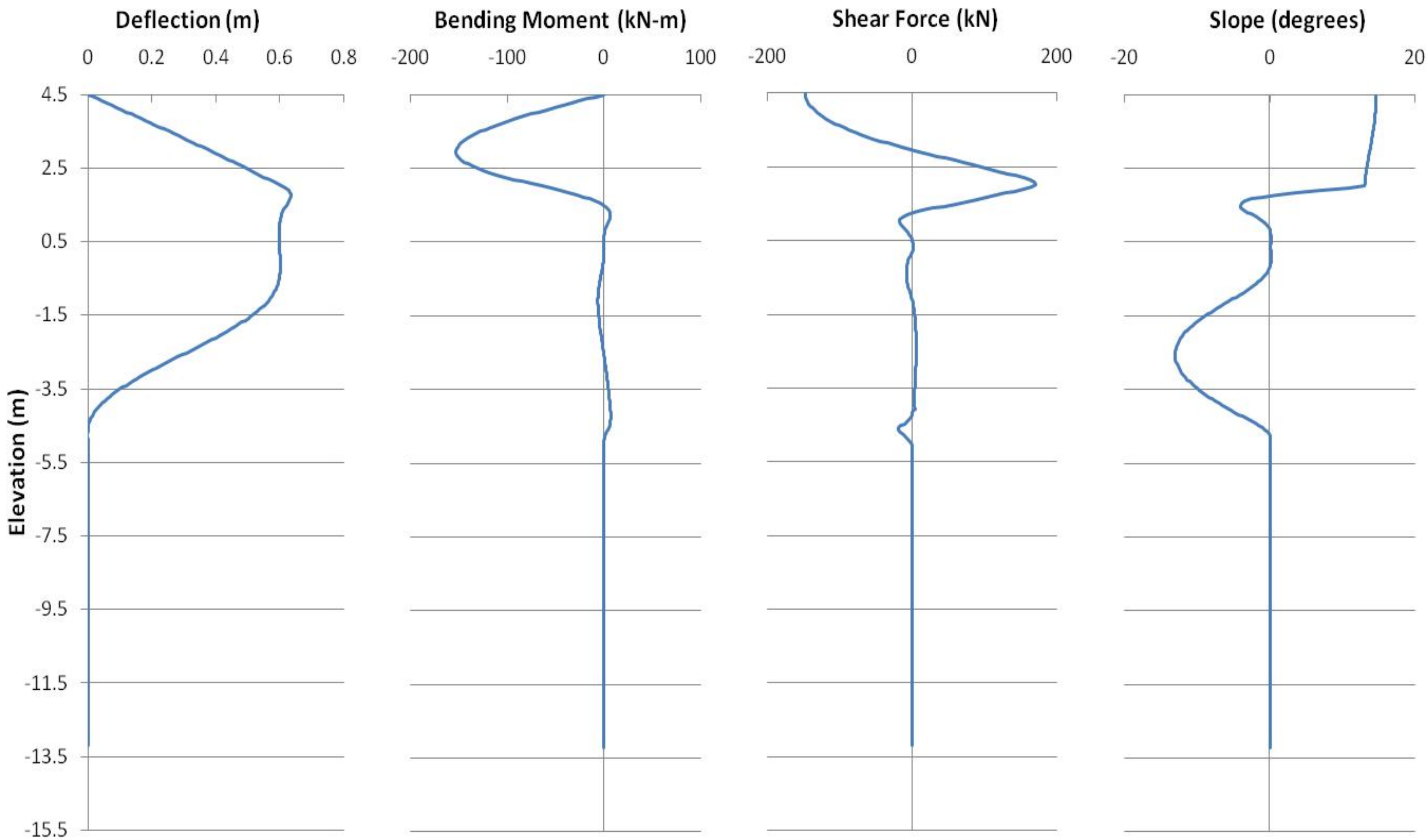

Figure 6-40: Deterministic computed pile response for the Rio Bananito Highway Bridge south abutment before bridge deck fell from its supports

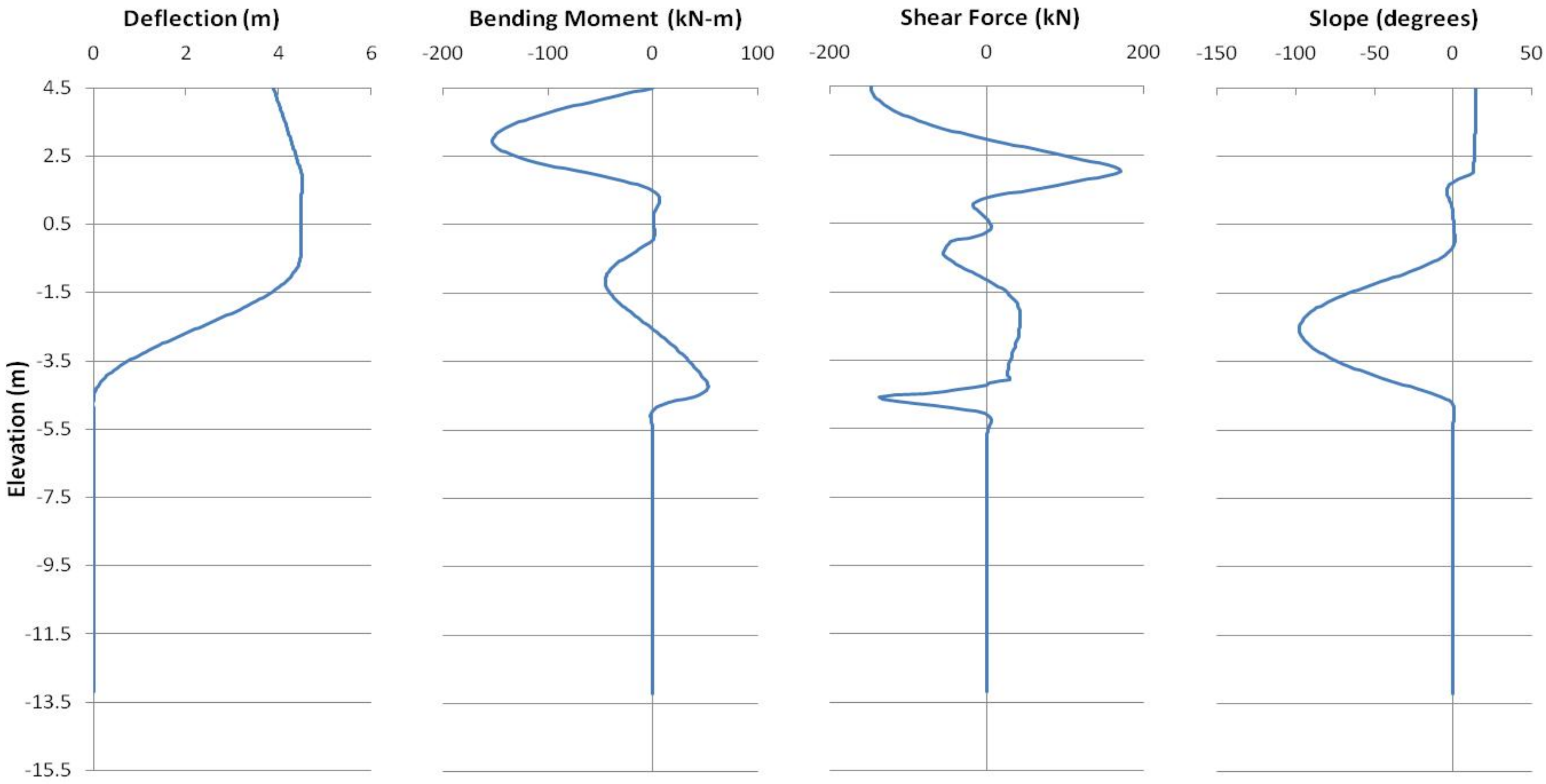

Figure 6-41: Deterministic computed pile response for the Rio Bananito Highway Bridge south abutment after the bridge deck fell from its supports

6.6 Rio Bananito Railway Bridge

The railway bridge over the Rio Bananito is single-span truss bridge supporting the rail line from Bananito Norte to Bananito Sur. The bridge is located about 15 kilometers upstream from the Rio Bananito Highway Bridge and is the only structure crossing the Rio Bananito upstream from the highway Route 36 at the coast (McGuire, 1994). Today, the bridge is used as both a road and a railway crossing over the Rio Bananito. At the time of the earthquake, the bridge was used primarily for the rail transport of bananas to ports on the east coast of Costa Rica. The latitudinal and longitudinal coordinates for the bridge are 9.8765° North 83.0076° West.

According to bridge drawings from the Costa Rica Ministry of Transportation, the bridge was constructed some time prior to 1890. The through-truss bridge is approximately 50 meters in length, and each abutment is founded on two elliptically-shaped caissons that are 1.46 meters by 2.16 meters across the major axes (EERI, 1993). The caissons are constructed of a 12 mm steel shell composed of narrow sheet pile segments which were filled with concrete. Details regarding internal reinforcement of the caissons, if any, are unknown. For this study, it was assumed that no internal steel reinforcement was used in the concrete. The results of a dynamic wave equation analysis of the pile performed by Insuma S.A. during our field investigation in April 2010 suggested that the caissons are approximately 12 meters in length. At the time of the 1991 earthquake, the bridge was simply supported by these caissons and secured with a simple seating plate. The bridge has an at-grade crossing with no approach embankment for the rail.

6.6.1 Surface Conditions and Bridge Geometry

The surface geometry at the Rio Bananito Railway Bridge is relatively flat in the surrounding river plain, but steep in the river channel itself. Because the bridge plans provided by the Costa Rica Ministry of Transportation did not include any absolute elevations of the bridge structure, all of our measured elevations are relative to a datum point near the south abutment of the bridge and equal to an arbitrary elevation of 100 meters. According to our GPS site survey in April 2010, the relative ground surface elevation at each abutment is approximately 98 meters. From our estimation, the approximate relative ground surface elevation of the bottom of the river is 91 meters. The approximate slope of the river channel is 1.5H:1V. We estimated the relative elevation of the water surface in the Rio Bananito to be approximately 93 meters at the time of our investigation. Several houses and a soccer field lie adjacent to the northern abutment, and a few houses are located near the southern abutment.

A sketch of the profile and relative elevation contours based on our 2010 GPS site survey and the bridge plans provided by the Costa Rica Ministry of Transportation is presented in .

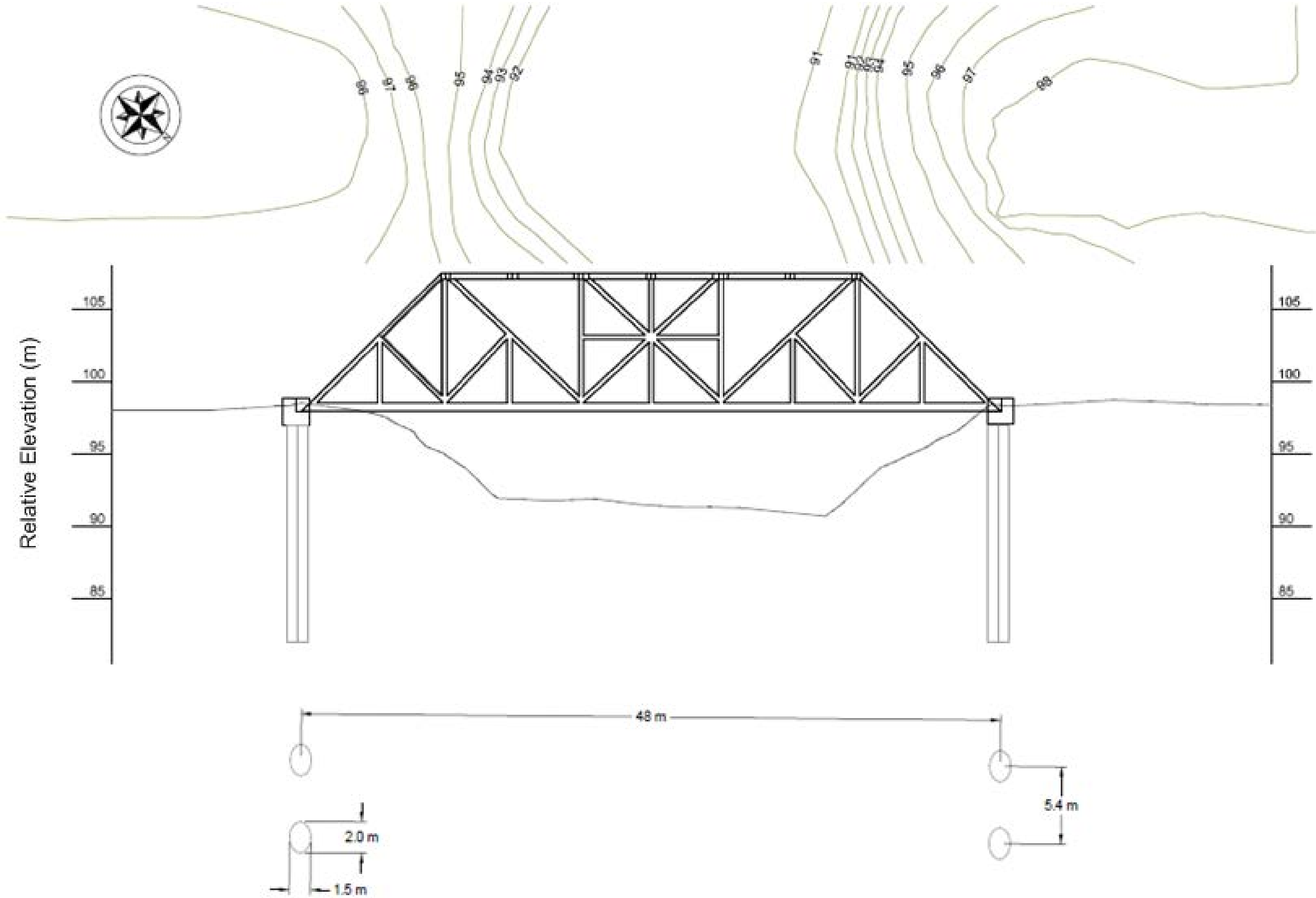

Figure 6-42: Simplified sketch of the plan and profile views of the Rio Bananito Railway Bridge

6.6.2 Subsurface Conditions

Insuma S.A. Geotechnical Consultants performed two borings in the vicinity of the northern abutment. Boring P-1 was performed approximately 200 feet from the northern abutment and was extended to an approximate depth of 14 meters. Boring P-2 was performed about 20 meters to the north of Boring P-1 and was extended to an approximate depth of 14 meters. The soils encountered in the borings were reported to consist primarily of very soft to soft clays near the ground surface overlying loose to medium-dense clayey or silty sands. The clays encountered appeared to have medium to high plasticity. The sands encountered appeared to be fine-grained and varied in fines content from about 14-percent to 23-percent.

The relative elevation of the ground surface at Boring P-1 was measured to be approximately 96.5 meters, and the relative elevation of the ground surface at Boring P-2 was measured to be approximately 97.9 meters. Groundwater was reported by the drillers at an approximate depth of 5.65 meters in Boring P-1 and 6.65 meters in Boring P-2, which correspond to approximate relative elevations of 90.8 meters and 91.2 meters, respectively. It is not unexpected that these relative elevations reported for groundwater appear low since piezometers were not used to obtain a more accurate measurement of the groundwater level and since the native soils represented very low-permeability fat clays. Simple diagrams of the soils encountered in the borings performed are shown in Figure 6-43 and Figure 6-44 below. Further details regarding the borings at the Rio Bananito Railway Bridge and the corresponding laboratory test results can be found in the Insuma Geotechnical Report included as Appendix A of this report.

Depth (m)	SPT N Value	
0.00 - 0.45	26	Fill that consists in a mixture of GRAVEL and silt.
0.45 - 0.90	11	
0.90 - 1.35	6	Brown clayey SAND, mixed with some gravel, loose.
1.35 - 1.80	4	
1.80 - 2.25	4	
2.25 - 2.70	4	
2.70 - 3.15	4	
3.15 - 3.60	1	Brown plastic CLAY, medium to high plasticity, very soft to soft consistency.
3.60 - 4.05	0	
4.05 - 4.50	0	
4.50 - 4.95	1	
4.95 - 5.40	2	
5.40 - 5.85	3	Greenish gray plastic CLAY, mixed with a fraction of sand size particles, soft.
5.85 - 6.30	7	
6.30 - 6.75	7	
6.75 - 7.20	7	Gray or brownish gray clayey SAND, mixed with particles of gravel, fines with medium plasticity, loose to dense relative density.
7.20 - 7.65	15	
7.65 - 8.10	20	
8.10 - 8.55	8	
8.55 - 9.00	24	
9.00 - 9.45	36	
9.45 - 9.90	20	
9.90 - 10.35	16	Greenish gray clayey SAND, fines with low to medium plasticity, predominantly medium relative density.
10.35 - 10.80	19	
10.80 - 11.25	21	
11.25 - 11.70	25	
11.70 - 12.15	23	
12.15 - 12.60	6	
12.60 - 13.05	17	
13.05 - 13.50	24	
13.50 - 13.95	18	

Figure 6-43: Boring P-1 performed at the Rio Bananito Railway Bridge

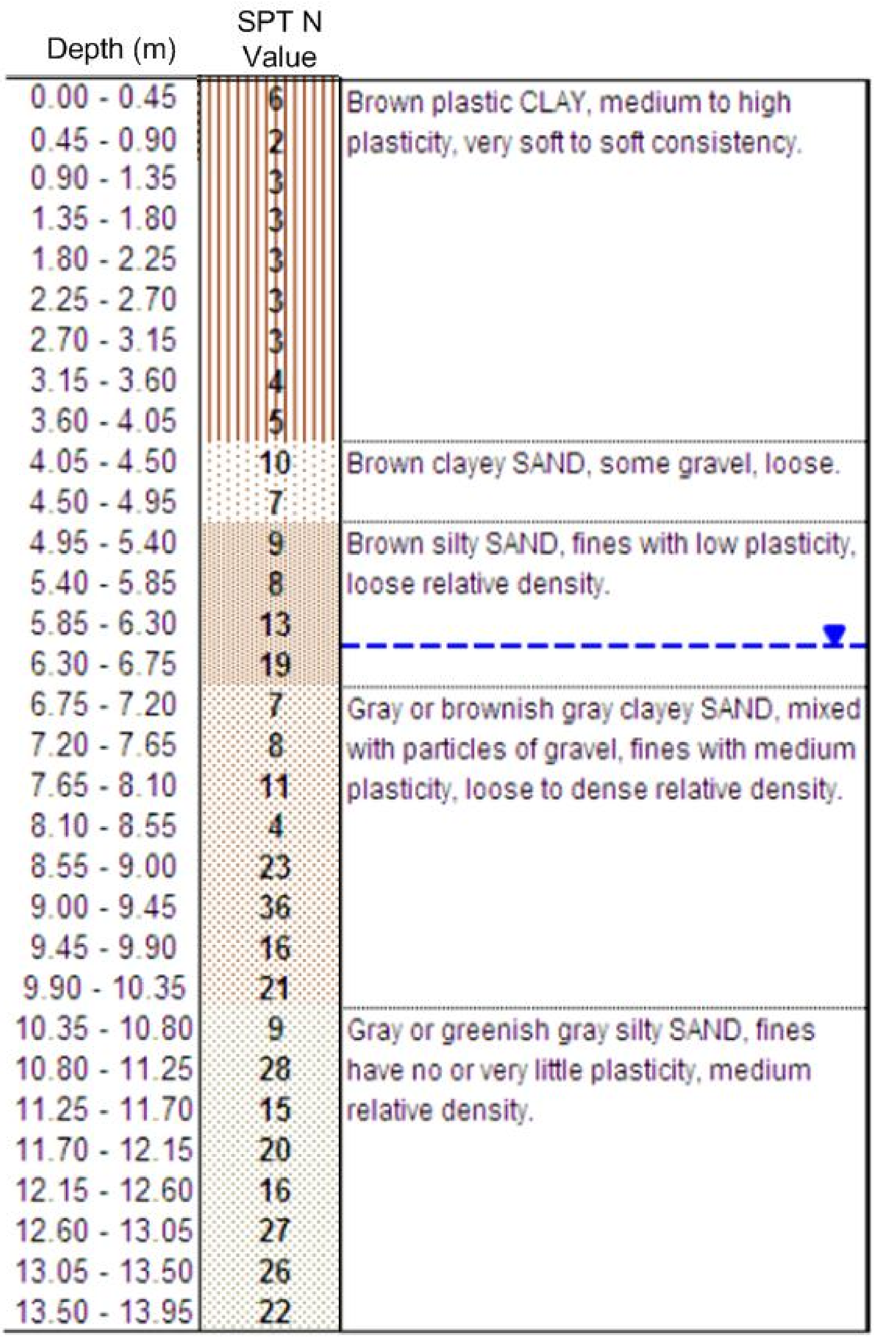

Figure 6-44: Boring P-2 performed at the Rio Bananito Railway Bridge

For the analysis at the northern abutment at the Rio Bananito Railway Bridge, an averaged profile of the SPT blowcounts and fines content was developed. A plot of the averaged SPT values used for the analysis of the Rio Bananito Railway Bridge is shown in Figure 6-45. From Relative Elevation 96 meters to 91.3 meters, some variability between Borings P-1 and P-2 was observed in the surficial clays. This observation suggests that there are likely some relatively small alluvial deposits of sand scattered throughout the clay layer. Therefore, engineering judgment was applied in modifying the averaged SPT blowcounts in order to better represent a generalized clay layer for modeling purposes.

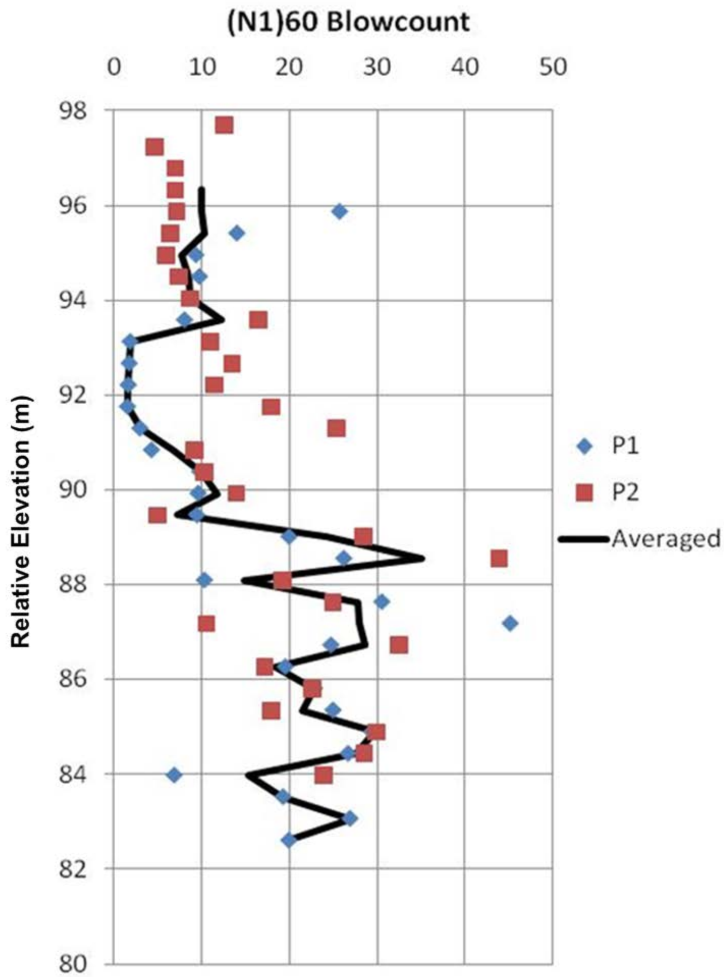

Figure 6-45: Averaged SPT blowcounts for the north abutment at the Rio Bananito Railway Bridge

The information from Borings P-1 and P-2 was used to develop a generalized soil profile for the northern abutment of the Rio Bananito Railway Bridge. Empirical correlations with SPT blowcounts were averaged to estimate the friction angle of granular soils. These correlations include Peck et al. (1974), Hatanaka and Uchida (1996), and Bowles (1977). Relative density of granular soils was estimated using the empirical correlation presented by Kulhawy and Mayne (1990). Corrected soil modulus estimates K^* of the granular soils for use with the API (1993) p-y relationship were estimated using the recommendations presented by Boulanger et al. (2003). Undrained strength of cohesive plastic soils was averaged from empirical correlations including Hara et al. (1971), Kulhawy and Mayne (1990), and Skempton (1957).

Field measurements of the shear strength of the surficial clays were also performed using simplified tests including the torvane and the pocket penetrometer. These field measurements showed remarkably good agreement for the clays between Relative Elevations 91 meters and 94 meters (i.e. up to 3 meters in height above the water level). At relative elevations higher than 94 meters, the field measurements showed greater shear strengths and more variability between the torvane and the pocket penetrometer. This trend could be due to dessication of the near-surface soils and/or increased sand content in the clay. In addition, shear strength parameters using Stress History and Normalized Soil Engineering Properties (SHANSEP) theory (Ladd and Foott, 1974) were estimated by fitting the parameters to the available field measurements and SPT correlations. Greater weight was given to the field measurements due to the reasonably good agreement between the torvane and pocket penetrometer results. The shear strength measurements using the various approaches described above are shown in Figure 6-46. The computed values of *S*, *OCR*, and *m* for the SHANSEP parameters are 0.25, 1.8, and 0.85, respectively. A minimum undrained shear strength value of 20 kPa could be assigned due to the high plasticity of the clay. For simplification, a uniform undrained strength of 27 kPa was used in the kinematic pile response analyses for this study.

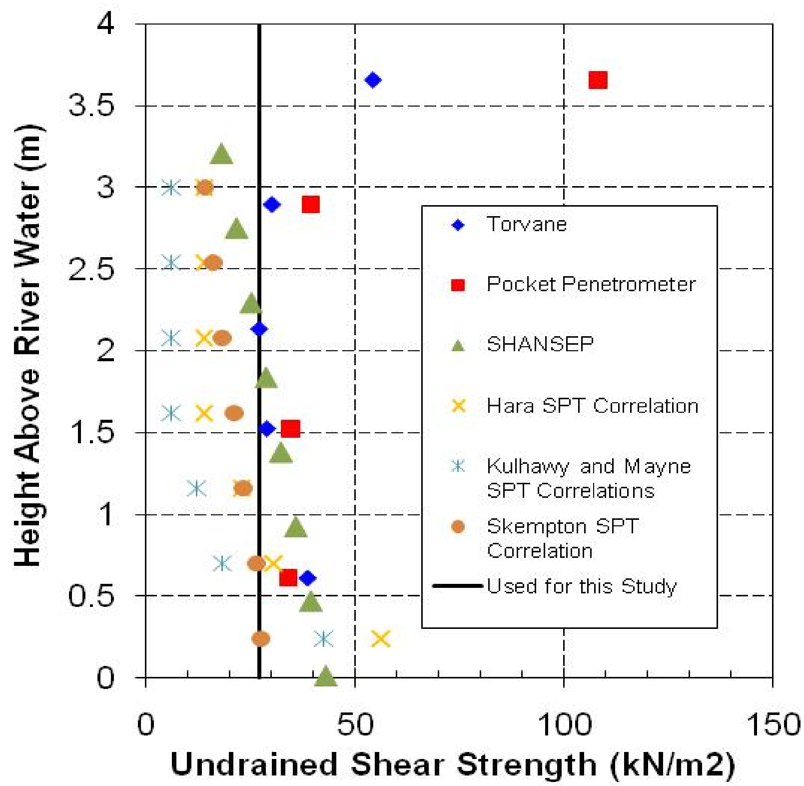

Figure 6-46: Shear strength data from the north abutment at the Rio Bananito Railway Bridge

Assumptions regarding the unit weight of the native soil as well as the strength properties of the embankment fill were made. Groundwater was modeled at an elevation of 91 meters (i.e. an estimated depth of 7.0 meters below the ground surface). Table 6-7 summarizes our generalized model of the soil profile at the north abutment of the Rio Bananito Railway Bridge.

Table 6-7: Generalized soil profile for the north abutment at the Rio Bananito Railway Bridge

Top Depth (m)	Top Elevation (m)	Thickness (m)	USCS Soil Class	Friction Angle (deg)	Moist Unit Weight (kN/m3)	Undrained Strength (kPa)	Relative Density (%)	Corrected Soil Modulus (kN/m3)	Liquefied p-multiplier
0	98.0	6.0	CH	---	18.85	27	---	---	NA
6.0	91.0	1.4	SC	32	8.25	---	45	8,800	0.12
7.4	89.6	3.7	SC/SM	37	9.00	---	68	16,200	0.43
11.1	85.9	2.8	SC/SM	35	9.00	---	58	11.150	0.28

6.6.3 Ground Motions and Liquefaction

The Rio Bananito Railway Bridge is located approximately 22 kilometers north from the epicenter of the April 22, 1991 e arthquake. Assuming an average V_{s30} value of 270 m/s, the average computed median spectral accelerations $\pm 1\sigma$ from the four selected NGA models are shown in Figure 6-47. The median computed PGA and spectral accelerations corresponding to 0.2-second and 1.0-second are approximately 0.232g, 0.483g, and 0.318g.

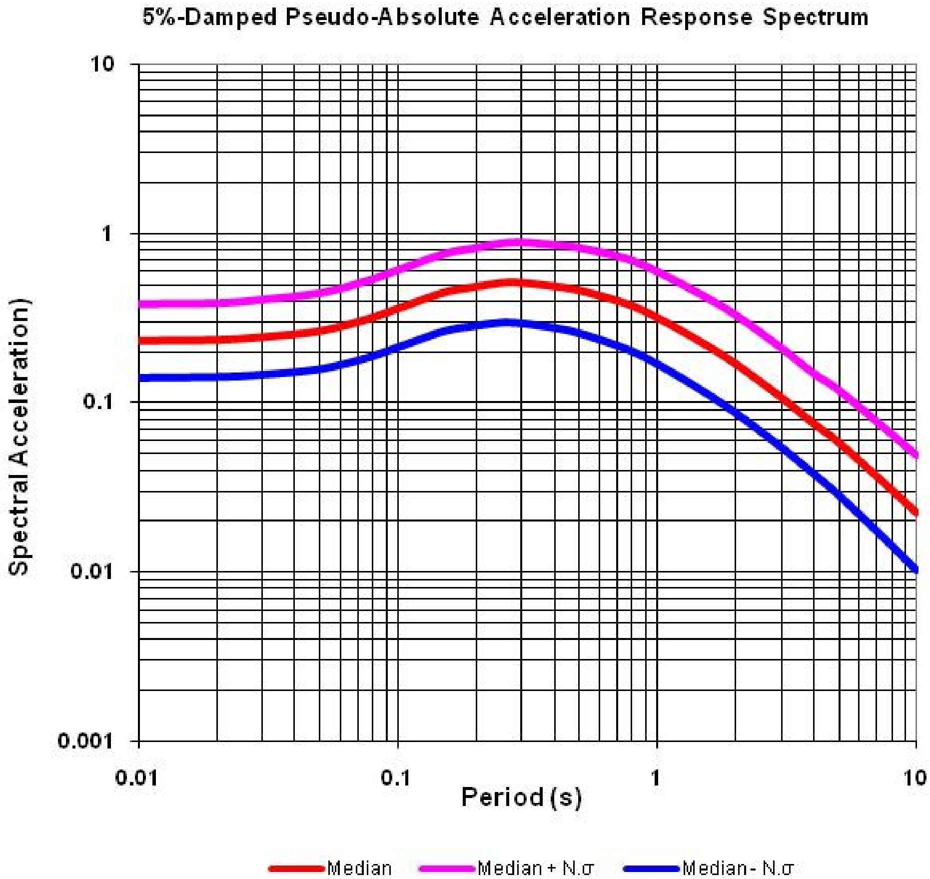

Figure 6-47: Computed deterministic response spectra for the Rio Bananito Railway Bridge from the 1991 earthquake. N = 1

Using the average deterministic ground motions from the NGA equations, the deterministic liquefaction triggering was evaluated at the Rio Bananito Railway Bridge for the M7.6 1991 Limon earthquake using the SPT blowcounts from both Borings P-1 and P-2. The results of the deterministic liquefaction triggering analysis are shown in Figure 6-48 and Figure 6-49. This evaluation included consideration of the Cetin et al. (2004), Idriss and Boulanger (2008), and Youd et al. (2001) simplified procedures. In general, good agreement was observed between the three procedures. The results of the analysis at Boring P-1 suggest that liquefaction triggered from depths of approximately 6.9 meters to 7.3 meters below the ground surface (R.EL 89.6m to R.EL 89.2m) and from depths of approximately 7.8 meters to 8.2 meters below the ground surface (R.EL 88.7m to R.EL 88.3m). In addition, occasional thin layers of sand are shown to liquefy below depths of about 12.3 meters (R.EL 84.2m). The results of the analysis at Boring P-2 suggest that liquefaction triggered from depths of approximately 7.0 meters to 8.9 meters below the ground surface (R.EL 90.8m to R.EL 88.9m). In addition, occasional thin layers of sand are shown to liquefy below depths of about 10.7 meters (R.EL 87.1m). Though there is a small discrepancy in the elevations of the principle liquefiable layers between Borings

P-1 and P-2, it is likely that there is a continuous liquefiable layer near the ground surface that likely governed the observed soil deformations following the 1991 Limon earthquake.

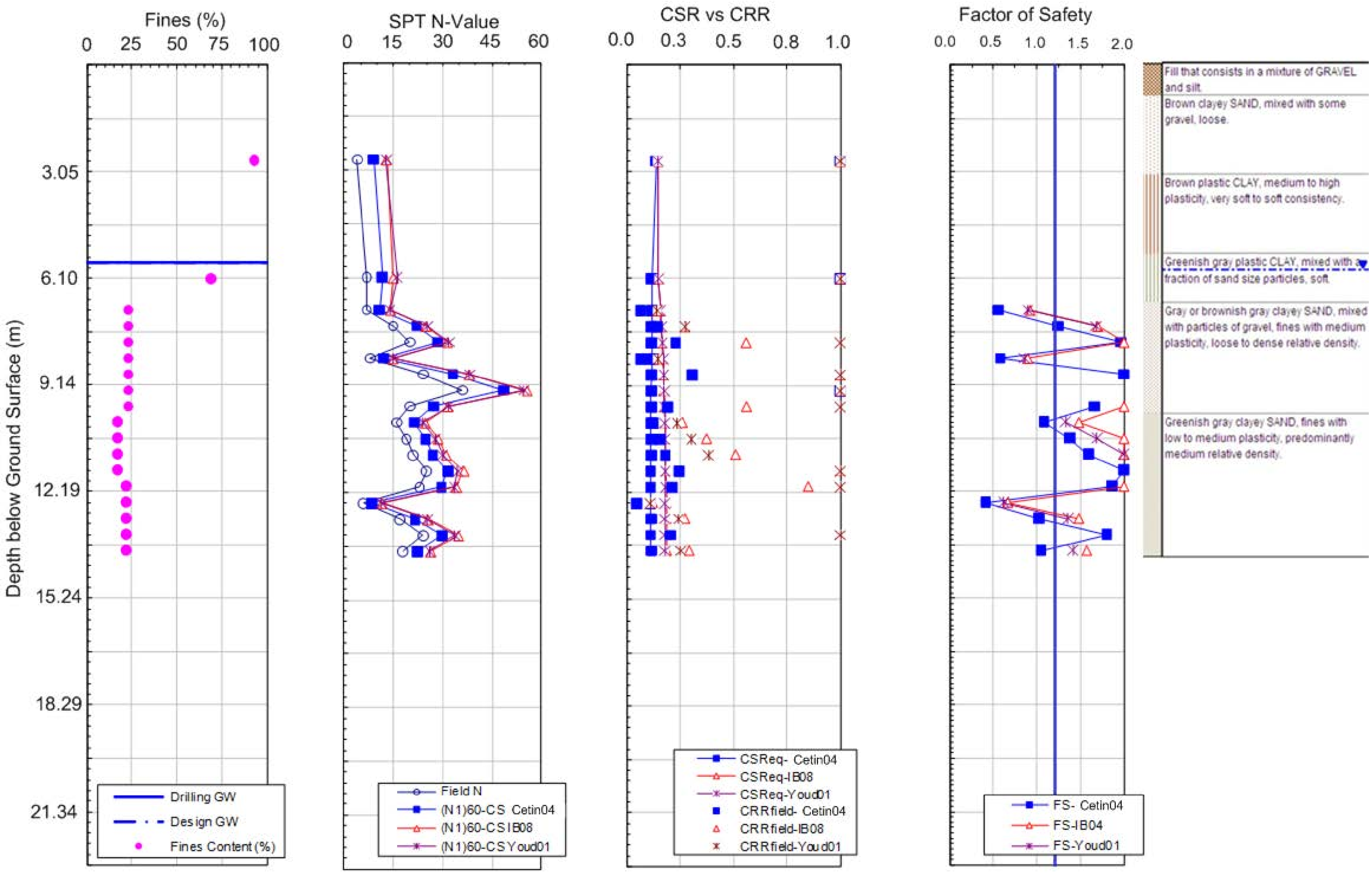

Figure 6-48: Deterministic liquefaction triggering results from Boring P-1 for the M7.6 1991 Limon earthquake at the Rio Bananito Railway Bridge

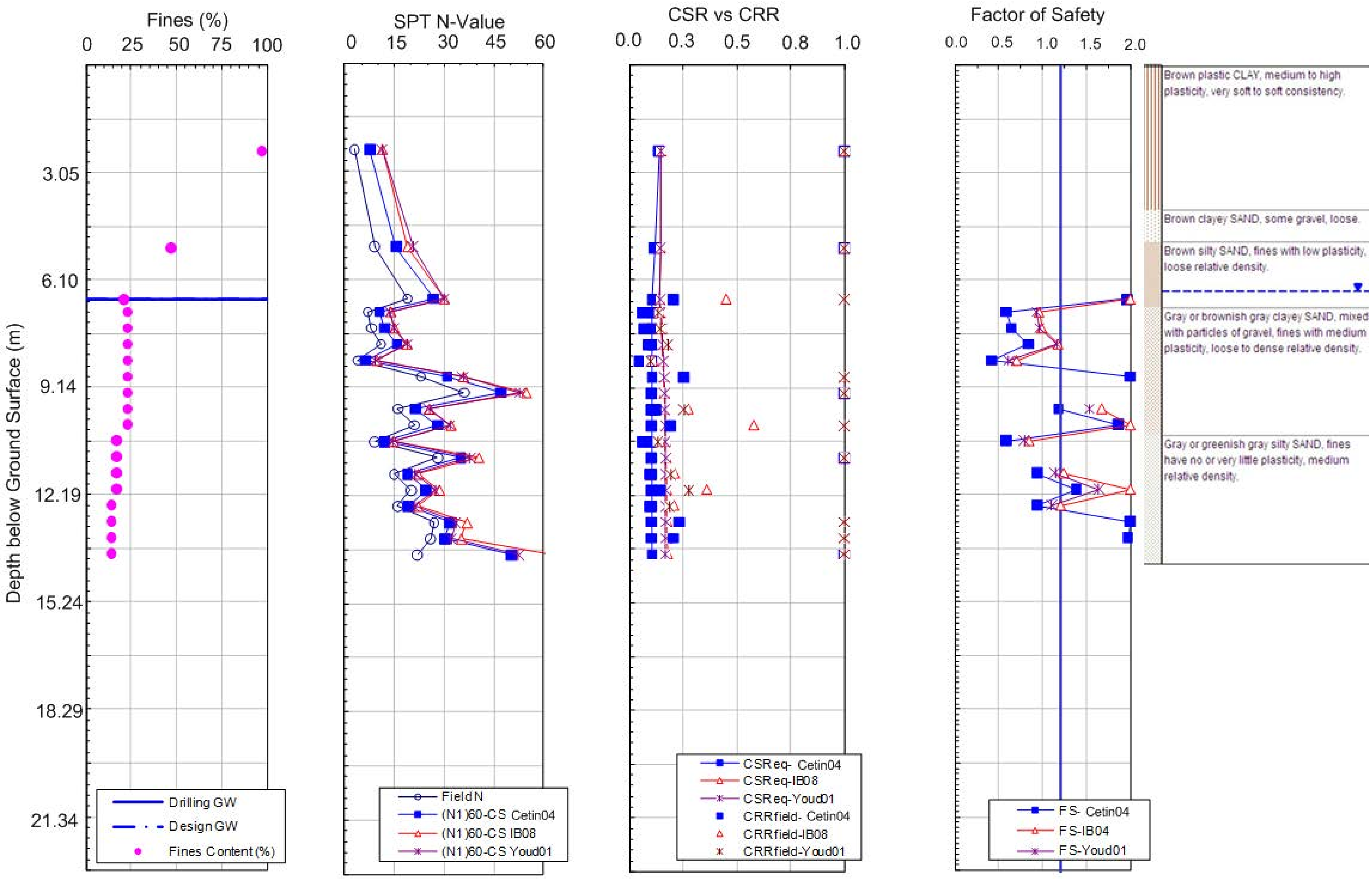

Figure 6-49: Deterministic liquefaction triggering results from Boring P-2 for the M7.6 1991 Limon earthquake at the Rio Bananito Railway Bridge

The results of our PSHA using EZ-FRISK software suggest that the seismicity at the bridge is moderate to high. The seismic hazard curve for the PGA is shown below in Figure 6-50.

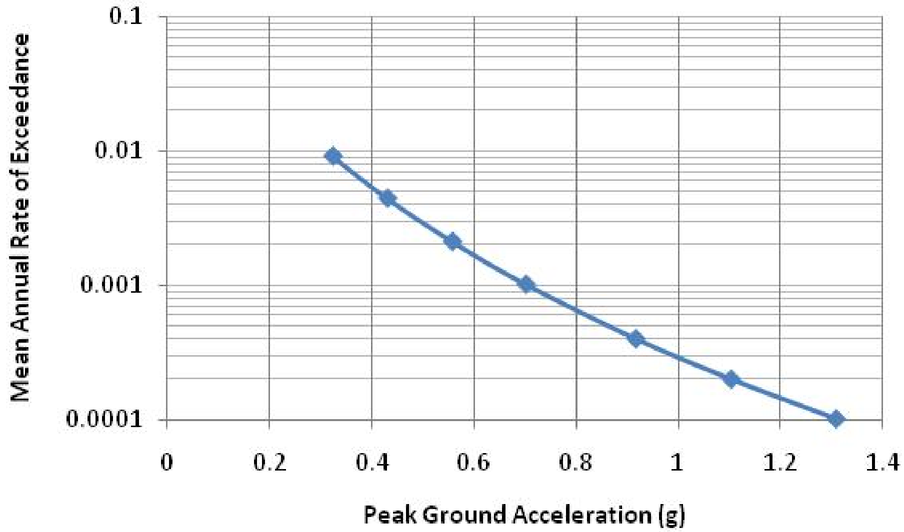

Figure 6-50: Computed seismic hazard curve for the PGA at the Rio Bananito Railway Bridge

The magnitude/distance deaggregations as estimated by EZ-FRISK for the PGA are shown in Figure 6-51. These magnitude deaggregations are used in conjunction with the seismic hazard curve for the PGA shown in Figure 6-50 to perform the performance-based liquefaction triggering analysis according to the Kramer and Mayfield (2007) procedure. The performance-based factors of safety against liquefaction for various return periods are shown in Figure 6-52. These factors of safety were computed using the averaged SPT blowcount information for Rio Bananito Railway Bridge as shown in Figure 6-45. A factor of safety less than or equal to 1.2 was assumed to be liquefiable for this study. Note that for fine-grained soil layers not considered susceptible to liquefaction due to plasticity, a generic factor of safety against liquefaction equal to 2.0 was assigned regardless of return period. A maximum factor of safety equal to 4.0 was assigned to layers with very high resistance to liquefaction triggering. In general, Figure 6-52 shows that for return periods greater than about 108 years, liquefaction triggers from depths of about 6.0 meters to 7.4 meters (EL. 91.0m to 89.6m) below the ground surface. At much higher return periods (i.e. >2,475 years), liquefaction was also computed to trigger in various soil layers below depths of about 10 meters (EL 87m).

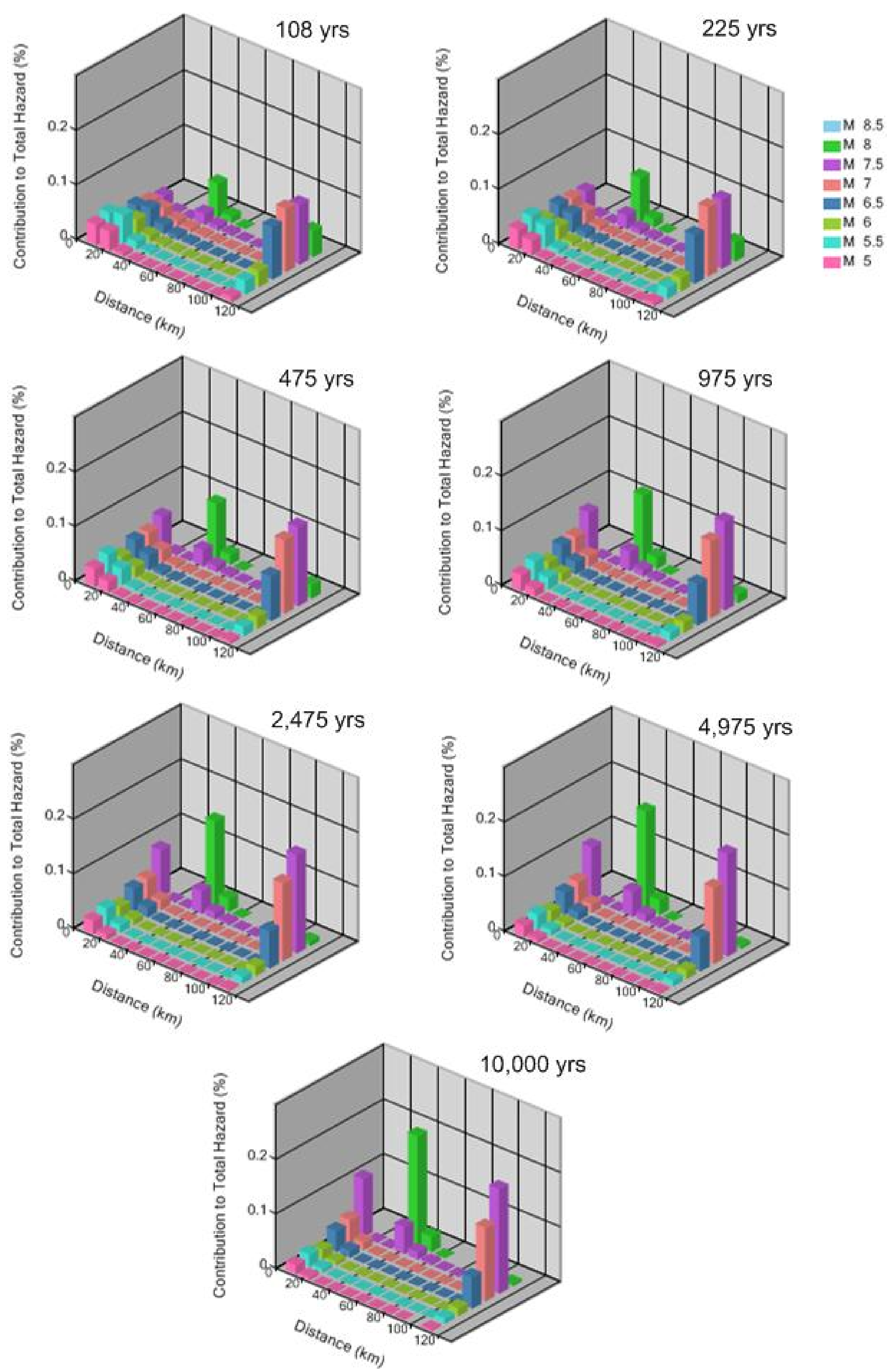

Figure 6-51: Magnitude/distance deaggregations for the PGA at the Rio Bananito Railway Bridge

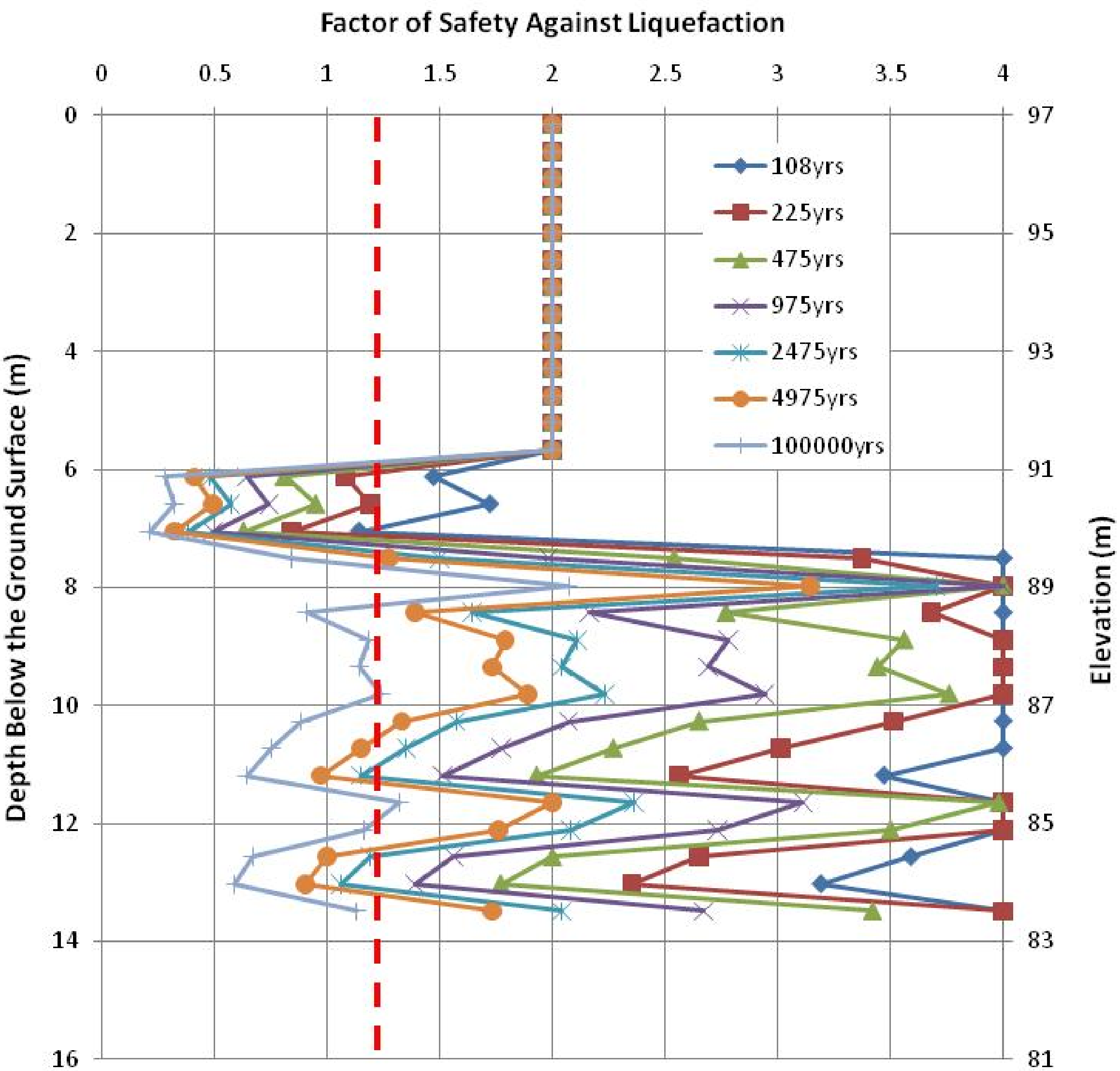

Figure 6-52: Performance-based liquefaction triggering results for the averaged SPT blowcounts at the Rio Bananito Railway Bridge

6.6.4 Lateral Spreading

EERI (1993) and McGuire (1994) documented much of the observed lateral spreading displacements and resulting damage to the Rio Bananito Railway Bridge following the 1991 Limon Earthquake. Survey measurements of the damaged bridge at the north abutment indicate lateral displacements of 4.3 and 5.7 meters (rotations of 26 and 37 degrees) for the east and west caissons, respectively. Measurements at the south abutment indicate lateral displacements of 2.83 and 1.9 meters (rotations of 19 and 7 degrees) for the east and west caissons, respectively. Survey measurements of the north abutment wall indicated lateral deformations between 2.0 and 2.5 meters, while measurements of the south abutment wall indicated lateral deformations between 1.0 and 1.5 meters. Survey measurements of the boundary lines of a soccer field just northwest of the north abutment indicated riverward (i.e. southward) surface deformations as large as 3.854 meters and eastward surface deformations as great as 1.860 meters. Finally, measurement and cumulative summation of the fissures in the ground suggest a total lateral deformation of 4.171 meters at the north river bank. Therefore, the total lateral spreading displacement that occurred at the north river bank at the Rio Bananito Railway Bridge was between 2.0 and 4.171 meters.

Empirical evaluation of the free-field soil displacements due to lateral spreading was performed using the Youd et al. (2002), Bardet et al. (2002), and Baska (2002) models. Our analysis assumed an earthquake magnitude of 7.6, a source-to-site distance of 22 kilometers, a free-face ratio of 67-percent, and a free-face height of 6 meters. The averaged SPT blowcounts from the generalized boring was used in the analysis. The mean grain size diameter for the generalized boring was estimated from Insuma sieve results for Borings P-1 and P-2. While a free-face ratio of 67-percent is a significant extrapolation beyond the maximum recommended value of 20-percent for the empirical models, the value was used nonetheless in order to properly represent the geometry at the bridge abutment. The median computed lateral spreading displacement value and the 95th-percentile confidence interval for each of the three empirical models is shown in Figure 6-53. The average computed median displacement from the three models is approximately 2.63 meters, which is within the range but near the low end of the displacement values reported by McGuire (1994).

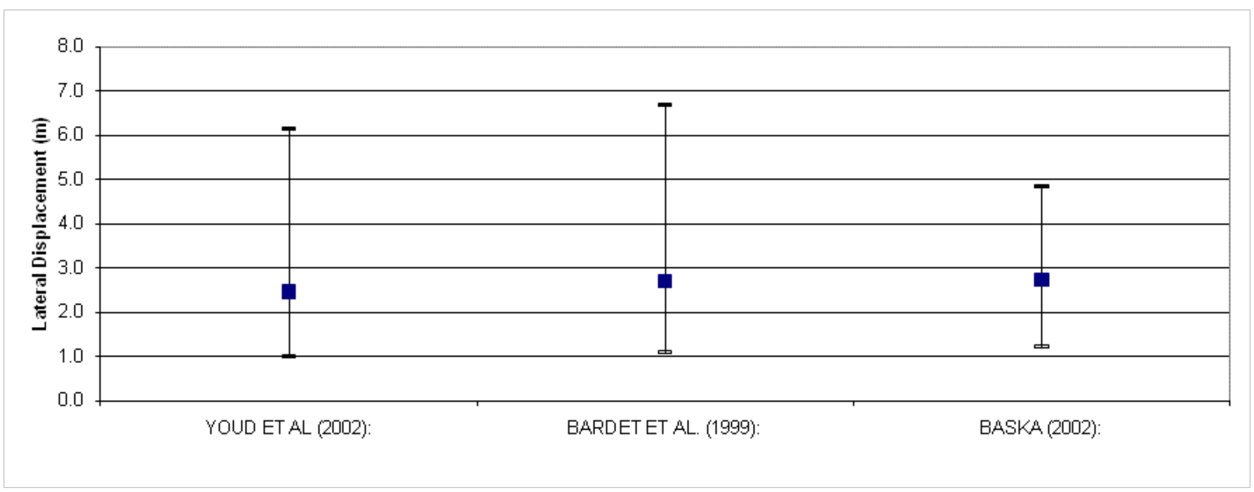

Figure 6-53: Deterministic median and 95-percentile evaluations of lateral spreading displacement using select empirical models for the Rio Bananito Railway Bridge

Since measured field displacements are available for the Rio Bananito Railway Bridge, a lateral spreading surface displacement of 3.85 meters is used for the deterministic evaluation of pile response in this study. The estimated deterministic lateral spreading displacement profile for the M7.6 1991 Limon earthquake was computed according to the procedure presented in Sections 2.7 and 2.8 of this report. This displacement profile is shown in Figure 6-54.

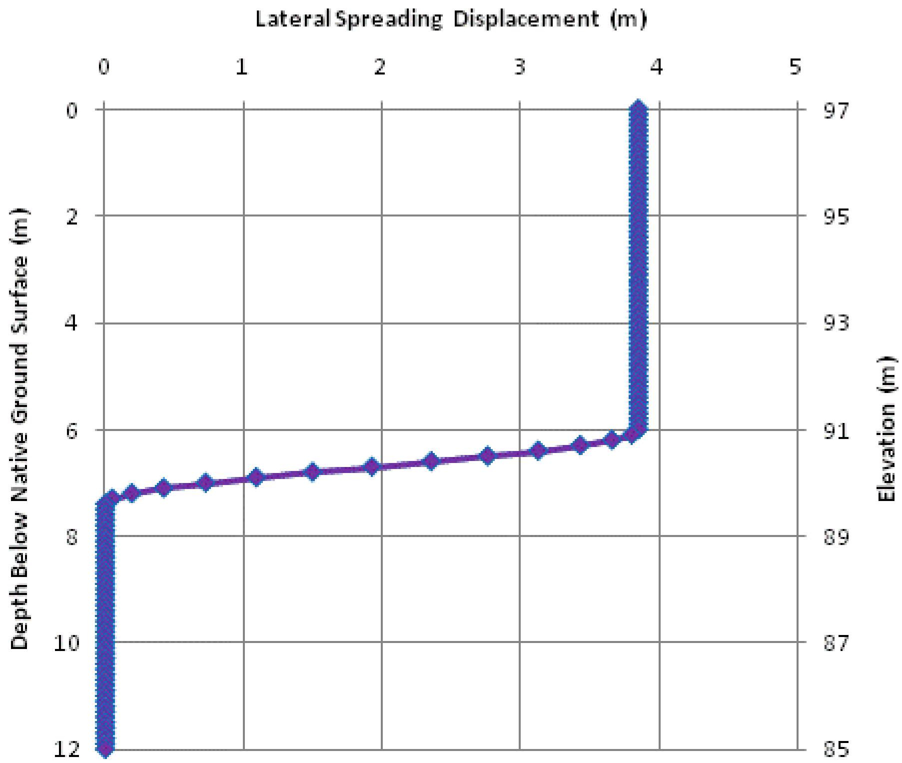

Figure 6-54: Computed deterministic lateral spreading displacement profile at the Rio Bananito Railway Bridge for the M7.6 1991 Limon earthquake

In the performance-based framework, values of $\mathscr{L}$ and $\mathscr{S}$ were computed at the Rio Blanco Bridge for each of the three empirical models. These values are shown in Table 6-8.

Table 6-8: $\mathscr{L}$ and $\mathscr{S}$ parameters for the performance-based lateral spreading analysis at the Rio Bananito Railway Bridge

	$\mathscr{L}$ parameter							$\mathscr{S}$ parameter
	108yrs	225yrs	475yrs	975yrs	2475yrs	4975yrs	100000yrs	
Youd et al. (2002)	8.453	9.115	9.621	9.975	10.130	10.140	10.200	-8.801
Bardet et al. (2002)	6.060	6.652	7.175	7.696	8.117	8.168	8.300	-6.296
Baska (2002)	6.748	7.288	7.700	8.004	8.112	8.120	8.160	-5.671

Using the values of $\mathscr{L}$ and $\mathscr{S}$ with the performance-based procedure for computing the lateral spreading displacement as described in Sections 5.6 and 5.7, performance-based estimates of lateral spreading deformation are computed and shown in Figure 6-55.

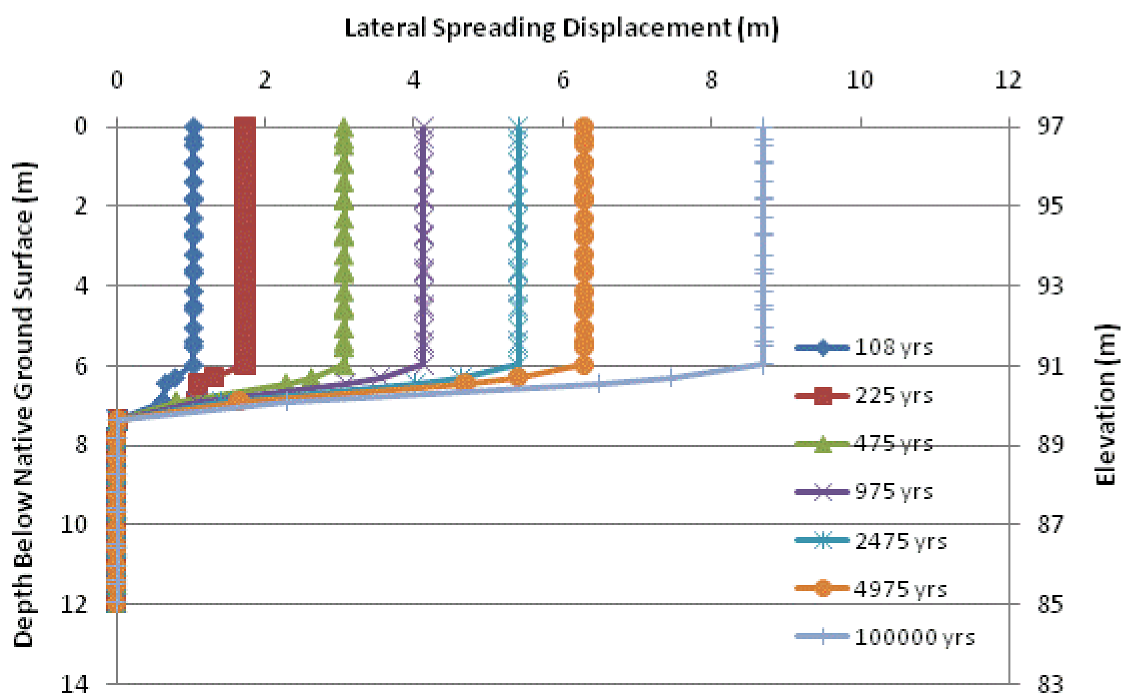

Figure 6-55: Performance-based lateral spreading displacement profiles for the Rio Bananito Railway Bridge

6.6.5 Deterministic Pile Response Analysis

With lateral spreading displacement profiles, an analysis of the pile response at the north abutment of the Rio Bananito Railway Bridge can be performed. A free-head condition was used for the caisson in the LPILE analysis, and linear-elastic modeling was incorporated to ensure model stability.

Since no bridge plans could be located for the Rio Bananito Railway Bridge, it was assumed that there was no reinforcing steel in the interior of the caisson for the computation of the initial composite flexural stiffness (i.e. EI). The resulting composite initial flexural stiffness of the piles was computed to be approximately 13,312 MN-m^2. A nonlinear pile response analysis was also performed in LPILE with a 2.16m-diameter circular caisson to estimate the yielding and plastic moments. The yield moment for the modeled caisson was computed to be approximately 1,300 kN-m and the plastic moment was computed to be approximately 7,900 kN-m. This approach likely over-computed the true yielding and plastic moments slightly due to the elliptical geometry of the actual caisson.

Applying the lateral spreading deformation shown in Figure 6-54 to the equivalent single pile, the modeled LPILE deterministic response from the caissons at the north abutment of the Rio Bananito Railway Bridge from the 1991 Limon earthquake is shown in Figure 6-56.

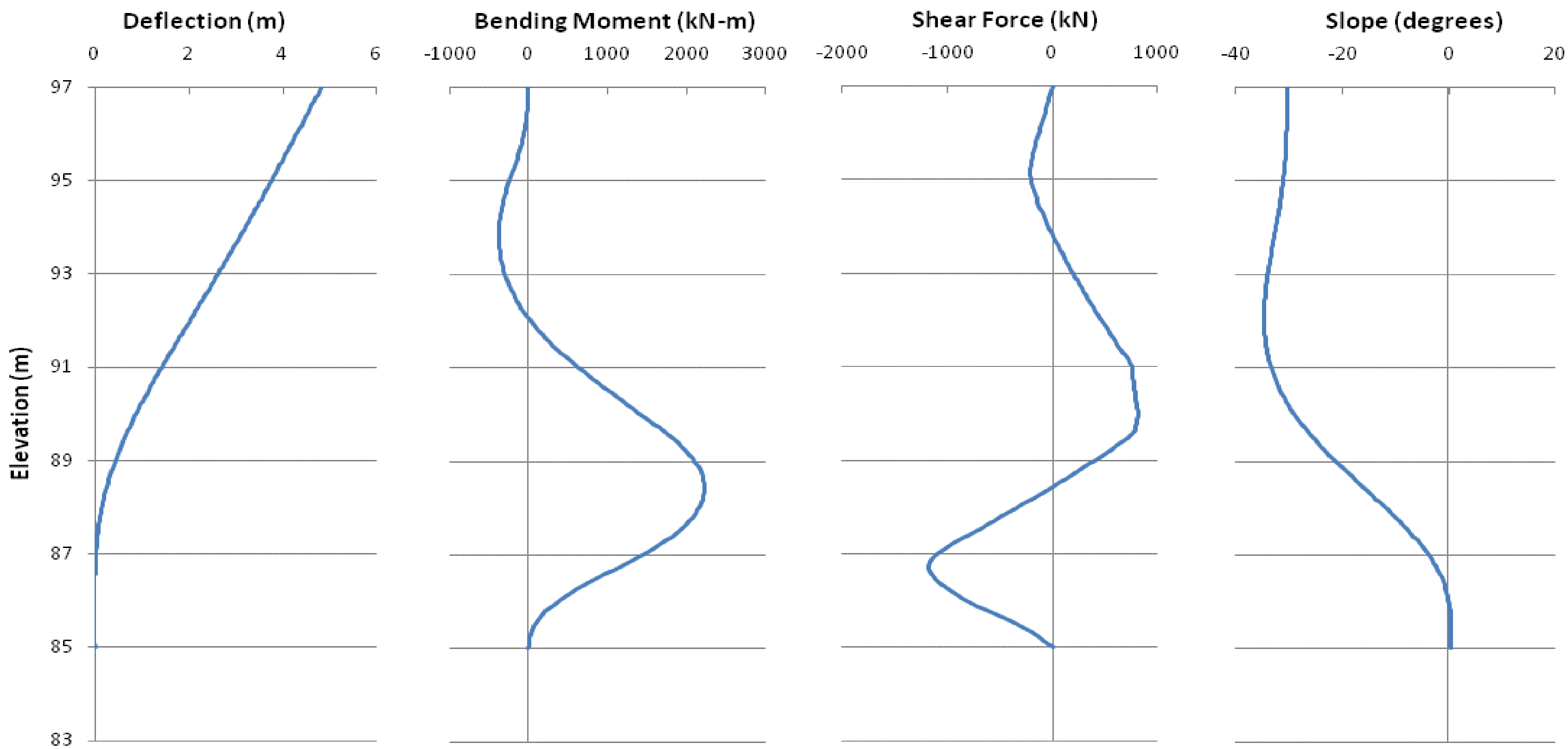

Figure 6-56: Deterministic computed pile response for the Rio Bananito Railway Bridge north abutment from the 1991 Limon earthquake

In general, the deterministic analysis reasonably replicated the response of the bridge foundation to the earthquake. Using a surface lateral spreading displacement of 3.85 meters, a head displacement of approximately 4.83 meters and a rotation of approximately 30 degrees was computed for the caisson. In addition, results from the dynamic wave equation analysis at the caisson suggest that concrete cracking has occurred between depths of 8 to 9 meters below the head of the caisson, which corresponds well with the depth of maximum computed moment in our analysis. Since the peak bending moment exceeds the computed yield moment of 1,300 kN-m, it is likely that yielding of the caisson occurred resulting in cracking of the concrete.

6.6.6 Performance-Based Pile Response

A performance-based pile response analysis was performed for a caisson at the north abutment of the Rio Bananito Railway Bridge according to the procedure described in Chapter 5 of this report. A Monte Carlo simulation was performed to estimate the variance of the caisson response to the various levels of kinematic loading in the performance-based procedure. The results of the performance-based analysis are shown in Figure 6-57.

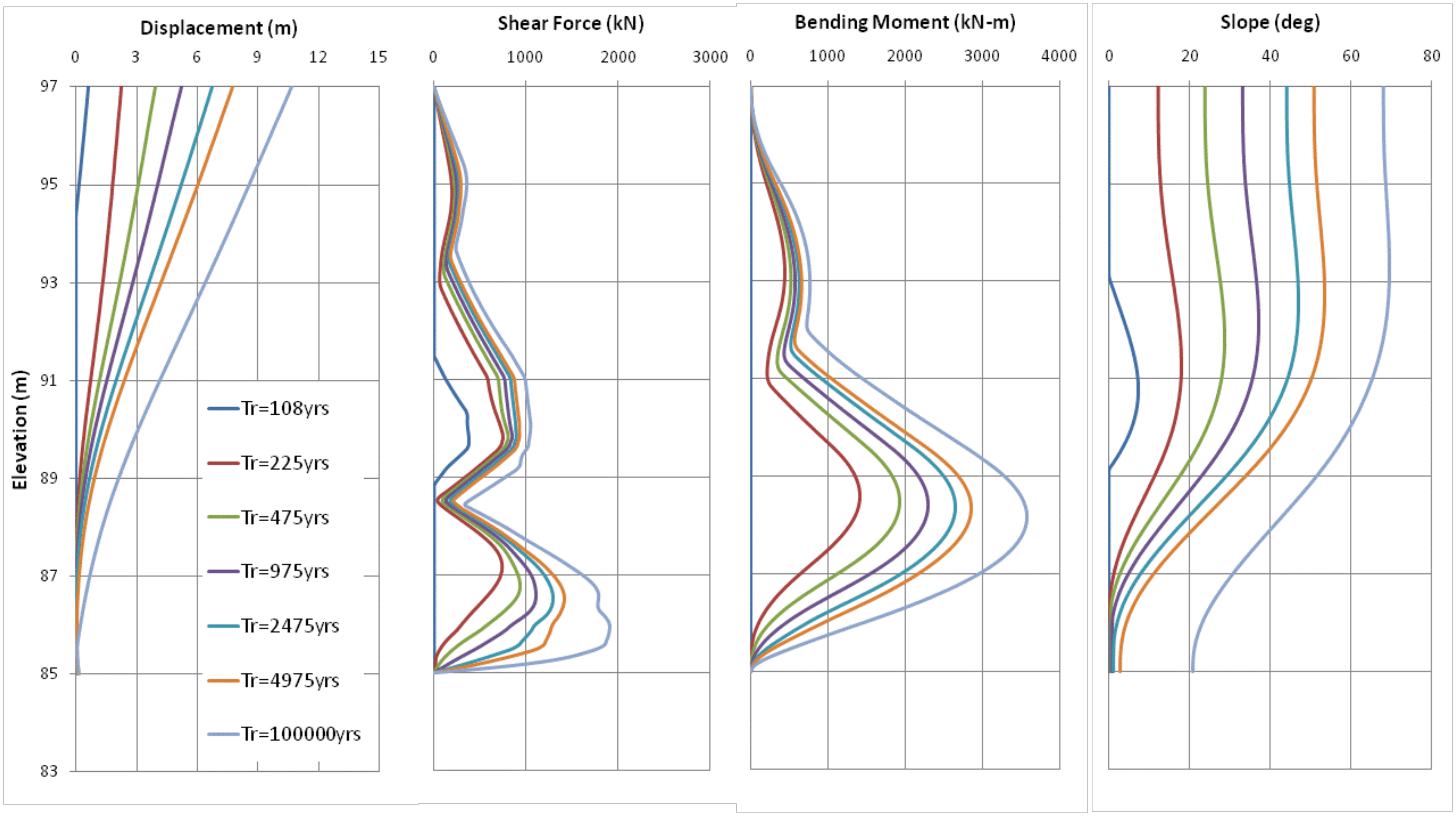

Figure 6-57: Performance-based pile response results for a single caisson at the Rio Bananito Railway Bridge

6.6.7 Discussion of Results

The results of performance-based pile response analysis at the Rio Bananito Railway Bridge appear reasonable and demonstrate that it is possible to combine simple pile response analysis procedures which are familiar to most practicing engineers in order to form a relatively sophisticated performance-based procedure. The analysis also demonstrates that it is possible to model the kinematic behavior of relatively large caissons/drilled shafts as long as sufficient information is available to reasonably model the caissons/shafts in the analysis.

One may note the discrepancy between the various pile responses (i.e. deflection, bending moment, shear, and slope) at the low return period of 108 years. This phenomenon is due to the fact that the pile responses are evaluated independently of one another in the performance-based probabilistic framework and may have different relative coefficients of variation computed from the Monte Carlo simulation. This means that the different forms of pile response should be evaluated independently from one another when considering the results of the analysis. For example, one should not assume that the pile displacement corresponding to a return period of 108 years could be computed by integrating the bending moment corresponding to a return period of 108 years.

According to the results of the performance-based kinematic pile response analysis, caisson head deflections of 4.3 and 5.7 meters correspond to return periods of approximately 600 years and 1,325 years, respectively. Caisson head rotations of 26 and 37 degrees correspond to return periods of approximately 560 years and 1,360 years, respectively. These results agree relatively well with one another, thus suggesting that the true return period corresponding to the observed caisson response following the 1991 Limon earthquake is between 560 and 1,360 years (i.e. probabilities of exceedance of 12.5% and 5.4% in 75 years, respectively).

6.7 Rio Estrella Bridge

The highway bridge over the Rio Estrella is a three-span steel and pre-stressed concrete bridge supporting two lanes of traffic. The two southern spans are approximately 75 meters in length and composed of steel trusses. The northern span is approximately 25 meters in length and composed of pre-stressed concrete girders. The total length of the bridge is approximately 178 meters. The bridge is located just north of the Town of Penhurst along National Route 36 and is the southern-most river crossing between Limon and Bribri. The latitude/longitude coordinates of the bridge are approximately 9.78760° North 82.9134° West.

According to bridge plans provided by the Costa Rican Ministry of Transportation and dated April 1971, the bridge is founded on a series of 12BP53 H-piles. The north abutment is supported by two rows of piles (5 piles in each row) that are approximately 17.2 meters in length and spaced at 1.5 meters in the transverse direction and 1 meter in the longitudinal direction. The northern bent is founded on two 2.90-meter x 4.94-meter pile caps. Each of these pile caps is supported by 15 12BP53 steel piles (three rows of five piles) that are 20 meters in length and spaced at 1 meter in both the transverse and longitudinal directions. The southern bent is founded on two 3.94-meter x 4.94-meter pile caps. Each of these pile caps is supported by 20 12BP53 steel piles (four rows of five piles) that are 20 meters in length and spaced at 1 meter in both the transverse and longitudinal directions. The southern abutment of the bridge was designed to be converted into a bent in the event of a bridge expansion. The abutment is founded on two 3.96-meter x 5.96 meter pile caps. Each of these pile caps is supported by 24 12BP53 steel piles (four rows of six piles) that are 20 meters in length and spaced at 1 meter in both the transverse and longitudinal directions.

6.7.1 Surface Conditions and Bridge Geometry

The Rio Estrella is a relatively wide river bounded on both sides by a gently sloping floodplain with extensive vegetation and banana plantations. According to elevations shown on the blueprints that were provided by the Costa Rican Ministry of Transportation, the river channel itself ranges in elevation from about -0.8 meter at the bottom of the river channel to approximately 3.5 meters at the river bank near the southern bridge abutment. However, at the time of the 1991 earthquake, the ground surface elevations measured near the southern abutment did not match the elevations shown on the bridge drawings, indicating that the elevations on the drawings were design elevations which may have changed due to erosion, deposition, or man-made changes in the river geometery. According to the bridge blueprints, the roadway elevation across the bridge is 8.90 meters. From the blueprints, it also appears that the approach embankment was constructed at a 1.5H:1V slope.

A simplified sketch of the plan and profile views of the Rio Estrella Bridge is shown in Figure 6-58. Note that the sketch includes an estimation of the approximate ground surface profile assumed at the time of the 1991 earthquake.

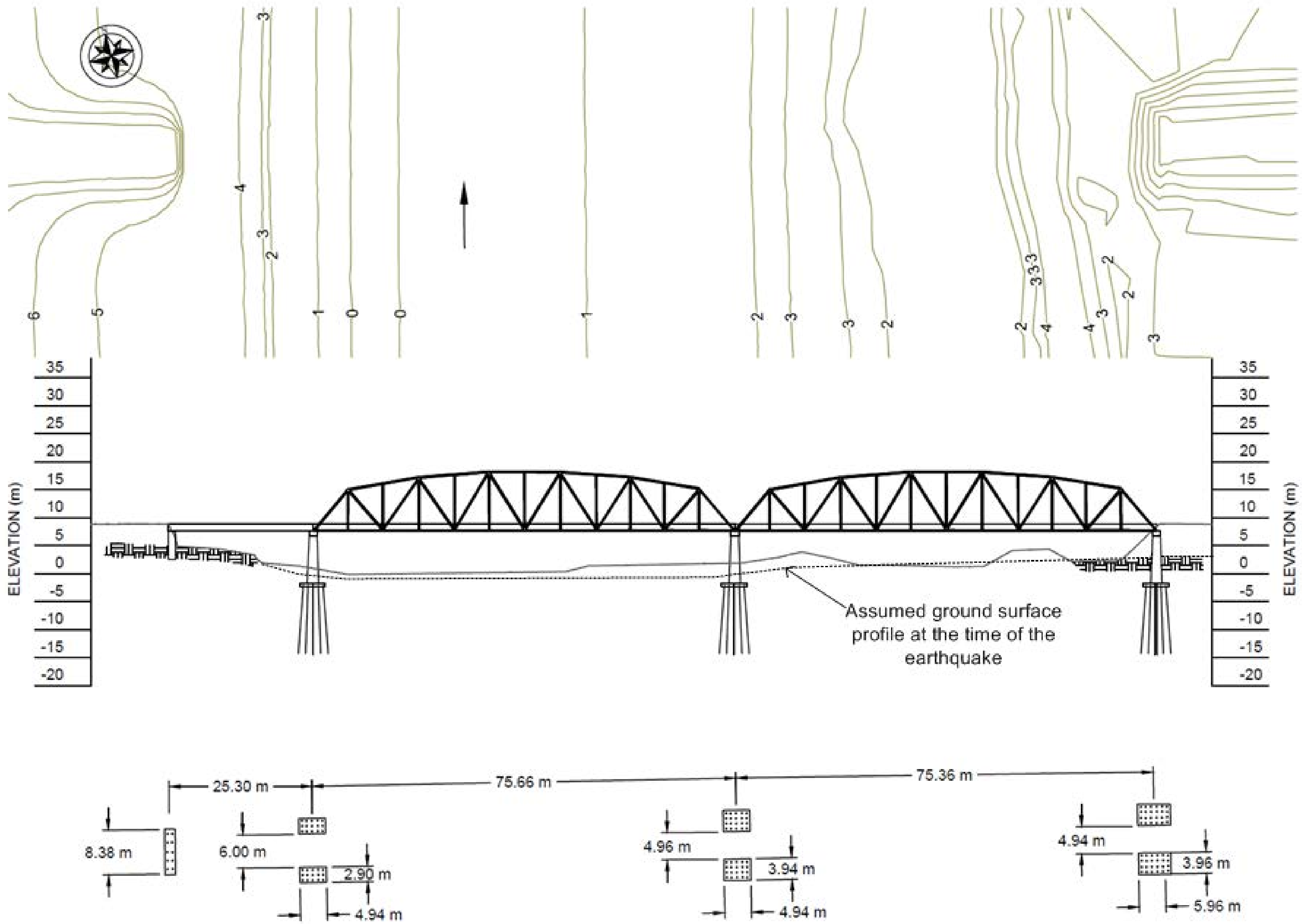

Figure 6-58: Simplified sketch of the plan and profile views of the Rio Estrella Bridge

6.7.2 Subsurface Conditions

Insuma S.A. Geotechnical Consultants performed a single boring immediately adjacent to southern abutment at the Rio Estrella Bridge. The boring extended to a depth of 20.25 meters. The soils encountered in the boring were reported to consist primarily of alluvial deposits composed primarily of clayey (i.e. elastic) silts and silty sands. The silts encountered in the boring were generally non-plastic. However, elastic silts near the ground surface were generally moderate to highly plastic. The sands encountered appeared to be fine-grained and generally silty. However, a zone of relatively clean sands and gravels was encountered at depths between approximately 4.9 and 10.4 meters. Groundwater was encountered in the boring at an approximate depth of 4.9 meters, which corresponds to an estimated elevation of approximately -1.4 meters. A simple diagram of the soils encountered in the boring performed is shown in Figure 6-59 below. Further details regarding the boring at the Rio Estrella Bridge and the corresponding laboratory test results can be found in the Insuma Geotechnical Report included as Appendix A of this report.

Depth (m)	SPT N Value	
0.00 - 0.45	10	Grayish brown or brown very sandy SILT and/or very silty SAND, fines are not plastic very loose to loose relative density.
0.45 - 0.90	7	
0.90 - 1.35	6	
1.35 - 1.80	2	
1.80 - 2.25	2	
2.25 - 2.70	1	
2.70 - 3.15	1	Brown clayey SILT, mixed with fraction of sand size particles, medium plasticity, soft
3.15 - 3.60	1	
3.60 - 4.05	2	
4.05 - 4.50	2	
4.50 - 4.95	2	Gray well graded sandy GRAVEL and/or gravelly SAND, no plasticity, medium.
4.95 - 5.40	14	
5.40 - 5.85	10	
5.85 - 6.30	16	
6.30 - 6.75	12	
6.75 - 7.20	7	
7.20 - 7.65	10	Gray well graded silty SAND, with some gravel, fines have no plasticity, medium to dense relative density.
7.65 - 8.10	10	
8.10 - 8.55	12	
8.55 - 9.00	10	
9.00 - 9.45	28	
9.45 - 9.90	34	
9.90 - 10.35	22	
10.35 - 10.80	24	Greenish gray very fine silty SAND, fines have no platicity, medium to dense relative density.
10.80 - 11.25	19	
11.25 - 11.70	19	
11.70 - 12.15	24	
12.15 - 12.60	17	
12.60 - 13.05	26	
13.05 - 13.50	27	
13.50 - 13.95	35	
13.95 - 14.40	24	
14.40 - 14.85	38	
14.85 - 15.30	35	
15.30 - 15.75	28	
15.75 - 16.20	36	
16.20 - 16.65	36	
16.65 - 17.10	17	
17.10 - 17.55	25	
17.55 - 18.00	21	
18.00 - 18.45	22	
18.45 - 18.90	33	
18.90 - 19.35	32	
19.35 - 19.80	36	
19.80 - 20.25	38	

Figure 6-59: Boring P-1 performed at the Rio Estrella Bridge

The information from Boring P-1 was used to develop a generalized soil profile for the southern abutment of the Rio Estrella Bridge. Empirical correlations with SPT blowcounts were averaged to estimate the friction angle of granular soils and non-plastic silts. These correlations include Peck et al. (1974), Hatanaka and Uchida (1996), and Bowles (1977). Relative density of granular soils was estimated using the empirical correlation presented by Kulhawy and Mayne (1990). Corrected soil modulus estimates K^* of the granular soils for use with the API (1993) p-y relationship were estimated using the recommendations presented by Boulanger et al. (2003). Undrained strength of cohesive plastic soils was averaged from empirical correlations including Hara et al. (1971), Kulhawy and Mayne (1990), and Skempton (1957). Assumptions regarding the unit weight of the native soil as well as the strength properties of the embankment fill were made. Groundwater is modeled at an elevation of -1.00 meter (i.e. an estimated depth of 9.9 meters from the top of the embankment). Table 6-9 summarizes our generalized model of the soil profile at the east abutment of the Rio Estrella Bridge.

Table 6-9: Generalized soil profile for the east abutment at the Rio Estrella Bridge

Top Depth (m)	Top Elevation (m)	Thickness (m)	USCS Soil Class	Friction Angle (deg)	Moist Unit Weight (kN/m3)	Undrained Strength (kPa)	Relative Density (%)	Corrected Soil Modulus (kN/m3)	Liquefied p-multiplier
0	8.90	5.40	SM (Fill)	35	18.5	---	62	24,800	NA
5.40	3.50	2.70	ML/SM	32	18.1	---	39	5,900	NA
8.10	0.80	1.80	MH	---	18.8	13.0	---	---	NA
9.90	-1.00	2.80	GW	34	8.3	---	53	10,300	0.19
12.70	-3.80	1.90	SW/SM	33	8.3	---	48	7,700	0.14
14.60	-5.70	1.30	SW/SM	40	8.5	---	77	20,000	NA
15.90	-7.00	2.70	SM	37	8.5	---	65	13,350	0.33
18.60	-9.70	1.40	ML/SM	39	8.5	---	73	15,600	NA
21.00	-11.10	5.70	SM	39	8.5	---	72	14,000	NA

6.7.3 Ground Motions and Liquefaction

The Rio Estrella Bridge is located approximately 21 kilometers northeast from the epicenter of the April 22, 1991 e arthquake. Assuming an average V_{s30} value of 270 m /s, the average computed median spectral accelerations ±1σ from the four selected NGA models are shown in Figure 6-60. The median computed PGA and spectral accelerations corresponding to 0.2-second and 1.0-second are approximately 0.244g, 0.506g, and 0.334g.

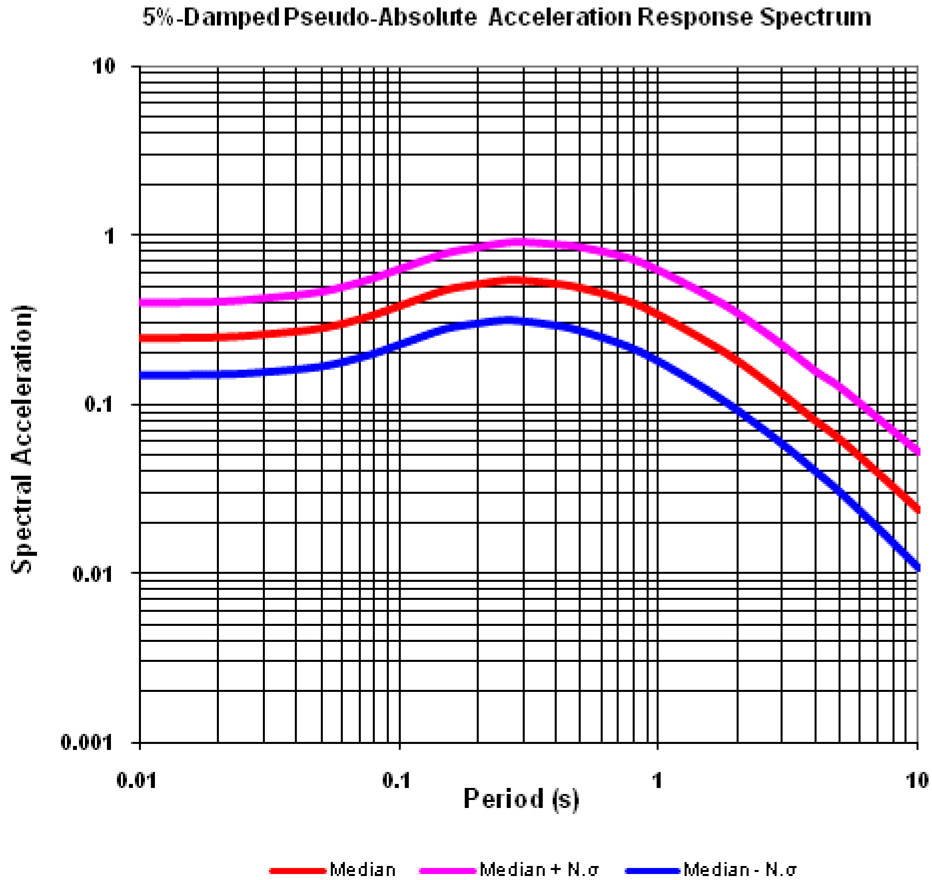

Figure 6-60: Computed deterministic response spectra for the Rio Estrella Bridge from the 1991 earthquake. N = 1

Using the average deterministic ground motions from the NGA equations, the deterministic liquefaction triggering was evaluated at the Rio Estrella Bridge for the M7.6 1991 Limon earthquake using the SPT blowcounts from Boring P-1. The results of the deterministic liquefaction triggering analysis are shown in Figure 6-61. This evaluation included consideration of the Cetin et al. (2004), Idriss and Boulanger (2008), and Youd et al. (2001) simplified procedures. In general, reasonable agreement was observed between the three procedures although the Cetin et al approach (2004) yields somewhat lower factors of safety against liquefaction. Assuming that the top of the boring is at an approximate elevation of 3.5 meters, the results of the analysis suggest that liquefaction triggered from depths of approximately 4.50 meters to 9.00 meters below the ground surface (EL -1.00m to EL -5.5m).

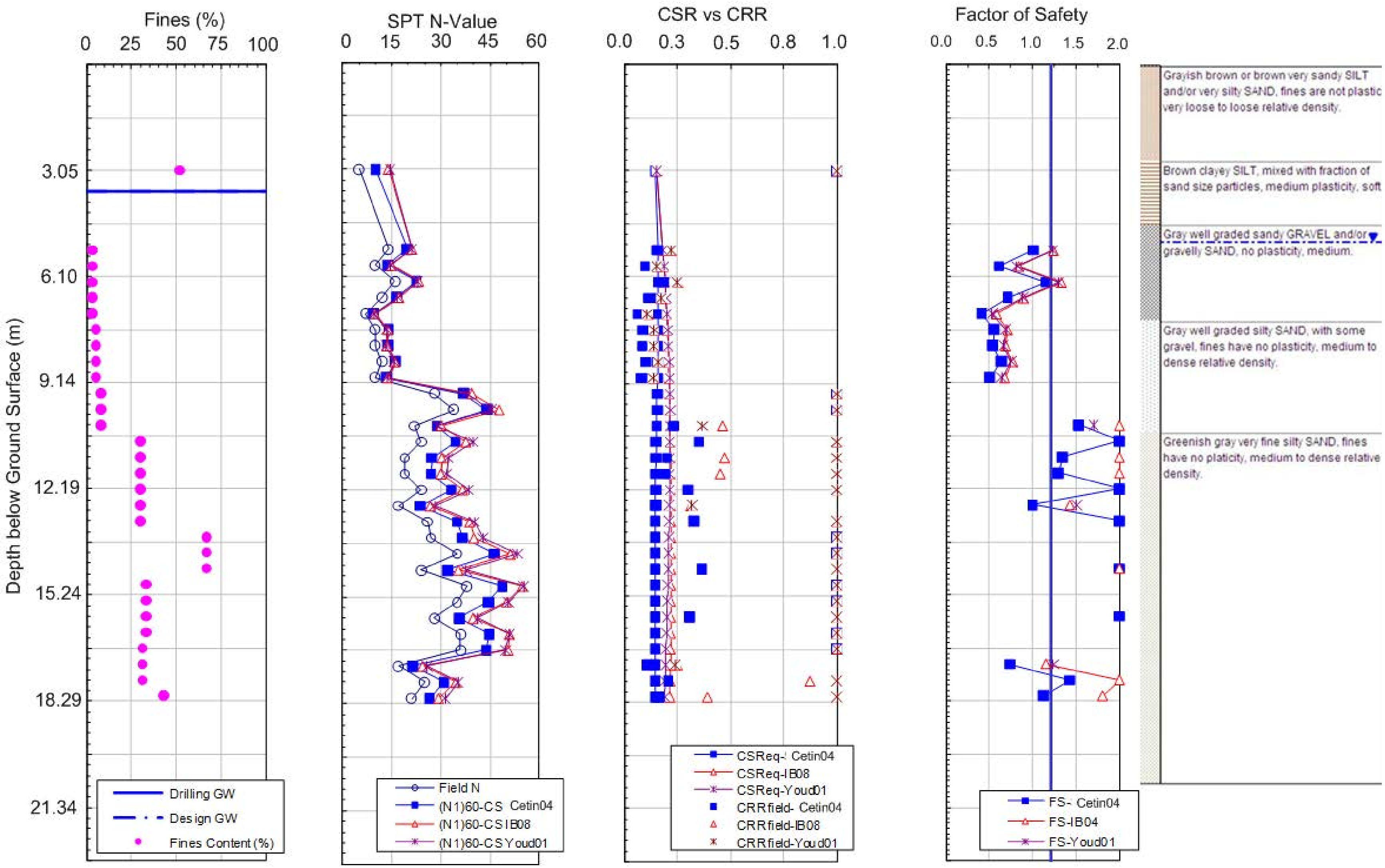

Figure 6-61: Deterministic liquefaction triggering results for the M7.6 1991 Limon earthquake at the Rio Estrella Bridge

In evaluating the soil stratigraphy at the south abutment of the Rio Estrella Bridge, the high plasticity non-liquefiable soil cap underlain by a coarse-grained and clean liquefiable soil layer leads one to hypothesize the occurrence of void redistribution and the development of a water film following the triggering of liquefaction during the Limon earthquake. Void redistribution is a well-documented phenomenon associated with liquefaction, and is perhaps most well known for its purported role in the flow liquefaction failure of the Lower San Fernando Dam following the 1971 San Fernando earthquake (Kramer, 1996). The phenomenon occurs when escaping pore water becomes trapped beneath a low permeability soil cap and is therefore unable to alleviate excess pore pressures. Under these conditions, the individual soil particles in the liquefied layer can redistribute themselves and consolidate. However, since the pore water is unable to escape, the overlying soil is unable to settle with the consolidated particles in the liquefied soil, thus creating a temporary water film between the non-liquefied soil cap and the liquefied soil. Due to its lack of shear strength, this water film can contribute to significant ground deformations including lateral spreading and/or flow failures. Currently, no analytical methods exist for objectively evaluating the occurrence of void redistribution and the development of a water film in a given soil profile subjected to seismic loading.

The results of our PSHA using EZ-FRISK software suggest that the seismicity at the bridge is moderate to high. The seismic hazard curve for the PGA is shown below in Figure 6-62.

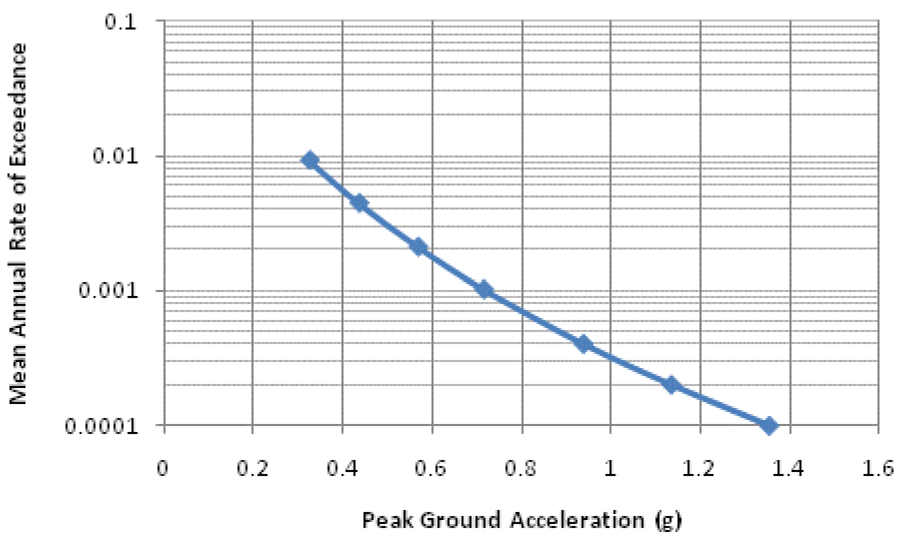

Figure 6-62: Computed seismic hazard curve for the PGA at the Rio Estrella Bridge

The magnitude/distance deaggregations as estimated by EZ-FRISK for the PGA are shown in Figure 6-63. These magnitude deaggregations are used in conjunction with the seismic hazard curve for the PGA shown in Figure 6-62 to perform the performance-based liquefaction triggering analysis according to the Kramer and Mayfield (2007) procedure. The performance-based factors of safety against liquefaction for various return periods are shown in Figure 6-64. These factors of safety were computed using the SPT blowcount information from Insuma boring P-1 at the Rio Estrella Bridge. A factor of safety less than or equal to 1.2 was assumed to be liquefiable for this study. Note that for fine-grained soil layers not considered susceptible to liquefaction due to plasticity, a generic factor of safety against liquefaction equal to 2.0 was assigned regardless of return period. A maximum factor of safety equal to 4.0 was assigned to layers with very high resistance to liquefaction triggering. In general, Figure 6-64 shows that for return periods greater than about 975 years, liquefaction triggers from depths of about 4.50 meters to 9.00 meters (EL. -1.00m to -5.50m) below the ground surface.

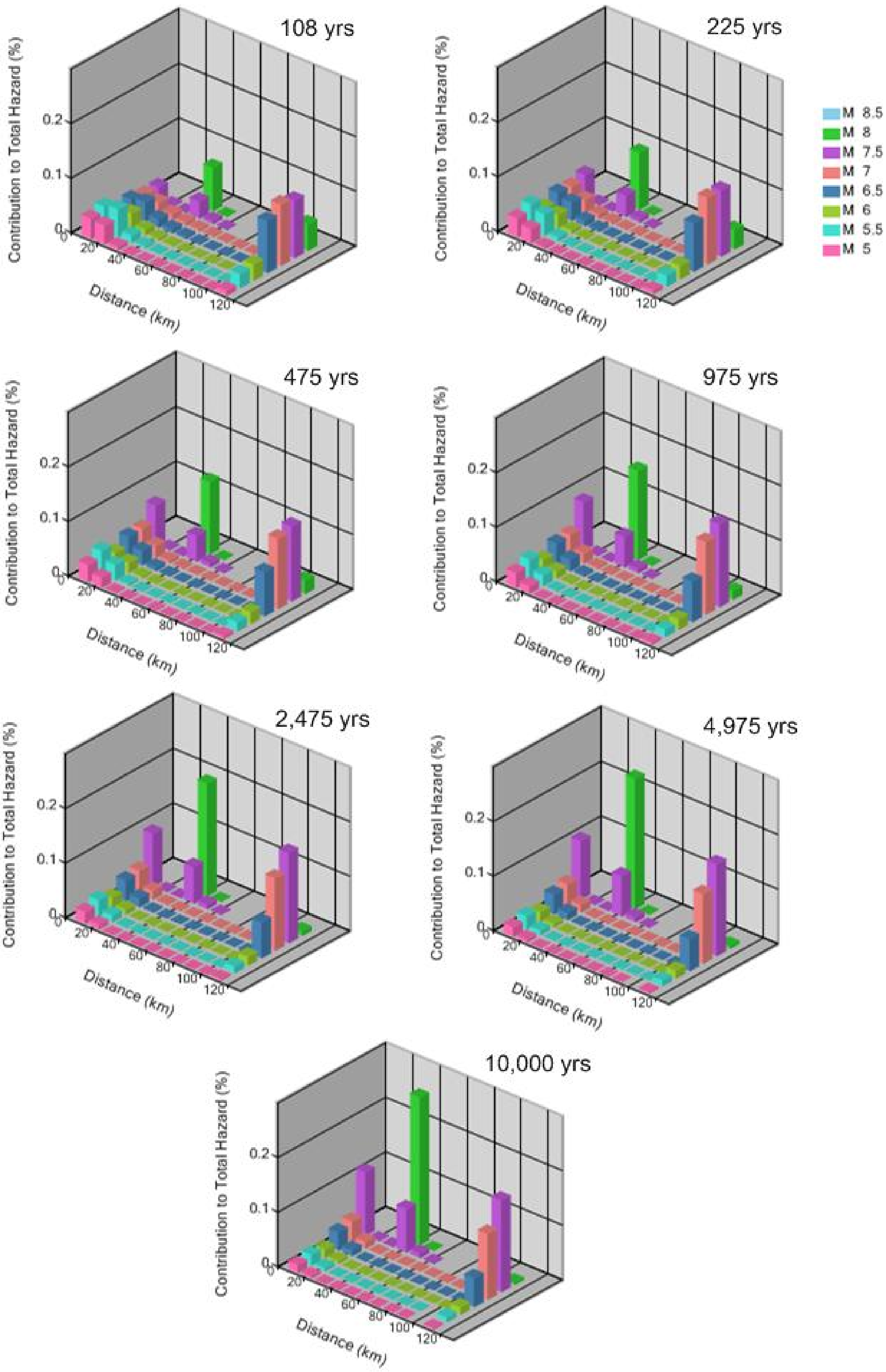

Figure 6-63: Magnitude/distance deaggregations for the PGA at the Rio Estrella Bridge

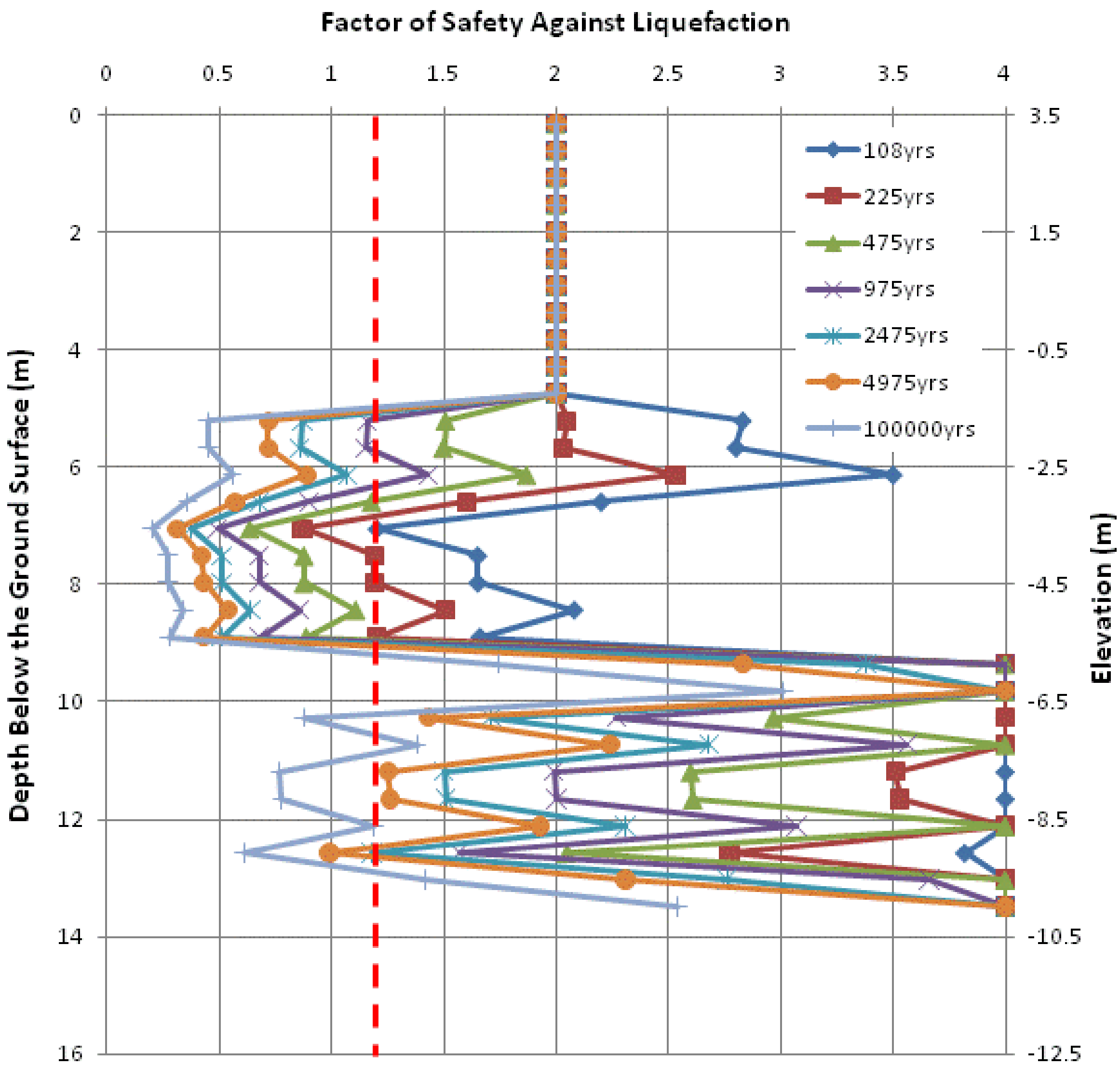

Figure 6-64: Performance-based liquefaction triggering results for the Rio Estrella Bridge

6.7.4 Lateral Spreading

Observed evidence of lateral spreading at the Rio Estrella Bridge is quite extensive. Youd (1993) estimated that up to 2 meters of displacement may have occurred in the vicinity of the south abutment. Priestley et al. (1991) and McGuire (1994) describe localized slope stability failures and liquefaction-induced settlements of up to 2 meters in the approach embankment at the south abutment. Despite this extensive amount of liquefaction-induced ground deformation, the foundation at the south abutment showed negligible amounts of damage and deformation as shown in Table 6-10 after Youd et al. (1992). However, the bridge itself sustained significant damage due to the unseating and subsequent collapse of both steel trusses from the transient ground motions.

Table 6-10: Measured distances at the Rio Estrella Bridge following the 1991 Limon Earthquake (after Youd et al., 1992)

Distance between center of bridge seats on:	*Plan distance* m	*Measured post-earthquake distance* *m*
North Abutment and Pier 1	25.00	24.96
Pier 1 and Pier 2	75.00	75.02
Pier 2 and South Abutment	75.00	75.24
North and South Abutments	176.32	176.14

Empirical evaluation of the free-field soil displacements due to lateral spreading was performed using the Youd et al. (2002), Bardet et al. (2002), and Baska (2002) models. Because evaluation of photos presented by Youd et al. (1992) and Youd (1993) suggest that the river was likely wider at the time of the earthquake than was measured during out 2010 GPS site survey, an adjusted ground surface profile based on engineering judgment, visual interpretation of the fore-mentioned photos and the elevations shown on the Costa Rican bridge plans was used in our lateral spreading analysis. Our analysis assumed an earthquake magnitude of 7.6, a source-to-site distance of 21 kilometers, a free-face ratio of 6-percent, and a free-face height of 4.6 meters. The mean grain size diameter for each soil sublayer in the analysis was estimated from the Insuma sieve results. The median computed lateral spreading displacement value and the 95th-percentile confidence interval for each of the three empirical models is shown in Figure 6-65. The average computed median displacement from the three models is approximately 0.45 meter. This value is significantly less than the reported lateral spreading displacements at the south abutment of the Rio Estrella Bridge, thus providing further evidence that a water film may have contributed to larger ground deformations. A profile sketch showing the location of the soil zones and possible location of a water film against the foundation at the south abutment of the Rio Estrella Bridge is shown in Figure 6-66.

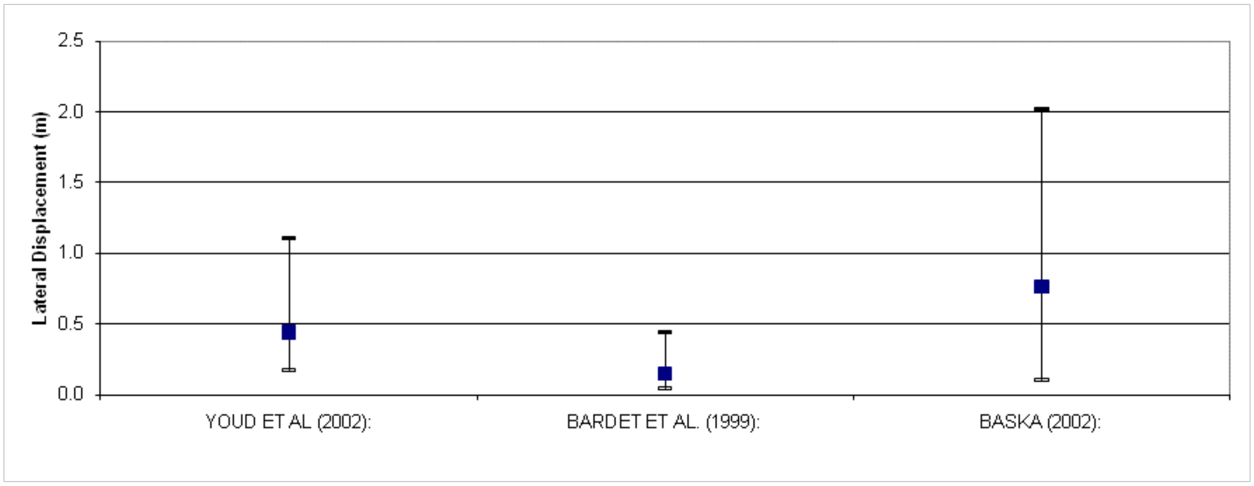

Figure 6-65: Deterministic median and 95-percentile evaluations of lateral spreading displacement using select empirical models for the Rio Estrella Bridge

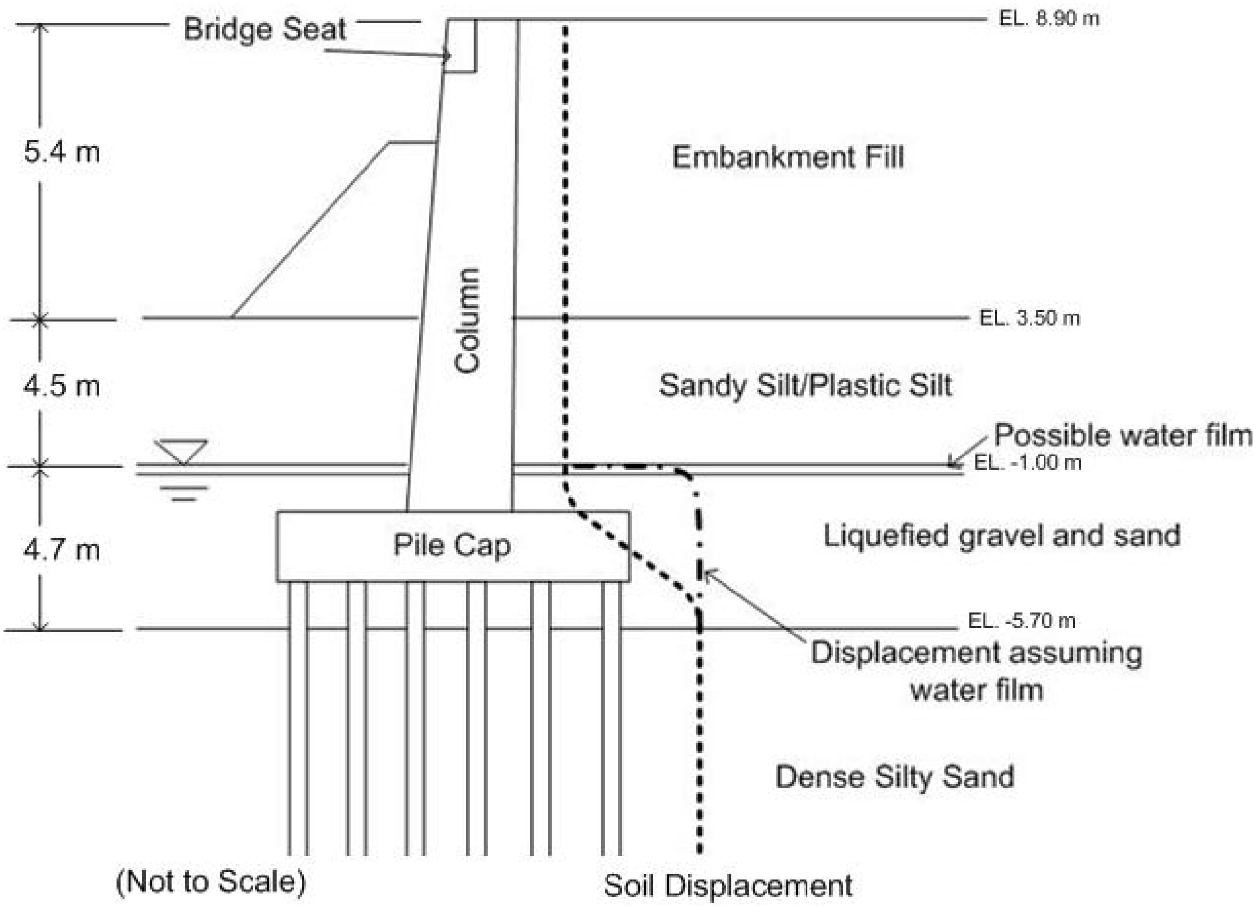

Figure 6-66: Simple sketch of the soil layering against the foundation at the south abutment of the Rio Estrella Bridge

Preliminary pile response analyses at the south abutment of the Rio Estrella Bridge suggested that even small soil deformations through the liquefied soil would likely result in foundation deformations exceeding 0.12 meter (~5 inches) at the abutment. However, further evaluation of the pile response assuming that the soil deformation was concentrated at the top of the liquefied layer in order to replicate a water film resulted in nearly no computed displacement of the foundation. Therefore, all subsequent pile response analyses at the south abutment of the Rio Estrella Bridge were performed assuming a water film at the top of the liquefiable layer. Since the empirically computed lateral spreading displacement for the 1991 Limon earthquake was significantly less than the observed lateral spreading displacement, a value of 2 meters was used for the deterministic pile response analysis in this study. No guidance on developing lateral displacement profiles with depth for liquefied soils with a water film could be found in the literature at the time of this study. Assuming a layer water film thickness of approximately 0.05 meter, soil displacements through the water film and the liquefied soil layer were assigned based on the relative water film displacements measured during the centrifuge tests reported by Boulanger et al. (2003). This approach assigned approximately 62-percent of the total displacement to the water film, 23-percent of the total displacement to the top 13-percent of the liquefiable layer, 11-percent of the total displacement to the next 16-percent of the liquefiable layer, and then 4-percent of the total displacement to the remaining 71-percent of the liquefiable layer. The resulting deterministic lateral spreading displacement profile computed from this approach is shown in Figure 6-67.

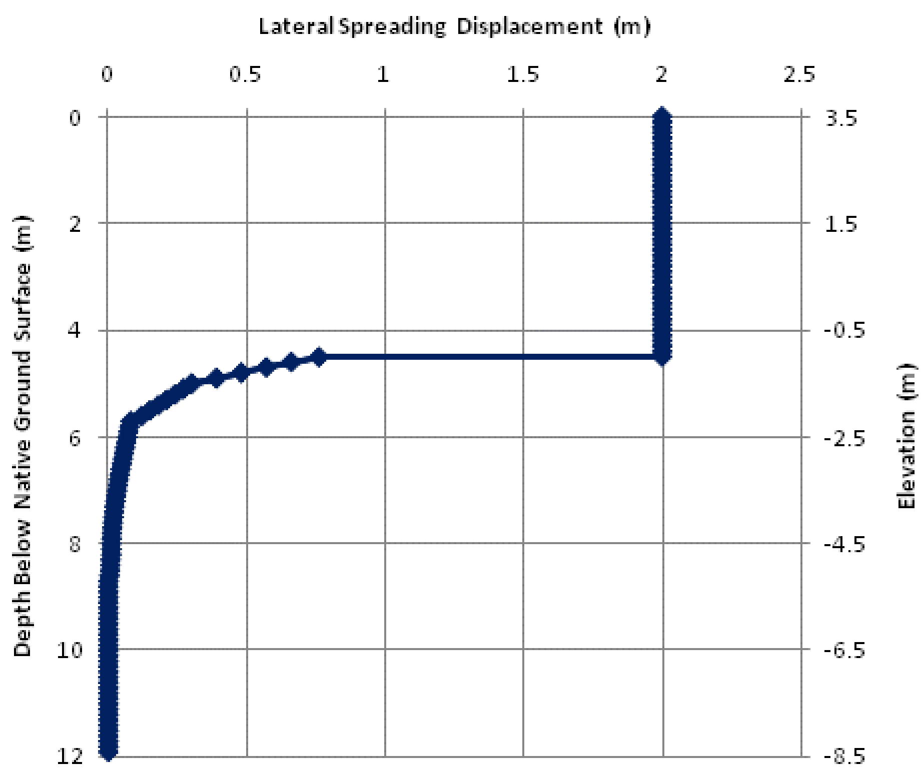

Figure 6-67: Deterministic lateral spreading displacement profile at the south abutment of the Rio Estrella Bridge for the M7.6 1991 Limon earthquake

Even though the discrepancy between the computed and the observed displacements following the 1991 Limon earthquake suggests that empirical methods likely under-predict the lateral spreading displacement at the Rio Estrella Bridge, a performance-based kinematic pile response analysis was still performed as part of this study for demonstration purposes. In the performance-based framework, values of $\mathscr{L}$ and $\mathscr{S}$ were computed at the Rio Estrella Bridge for each of the three empirical lateral spreading models. These values are shown in Table 6-11.

Table 6-11: $\mathscr{L}$ and $\mathscr{S}$ parameters for the performance-based lateral spreading analysis at the Rio Estrella Bridge

	$\mathscr{L}$ parameter							$\mathscr{S}$ parameter
	108yrs	225yrs	475yrs	975yrs	2475yrs	4975yrs	100000yrs	
Youd et al. (2002)	8.469	9.186	9.791	10.080	10.130	10.190	10.204	-9.588
Bardet et al. (2002)	6.090	6.728	7.394	7.954	8.152	8.300	8.304	-6.816
Baska (2002)	6.764	7.347	7.834	8.006	8.115	8.150	8.160	-6.508

Using the values of $\mathscr{L}$ and $\mathscr{S}$ with the performance-based procedure for computing the lateral spreading displacement as described in Sections 5.6 and 5.7, performance-based estimates of lateral spreading deformation are computed and shown in Figure 6-68. Note that these lateral spreading estimates assume the same approach involving a water film as described above for the deterministic lateral spreading displacement profile.

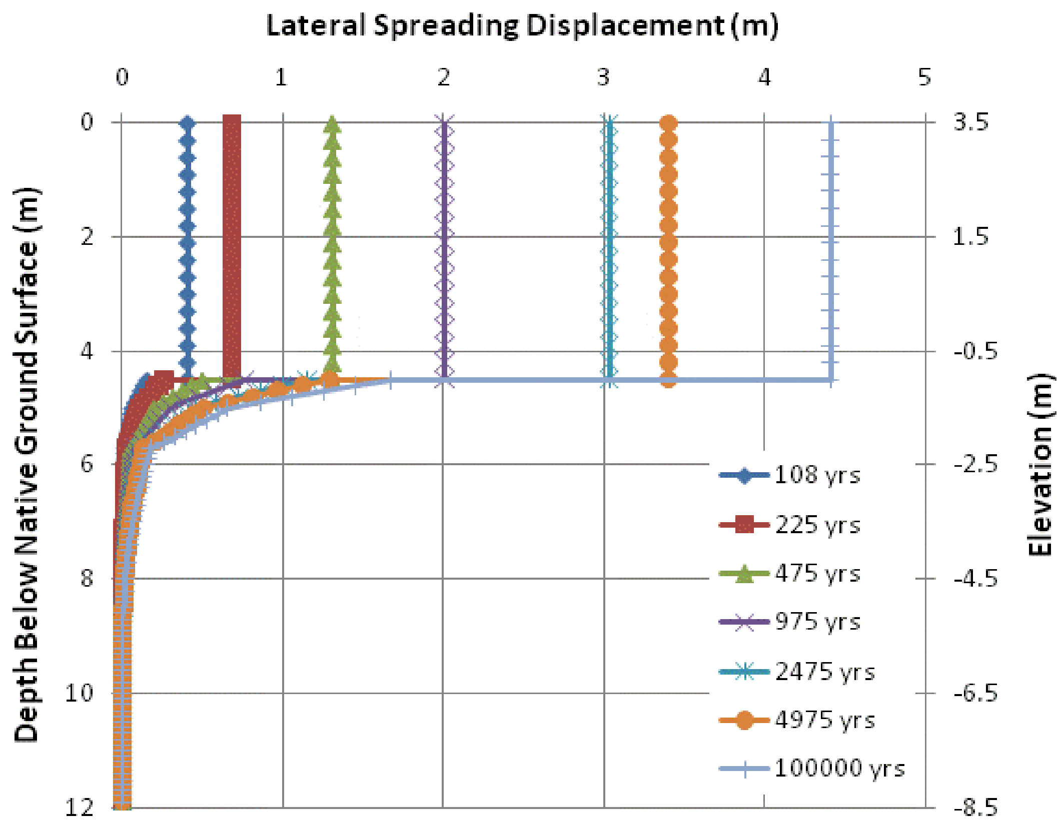

Figure 6-68: Performance-based lateral spreading displacement profiles for the Rio Estrella Bridge

6.7.5 Deterministic Pile Response Analysis

With lateral spreading displacement profiles, an analysis of the pile response at the south abutment of the Rio Estrella Bridge can be performed. Since the pile caps are located beneath the top of the liquefied soil layer with piers extending to the bridge abutment, the kinematic loading of the piers was also considered in the analysis. This was performed in the LPILE model by manually computing the total passive force exerted on piers from the laterally spreading embankment and applying it as an inertial load and moment at the head of the equivalent single pile.

The passive behavior of a non-liquefied soil during lateral spreading is still relatively poorly understood. The centrifuge study performed by Brandenberg et al. (2007) observed that Rankine passive earth pressures reasonably modeled the passive pressures measured in their model. In addition, it is unclear how the possible presence of a water film above the liquefied layer could affect the passive force exerted by the non-liquefied soil crust on the bridge piers. Therefore, this study incorporated Rankine passive earth pressures to model the kinematic loading of the non-liquefied soil crust on the bridge piers at the south abutment. Since significant settlement of the approach embankment was observed during the Limon earthquake, the embankment height was reduced by 1 meter. Using the geometry of the bridge piers shown on the bridge plans provided by the Costa Rican Ministry of Transportation, a total passive force of 10,870 kN and moment of 274,100 kN-m were computed. Our analysis assumed that the piles behaved as end-bearing piles when loaded kinematically, and the frictional resistance from a single pile was computed to be approximately 987 kN. The resulting overturning resisting moment from the 48 pile group at the abutment was computed to be approximately 121,730 kN-m. Using Rollins et al. (2006), an average group p-multiplier of 26.2 was computed to convert the pile group to an equivalent single pile. Using a total computed moment of 395,830 kN-m (i.e., 274,100 kN-m + 121,730 kN-m) and a rotation angle of 0.008 radians (fixed-end condition, assumed frictional mobilization distance of 0.008 meter), the rotational stiffness for the equivalent single pile was computed as 49,478,750 kN-m/rad.

Applying the lateral spreading deformation shown in Figure 6-67 to the equivalent single pile, the LPILE deterministic pile response from the 1991 Limon earthquake was computed and is shown in Figure 6-69.

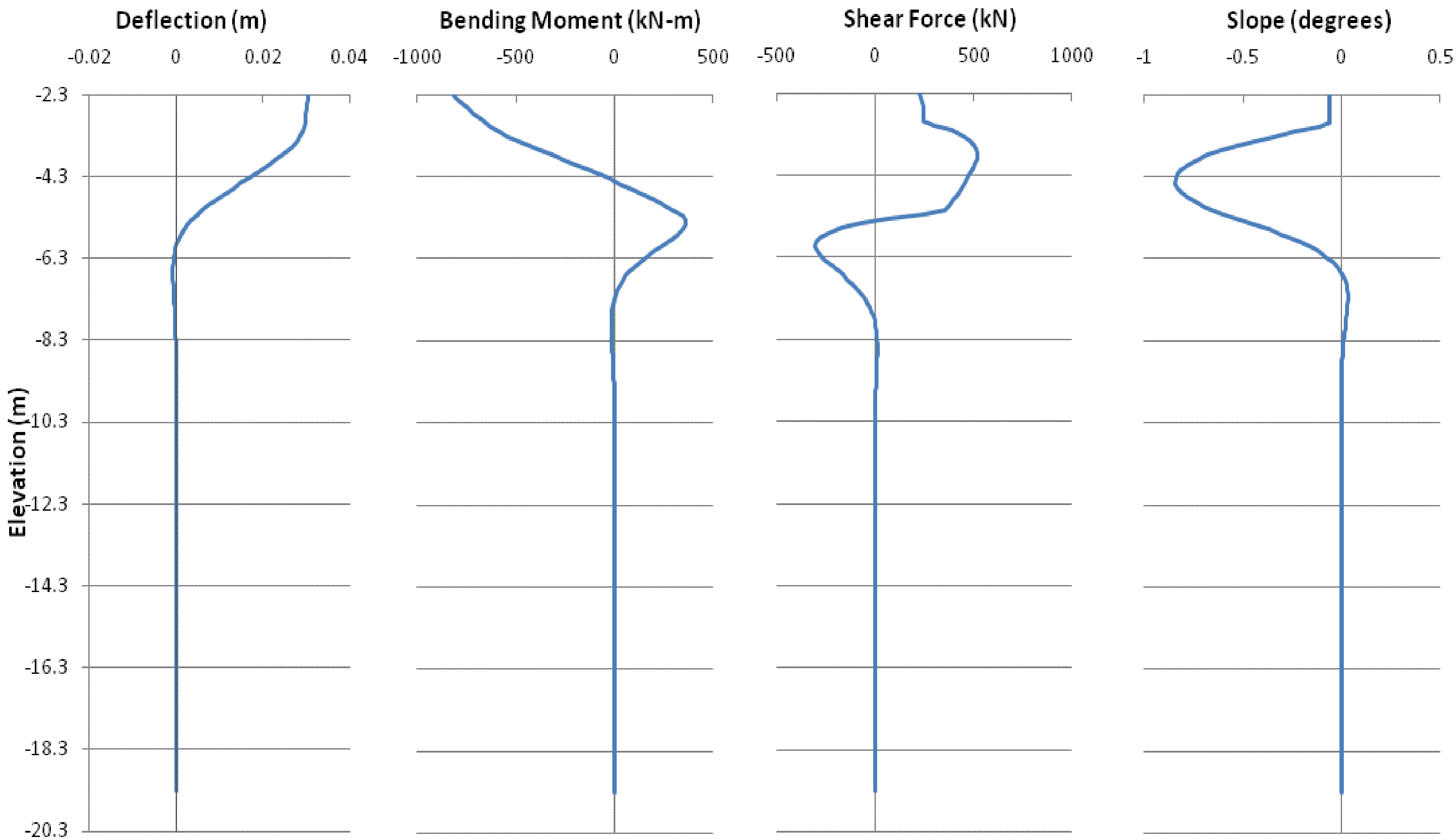

Figure 6-69: Deterministic computed pile response for the Rio Estrella Bridge south abutment from the 1991 Limon earthquake

By assuming the development of a water film and limiting the majority of the lateral spreading displacement to the top of the liquefied layer, the deterministic analysis was able to reasonably replicate the pile response results observed in the field following the 1991 Limon earthquake. Because the pile caps at the southern abutment of the Rio Estrella Bridge are located approximately 5.8 meters below the native ground surface, it is impossible to measure the true displacement and rotation of the pile caps. However, Youd et al. (1992) reported that the surveyed location of the top of the south abutment following the earthquake was within about 0.24 meter of its proper location according to the bridge plans. This error is likely caused by typical construction inaccuracies and has little or nothing to do with the earthquake itself, because the measurements show a lengthening of the bridge rather than a compression as would result from lateral spread displacements. Regardless, it is clear that no significant deformations of the pile cap occurred or else more noticeable deformations/rotations of the bridge abutment would have been measured following the earthquake.

6.7.6 Performance-Based Pile Response

A performance-based pile response analysis was performed for the equivalent single pile representing the foundation at the southern abutment of the Rio Estrella Bridge according to the procedure described in Chapter 5 of this report. A Monte Carlo simulation was performed using coefficients of variation within the ranges of those shown on Table 5-1 to estimate the variance of the pile response to the various levels of kinematic loading in the performance-based procedure. Because there is considerable uncertainty surrounding the passive load applied to the abutment piers from the overlying non-liquefied soil crust and approach embankment, the resulting overturning moment and corresponding total passive force was randomized using a log-normal probability distribution with mean moment equal to 274,100 kN-m and a logarithmic standard deviation equal to 0.16. Again, the presence of a water film was assumed in the analysis, and the lateral spreading displacement profiles shown in Figure 6-68 were used in the analysis. The results of the performance-based pile response analysis are shown in Figure 6-70.

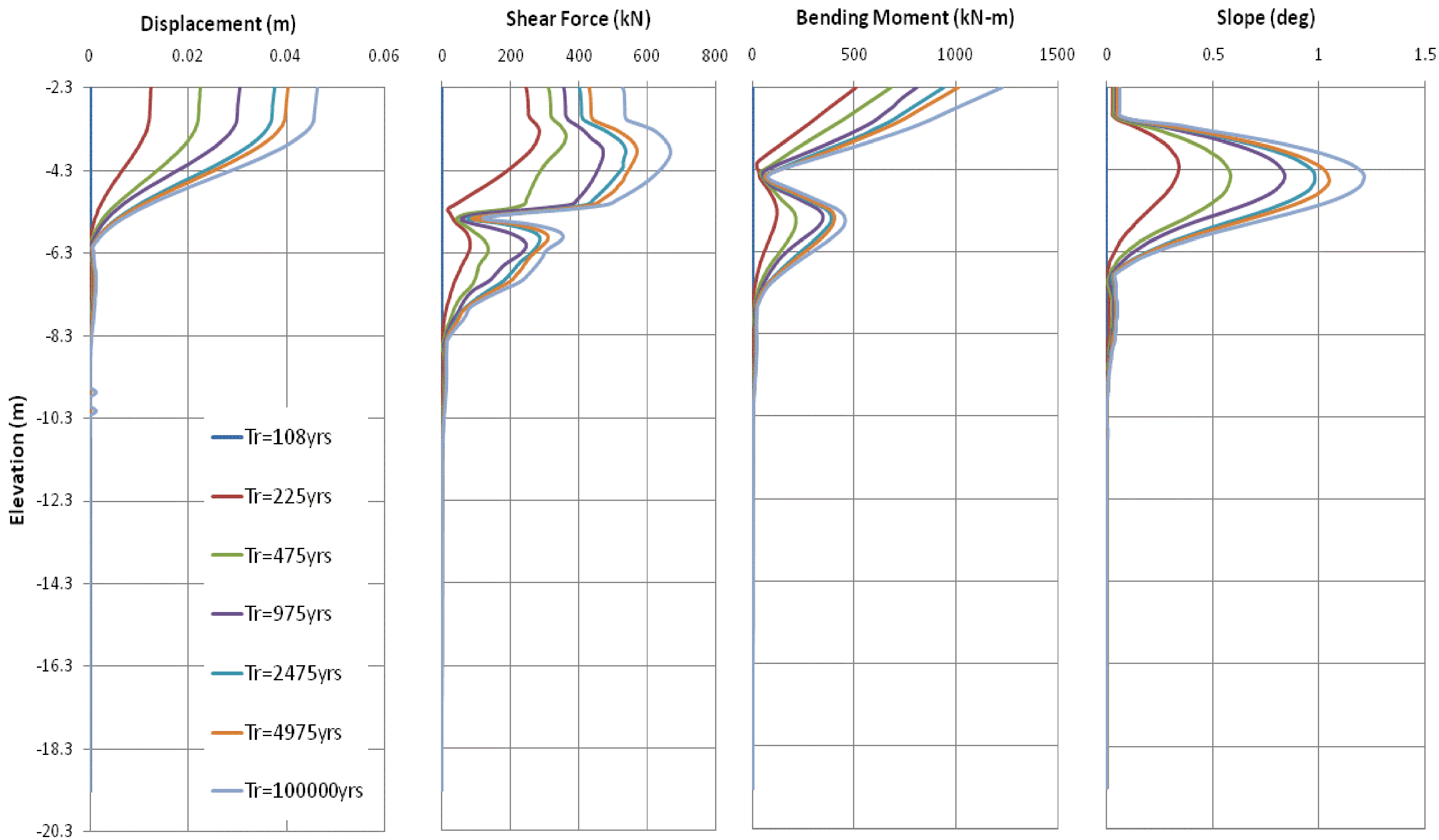

Figure 6-70: Performance-based pile response results for an average single pile at the south abutment of the Rio Estrella Bridge assuming the majority of lateral spreading is concentrated in a water film at an approximate elevation of approximately -1.0 meter.

6.7.7 Discussion of Results

The performance-based pile response analysis at the southern abutment of the Rio Estrella Bridge demonstrates that the magnitude of lateral spreading displacement likely would have been negligible as long as the majority of that displacement was concentrated in a water film at the top of the liquefiable layer (~elevation -1.0 meter). If we assume that such a water film developed during soil liquefaction, foundation deformations would have been limited due to the fact that the pile caps would have been located approximately 1.3 meters below the water film, and most of the lateral spreading deformations would have loaded the relatively narrow abutment piers rather than the relatively wide pile caps. While it is currently impossible to conclusively state that such a water film developed in conjunction with liquefaction during the 1991 Limon earthquake, the back-calculated analytical evidence and the observed soil stratigraphy support the theory. A potentially useful future study would be to attempt to model the abutment using a dynamic finite element model and/or a scaled centrifuge model in order to observe whether a water film develops during dynamic loading and liquefaction of the soil.

The computed deterministic pile response shown in Figure 6-69 showed a peak pile displacement of approximately 0.03 meter, a peak bending moment of approximately 820 kN-m, a peak shear force of approximately 500 kN, and a maximum slope of 0.84 degrees. These values of pile response correspond to return periods of 907, 1046, 1906, and 1012 years, respectively. These return periods correspond to probabilities of exceedance equal to 7.9%, 6.9%, 3.9%, and 7.1% in 75 years, respectively. These return periods also match reasonably well those computed in the performance-based pile response analysis for the Rio Bananito Railway Bridge.

7 Summary and Conclusions

Lateral spreading is a term commonly used to describe the permanent deformation of the ground resulting from soil liquefaction due to earthquake shaking. Its effects on infrastructure and critical lifelines can be devastating. This study reviewed and summarized many of the basic mechanics behind liquefaction initiation and subsequent occurrence of lateral spreading. In addition, several of the simplified empirical procedures currently used in engineering practice to design for these phenomena were presented and briefly discussed.

This study introduced a new pile response procedure based on the Pacific Earthquake Engineering Research Center's performance-based earthquake engineering framework for computing performance-based kinematic pile response due to lateral spreading displacement. Unlike previously published performance-based models for computing kinematic pile response, the procedure presented in this study is not aimed solely at bridge foundations, and has the capability of producing probabilistic estimates of kinematic pile response for any deep foundation system subjected to lateral spreading displacements. The procedure utilizes and combines previously published methodologies for evaluating liquefaction triggering, estimating lateral spreading displacements, and computing pile response using p-y soil springs with popular analytical software such as LPILE in order to produce probabilistic estimates of kinematic pile response for either single piles or pile groups.

This study developed and presented five separate lateral spreading case histories involving bridges that were damaged following the April 22, 1991 earthquake which struck the Limon Province in Costa Rica. The magnitude 7.6 earthquake killed 53 people, injured another 193 people, and disrupted an estimated 30-percent of the highway pavement and railways in the region due to fissures, scarps, and soil settlements resulting from liquefaction. As part of this study, a subsurface exploration program was developed to evaluate the soil conditions at each of the five selected bridges, where post-earthquake structural damage was observed to range from moderate to severe. As a result, this study will significantly increase the number of available case histories for researchers investigating lateral spreading and its effects on bridge structures and their foundations, and should prove to be a valuable addition to the field of earthquake hazard mitigation.

Deterministic estimates of kinematic pile response were computed in this study and (where appropriate) compared against the results of the performance-based kinematic pile response procedure. This comparison demonstrates that the proposed performance-based procedure for estimating kinematic pile response due to lateral spreading displacement produces reasonable probabilistic estimates of pile response and could be used by engineers and owners to objectively evaluate the risk posed to a given deep foundation system from liquefaction-induced lateral spreading. This study demonstrates that both deterministic and performance-based simplified pile response procedures are capable of reasonably modeling the response of even fairly complex systems for most cases given that sufficient information regarding the forces, mechanisms, and uncertainties involved is available for incorporation into the model.

The following conclusions can be reached from the observed results of this study:

1. Empirical and simplified procedures for computing liquefaction triggering and lateral spreading displacements can produce reasonable results if proper input parameters are used;

2. The three empirical lateral spreading models applied in this study (Youd et al., 2002; Bardet et al., 2002; and Baska, 2002) each computed lateral spreading displacements that matched reasonably well with observed lateral spreading displacements following the 1991 Limon earthquake. All observed displacements (with the exception of Rio Bananito Highway Bridge) fell within the computed 95-percent confidence interval for each model. The three models were generally in good agreement with one another for every case history analyzed, with the Baska (2002) model consistently computing the largest displacements. The models appear to possibly under-predict lateral spreading displacements for cases where shear forces in the soil are likely relatively large (e.g., free-face ratios greater than 20-percent) or for cases where void redistribution/water film development may govern the soil deformation behavior.

3. Extrapolation of empirical lateral spreading models may produce reasonable results, but caution and engineering judgment should be applied in interpreting and utilizing such results;

4. Simplified kinematic pile response analysis methods incorporating equivalent single pile techniques appear capable of producing reasonable approximations of the average pile response from a given deterministic event if all of the significant contributing factors to the pile response (e.g. restraining "strut" loads from a bridge deck, etc.) are adequately accounted for;

5. Modern procedures for computing kinematic pile response at bridges may not adequately consider the restraining force supplied by the possible presence of the bridge deck. Results from this study suggest that for rigid abutments, the bridge deck may significantly alter the kinematic pile response by limiting lateral displacements at the head of the pile group and causing the abutment to rotate beneath the bridge deck;

6. Both lateral spreading displacement in the native soils and seismic slope displacement in an approach embankment can apply significant kinematic loads to the pile foundations of a bridge. Therefore, both modes of ground deformation should be considered in a deterministic analysis, and the governing deformation should drive the pile response model;

7. Flow liquefaction failure can impose significant damage to deep foundations and the structures which they support. Therefore, ground improvement or other preventative measures should be incorporated to either mitigate the triggering of liquefaction or to limit its effects if flow failure is determined to be a viable risk.

8. The occurrence of a water film due to particle redistribution during liquefaction can significantly increase the ground deformations resulting from an earthquake. Therefore, if the development of a water film is considered a viability, ground deformations resulting from the design earthquake may be much larger than those computed by traditional analysis methods;

9. Due to the observed performance of the foundation beneath the south abutment of the Rio Estrella Bridge and the results of the pile response analyses of this study, it may be possible to significantly limit the deformations and corresponding damage to a given structure if the foundation is placed below the depth where significant soil deformations are occurring due to liquefaction and lateral spreading. We acknowledge that few cases would likely exist where such a solution would be considered economical, but for cases where the footings or pile cap must be placed at depth for other design requirements (e.g. scour limitations), no additional ground improvement for liquefaction/lateral spreading mitigation may be necessary if an analysis demonstrates that the foundation will be able to resist the anticipated kinematic loads;

10. The results from the performance-based kinematic pile response analysis performed at the Rio Bananito Railway Bridge and the Rio Estrella Bridge suggest that the kinematic pile response observed during the 1991 Limon earthquake corresponds to a return period between about 600 years and 1900 years (probabilities of exceedance equal to 8% and 2.6% in 50 years, respectively).

References

Abdoun, T. H., Dobry, R., O'Rourke, T. D., & Chaudhuri, D. (1996). Centrifuge modeling of seismically-induced lateral deformation during liquefaction and its effects on a pile foundation. *6th Japan - U.S. Workshop on Earthquake Resistant Design of Lifeline Facilities and Countermeasures Against Soil Liquefaction, Report No. NCEER-96-0012* , 525-539. Buffalo, New York: SUNY.

Abdoun, T., Dobry, R., & O'Rourke, T. D. (1997). Centrifuge and numerical modeling of soil-pile interaction during earthquake induced soil liquefaction and lateral spreading. *Observation and Modeling in Numerical Analysis and Model Tests in Dynamic Soil-Structure Interaction Problems, Geotechnical Special Publication No. 64* , 76-90. New York: ASCE.

Abrahamson, N. A., & Silva, W. J. (2008). Summary of the Abrahamson & Silva NGA ground-motion relations. *Earthquake Spectra , 24* (1), 67-98.

Abramowitz, & Stegun. (1965). *Handbook of Mathematical Functions.* Dover Publications (originally published by the National Bureau of Standards, 1964).

Adachi, N., Miyamoto, Y., & Koyamada, K. (1998, September 25). Shaking table test and lateral loading for pile foundation in saturated sand. *Proceedings, International Conference Centrifuge '98* , 289-294. (T. Kimura, O. Kusakabe, & J. Takemura, Eds.) Tokyo, Japan.

Al Atik, L. (2009, September). NGA Excel Spreadsheet, Version 1.0. Pacific Earthquake Engineering Research Center; http://peer.berkeley.edu/products/rep_nga_models.html.

Ambraseys, N. (1988). Engineering seismology. *Journal of Earthquake Engineering and Stuctural Dynamics , 17*, 1-105.

American Petroleum Institute (API). (1993). *Recommended practice for planning, design, and constructing fixed offshore platforms, API-RP-2A-WSD, 20th Ed.* Washington D.C.: API.

Arduino, P., Ilankatharan, M., Kramer, S. L., Kutter, B. L., & Shin, H. -S. (2006). Experimental and numerical analysis of seismic soil-pile-structure interaction of a two-span bridge. *Proceedings, 8th U.S. National Conference on Earthquake Engineering, Paper No. 504* . San Francisco, CA.

Ashford, S. A., & Rollins, K. M. (2002). TILT: Treasure Island liquefaction test final report. *Report No. SSRP-2001/17* . Department of Structural Engineering, University of California, San Diego.

Ashford, S. A., Juirnarongrit, T., Sugano, T., & Hamada, M. (2006). Soil-pile response to blast-induced lateral spreading I: Field Test. *Journal of Geotechnical and Geoenvironmental Engineering , 132 , 2*, 152-162. ASCE.

Atkinson, G. M., & Boore, D. M. (2003). Empirical ground-motion relations for subduction-zone earthquake and their application to Cascadia and other regions. *Bulletin of the Seismological Society of America , 93 , 4*, 1703-1729.

Balakrishnan, A., Kutter, B. L., & Idriss, I. M. (1997). Liquefaction remediation at bridge sites - centrifuge data report for BAM05. *Report No. UCD/CGMDR-91/10* . Center for Geotechnical Modeling, University of California at Davis.

Bardet, J. P., Tobita, T., Mace, N., & Hu, J. (2002). Regional modeling of liquefaction-induced ground deformation. *Earthquake Spectra , 18* (1), 19-46.

Bartlett, S. F., & Youd, T. L. (1992). Empirical analysis of horizontal ground displacement generated by liquefaction-induced lateral spread. *Technical Report No. NCEER-92-0021* , 114 pp. Buffalo, New York: National Center for Earthquake Engineering Research, State University of New York.

Bartlett, S. F., & Youd, T. L. (1995). Empirical prediction of liquefaction-induced lateral spread. *Journal of Geotechnical Engineering , 121* (4), 316-329.

Bartlett, S. (2009, June). Personal communication via email.

Baska, D. (2002). An analytical model for prediction of lateral spread displacement. *PhD Dissertation* . Seattle, Washington: University of Washington.

Bertero, R. D., & Bertero, V. V. (2004). Performance-based seismic engineering: Development and application of a comprehensive conceptual approach to the design of buildings. *Chapter 8, Earthquake Engineering: From Engineering Seismology to Performance-Based Engineering* . (Y. Bozorgnia, & V. V. Bertero, Eds.) Boca Raton, FL: CRC Press, LLC.

Boore, D. M., & Atkinson, G. M. (2008). Ground-motion prediction equations for the average horizontal component of PGA, PGV, and 5%-damped PSA at spectral periods between 0.01 s and 10.0 s. *Earthquake Spectra , 24* (1), 99-138.

Boulanger, R. W., Chang, D., Brandenberg, S. J., Armstrong, R. J., & Kutter, B. L. (2007). Chapter 12: Seismic design of pile foundations for liquefaction effects. In K. D. Pitilakis, *Earthquake Geotechnical Engineering: 4th International Conference on Earthquake Geotechnical Engineering-Invited Lectures* (pp. 277-302). Springer.

Boulanger, R. W., Kutter, B. L., Brandenberg, S. J., Singh, P., & Chang, D. (2003). Pile foundations in liquefied and laterally spreading ground: Centrifuge experiments and analysis. *Report UCD/CGM-03/01* , 205 pp. Davis, California: Center for Geotechnical Modeling, University of California.

Boulanger, R. W., Mejia, L. H., & Idriss, I. M. (1997). Liquefaction at Moss Landing during Loma Prieta earthquake. *Journal of Geotechnical and Geoenvironmental Engineering , 123* (5), 453-467.

Bowles, J. E. (1977). *Foundation Analysis and Design* , 750pp. McGraw-Hill.

Bowles, S. I. (2005). Statnamic load testing and analysis of a drilled shaft in liquefied sand. *MS Thesis* . Provo, Utah: Department of Civil and Environmental Engineering, Brigham Young University.

Brandenberg, S. J. (2005). Behavior of pile foundations in liquefied and laterally spreading ground. *PhD Dissertation* . Davis, California: University of California, Davis.

Brandenberg, S. J., Boulanger, R. W., Kutter, B. L., & Chang, D. (2007b). Liquefaction-induced softening of load transfer between pile groups and laterally spreading crusts. *Journal of Geotechnical and Geoenvironmental Engineering , 133 , 1*, 91-103. ASCE.

Brandenberg, S. J., Boulanger, R. W., Kutter, B. L., & Chang, D. (2007a). Static pushover analyses of pile groups in liquefied and laterally spreading ground in centrifuge tests. *Journal of Geotechnical and Geoenvironmental Engineering , 133 , 9*, 1055-1066. ASCE.

Bray, J. D., & Sancio, R. B. (2006). Assessment of the liquefaction susceptibility of fine-grained soils. *Journal of Geotechnical and Geoenvironmental Engineering , 132* (9), 1165-1177.

Bray, J. D., & Travasarou, T. (2007). Simplified procedure for estimating earthquake-induced deviatoric slope displacements. *Journal of Geotechnical and Geoenvironmental Engineering , 133* (4), 381-392.

Brown, D. A., & Reese, L. C. (1985). Behavior of a large scale pile group subjected to cyclic lateral loading. *Report to the minerals Management Services* . U.S. Dept. of Interior, Reston, VA.; Dept. of Research, FHWA, Washington D.C.; and U.S. Army Engineer Waterways Experiment Station, Vicksburg, MS.

Campbell, K. W., & Bozorgnia, Y. (2008). NGA ground motion model for the geometric mean horizontal component of PGA, PGV, PGD and 5% damped linear elastic response spectra for period ranging from 0.01 to 10 s. *Earthquake Spectra , 24* (1), 139-172.

Castro, G. (1969). Liquefaction of sands. *PhD Dissertation* . Cambridge, Massachusetts: Harvard University.

Cetin, K. O., Seed, R. B., Der Kiureghian, A., Tokimatsu, K., Harder Jr., L. F., Kayen, R. E., et al. (2004). Standard penetration-based probabilistic and deterministic assessment of seismic soil liquefaction potential. *Journal of Geotechnical and Geoenvironmental Engineering , 130* (12), 1314-1340.

Chen, L., Yuan, X., Zhenzhong, C., Longqing, H., Sun, R., Dong, L., et al. (2009). Liquefaction macrophenomena in the great Wenchuan earthquake. *Earthquake Engineering and Engineering Vibration , 8* (2), 219-229.

Cheng, Z., & Jeremic, B. (2009, March 15-19). Numerical modeling and simulation of soil lateral spreading against piles. *Proceedings, International Foundation Congress and Equipment Expo , 1* , 183-189. Orlando, FL.

Chiou, B. S.-J., & Youngs, R. R. (2008). An NGA model for the average horizontal component of peak ground motion and response spectra. *Earthquake Spectra , 24* (1), 173-216.

Coduto, D. P. (2001). *Foundation Design: Principles and Practices.* Upper Saddle River, NJ: Prentice-Hall, Inc.

Cornell, C. A. (1968). Engineering seismic risk analysis. *Bulletin of the Seismological Society of America , 58 , 5*.

Cornell, C. A. (1971). Probabilistic analysis of damage to structures under seismic loading. *Dynamic Waves in Civil Engineering* . London, England: Interscience.

Cornell, C. A., & Krawinkler, H. (2000, April). Progress and challenges in seismic performance assessment. *PEER News* , 1-3. Pacific Earthquake Engineering Research Center.

Coulter, M., & Migliaccio, L. (1966). Effects of the earthquake of March 27, 1964 at Valdez, Alaska. *Professional Paper 542-C* . Washington, D.C.: U.S. Geological Survey, U.S. Department of the Interior.

Cubrinovski, M., & Ishihara, K. (2004). Simplified method for analysis of piles undergoing lateral spreading in liquefied soils. *Soils and Foundations , 44* (5), 119-133.

Das, B. M. (2004). *Principles of Foundation Engineering, 5th Edition.* Pacific Grove, CA: Brooks/Cole-Thomson Learning.

Deierlein, G. G., Krawinkler, H., & Cornell, C. A. (2003). A framework for performance-based earthquake engineering. *Proceedings, 2003 Pacific Conference on Earthquake Engineering* .

Der-Kiureghian, A., & Ang, A. S. (1977). A fault-rupture model for seismic risk analysis. *Bulletin of the Seismological Society of America , 67 , 4*, 1173-1194.

Dobry, R., Abdoun, T., O'Rourke, T. D., & Goh, S. H. (2003). Single piles in lateral spreads: Field bending moment evaluation. *Journal of Geotechnical and Geoenvironmental Engineering , 129 , 10*, 879-889. ASCE.

Duncan, J. M. (2000). Factors of safety and reliability in geotechnical engineering. *Journal of Geotechnical and Geoenvironmental Engineering , 126* (4), 307-316.

Earthquake Engineering Research Institute (EERI). (1991). Costa Rica Earthquake Reconnaissance Report. *Earthquake Spectra , 7 , Sup B*, 127 p. EERI.

Ensoft. (2004). *LPILE Plus 5.0* . developed by Ensoft, Inc.

Faccioli, E., Paolucci, R., & Pessina, V. (2002). Engineering assessment of seismic hazard and long period ground motions at the Bolu Viaduct site following the November 1999 earthquake. *Journal of Seismology , 6 , 3*, 307-327.

Finn, W. D., & Thavaraj, T. (2001). Deep foundations in liquefiable soils: case histories, centrifuge tests and methods of analysis. *Proceedings, 4th International Conference on Recent Advances in Geotechnical Earthquake Engineering and Soil Dynamics, Paper No. SOAP-1* , 1-11. (S. Prakash, Ed.) Rolla, Missouri: University of Missouri-Rolla.

Franke, K. W. (2005). Development of a performance-based model for the prediction of lateral spreading displacements. *MS Thesis* , 276 pp. Seattle, WA: The University of Washington.

Gonzalez, L., Abdoun, T., & Dobry, R. (2005, March 16-19). Effect of soil permeability on centrifuge modeling of pile response to lateral spreading. *Seismic Performance and Simulation of Pile Foundations in Liquefied and Laterally Spreading Ground, Proceedings* . Davis, California: University of California, Davis.

Gu, W. H., Morgenstern, N. R., & Robertson, P. K. (1994). Post-earthquake deformation analysis of wildlife site. *Journal of Geotechnical Engineering , 120* (2), 274-289.

Gutenberg, B., & Richter, C. F. (1944). Frequencey of earthquakes in California. *Bulletin of the Seismological Society of America , 34 , 4*, 1985-1988.

Hahn, G. J., & Shapiro, S. S. (1967). *Statistical Models in Engineering.* John Wiley.

Haigh, S. K. (2002). Effects of liquefaction on pile foundations in sloping ground. *PhD Dissertation* . Cambridge, England: Cambridge University.

Haigh, S. K., & Madabhushi, S. P. (2002). Centrifuge modeling of lateral spreading past pile foundations. *Proceedings, International Conference on Physical Modeling in Geotechnics* . St. John's, Newfoundland, Canada.

Hales, L. J. (2003). Cyclic lateral load testing and analysis of a CISS pile in liquefied sand. *MS Thesis* . Provo, Utah: Department of Civil and Environmental Engineering, Brigham Young University.

Hara, A., Ohata, T., & Niwa, M. (1971). Shear modulus and shear strength of cohesive soils. *Soils & Foundations , 14 , 3*, 1-12. Japanese Geotechnical Society.

Harr, M. E. (1984). Reliability-based design in civil engineering. *1984 Henry M. Shaw Lecture* . Raleigh, NC: Dept. of Civil Engineering, North Carolina State University.

Hatanaka, M., & Uchida, A. (1996). Empirical correlation between penetrationresistance and effective friction of sandy soils. *Soils & Foundations , 36 , 4*, 1-9. Japanese Geotechnical Society.

He, L., Elgamal, A., Abdoun, T., Abe, A., Dobry, R., Hamada, M., et al. (2009). Liquefaction-induced lateral load on pile in a medium Dr sand layer. *Journal of Earthquake Engineering , 13 , 7*, 916-938.

Holzer, T. L., & Youd, T. L. (2007). Liquefaction, ground oscillation, and soil deformation at the Wildlife array, California. *Bulletin of the Seismological Society of America , 97* (3), 961-976.

Idriss, I. M. (2008). An NGA empirical model for estimating the horizontal spectral values generated by shallow crustal earthquakes. *Earthquake Spectra , 24* (1), 217-242.

Idriss, I. M., & Boulanger, R. W. (2007, March 5-9). Residual shear strength of liquefied soils. *Proceedings, 27th USSSD Annual meeting and Conference, Modernization and Optimization of Existing Dams and Reservoirs* . Philadelphia, Pennsylvania: U.S. Society on Dams.

Idriss, I. M., & Boulanger, R. W. (2008). *Soil Liquefaction During Earthquakes* (Vols. Monograph MNO-12). Oakland, CA: Earthquake Engineering Research Institute.

Ishihara, K. (1993). Liquefaction and flow failure during earthquakes. *Geotechnique , 43* (3), 351-415.

Ishihara, K. (1984). Post-earthquake failure of a tailings dam due to liquefaction of the pond deposit. *Proceedings, International Conference on Case Histories in Geotechnical Engineering. Vol. 3*, pp. 1129-1143. St. Louis, MO: University of Missouri.

JRA. (2002, November). *Specifications for Highway Bridges* . Japan: Japan Road Association, Preliminary English version prepared by Public Works Research Institute (PWRI) and Civil Engineering Research Laboratory (CRL.

Juirnarongrit, T., & Ashford, S. A. (2006). Soil-pile response o blast-induced lateral spreading II: Analysis and assessment of the p-y method. *Journal of Geotehcnical Engineering , 132 (2)* , 163-172. ASCE.

Kovacs, W. D., Salomone, L. A., & Yokel, F. Y. (1983). Comparison of energy measurements in the Standard Penetration Test using the cathead and rope method. *Final Report* , 99 pp. U.S. Nuclear Regulatory Commission.

Kramer, S. L. (1996). *Geotechnical Earthquake Engineering.* Upper Saddle River, NJ: Prentice Hall, Inc.

Kramer, S. L., & Mayfield, R. T. (2007). The return period of soil liquefaction. *The Journal of Geotechnical and Geoenvironmental Engineering , 133 , 7*, 1-12. ASCE.

Kramer, S. L., & Seed, H. B. (1988). Initiation of soil liquefaction under static loading conditions. *Journal of Geotechnical Engineering , 114* (4), 412-430.

Krawinkler, H. (2002). A general approach to seismic performance assessment. *Proceedings, International Conference on Advances and New Challenges in Earthquake Engineering Research* . Hong Kong, China: ICANCEER.

Krawinkler, H., & Miranda, E. (2004). Performance-based earthquake engineering. *Chapter 9, Earthquake Engineering: From Seismology to Performance-Based Engineering* . (Y. Bozorgnia, & V. V. Bertero, Eds.) Boca Raton, FL: CRC Press, LLC.

Kulhawy, F. H. (1992). On the evaluation of soil properties. *ASCE Geotechnical Special Publication No. 31* , 95-115. ASCE.

Kulhawy, F. H., & Mayne, P. W. (1990). Manual on Estimating Soil Properties for Foundation Design. *Report No. EL-6800* , 306 p. . Palo Alto, CA: Electric Power Research Institute.

Lacasse, S., & Nadim, F. (1997). Uncertainties in characterizing soil properties. *Publication No. 201* , 49-75. Oslo, Norway: Norwegian Geotechnical Institute.

Ladd, C. C., & Foott, R. (1974, July). New design procedure for stability of soft clays. *Journal of Geotechnical Engineering Division , 100 , GT7*, 763-786. ASCE.

Lam, I. P., Arduino, P., & Mackenzie-Helnwein, P. (2009, March 15-19). OPENSEES soil-pile interaction study under lateral spread loading. *Proceedings, International Foundation Congress and Equipment Expo , 1* , 206-213. Orlando, FL.

Ledezma, C., & Bray, J. D. (2010). Probabilistic performance-based procedure to evaluate pile foundations at sites with liquefaction-induced lateral displaement. *Journal of Geotechnical and Geoenvironmental Engineering , 136* (3), 464-476.

Li, X. S., & Dafalias, Y. F. (2000). Dilatancy for cohesionless soils. *Geotechnique , 50 , 4*, 449-460.

Liu, L., & Dobry, R. (1995). Effect of liquefaction on lateral response of piles by centrifuge model tests. *NCEER Bulletin , 9 , 1*, 7-11.

Lomnitz-Adler, J., & Lomnitz, C. (1979). A modified form of the Gutenberg-Richter magnitude-frequency law. *Bulletin of the Seismological Society of America , 63* , 1999-2003.

Makdisi, F. I., & Seed, H. B. (1977). A simplified procedure for estimating earthquake-induced deformations in dams and embankments. *Earthquake Engineering Research Center Report UCB/EERC-77/19* , 33 p. University of California, Berkeley.

Malvick, E. J., Kutter, B. L., Boulanger, R. W., & Kulasingam, R. (2006). Shear localization due to liquefaction-induced void redistribution in a layered infinite slope. *Journal of Geotechnical and Geoenvironmental Engineering , 132* (10), 1293-1303.

Matlock, H. (1970). Correlations for design of laterally loaded piles in soft clay. *Proceedings, 2nd Offshore Technology Conference, Paper No. OTC 1204 , 1* , 577-594. Houston, Texas.

McGuire, J. J., Zhao, L., & Jordan, T. H. (2002). Predominance of unilateral rupture for global catalog of large earthquakes. *Bulletin of the Seismological Society of America , 92 , 8*, 3309-3317.

McGuire, J. P. (1994, January 20). Liquefaction induced bridge damage in the Costa Rica earthquake of April 22, 1991. *Master's Thesis* , 91 pp. Brigham Young University.

McGuire, R. K., & Arabasz, W. J. (1990). An introduction to probabilistic seismic hazard analysis. *Geotechnical and Environmental Geophysics , 1* , 333-353. (S. H. Ward, Ed.) Society of Exporation Geophysicists.

McGuire, R. (2004). Seismic hazard and risk analysis. *Second Monograph Series MNO-10* . Earthquake Engineering Research Institute.

McVay, M., Bloomquist, D., Vanderlinde, D., & Clausen, J. (1994). Centrifuge modeling of laterally loaded pile groups in sands. *Geotechnical Tesing Journal , 17* , 129-137.

McVay, M., Casper, R., & Shang, T. (1995). Lateral response of three-row groups in loose to dense sands at 3D and 5D pile spacing. *Journal of Geotechnical Engineering , 121 , 5*, 436-441. ASCE.

Merz, H. L., & Cornell, C. A. (1973). Seismic risk analysis based on quadratic magnitude-frequency law. *Bulletin of the Seismological Society of America , 63 , 6*.

Miyajima, Kitaura, & Ando. (1991). Experiments on liquefaction-induced large ground deformation. *Proceedings, 3rd Japan-U.S. Workshop on earthquake Resistant Design of Liefeline Facilities and Countermeasures for Soil Liquefaction, Technical Report NCEER-91-0001* , 269-292. (O'Rourke, & Hamada, Eds.)

Mokwa, R. L. (1999). Investigation of the resistance of pile caps to lateral spreading. *PhD Thesis* . Blacksburg, Virginia: Department of Civil Engineering, Virginia Polytechnic Institute and State University.

Mokwa, R. L., & Duncan, J. M. (2003). Rotational restraint of pile caps during lateral loading. *Journal of Geotechnical and Geoenvironmental Engineering , 129 , 9*, 829-837. ASCE.

Morrison, C., & Reese, L. C. (1986). A lateral-load test of full-scale pile group in sand. *GR86-J* . Washington, D.C.: FHWA.

Nakase, H., Hiro-oka, A., & Yanagihata, T. (1997). Deformation characteristics of liquefied loose sand by triaxial compression tests. *Proceedings, IS-Nagoya 97, Deformation and Progressive Failure in Geomechanics* , 559-564. (A. Asaoka, T. Adachi, & F. Oka, Eds.) Pergamon, Elsevier Science.

Obermeier, S. F., & Pond, E. C. (1999). Issues in using liquefaction features for paleoseismic analysis. *Seismological Research Letters , 70* (1), 34-58.

Olson, S. M., & Johnson, C. I. (2008). Analyzing liquefaction-induced lateral spreading strength ratios. *Journal of Geotechnical and Geoenvironmental Engineering , 134* (8), 1035-1049.

Olson, S. M., & Stark, T. D. (2002). Liquefied srength ratio from liquefaction flow failure case histories. *Canadian Geotechnical Journal , 39* (3), 629-647.

Peck, R. B., Hanson, W. E., & Thornburn, T. H. (1974). *Foundation Engineering* , 514 pp. John Wiley & Sons.

Priestley, M. J., Nigel, Singh, J. P., Youd, T. L., & Rollins, K. M. (1991). Costa Rica Earthquake of April 22, 1991, Reconnaissance Report. *Earthquake Spectra, Supplement B , 7* , 79-90. EERI.

Reese, L. C., Cox, W. R., & Koop, F. D. (1974). Analysis of laterally loaded piles in sand. *Proceedings, 6th Offshore Technology Conference, Paper No. OTC 2090 , 2* , 473-483. Houston, Texas.

Reese, L. C., Cox, W. R., & Koop, F. D. (1975). Field testing and analysis of laterally loaded piles in stiff clay. *Proceedings, 7th Offshore Technology Conference, Paper No. OTC 2312* , 671-690. Houston, Texas.

Reese, L. C., Wang, S. T., Isenhower, W. M., & Arrellaga, J. A. ((2000)). *Computer program LPILE plus version 4.0 technical manual* . Ensoft, Inc., Austin, Texas.

Reid, H. F. (1911). The elastic rebound theory of earthquakes. *Bulletin of the Department of Geology , 6* , 413-444. Berkeley, CA: University of California, Berkeley.

Reiter, L. (1990). *Earthquake Hazard Analysis - Issues and Insights.* New York, NY: Columbia University Press.

Risk Engineering. (2010). EZ-FRISK version 7.43. Boulder, CO.

Rollins, K. M., Gerber, T. M., Lane, J. D., & Ashford, S. (2005). Lateral resistance of a full-scale pile group in liquefied sand. *Journal of Geotechnical and Geoenvironmental Engineering , 131 , 1*, 115-125. ASCE.

Rollins, K. M., Olsen, K. G., Jensen, D. H., Garrett, B. H., Olsen, R. J., & Egbert, J. J. (2006). Pile spacing effects on lateral pile group behavior: Analysis. *Journal of Geotechnical and Geoenvironmental Engineering , 132 , 10*, 1272-1283. ASCE.

Rollins, K. M., Peterson, K. T., & Weaver, T. J. (1998). Lateral load behavior of full-scale pile group in clay. *Journal of Geotechnical and Geoenvironmental Engineering , 124 , 6*, 468-478. ASCE.

Santana, G. (1992, July 19-24). Lessons learned and socio-economic issues arising from recent catastrophic earthquakes. *Proceedings, 10th World Conference on Earthquake Engineering* . Madrid, Spain.

Santana, G. (1991). Reporte preliminar de los registros de aceleraciones obtenidos durante el sismo del 22 de diciembre 1990. Laboratorio de Ingenieria Sismica, Instituto de Investigaciones en Ingenieria, Universidade de Costa Rica.

Santana, G., Vargas, W., Sancho, V., Segura, C., Ramirez, A., & Sibaja, R. (1991). Registro de aceleraciones del terremoto de Limon, 22 de abril de 1991. *Reporte INII 48* , 58-91. Laboratorio de Ingenieria Sismica, Instituto de Investigaciones en Ingenieria, Universidad de Costa Rica.

Sasaki, Tokaida, Matsumoto, & Saya. (1991). Shake table tests on lateral ground flow induced by soil liquefaction. *Proceedings, 3rd Japan-U.S. Workshop on Earthquake Resistant Design of Lifeline Facilities and Countermeasures for Soil Liquefaction, Technical Report NCEER-91-0001* , 371-385. (O'Rourke, & Hamada, Eds.)

Saygili, G., & Rathje, E. M. (2008). Empirical predictive models for earthquake-induced sliding displacements of slopes. *Journal of Geotechnical and Geoenvironmental Engineering , 134* (6), 790-803.

Seed, H. B. (1986). Design problems in soil liquefaction. *Journal of Geotechnical Engineering , 113* (8), 827-845.

Seed, H. B. (1979). Soil liquefaction and cyclic mobility evaluation for level ground during earthquakes. *Journal of Geotechnical Engineering , 105* (2), 201-255.

Seed, H. B., & Idriss, I. M. (1971). Simplified procedure for evaluating soil liquefaction potential. *Journal of Soil Mechanics and Foundations Div. , 97* (SM9), 1249-1273.

Seed, H. B., Idriss, I. M., & Arango, I. (1983). Evaluation of liquefaction potential using field performance data. *Journal of Geotechnical Engineering , 109* (3), 458-482.

Seed, R. B., & Harder, L. F. (1990). SPT-based analysis of cyclic pore pressure generation and undrained residual strength. *Proceedings, H. Bolton Seed Memorial Symposium , 2* , 351-376. (J. Duncan, Ed.) Berkeley, California: University of California.

Shah, H. C., Mortgat, C. P., Kiremidjian, A. S., & Zsutty, T. C. (1975). A study of seismic risk for Nicaragua, Part I. *Report 11* . Palo Alto, CA: The John A. Blume Earthquake Engineering Center, Stanford University.

Shamoto, Y., Zhang, J.-M., & Goto, S. (1997). Mechanism of large post-liquefaction deformation in saturated sand. *Soils and Foundations , 37* (2), 71-80.

Singh, P. (2002). Behavior of pile in earthquake-induced lateral spreading. *MS Thesis* . University of California, Davis.

Singh, V. P., Sharad, K. J., & Aditya, T. (2007). *Risk and Reliability Analysis.* Reston, VA: ASCE Press.

Skempton, A. W. (1957). The planning and design of of new Hong Kong airport. *Proceedings, The Institute of Civil Engineers , 7* , 305-307. London, UK.

Sladen, J. A., D'Hollander, R. D., & Krahn, J. (1985). The liquefaction of sands: a collapse surface approach. *Canadian Geotechnical Journal , 22* (4), 564-578.

Speidel, D. H. (1998). Seismicity patterns and the 'characteristic' earthquake in the Central Mississippi Valley, USA . *Engineering Geology , 50 , 1-2*, 1-8.

Toboada, V. M., Abdoun, T., & Dobry, R. (1996). Prediction of liquefaction-induced lateral spreading by dilatant sliding block model calibrated by centrifuge tests. *Proceedings, 11th World Conference on Earthquake Engineering* , Paper No. 1037. Acapulco, Mexico.

Toboada-Urtuzuastegui, V. M., & Dobry, R. (1998). Centrifuge modeling of earthquake-induced lateral spreading in sand. *Journal of Geotechnical and Geoenvironmental Engineering , 124* (12), 1195-1206.

Tokimatsu, K. (1999, June 21-25). Performance of pile foundations in laterally spreading soils. *Proceedings, 2nd International Conference of Earthquake Geotechnical Engineering , 3* , 957-964. (Seco, & P. Pinto, Eds.) Lisbon, Portugal.

Tokimatsu, K., & Asaka, A. (1998). Effects of liquefaction-induced ground displacements on pile performance in the 1995 Hyogoken-Nambu earthquake. *Soils and Foundations, Special Issue No. 2* , 163-178.

Tokimatsu, K., & Suzuki, H. (2004). Pore water pressure response around pile and its effects on p-y behavior duing soil liquefaction. *Soils and Foundations , 43 , 6*, 101-110.

Tokimatsu, K., Suzuki, H., & Suzuki, Y. (2001). Backcalculated p-y relation of liquefied soils from large shaking table tests. *Proceedings, 4th International Conference on Recent Advances in Geotechnical Earthquake Engineering and Soil Dynamics, Paper No. 6.24* . (S. Prakash, Ed.) Rolla, Missouri: University of Missouri-Rolla.

Towhata, I., Sasaki, K., Tokida, K., Matsumoto, H., Tamari, Y., & Yamuda, K. (1992). Prediction of permanent displacement of liquefied ground by means of minimum energy principle. *Soils and Foundations , 32* (3), 97-116.

United States Geologic Survey. (2008, November 8). *Shakemap atlas 199104222156*. Retrieved February 7, 2011, from USGS Shakemap Atlas: http://earthquake.usgs.gov/earthquakes/shakemap/atlas/shake/199104222156/

USGS Earthquake Hazard Program. (2010). *USGS National Seismic Hazard Mapping Project*. (EHP Web Team) Retrieved November 2, 2010, from http://earthquake.usgs.gov/hazards

Valsamis, A., Bouckovalas, G., & Dimitriadi, V. (2007, June). Numerical evaluation of lateral spreading displacements in layered soils. *Proceedings, 4th International Conference on Earthquake Geotechnical Engineering, Paper No. 1644* . Thessaloniki, Greece.

Vasquez-Herrera, A., Dobry, R., & Baziar, M. H. (1990). Re-evaluation of liquefaction triggering and flow sliding in the Lower San Fernando Dam during the 1971 earthquake. *Proceedings, 4th U.S. National Conference on Earthquake Engineering* , 783-792. Palm Springs, California.

Wang, S. T., & Reese, L. C. (1998). Design of pile foundations in liquefied soils. *Geotechnical Earthquake Engineering and Soil Dynamics III, Geotechnical Special Pub. No. 75 , 2* , 1331-1343. (P. Dakoulas, M. Yegian, & R. Holtz, Eds.) ASCE.

Weaver, T. J., Ashford, S. A., & Rollins, K. M. (2005). Response of 0.6 m cast-in-steel-shell pile in liquefied soil under lateral loading. *Journal of Geotechnical and Geoenvironmental Engineering , 131 , 1*, 94-102. ASCE.

Wells, D. L. (2000). Probabilistic seismic hazard analysis and source characterization for central and eastern North America. *Proceedings, 6th International Conference on Seismic Zonation: Managing Earthquake Risk in the 21st Century* . Oakland, CA: Earthquake Engineering Research Institute.

Wesnousky, S. G. (1994). The Gutenberg-Richter or Characteristic Earthquake distribution, Which is it? *Bulletin of the Seismological Society of America , 84* , 1940-1959.

Wesnousky, S. G., Scholz, C. H., Shimazaki, K., & Matsuda, T. (1984). Integration of geological and seismological data for the analysis of seismic hazard: a case study of Japan. *Bulletin of the Seismological Society of America , 74* , 687-708.

Whitman, R. V. (1971). Resistance of soil to liquefaction and settlement. *Soils and Foundations , 11* (4), 59-68.

Wilson, D. W. (1998). Soil-pile-superstructure interaction in liquefying sand and soft clay. *PhD Dissertation* . Davis, California: University of California at Davis.

Wilson, D. W., Boulanger, R. W., & Kutter, M. L. (2000). Observed seismic lateral resistance of liquefying sand. *Journal of Geotechnical and Geoenvironmental Engineering , 126* (10), 898-906.

Wilson, D. W., Boulanger, R. W., & Kutter, M. L. (2000). Observed seismic lateral resistance of liquefying sand. *Journal of Geotechnical and Geoenvironmental Engineering , 126 , 10*, 898-906. ASCE.

Wong, R. T., Seed, H. B., & Chan, C. K. (1975). Liquefaction of gravelly soil under cyclic loading conditions. *Journal of the Geotechnical Engineering Division , 101* (GT6), 571-583.

Yang, Z. (2000). Numerical modeling of earthquake site response including dilation and liquefaction. *PhD Dissertation* . Graduate School of Arts and Science, Columbia University.

Yang, Z., Elgamal, A., & Parra, E. (2003). A computational model for liquefaction and associated shear deformation. *Journal of Geotechnical and Geoenvironmental Engineering , 129* (12).

Yasuda, S., Masuda, T., Yoshida, N., Kiku, H., Itafuji, S., Mine, K., et al. (1994). Torsional shear and triaxial compression tests on deformation characteristics of sands before and after liquefaction. *Proceedings, 5th U.S.-Japan Workshop on Earthquake Resistant Design of Lifeline Facitilities and Countermeasures Against Soil Liquefaction, NCEER-94-0026* , 249-266. Salt Lake City, UT.

Yasuda, S., Nagase, H., Kiku, H., & Uchida, Y. (1991). A simplified procedure for the analysis of the permanent ground displacement. *Proceedings, 3rd Japan-U.S. Workshop on Earthquake Resistant Design of Lifeline Facilities and Countermeasures for Soil Liquefaction, Technical Report NCEER-91-0001* , 225-236. (O'Rourke, & Hamada, Eds.)

Yoshida, N., & Hamada, M. (1990). Analysis of damages of foundation piles due to liquefaction-induced permanent ground displacements. *Proceedings, 8th Japan Earthquake Engineering Symposium , 1* , 55-60.

Youd, T. L. (1993, January). Liquefaction, ground failure, and consequent damage during the 22 April 1991 Costa Rica earthquake. *Proceedings, U.S.-Costa Rica Workshop, Costa Rica Earthquakes of 1990-1991, Effects on Soils and Structures, EERI Publication No. 93-A* , 74-95. EERI.

Youd, T. L. (2005, October). Liquefaction-induced flow, lateral spread, and ground oscillation. *Proceedings, GSA Annual Meeting, Paper No. 110-6* . Salt Lake City, Utah: Geological Society of America.

Youd, T. L. (2009, June). Personal communication.

Youd, T. L. (1984). Recurrence of liquefaction at the same site. *Proceedings, 8th World Conference on Earthquake Engineering*, *Vol. 3*, pp. 231-238.

Youd, T. L., & Hoose, S. N. (1977). Liquefaction susceptibility and geologic setting. *Proceedings, 6th World Conference on Earthquake Engineering*, *Vol. 3*, pp. 2189-2194. New Delhi.

Youd, T. L., DeDen, D. W., Bray, J. D., Sancio, R. B., Cetin, K. O., & Gerber, T. M. (2009). Zero-displacement lateral spreads, 1999 Kocaeli, Turkey, earthquake. *Journal of Geotechnical and Geoenvironmental Engineering , 135* (1), 46-61.

Youd, T. L., Idriss, I. M., Andrus, R. D., Arango, I., Castro, G., Christian, J. T., et al. (2001). Liquefaction resistance of soils; summary report from the 1996 NCEER and 1998 NCEER/NSF workshops on evaluation of liquefaction resistance of soils. *Journal of Geotechnical and Geoenvironmental Engineering , 127* (10), 817-833.

Youd, T. L., Rollins, K. M., Salazar, A. F., & Wallace, R. M. (1992, July 19-25). Bridge damage caused by liquefaction during the 22 April 1991 Costa Rica earthquake. *Proceedings, 10th World Conference on Earthquake Engineering , 1* , 153-158. Madrid, Spain.

Youngs, R. R., & Coppersmith, K. J. (1985). Implications of fault slip rates and earthquake recurrence models to probabilistic seismic hazard assessments. *Bulletin of the Seismological Society of America , 75 , 4*, 939-964.

Youngs, R. R., Chiou, S. J., Silva, W. J., & Humphrey, J. R. (1997). Strong ground motion attenuation relationships for subduction zone earthquake. *Seismological Research Letters , 68* (1), 58-73.

Zhao, J. X., Zhang, J., Asano, A., Ohno, Y., Oouchi, T., Takahashi, T., et al. (2006). Attenuation relations of strong ground motoin in Japan using site classification based on predominat period. *Bulletin of Seismological Society of America , 96 , 3*, 898-913.

Appendix A. Geotechnical Study Report

INGENIERIA SUELOS Y MATERIALES

INSUMA S.A.

INGENIEROS Y GEOLOGOS CONSULTORES

BRIGHAM YOUNG UNIVERSITY

GEOTECHNICAL STUDY

BRIDGES IN LIMÓN

PROVINCE OF LIMÓN, COSTA RICA

INSUMA S.A.
Geotechnical Consultants

July, 2010

Apartado: 2128-1002 Paseo Estudiantes · Tels.: (506) 2234-5070 · Tel.Fax: (506) 2234-9290 San José, Costa Rica
E-mail: insuma@racsa.co.cr

INGENIERIA SUELOS Y MATERIALES
insuma s.a.
INGENIEROS Y GEOLOGOS CONSULTORES

San José, July 12th, 2010
2056-10

Prof. Kyle Rollins
Department of Civil and Environmental Engineering
Brigham Young University
Provo, Utah

Dear Prof. Rollins:

We present the results of the Geotechnical Study carried out in several bridge sites of the province of Limón, in Costa Rica. The investigated sites correspond to several bridge structures that suffered damages during the Limón-Telire Earthquake, occurred in April of 1991. The investigated sites are listed below:

- Río Cuba Highway Bridge
- Río Blanco Highway Bridge
- Río Bananito Highway Bridge
- Río Estrella Highway Bridge
- Río Bananito Railroad Bridge

The objective of the investigation was to determine the geotechnical conditions of each of the different sites. This objective was achieved through the execution of field and laboratory tests. This report includes, among other things, the field and laboratory information that was used to determine the soil profile and the physical and mechanical characteristics of the materials.

We hope that this report is to your satisfaction and we are available for any further consultation you may have.

Sincerely,
INSUMA S.A.
Geotechnical Consultants

Ing. José A. Rodríguez Barquero **Ing. José P. Rodríguez Calderón, MSc.**

C: File

Apartado: 2128-1002 Paseo Estudiantes · Tels.: (506) 2234-5070 · Tel.Fax: (506) 2234-9290 San José, Costa Rica
E-mail: insuma@racsa.co.cr

TABLE OF CONTENTS

1. INTRODUCTION

Attending the request of Prof. Kyle Rollins from Brigham Young University and as proposed in document C114-10, INSUMA executed a geotechnical study in several bridge sites of the province of Limón, in Costa Rica. The bridge sites that were investigated are indicated in Table 1 and their location is presented in Figure 1.

Table 1: Bridge sites that were investigated in Limón, Costa Rica

Bridge Site	Location	
	Latitude	Longitude
Río Blanco Highway Bridge	9.99178	-83.125333
Río Cuba Highway Bridge	10.02237	-83.217967
Río Bananito Railroad Bridge	9.8765	-83.0076
Río Bananito Highway Bridge	9.88492	-82.966883
Río Estrella Highway Bridge	9.78760	-82.9134

Figure 1: Location of the different sites investigated during the study

The geotechnical study was requested as part of a research investigation being carried out by Prof. Rollins, which is related to the topic of soil liquefaction. Each of the investigated sites have the particular characteristic that they host bridge structures that were damaged during the occurrence of the Limón-Telire Eartquake, in April of 1991. The damages in the bridges were mainly due to the effects of liquefaction.

The objective of the investigation was to determine the geotechnical characteristics at each of the investigated sites. These characteristics include, among other things, the soil profiles and the physical and mechanical properties of the soil layers present at the subsurface levels. This objective was achieved through the execution of borings and laboratory tests that was analyzed in order to establish the geotechnical profiles and the soil properties. The results of the study are presented in this report, which has been divided into several sections.

Section 1 of the report corresponds to the introduction and it mainly describes the content of the report. The objectives and the scope of the investigation are described in Section 2, while the executed works and the methods followed to carry out the works are explained in Section 3.

In order to make a better interpretation of the geotechnical conditions of the site, it is necessary to have a good understanding of the regional geological conditions. Therefore, Section 4 presents a brief description of the geological framework present at the different sites that have been investigated. Even though these sites are distant from one another, the geological and geomorphological conditions are very similar throughout the region.

Once the geological framework has been established, the results obtained for each particular site are presented. Sections 5 through 9 are related to the specific results and geotechnical conditions detected for each of the investigated bridges. The following information is included for each of these sections: 1) brief description of the bridge site and summary of the works executed at the site, 2) description and properties of the soil layers that appear, and 3) soil profile interpreted from the field and laboratory information.

The specific results for each of the studied bridge sites are followed by Section 10 which corresponds to the conclusions of the investigation. To complement the report, five appendices are included and they correspond to the boring logs for each of the boreholes executed at the different bridge sites.

2. OBJECTIVES AND SCOPE OF THE STUDY

The main objective of the investigation is to determine the geotechnical conditions of each of the 5 bridge sites that were defined previously. In order to achieve this general objective, several specific objectives have been defined. Some of the specific objectives are: to determine the geological conditions of the region, to determine the physical and mechanical properties of the different soil layers that appear at the site, and to elaborate a geotechnical model based on the obtained information and based on INSUMA's interpretation.

In order to achieve the mentioned objectives, field and laboratory works were executed and the geotechnical information required to fulfill the objectives was acquired. A detail of the executed works is included in Section 3 of the report.

The executed investigation was carried out following methods that are currently accepted in geotechnical engineering and that comply both with national and international standards. The field and laboratory tests performed as part of the investigation were executed following procedures defined in the ASTM standards.

The scope of the study has been limited to determining the geotechnical conditions of the site; therefore, it does not include any type of analysis regarding foundation of structures, mathematical modeling and/or other types of analysis such as soil liquefaction. It should be understood that these types of analysis and models will probably be done in latter stages of the research project which is underway.

3. EXECUTED WORKS

The geotechnical investigation was divided into three different phases: 1) Field Works, 2) Laboratory Works, and 3) Analysis and interpretation. A more detailed description of each phase is presented below.

3.1 Field Works

The first activity of this phase of the investigation consisted in visits by engineers José A. Rodríguez Barquero and José P. Rodríguez Calderón from INSUMA. These visits were carried out with Prof. Kyle Rollins from BYU and their objective was to coordinate logistical aspects, see the advance of the field works, coordinate the location of the boreholes and gather the basic geological/geotechnical information of each of the sites.

The second activity of the field works consisted in the execution of the boreholes. This activity was supervised by personnel associated to BYU. The location of the boreholes was selected by Prof. Rollins and most of these drillings were executed in the right margin of each of the rivers, with the exception of the Río Bananito Railroad Bridge whose boreholes were done in the left margin. Table 2 summarizes the boreholes executed in each bridge site, the depth reached in the borehole, and the method of drilling used.

Table 2: Summary of the executed boreholes – Bridges in Limón, Costa Rica

Bridge Site	Quantity of Boreholes	Depth of Borehole	Method of Drilling
Río Cuba Highway Bridge	1	15 m	SPT + Casing
Río Blanco Highway Bridge	1	15 m	SPT + Casing
Río Bananito Highway Bridge	2	20 m 20 m	SPT + Casing
Río Estrella Highway Bridge	1	20 m	SPT + Casing
Río Bananito Railroad Bridge	2	14 m 14 m	SPT + Casing

As indicated in Table 2, the boreholes were executed following the procedure of the standard penetration test (SPT). The drillings were carried out in accordance to standard ASTM D-1586. Given that loose, non-plastic saturated sands were detected at each of the sites it was necessary to use casing to prevent the drillhole from collapsing. Continuous sampling was used in all of the boreholes; hence, it was possible to determine the soil profile down to the investigated depth.

The SPT drilling method is exclusive for soils; therefore, it is not possible to drill through very hard consistency materials (e.g. rocks, boulders or rock masses). This type of drilling procedure has been used worldwide and it consists in driving a split spoon sampler with the use of a hammer. A simple sketch of the drilling procedure is indicated in Figure 2.

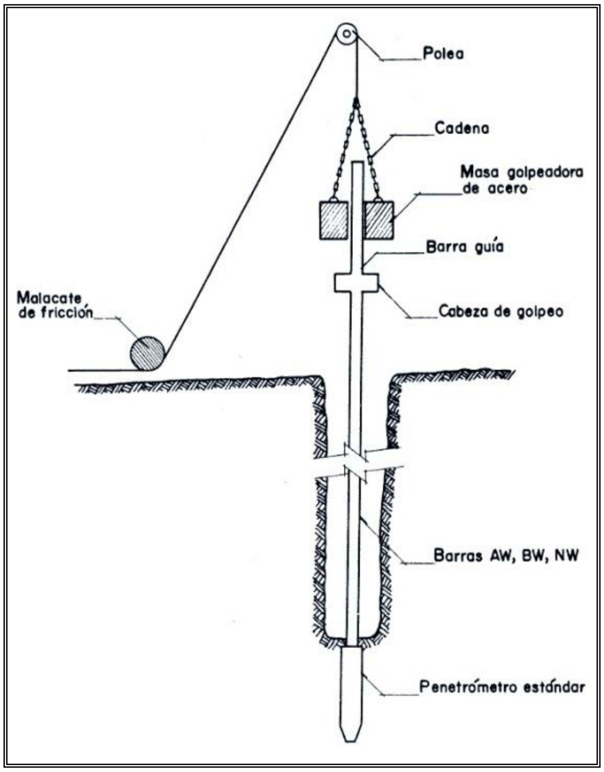

Figure 2: Sketch of the standard penetration test method (ASTM D-1586)

The dimensions of the split spoon sampler, the fall and weight of the hammer, the diameter of the bars and the rest of the materials used in the SPT method are standardized according to the specifications in ASTM D-1586. Figures 3 and 4 present some of the equipment used in the drilling procedure.

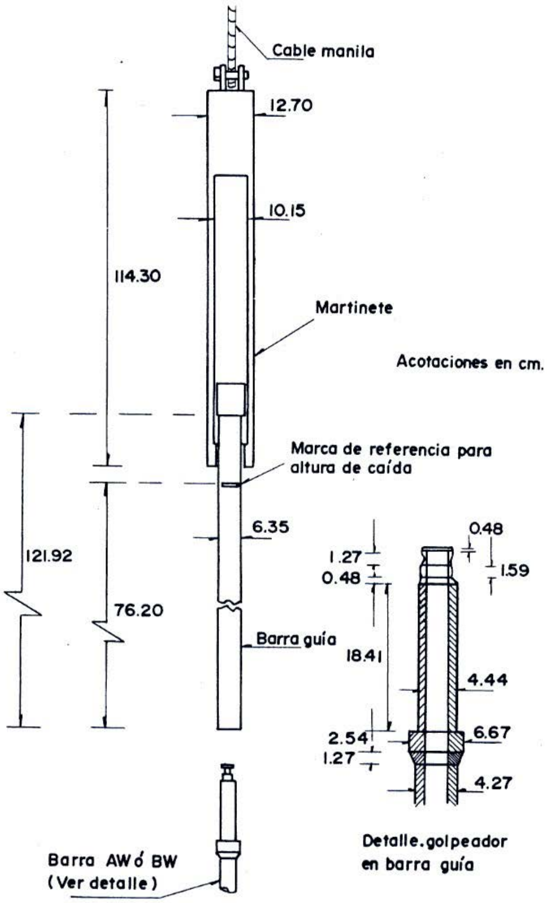

Figure 3: Detail of the 64 kg hammer and the specifications for the fall of the weight

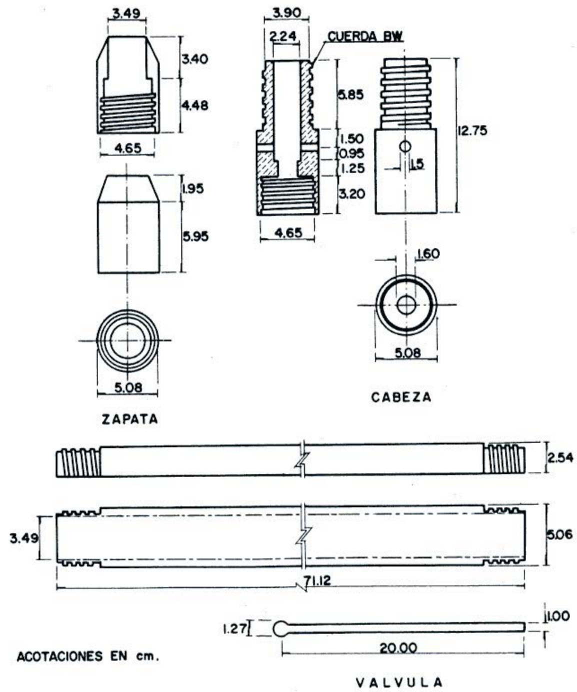

Figure 4: Detail of the standard split spoon sampler

The SPT method allows the correlation of the soil consistency with the N_{SPT} value. This value corresponds to the number of blows required to drive the standard sampler a distance of 0.3 m. In order to be able to define the N_{SPT} value and make it comparable to other investigations, it was necessary to carry out tests in order to determine the efficiency of the SPT drilling rig and its operator. These measurements were carried out directly by BYU personnel and according to the information provided the measured efficiency was higher than 90%; however, these results are not currently available to INSUMA.

The samples collected from the execution of the boreholes were described visually by the foreman of the drilling crew and they were later placed in plastic bags in order to prevent the loss of the natural water content. The samples were later transported to INSUMA's laboratory for the corresponding storage and analysis.

3.2 Laboratory Works

The second phase of the geotechnical study corresponds to the execution of the laboratory works. As indicated, the soil samples collected from the boreholes were transported to INSUMA's laboratory where a visual description was carried out by the laboratory technician. This visual description was executed to all the samples collected from the boreholes.

The visual description was complemented with the execution of the following index property tests:

- Gradation
- Percent washed in 200 Sieve
- Natural water content
- Atterberg limits

These tests were not executed on every sample, but they were carried out with a frequency of every 1.5 – 1.75 m and whenever a different type of soil was detected. All of the tests were carried out following the procedures described in the different ASTM standards. The results obtained from the laboratory tests enabled the classification of the different soil layers with the Unified Soil Classification System.

3.3 Analysis and interpretation

Once all the field and laboratory information was available, it was integrated and analyzed in order to elaborate and present the geotechnical profile of each site. It is important to indicate, as it was described in the scope of the investigation, that this phase of the investigation does not include any type of liquefaction or foundation analysis and/or recommendations. This will probably be done in a later stage of the research project that is being executed.

4. GEOLOGY OF THE AREA

Even though the different bridge sites are distant from one another, the geological conditions of the region are very similar. These geological conditions have a direct influence on the type of materials detected at the different sites, as well as on their mechanical properties and therefore, on the similar geotechnical behavior observed for each of the bridges.

Based on the geological map of Limón (CR2CM-6), scale 1:200.000, the geology of the area consists of Alluvial and coastal deposits (Qal). From the lithological point of view and specifically in the areas near the coast, these deposits are made up of fine sediments with sandy and clayey textures. An extract of Limón's geological map is presented in Figure 5 below. The location of each of the investigated bridge sites is shown in the map.

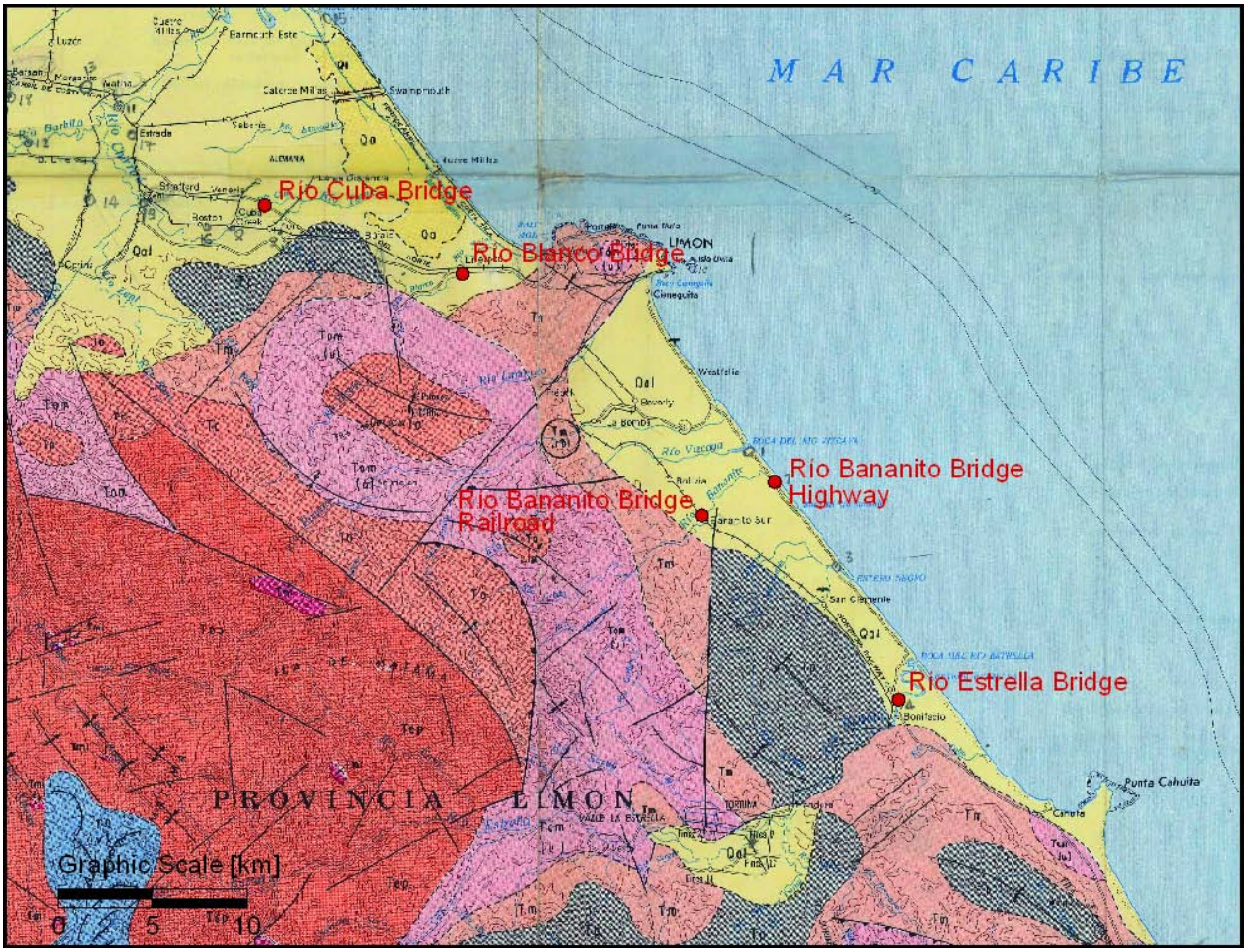

Figure 5: Geologic map of Limón (CR2CM-6) scale 1:200.000

Regarding the map shown in Figure 5, it can be observed that all five of the investigated sites lie within the areas of Alluvial and coastal deposits (Qal) which are indicated in the map with a pale yellow color. This type of geologic formation is located off the Atlantic Coast of the country but it also extends toward the north. Notice that towards the west, the geological formations change and they correspond to volcanic and sedimentary rocks associated to the Cordillera of Talamanca. This other geological formations are represented by the other colors shown in the map of Figure 5.

Regarding the geomorphological conditions of the area, the bridge sites are located in forms of alluvial sedimentation. The origin of this type of geomorphological units is associated with the sedimentation caused by rivers and/or creeks. In some cases, specifically in those areas located near the coast, there is a marine influence related to this soil deposits.

The specific alluvial unit where the bridge sites are located corresponds to the Alluvial Plain of San Carlos and the Atlantic. This unit is divided into two subunits, and the one of interest for this investigation corresponds to the one near the coast, which may have some marine influence in the formation of the soil deposits. One of the main characteristics of this unit consists in the relative flat topography.

From the seismic point of view, within the area of interest there are several active faults that can be the source of important earthquakes. The faults closer to the bridge sites are: Deformed Belt of North Panama – Limón (F2), Siquirres – Matina Fault (F1) and La Estrella Fault (F8). All of these faults are from the Quaternary (relatively recent) and they are considered active. They are indicated in Figure 6 below.

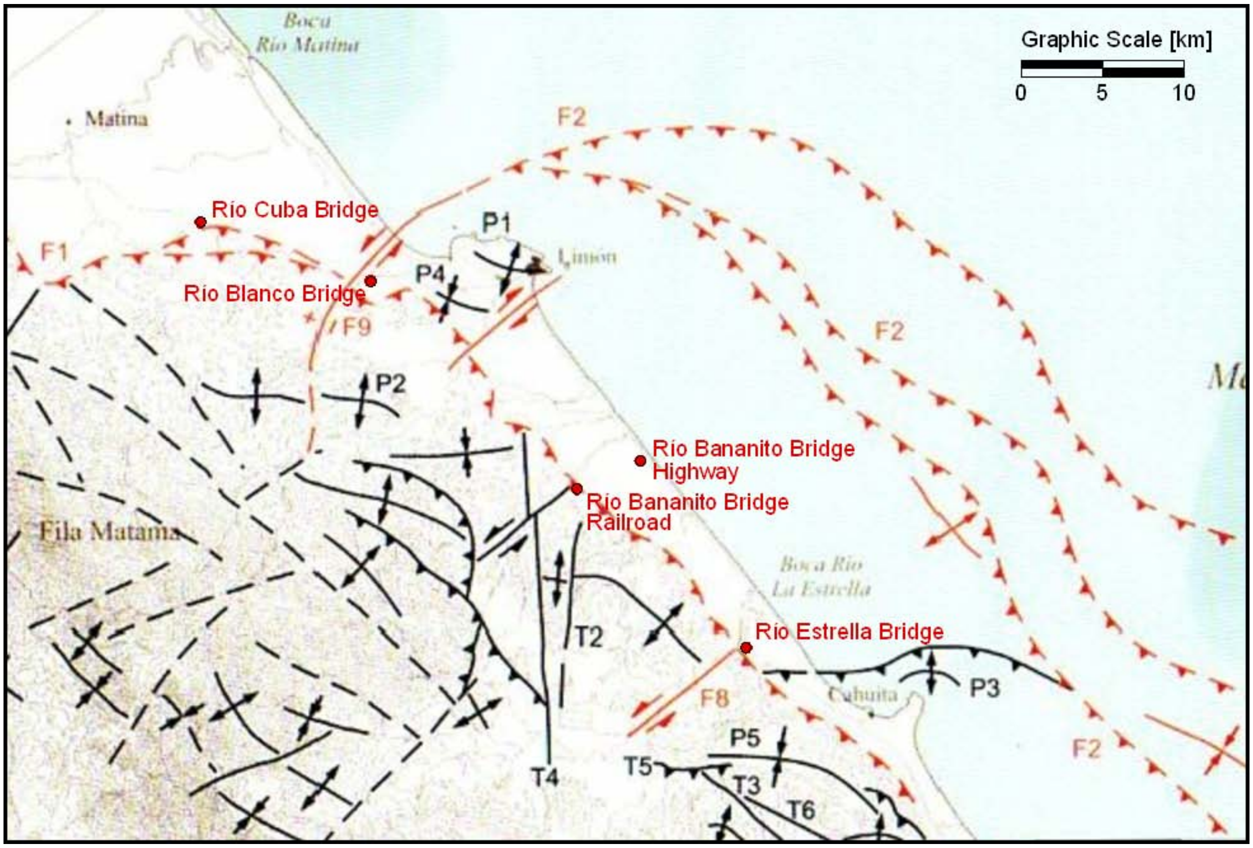

Figure 6: Tectonic map of the province of Limón (Source: Costa Rican Tectonic Atlas)

It is important to clarify that the active and recent faults from the Quaternary are shown in Figure 6 as red lines. The black lines correspond to paleotectonic faults and other geological structures that have not shown activity in the recent geologic past.

With regards to the seismicity of the area, the Limón-Telire earthquake that occurred in April 1991 is a clear example of the seismic potential of the area. For design purposes, the Costa Rican Seismic Code has identified the area as being within Zone III (see Figure 7).

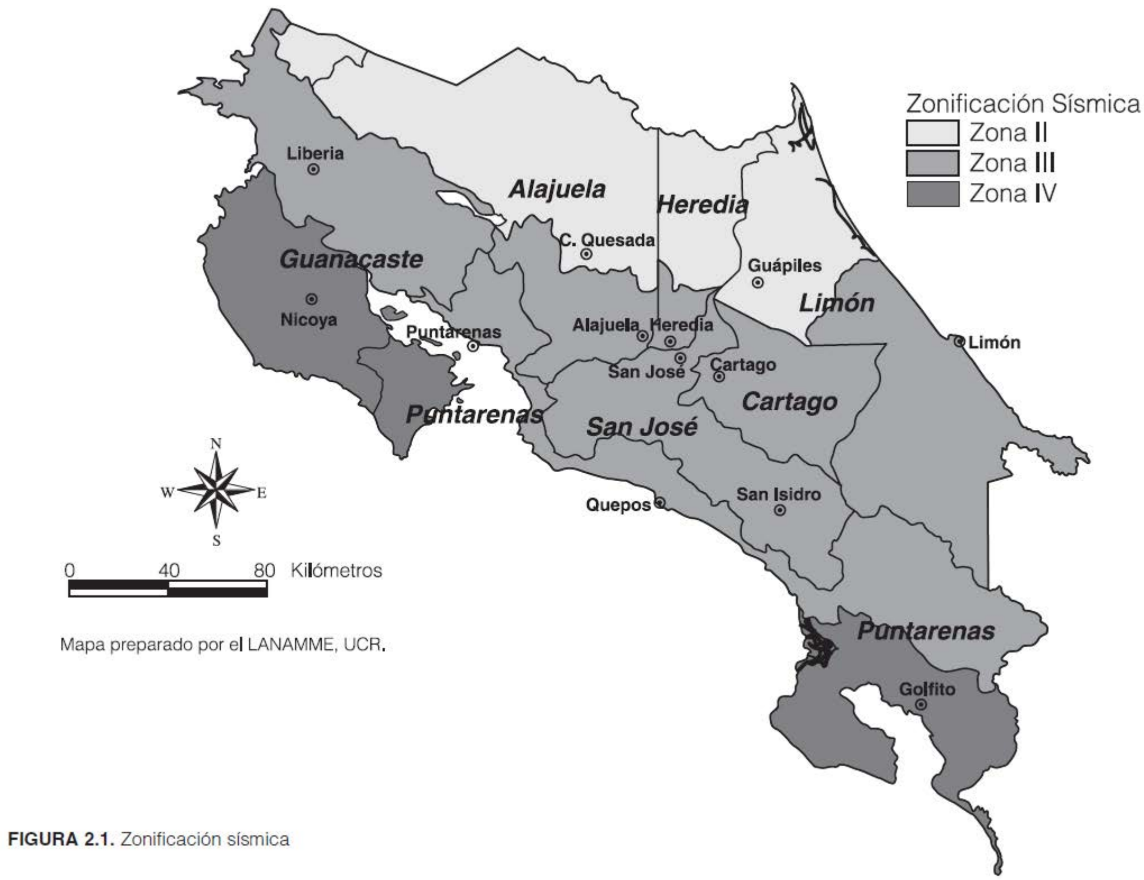

Figure 7: Seismic zoning proposed for Costa Rica (Source: Costa Rican Seismic Code 2002)

Within this area and based on the seismic threat studies that have been carried out, the design peak effective acceleration defined by the Costa Rican Seismic Code 2002 is between 0.30 and 0.36g. The peak effective acceleration will depend on the type of soil present at the site (i.e. rock, hard soils, soft soils, etc). With regards to the peak effective accelerations it is important to indicate that these values are for design and that during the Limón-Telire earthquake there were areas where the accelerations measured were higher.

With this brief geological framework of the area, it is possible to proceed with the specific results obtained for each of the investigated bridge sites.

5. RIO CUBA BRIDGE

This chapter includes the results obtained for the Río Cuba Bridge. A brief description of the site and the work executed is presented. This description is followed by a description of the geotechnical profile. The detailed results of the borings and the lab tests are presented in Appendix A, which corresponds to the boring logs.

5.1 Location and executed works

The Rio Cuba Bridge is located along national route 32, near the town of Maravilla. From the administrative/political point of view, the bridge site is located in the 7th province Limón, 5th county Matina, 3rd district Carrandí. From the geographical point of view, the site is located at coordinates 10.02237º and -83.217967º. These coordinates can be located in the map Moin, scale 1:50.000, of the Costa Rican Geographical Institute (see Figure 8).

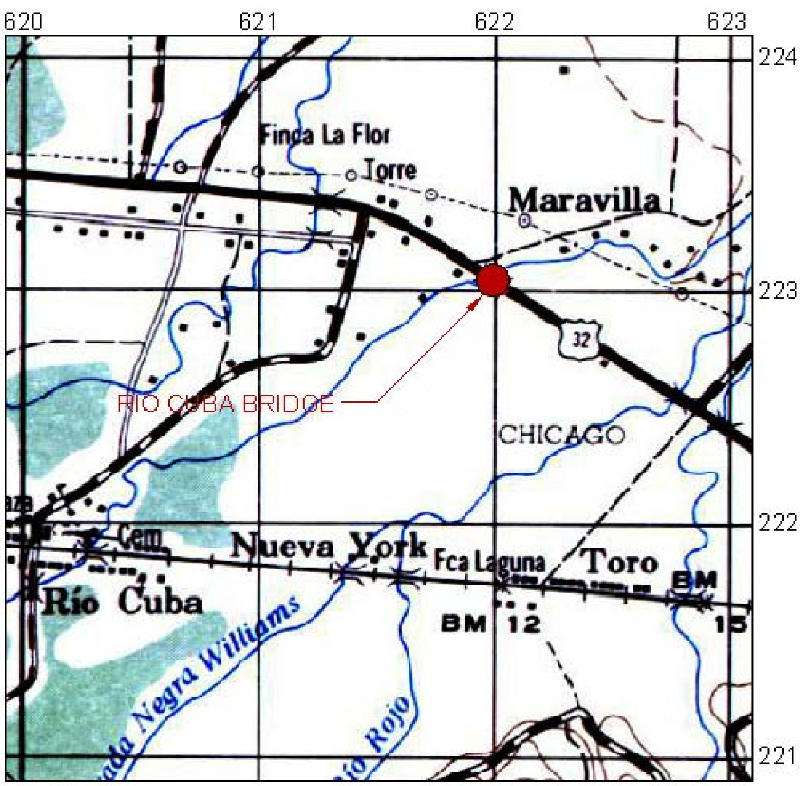

MOIN MAP - Scale 1:50.000 (IGN)

Figure 8: Location of Rio Cuba Bridge. The coordinates indicated in the map correspond to North Lambert Projection System which is used locally.

The field work carried out at the Rio Cuba Bridge consisted in one SPT borehole. The location and depth of this borehole is indicated in the Table 2. A photograph of the executed drilling is presented in Photo 1.

Table 3: Location and depth of the executed boreholes – Rio Cuba Bridge

Borehole ID	Date	GPS Coordinates		Borehole Depth [m]
		North	West	
P-1	29-Apr-10	N10 01.327	W83 13.085	15

Photo 1: View of the site where the borehole was executed. The borehole is on the right margin of the river.

As observed in Photo 1 the borehole was executed at the base of the bridge's approach fill. The ground surrounding the area of the borehole is relatively flat and there is some small vegetation. The area is also surrounded by a banana plantation.

5.2 Geotechnical profile

The soil profile detected at the site is typical of this type of alluvial deposits/plains. It consists in sequences and/or alternations of clays, silts and sands. Specifically at this site, the clays detected have a high plasticity, the silts are predominantly not plastic or have very low plasticity, and the sands are clean and/or silty but with no plastic fines. The soil profile interpreted for the site is presented in Figure 9. The detailed profile, which includes the characteristics of each type of soil is included in the boring log of Appendix A.

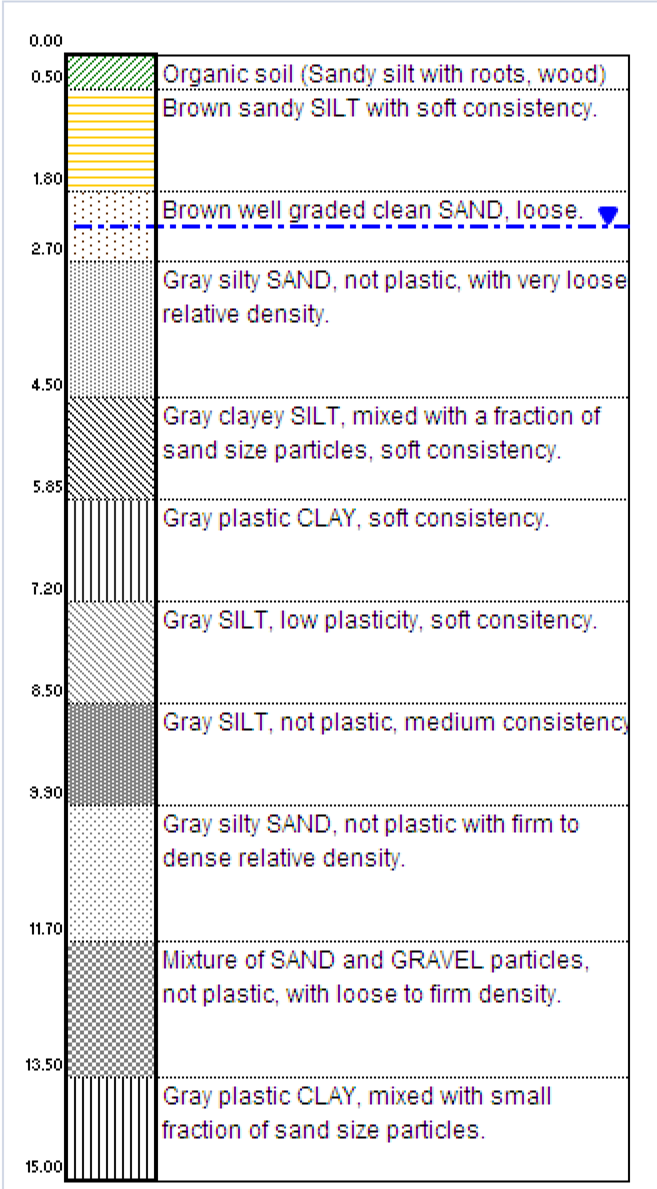

Figure 9: Soil profile detected at the Río Cuba Bridge site

As indicated in the profile above, the phreatic level appears at a depth of 2.10 m below the ground level. In order to complement the soil profile of Figure 9, a summary of the N_{SPT} values obtained in the boreholes is presented in Table 4. This summary includes the same symbol key used to represent the soils of Figure 9. This in order to differentiate the different N_{SPT} values detected for each type of soil. It is important to indicate that these values are the ones measured in the boring and they haven't been corrected.

Table 4: Summary of the N_{SPT} values detected at the Río Cuba Bridge Site

Depth [m]	P-1
0.00 - 0.45	15
0.45 - 0.90	9
0.90 - 1.35	4
1.35 - 1.80	2
1.80 - 2.25	5
2.25 - 2.70	7
2.70 - 3.15	12
3.15 - 3.60	4
3.60 - 4.05	2
4.05 - 4.50	2
4.50 - 4.95	2
4.95 - 5.40	2
5.40 - 5.85	3
5.85 - 6.30	2
6.30 - 6.75	4
6.75 - 7.20	2
7.20 - 7.65	6
7.65 - 8.10	5
8.10 - 8.55	11
8.55 - 9.00	17
9.00 - 9.45	11
9.45 - 9.90	15
9.90 - 10.35	22
10.35 - 10.80	24
10.80 - 11.25	24
11.25 - 11.70	33
11.70 - 12.15	23
12.15 - 12.60	15
12.60 - 13.05	10
13.05 - 13.50	6
13.50 - 13.95	6
13.95 - 14.40	6
14.40 - 14.85	10

Based on the results presented in Table 4, it can be observed that from the surface down to a depth of approximately 8 m the soils that appear have a soft/loose consistency. From depths between 8 – 12 m the materials have a better consistency which again decreases when a clayey layer is detected.

6. RIO BLANCO BRIDGE

This chapter includes the results obtained for the Río Blanco Bridge. A brief description of the site and the work executed is presented. This description is followed by a description of the geotechnical profile. The detailed results of the borings and the lab tests are presented in Appendix B, which corresponds to the boring logs.

6.1 Location and executed works

The Rio Blanco Bridge is located along national route 32 near the town of Liverpool. From the administrative/political point of view, the bridge site is located in the 7th province Limón, 1st county Limón, 3rd district Río Blanco. From the geographical point of view, the site is located at coordinates 9.99178º and -83.125333º. These coordinates can be located in the map Rio Banano, scale 1:50.000, of the Costa Rican Geographical Institute (see Figure 10).

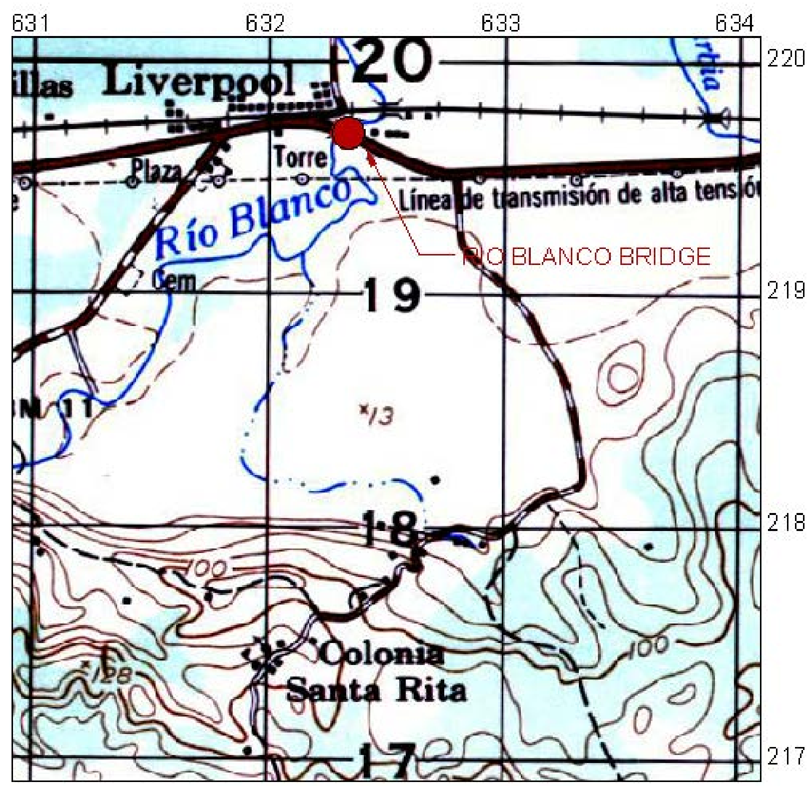

RÍO BANANO MAP - Scale 1:50.000 (IGN)

Figure 10: Location of Rio Blanco Bridge. The coordinates indicated in the map correspond to North Lambert Projection System which is used locally.

The field work carried out at the Rio Blanco Bridge consisted in one SPT borehole. The location and depth of this borehole is indicated in the Table 5. A photograph of the executed drilling is presented in Photo 2.

Table 5: Location and depth of the executed boreholes – Rio Blanco Bridge

Borehole ID	Date	GPS Coordinates		Borehole Depth [m]
		North	West	
P-1	28-Apr-10	N9 59.511	W83 07.482	15

Photo 2: View of the site of Río Blanco Bridge where the borehole was executed. The borehole is on the right margin of the river.

As observed in Photo 2 the borehole was executed at the base of the bridge's approach fill. The ground surrounding the area of the borehole is relatively flat and there is some small vegetation.

6.2 Geotechnical profile

The soil profile detected at the site is typical of alluvial transported deposits/plains. The types of soils recovered in the boreholes correspond to clays and silty sands or mixtures of these two materials. A particular characteristic of this site is that at depths between 3 and 7 m there are clays where traces of wood were observed. Furthermore, between 10 and 11 m, sands with pieces of wood also appeared. The pieces of wood that appear at the site are probably transported and deposited by the river. This wood is indicative of the recent soil deposits detected at this site.

The soil profile interpreted for the Rio Blanco site is presented in Figure 11. The detailed profile, which includes the laboratory results, is presented in Appendix B.

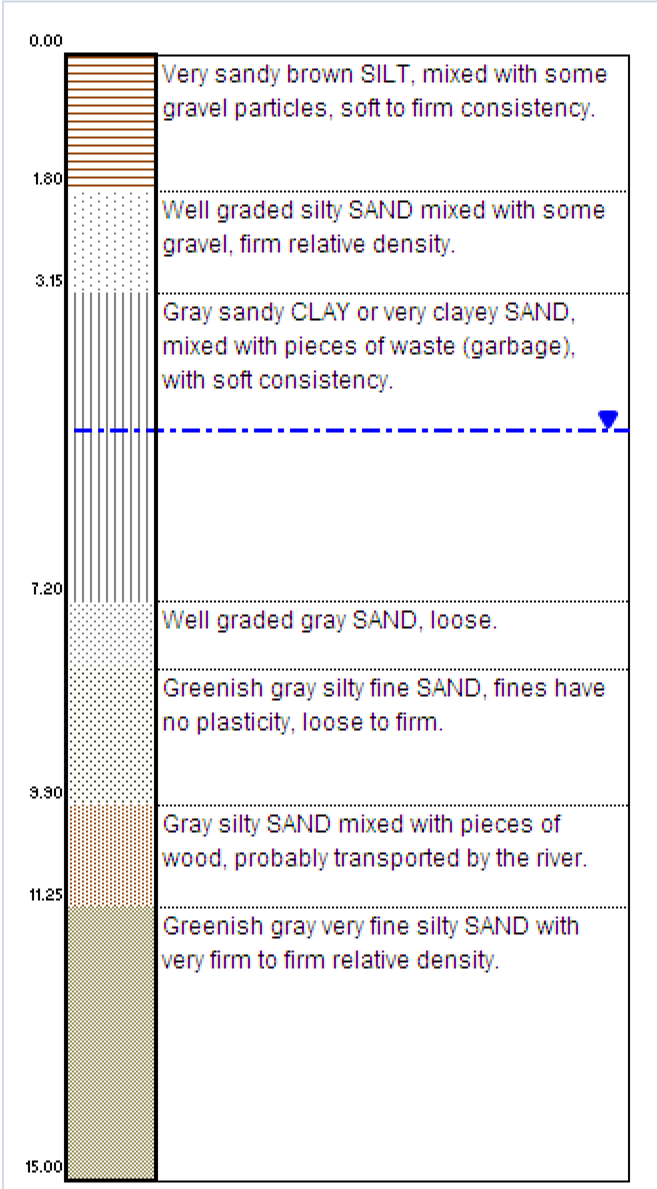

Figure 11: Soil profile detected at the Río Blanco Bridge site

The water table at this site appears at a depth of 4.80 m below the ground level. With regards to the soil profile, it is important to indicate that layer 3 corresponds to a mixture of clays and sands. Based on the laboratory results, this third layer is classified according to the USCS as very sandy CLAY or very clayey SAND.

In order to complement the soil profile of Figure 11, a summary of the N_{SPT} values obtained in the boreholes is presented in Table 6. This summary includes the same symbol key used to represent the soils of Figure 11. This in order to differentiate the different N_{SPT} values detected for each type of soil. It is important to indicate that these values are the ones measured in the boring and they haven't been corrected.

Table 6: Summary of the N_{SPT} values detected at the Río Blanco Bridge Site

Depth [m]	P-1
0.00 - 0.45	1
0.45 - 0.90	6
0.90 - 1.35	11
1.35 - 1.80	11
1.80 - 2.25	10
2.25 - 2.70	28
2.70 - 3.15	11
3.15 - 3.60	11
3.60 - 4.05	6
4.05 - 4.50	4
4.50 - 4.95	4
4.95 - 5.40	3
5.40 - 5.85	2
5.85 - 6.30	3
6.30 - 6.75	5
6.75 - 7.20	3
7.20 - 7.65	7
7.65 - 8.10	10
8.10 - 8.55	10
8.55 - 9.00	9
9.00 - 9.45	10
9.45 - 9.90	12
9.90 - 10.35	10
10.35 - 10.80	17
10.80 - 11.25	21
11.25 - 11.70	10
11.70 - 12.15	24
12.15 - 12.60	27
12.60 - 13.05	24
13.05 - 13.50	26
13.50 - 13.95	25
13.95 - 14.40	35
14.40 - 14.85	37

Based on the results presented in Table 6, it can be observed that soils of soft/loose consistency appear at depths between 3 and 10 m. Towards the end of the borehole, the consistency of the soils considerably improves and the materials that appear are dense silty SANDS.

7. RIO BANANITO HIGHWAY BRIDGE

This chapter includes the results obtained for the Río Bananito Highway Bridge. A brief description of the site and the work executed is presented. This description is followed by a description of the geotechnical profile. The detailed results of the borings and the lab tests are presented in Appendix C, which corresponds to the boring logs.

7.1 Location and executed works

The Rio Bananito Highway Bridge is located along national route 36 near Bananito Beach. From the administrative/political point of view, the bridge site is located in the 7th province Limón, 1st county Limón, 2nd district Valle de la Estrella. From the geographical point of view, the site is located at coordinates 9.88492º and -82.966883º. These coordinates can be located in the map San Andrés, scale 1:50.000, of the Costa Rican Geographical Institute (see Figure 12).

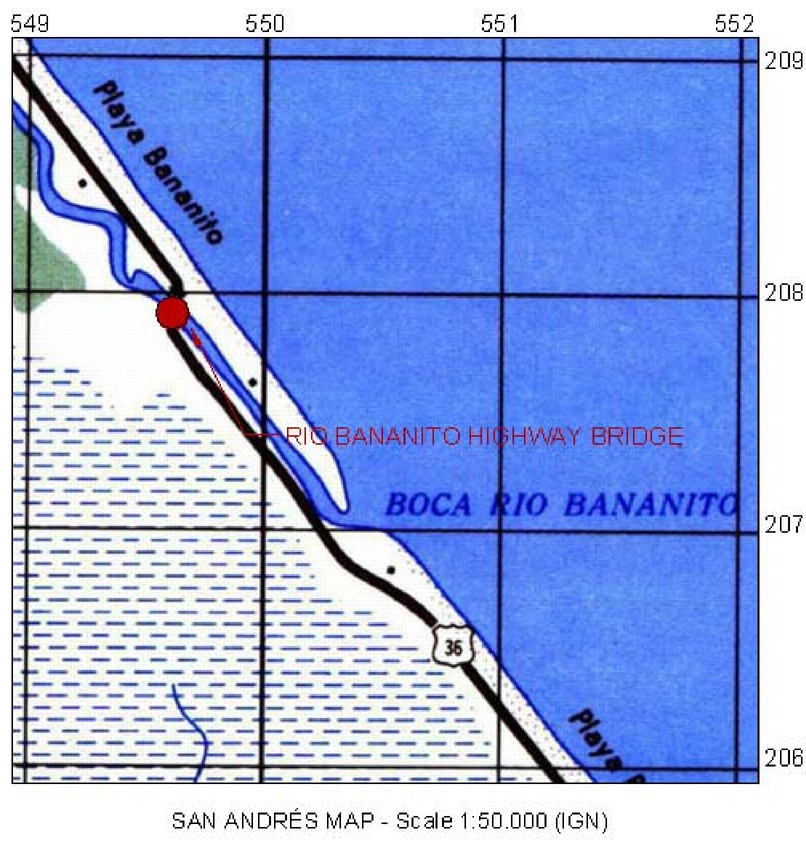

Figure 12: Location of Rio Bananito Highway Bridge. The coordinates indicated in the map correspond to Lambert Projection System which is used locally.

The field work carried out at the Rio Bananito Highway Bridge consisted in two SPT boreholes. The location and depth of each borehole is indicated in the Table 7. Photographs of the executed drillings are presented in Photos 3 and 4.

Table 7: Location and depth of the executed boreholes – Rio Bananito Highway Bridge

Borehole ID	Date	GPS Coordinates		Borehole Depth [m]
		North	West	
P-1	23-Apr-10	N9 53.056	W82 58.011	20
P-2	25-Apr-10	N9 53.046	W82 58.012	20

Photo 3: View of the site of borehole P-1 at the Río Bananito Highway Bridge. The borehole is on the right margin of the river.

Photo 4: View of the site of borehole P-2 at the Río Bananito Highway Bridge.

As observed in Photo 3 borehole P-1 was executed practically in the margin of the river. Boreholes P-2 was executed about 20 m from borehole P-1, also on the right margin and following the alignment of route 36.

7.2 Geotechnical profile

The soil profile detected at the site is typical of alluvial transported deposits. The types of soils recovered in the boreholes correspond to silty SANDS and/or very sandy not plastic SILTS. A particular characteristic of this site is in some of the samples there is presence of seashells, which is indicative of the marine influence. This can be expected given the bridges proximity to the coast.

With regards to the soil profile, a sandy or silty poorly graded gravel is detected near the surface in borehole P-2. This material is probably associated to the construction of the road. The soil profile interpreted for the Rio Bananito highway site is presented in Figure 13. The detailed boring logs, which include the laboratory test results, are presented in Appendix C.

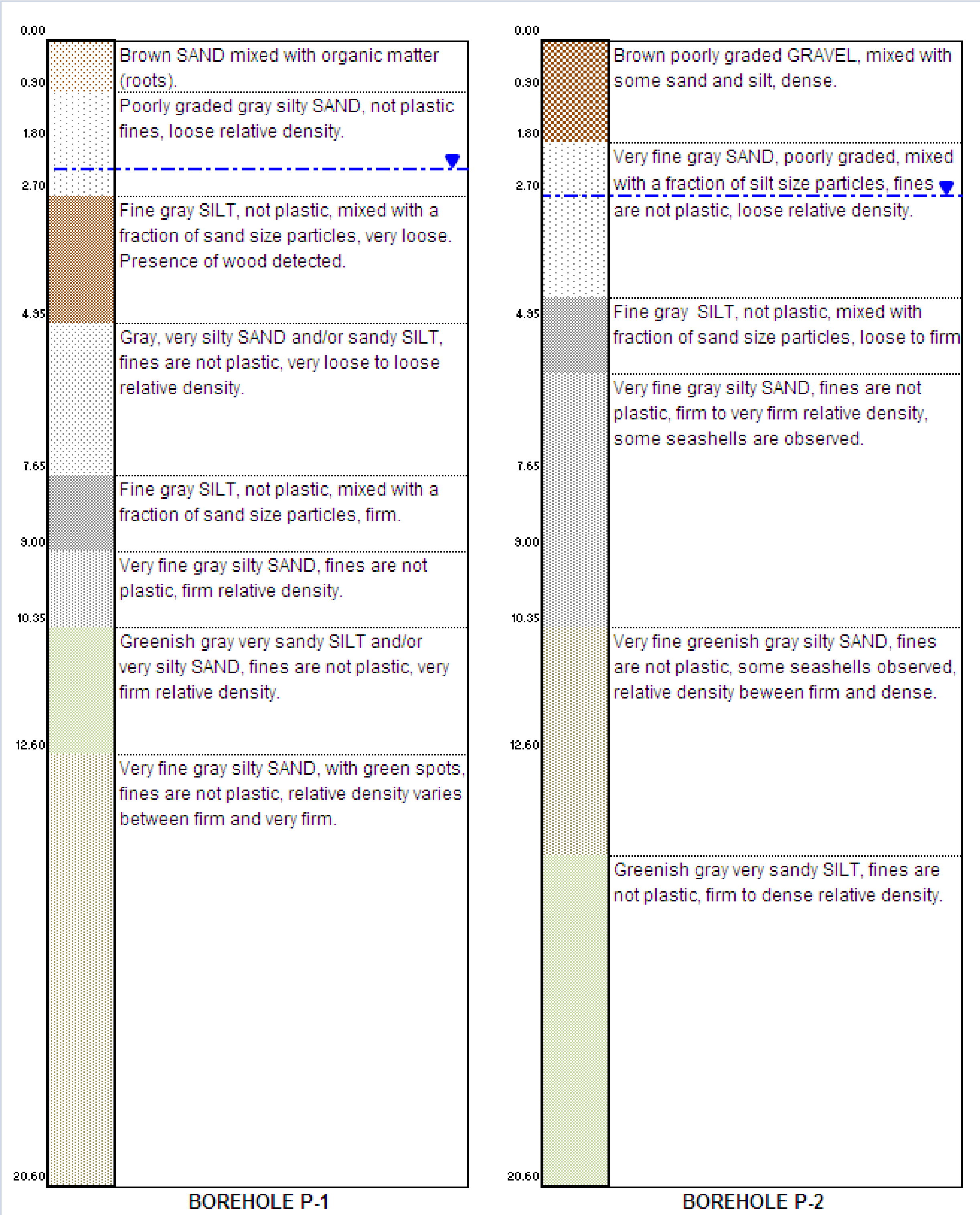

Figure 13: Soil profile detected at the Río Bananito Highway Bridge site

The water table at this site appears at a depth of 2 m below the ground level in P-1 and 2.65 m in boreholes P-2, which is farther away from the river. In order to complement the soil profile of Figure 13, a summary of the N_{SPT} values obtained in the boreholes is presented in Table 8.

Table 8: Summary of the N_{SPT} values detected at the Río Bananito Highway Bridge Site

Depth [m]	P-1	P-2
0.00 - 0.45	4	36
0.45 - 0.90	2	39
0.90 - 1.35	3	43
1.35 - 1.80	10	35
1.80 - 2.25	5	21
2.25 - 2.70	2	28
2.70 - 3.15	1	17
3.15 - 3.60	1	8
3.60 - 4.05	2	8
4.05 - 4.50	3	7
4.50 - 4.95	1	6
4.95 - 5.40	3	6
5.40 - 5.85	4	12
5.85 - 6.30	4	28
6.30 - 6.75	12	16
6.75 - 7.20	*	24
7.20 - 7.65	*	23
7.65 - 8.10	23	19
8.10 - 8.55	18	25
8.55 - 9.00	14	22
9.00 - 9.45	12	13
9.45 - 9.90	24	21
9.90 - 10.35	15	23
10.35 - 10.80	28	31
10.80 - 11.25	9	23
11.25 - 11.70	20	23
11.70 - 12.15	22	18
12.15 - 12.60	25	11
12.60 - 13.05	12	19
13.05 - 13.50	21	23
13.50 - 13.95	13	30
13.95 - 14.40	11	22
14.40 - 14.85	22	24
14.85 - 15.30	10	32
15.30 - 15.75	24	18
15.75 - 16.20	20	23
16.20 - 16.65	14	23
16.65 - 17.10	21	17
17.10 - 17.55	18	26
17.55 - 18.00	19	14
18.00 - 18.45	13	16
18.45 - 18.90	13	16
18.90 - 19.35	14	18
19.35 - 19.80	15	22
19.80 - 20.25	15	20

8. RIO BANANITO RAILROAD BRIDGE

This chapter includes the results obtained for the Río Bananito Railroad Bridge. A brief description of the site and the work executed is presented. This description is followed by a description of the geotechnical profile. The detailed results of the borings and the lab tests are presented in Appendix D, which corresponds to the boring logs.

8.1 Location and executed works

The Rio Bananito Railroad Bridge is located near the town of Bananito. Currently this bridge is used by vehicles and occasionally by the train. From the administrative/political point of view, the bridge site is located in the 7th province Limón, 1st county Limón, 4th district Matama. From the geographical point of view, the site is located at coordinates 9.8765º and -83.0076º. These coordinates can be located in the map Rio Banano, scale 1:50.000, of the Costa Rican Geographical Institute (see Figure 14).

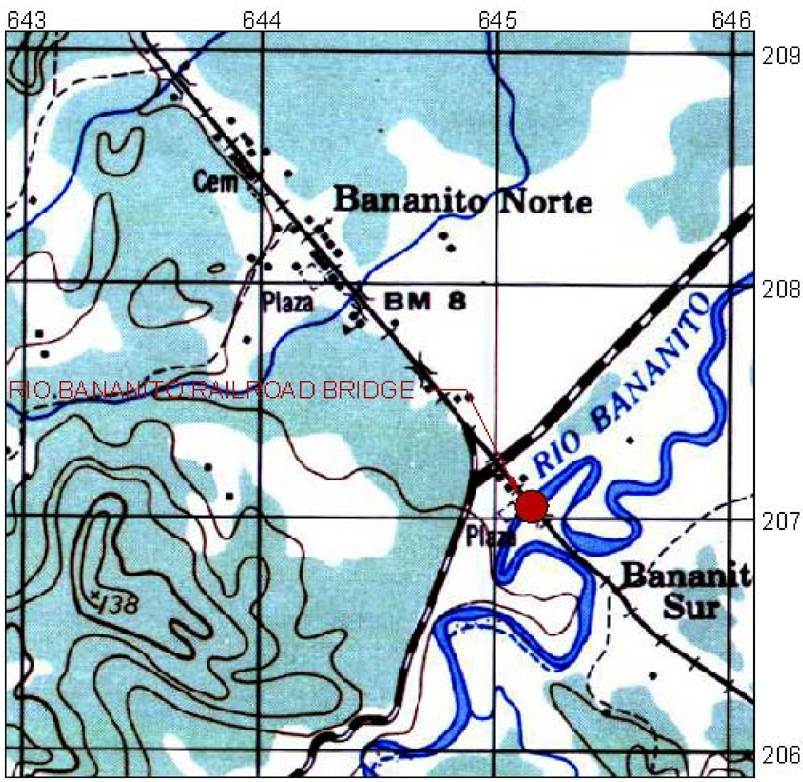

RIO BANANO MAP - Scale 1:50.000 (IGN)

Figure 14: Location of Rio Bananito Railroad Bridge. The coordinates indicated in the map correspond to Lambert Projection System which is used locally.

The field work carried out at the Rio Bananito Railroad Bridge consisted in two SPT boreholes. The location and depth of each borehole is indicated in the Table 9. Photographs of the executed drillings are presented in Photos 5 and 6.

Table 9: Location and depth of the executed boreholes – Rio Bananito Railroad Bridge

Borehole ID	Date	GPS Coordinates		Borehole Depth [m]
		North	West	
P-1	20-Apr-10	N9 52.619	W83 00.489	14
P-2	21-Apr-10	N9 52.623	W83 00.498	14

Photo 5: View of the site of borehole P-1 at the Río Bananito Railroad Bridge. The borehole is on the left margin of the river.

Photo 6: View of the site of borehole P-2 at the Río Bananito Railroad Bridge. The borehole is about 15 – 20 m apart from P-1.

As observed in Photo 4 and 5, the area where the boreholes were executed is relatively flat. Borehole P-2 was executed next to a pump station as observed in Photo 6.

8.2 Geotechnical profile

The soil profile detected at the site is also characteristics of the type of geologic formation and it consists mainly of two different types of materials: a clayey material near the surface underlain by clayey or silty SANDS. These sands have fines with some plasticity and in general, the relative density varies between loose and medium. On the other hand, the CLAY detected at the site has very soft to soft consistency.

The soil profile interpreted for the Rio Bananito Railroad site is presented in Figure 15. The detailed boring logs, which include the laboratory test results, are presented in Appendix D.

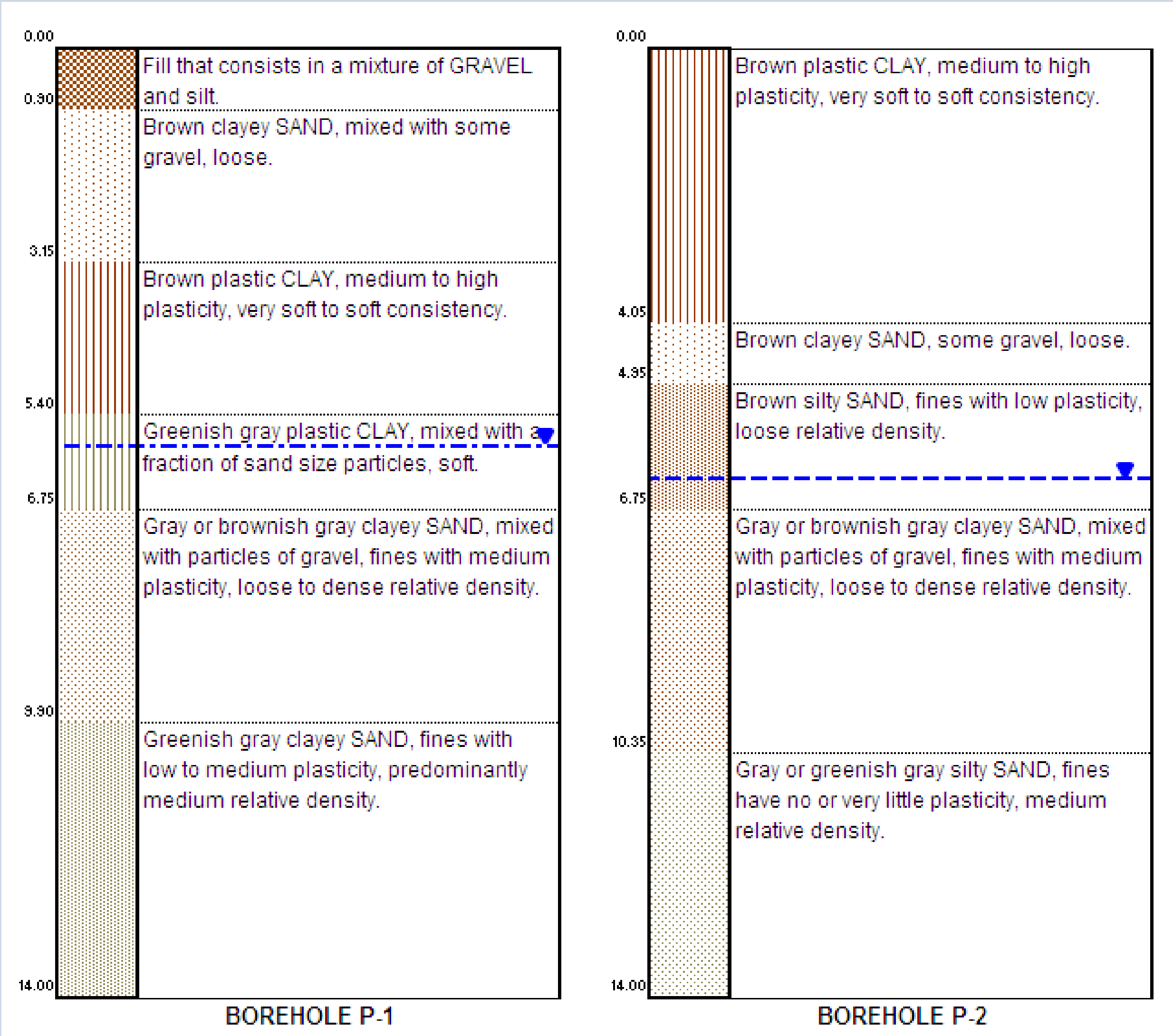

Figure 15: Soil profile detected at the Río Bananito Railroad Bridge site

The water table at this site appears at a depth of 5.65 m below the ground level in P-1 and 6.65 m in borehole P-2, which is farther away from the river. In order to complement the soil profile of Figure 15, a summary of the N_{SPT} values obtained in the boreholes is presented in Table 10.

Table 10: Summary of the N_{SPT} values detected at the Río Bananito Railroad Bridge Site

Depth [m]	P-1	P-2
0.00 - 0.45	26	6
0.45 - 0.90	11	2
0.90 - 1.35	6	3
1.35 - 1.80	4	3
1.80 - 2.25	4	3
2.25 - 2.70	4	3
2.70 - 3.15	4	3
3.15 - 3.60	1	4
3.60 - 4.05	0	5
4.05 - 4.50	0	10
4.50 - 4.95	1	7
4.95 - 5.40	2	9
5.40 - 5.85	3	8
5.85 - 6.30	7	13
6.30 - 6.75	7	19
6.75 - 7.20	7	7
7.20 - 7.65	15	8
7.65 - 8.10	20	11
8.10 - 8.55	8	4
8.55 - 9.00	24	23
9.00 - 9.45	36	36
9.45 - 9.90	20	16
9.90 - 10.35	16	21
10.35 - 10.80	19	9
10.80 - 11.25	21	28
11.25 - 11.70	25	15
11.70 - 12.15	23	20
12.15 - 12.60	6	16
12.60 - 13.05	17	27
13.05 - 13.50	24	26
13.50 - 13.95	18	22

Based on the results presented in Table 10, it is possible to observe that the CLAY layer is deeper near the river (borehole P-1).

9. RIO ESTRELLA BRIDGE

This chapter includes the results obtained for the Río Estrella Bridge. A brief description of the site and the work executed is presented. This description is followed by a description of the geotechnical profile. The detailed results of the borings and the lab tests are presented in Appendix E, which corresponds to the boring logs.

9.1 Location and executed works

The Rio Estrella Bridge is located along national route 36 near the town of Penshurt. From the administrative/political point of view, the bridge site is located in the 7th province Limón, 1st county Limón, 2nd district Valle de la Estrella. From the geographical point of view, the site is located at coordinates 9.78760º and -82.9134º. These coordinates can be located in the map Cahuita, scale 1:50.000, of the Costa Rican Geographical Institute (see Figure 16).

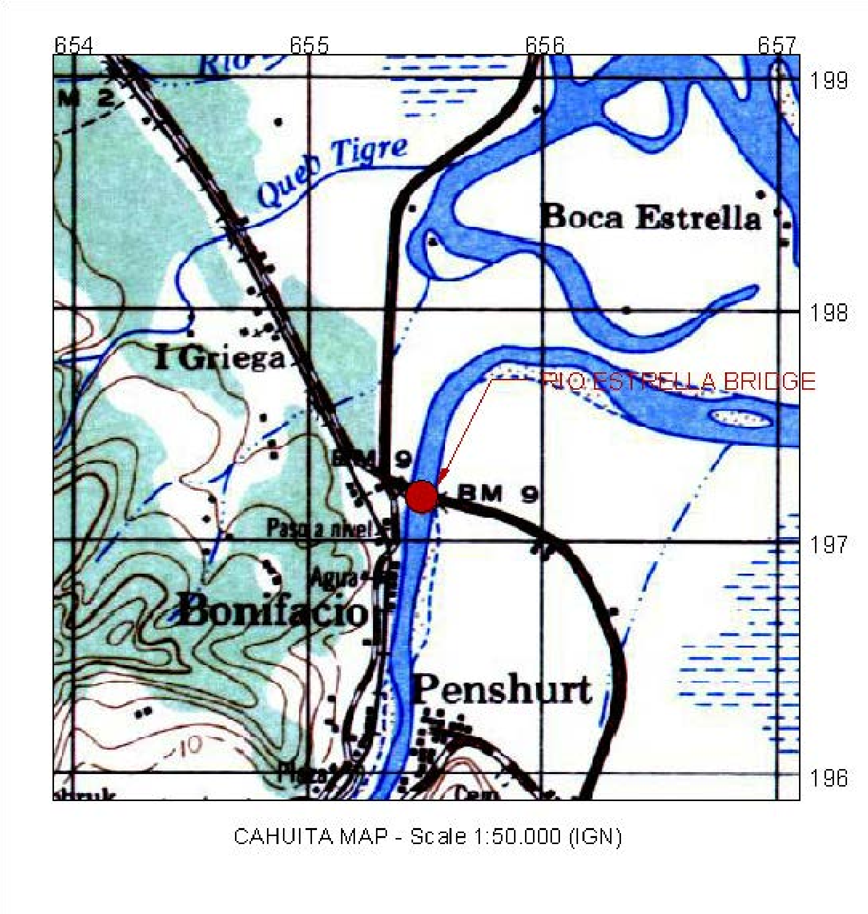

Figure 16: Location of Rio Estrella Bridge. The coordinates indicated in the map correspond to Lambert Projection System which is used locally.

The field work carried out at the Rio Estrella Bridge consisted in one SPT borehole. The location and depth of this borehole is indicated in the Table 11. A photograph of the executed drilling is presented in Photo 7.

Table 11: Location and depth of the executed boreholes – Rio Blanco Bridge

Borehole ID	Date	GPS Coordinates		Borehole Depth [m]
		North	West	
P-1	27-Apr-10	N9 47.245	W82 54.816	20

Photo 7: View of the site of Río Estrella Bridge where the borehole was executed. The borehole is on the right margin of the river. Notice the bridge to the right.

As observed in Photo 7 the borehole was executed at the base of the bridge's approach fill. The borehole is in the vicinity of one of the bridge's abutments. The ground surrounding the area of the borehole is relatively flat and the vegetation corresponds to a banana plantation.

9.2 Geotechnical profile

The soil profile detected at the site is typical of this type of geological formations. The types of soils recovered in the boreholes correspond to clayey silts and silty sands. Between 4.50 and 7.20 m there is a layer of a coarser alluvial material that consists in very sandy gravels or sands with some gravel particles.

The soil profile interpreted for the Rio Estrella site is presented in Figure 17. The detailed profile, which includes the laboratory results, is presented in Appendix E.

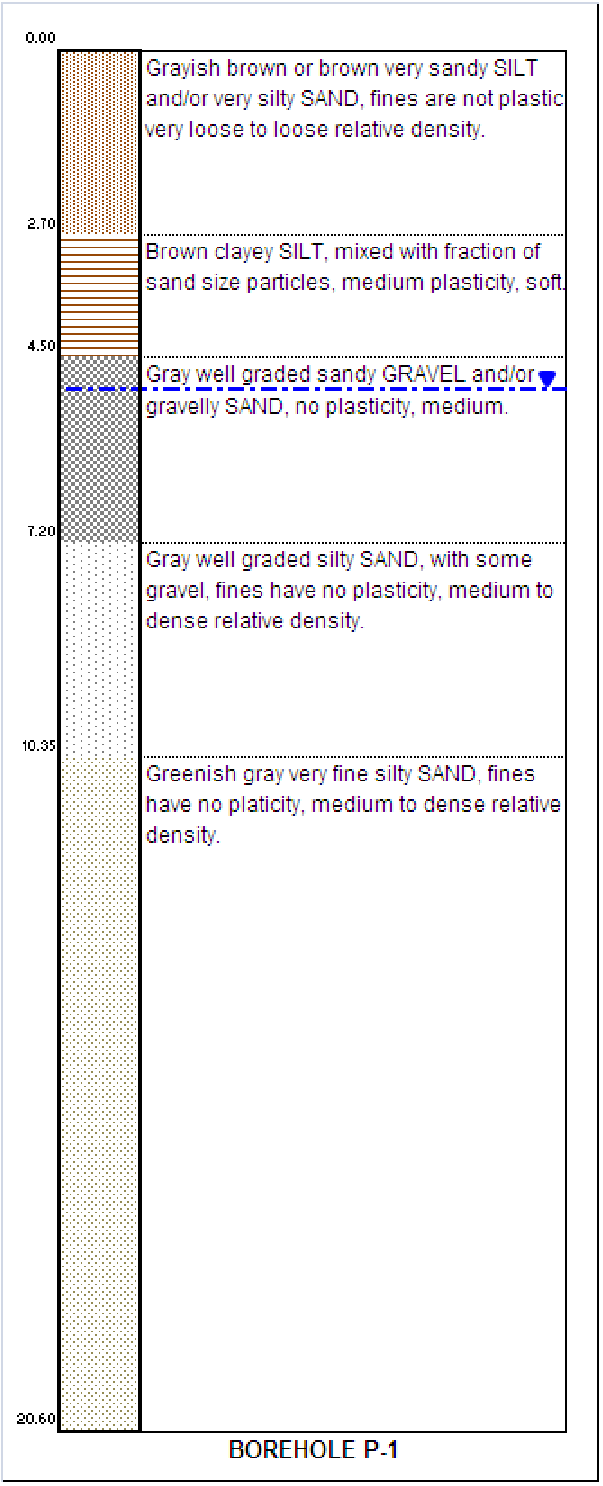

Figure 17: Soil profile detected at the Río Estrella Bridge site

The water table at this site appears at a depth of 4.90 m below the ground level. In order to complement the soil profile of Figure 17, a summary of the N_{SPT} values obtained in the boreholes is presented in Table 12.

Table 12: Summary of the N_{SPT} values detected at the Río Estrella Bridge Site

Depth [m]	P-1
0.00 - 0.45	10
0.45 - 0.90	7
0.90 - 1.35	6
1.35 - 1.80	2
1.80 - 2.25	2
2.25 - 2.70	1
2.70 - 3.15	1
3.15 - 3.60	1
3.60 - 4.05	2
4.05 - 4.50	2
4.50 - 4.95	2
4.95 - 5.40	14
5.40 - 5.85	10
5.85 - 6.30	16
6.30 - 6.75	12
6.75 - 7.20	7
7.20 - 7.65	10
7.65 - 8.10	10
8.10 - 8.55	12
8.55 - 9.00	10
9.00 - 9.45	28
9.45 - 9.90	34
9.90 - 10.35	22
10.35 - 10.80	24
10.80 - 11.25	19
11.25 - 11.70	19
11.70 - 12.15	24
12.15 - 12.60	17
12.60 - 13.05	26
13.05 - 13.50	27
13.50 - 13.95	35
13.95 - 14.40	24
14.40 - 14.85	38
14.85 - 15.30	35
15.30 - 15.75	28
15.75 - 16.20	36
16.20 - 16.65	36
16.65 - 17.10	17
17.10 - 17.55	25
17.55 - 18.00	21
18.00 - 18.45	22
18.45 - 18.90	33
18.90 - 19.35	32
19.35 - 19.80	36
19.80 - 20.25	38

Based on the results presented in Table 12, it can be observed that soils of soft/loose consistency appear at depths between 0 and 9 m. Towards the end of the borehole, the consistency of the soils improves considerably.

10. CONCLUSIONS

The following conclusions can be obtained from the execution of the geotechnical investigation:

- The five bridge sites that were investigated lie within a same geological formation known as Alluvial and coastal deposits, which is characterized by consisting of sediments of clayey, silty and sandy textures. Given the same geological conditions for each site, it can be expected that the sites will be composed of similar soil profiles with a similar geotechnical behavior.

- As indicated in section 4, the bridge sites that were studied, as well as the rest of the Costa Rican territory, is subject to the risk of earthquake. Near the investigated bridge sites there are several active faults and geological structures that can have the potential of producing earthquakes. Proof of the seismicity that can affect the area is the Limón-Telire Earthquake that occurred in April of 1991.

- In all of the five sites, the soil profiles are typical of the geological formation of alluvial and coastal deposits. In general, these soil profiles consist of sequence of clays, silts, sands and mixtures of each of these types of soils. The materials are not consolidated, not cemented and they have a loose/soft consistency near the surface.

- Based on the boreholes and the laboratory tests carried at the different sites, it was possible to determine the physical and mechanical properties of the soils. This information will be helpful for the modeling and interpretation that will be done for the future stages of the research investigation.

- For each investigated site, it was possible to establish that the requirements for liquefaction to occur under a seismic are present (i.e. loose saturated soils, granular not plastic materials, etc). It is important to indicate that a thorough liquefaction analysis was not carried out; however, the precedent of the liquefaction problems that occurred during the Limón-Telire Earthquake is well established.

APPENDIX A

RIO CUBA BRIDGE
BORING LOG

insuma s.a. — Ingeniería Suelos y Materiales — Ingenieros y Geólogos Consultores	**PROJECT:**	Rio Cuba Bridge		**File:**	
	LOCATION:	Maravilla, Limón, Costa Rica		**CODE:**	
	BOREHOLE:	**P-1**		**DATE:**	29/04/2010
	ELEVATION:		m.s.n.m.	**DEPTH:**	14.85 m
BORING LOG	**EQUIPMENT:**	SPT and Casing		**DIAMETER:**	AWJ
	DRILLER:	V. Murillo		**WATER TABLE:**	2.1 m

#	DEPTH (m) From	DEPTH (m) To	N_{SPT}	% Recovery	Description	LL	PI	WN (%)	%<#200	USCS
1	0.00	0.45	15	22	Organic soil (Sandy silt with roots, wood)					
2	0.45	0.90	9	33	Brown sandy SILT with soft consistency.					
3	0.90	1.35	4							
4	1.35	1.80	2							
5	1.80	2.25	5	22	Brown well graded clean SAND, loose.					
6	2.25	2.70	7	89	%Passing: 3/8 = 96; #4=91; #10=82; #40=17;	NP	NP	21.2	4	SW
7	2.70	3.15	12	67	Gray silty SAND, not plastic, with very loose					
8	3.15	3.60	4	56	relative density.					
9	3.60	4.05	2	22						
10	4.05	4.50	2	22	%Passing: 3/8 = 77; #4=73; #10=64; #40=24;	NP	NP	14.8	15	SM
11	4.50	4.95	2	56	Gray clayey SILT, mixed with a fraction of					
12	4.95	5.40	2	33	sand size particles, soft consistency.					
13	5.40	5.85	3	33	%Passing: #40=100;	47	16	62.4	71	ML
14	5.85	6.30	2	78	Gray plastic CLAY, soft consistency.					
15	6.30	6.75	4	78	%Passing: #40=100;	78	51	66.0	94	CH
16	6.75	7.20	2	78						
17	7.20	7.65	6	67	Gray SILT, low plasticity, soft consitency.					
18	7.65	8.10	5	89	%Passing: #40=100;	41	15	36.9	96	ML
19	8.10	8.55	11	89						
20	8.55	9.00	17	33	Gray SILT, not plastic, medium consistency.					
21	9.00	9.45	11	67	%Passing: #40=100;	NP	NP	34.1	90	ML
22	9.45	9.90	15	78						
23	9.90	10.35	22	89						
24	10.35	10.80	24	67	%Passing: 3/8 = 92; #4=91; #10=88; #40=47;	NP	NP	20.9	14	SM
25	10.80	11.25	24	67	Gray silty SAND, not plastic with medium to					
26	11.25	11.70	33	78	dense relative density.					
27	11.70	12.15	23	78	%Pas: 3/4=72; 3/8=59; #4=45; #10=35; #40=11;	NP	NP	8.7	5	GP
28	12.15	12.60	15	33	Mixture of SAND and GRAVEL particles,					
29	12.60	13.05	10	33	not plastic, with loose to medium density.					
30	13.05	13.50	6	33	%Passing: 3/8 = 78; #4=51; #10=27; #40=2;	NP	NP	8.0	1	SW
31	13.50	13.95	6	33	%Passing: #10=100; #40=89;	63	35	62.2	87	CH
32	13.95	14.40	6		Gray plastic CLAY, mixed with small					
33	14.40	14.85	10		fraction of sand size particles.					
34					^ ^ ^ End of borehole: 14.85 m ^ ^ ^					
35										
36										

Observations:

Described by:	J.P. Rodríguez	*Revised by:*	J. Rodríguez	*Approved by:*	J. Rodríguez
Date:	15/07/2010	*Date:*	15/07/2010	*Date:*	15/07/2010
Signature:		*Signature:*		*Signature:*	

APPENDIX B

RIO BLANCO BRIDGE
BORING LOG

INGENIERIA SUELOS Y MATERIALES
INSUMA S.A.
INGENIEROS Y GEOLOGOS CONSULTORES

BORING LOG

PROJECT:	Río Blanco Bridge	*File:*	
LOCATION:	Liverpool, Limón, Costa Rica	**CODE:**	
BOREHOLE:	**P-1**	**DATE:**	28/04/2010
ELEVATION:	m.s.n.m.	**DEPTH:**	14.85 m
EQUIPMENT:	SPT and Casing	**DIAMETER:**	AWJ
DRILLER:	V. Murillo	**WATER TABLE:**	4.8 m

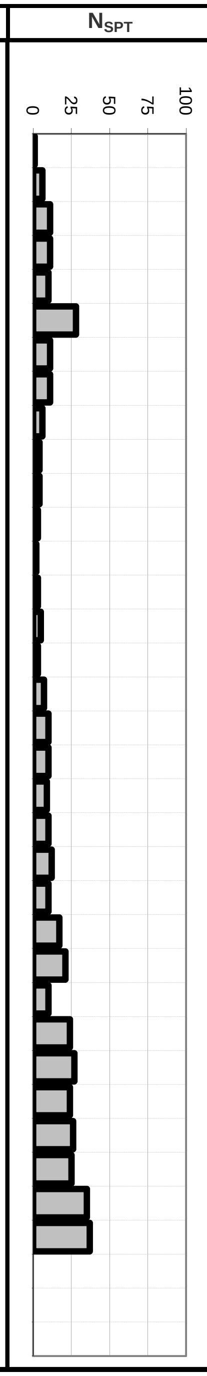

#	DEPTH (m) From	To	N_{SPT}	% Recovery	Description	LL	PI	WN (%)	%>#200	SUCS
1	0.00	0.45	**1**	56						
2	0.45	0.90	**6**	33	% Passing: #4=89; #10=83; #40=65;	27	3	24.6	53	ML
3	0.90	1.35	**11**	22	Very sandy brown SILT, mixed with some					
4	1.35	1.80	**11**	33	gravel particles, soft to medium consistency.					
5	1.80	2.25	**10**	44	% Pas: 3/4=79;3/8=68; #4=54; #10=43; #40=18;	NP	NP	8.7	7	SW-S
6	2.25	2.70	**28**	44	Well graded silty SAND mixed with some					
7	2.70	3.15	**11**	44	gravel, medium relative density.					
8	3.15	3.60	**11**	22	% Passing: #4=89; #10=81; #40=61;	50	27	25.7	48	SC
9	3.60	4.05	**6**	44						
10	4.05	4.50	**4**	89	Gray sandy CLAY or very clayey SAND,					
11	4.50	4.95	**4**		mixed with pieces of wood, with soft					
12	4.95	5.40	**3**		consistency.					
13	5.40	5.85	**2**							
14	5.85	6.30	**3**	78						
15	6.30	6.75	**5**	78	% Passing: #40=100;	53	30	64.8	93	CH
16	6.75	7.20	**3**	78						
17	7.20	7.65	**7**	56	Well graded gray SAND, loose.					
18	7.65	8.10	**10**	56	% Passing: #4=82; #10=70; #40=31;	NP	NP	25.3	4	SW
19	8.10	8.55	**10**	67	Greenish gray silty fine SAND, fines have					
20	8.55	9.00	**9**	78	no plasticity, loose to medium.					
21	9.00	9.45	**10**	78	% Passing: #40=100;	NP	NP	36.3	36	SM
22	9.45	9.90	**12**	78						
23	9.90	10.35	**10**	67	Gray silty SAND mixed with pieces of					
24	10.35	10.80	**17**	44	wood, probably transported by the river.					
25	10.80	11.25	**21**	56	% Passing: #4=94; #10=89; #40=65;	NP	NP	23.4	21	SM
26	11.25	11.70	**10**	33	Greenish gray very fine silty SAND with					
27	11.70	12.15	**24**	44	medium to dense relative density.					
28	12.15	12.60	**27**	56	% Passing: #40=100;	NP	NP	25.9	45	SM
29	12.60	13.05	**24**	67						
30	13.05	13.50	**26**	56						
31	13.50	13.95	**25**	56						
32	13.95	14.40	**35**	67	% Passing: #40=100;	NP	NP	24.5	59	ML
33	14.40	14.85	**37**	56						
34					^ ^ ^ End of borehole: 14.85 m ^ ^ ^					
35										
36										

Observations:

Described by:	J.P. Rodríguez	*Revised by:*	J. Rodríguez	*Approved by:*	J. Rodríguez
Date:	15/07/2010	*Date:*	15/07/2010	*Date:*	15/07/2010
Signature:		*Signature:*		*Signature:*	

APPENDIX C

RIO BANANITO HIGHWAY BRIDGE BORING LOGS

PROJECT:	Bananito River Bridge (Highway)	File:	
LOCATION:	Province of Limón	CODE:	
BOREHOLE:	P-1	DATE:	22/04/2010
ELEVATION:	m.s.n.m.	DEPTH:	20.25 m
EQUIPMENT:	SPT and Casing	DIAMETER:	AWJ
DRILLER:	V. Murillo	WATER TABLE:	2 m

INGENIERIA SUELOS Y MATERIALES
insuma s.a.
INGENIEROS Y GEOLOGOS CONSULTORES

BORING LOG

#	DEPTH (m) From	DEPTH (m) To	N_{SPT}	% Recovery	Description	LL	PI	WN (%)	%<#200	SUCS
1	0.00	0.45	4	89	Brown SAND mixed with organic matter					
2	0.45	0.90	2	44	(roots).					
3	0.90	1.35	3	67	Poorly graded gray silty SAND, not plastic					
4	1.35	1.80	10	67	fines, loose relative density.					
5	1.80	2.25	5	56	% Passing: #40=97;	NP	NP	23.1	12	SP-SI
6	2.25	2.70	2	67						
7	2.70	3.15	1	33						
8	3.15	3.60	1	22	% Passing: #10=100; #40=97;	NP	NP	49.9	84	ML
9	3.60	4.05	2	11	Fine gray SILT, not plastic, mixed with a					
10	4.05	4.50	3	44	fraction of sand size particles, very loose.					
11	4.50	4.95	1	78	Presence of wood detected.					
12	4.95	5.40	3	67						
13	5.40	5.85	4	78	% Passing: #4=100; #10=97; #40=84;	NP	NP	41.1	48	SM
14	5.85	6.30	4	33	Gray, very silty SAND and/or sandy SILT,					
15	6.30	6.75	12	44	fines are not plastic, very loose to loose					
16	6.75	7.20	*		relative density.					
17	7.20	7.65	*							
18	7.65	8.10	23	56	% Passing: #40=96;	NP	NP	24.6	78	ML
19	8.10	8.55	18	78	Fine gray SILT, not plastic, mixed with a					
20	8.55	9.00	14	44	fraction of sand size particles, medium.					
21	9.00	9.45	12	56	Very fine gray silty SAND, fines are not					
22	9.45	9.90	24	56	plastic, medium relative density.					
23	9.90	10.35	15	44	% Passing: #40=100;	NP	NP	28.4	17	SM
24	10.35	10.80	28	56	Greenish gray very sandy SILT and/or					
25	10.80	11.25	9	56	very silty SAND, fines are not plastic,					
26	11.25	11.70	20	89	medium relative density.					
27	11.70	12.15	22	67						
28	12.15	12.60	25	56	% Passing: #40=100;	NP	NP	27.9	55	ML
29	12.60	13.05	12	56						
30	13.05	13.50	21	56	Very fine gray silty SAND, with green spots,					
31	13.50	13.95	13	56	fines are not plastic, relative density					
32	13.95	14.40	11	33	medium.					
33	14.40	14.85	22	33						
34	14.85	15.30	10	44	% Passing: #40=100;	NP	NP	31.7	35	SM
35	15.30	15.75	24	22						
36	15.75	16.20	20	22						

Observations: (*) Washed away during installation of the casing.

Described by:	J.P. Rodríguez	*Revised by:*	J. Rodríguez	*Approved by:*	J. Rodríguez
Date:	15/07/2010	*Date:*	15/07/2010	*Date:*	15/07/2010
Signature:		*Signature:*		*Signature:*	

INGENIERIA SUELOS Y MATERIALES insuma s.a. INGENIEROS Y GEOLOGOS CONSULTORES					
	PROJECT:	Bananito River Bridge (Highway)	*File:*	
	LOCATION:	Province of Limón	**CODE:**	
	BOREHOLE:	**P-1 (Continued)**	**DATE:**	22/04/2010
	ELEVATION:	m.s.n.m.	**DEPTH:**	20.25 m
BORING LOG	**EQUIPMENT:**	SPT and Casing	**DIAMETER:**	AWJ
	DRILLER:	V. Murillo	**WATER TABLE:**	2 m

#	DEPTH (m) From	DEPTH (m) To	N_{SPT}	% Recovery (0 25 50 75 100)	N_{SPT} (0 25 50 75 100)	Symbol	Description	LL	PI	WN (%)	%>#200	SUCS
37	16.20	16.65	**14**	33								
38	16.65	17.10	**21**	44								
39	17.10	17.55	**18**	22			% Passing: #10 = 100; #40=99;	NP	NP	30.2	35	SM
40	17.55	18.00	**19**	22			Very fine gray silty SAND, with green spots,					
41	18.00	18.45	**13**	22			fines are not plastic, relative density is					
42	18.45	18.90	**13**	22			medium.					
43	18.90	19.35	**14**	22								
44	19.35	19.80	**15**	22			% Passing: #40=100;	NP	NP	28.9	49	SM
45	19.80	20.25	**15**	33								
46							^ ^ ^ End of borehole: 20.25 m ^ ^ ^					
47												
48												
49												
50												
51												
52												
53												
54												
55												
56												
57												
58												
59												
60												
61												
62												
63												
64												
65												
66												
67												
68												
69												
70												
71												
72												

Observations:

Described by:	J.P. Rodríguez	*Revised by:*	J. Rodríguez	*Approved by:*	J. Rodríguez
Date:	15/07/2010	*Date:*	15/07/2010	*Date:*	15/07/2010
Signature:		*Signature:*		*Signature:*	

PROJECT:	Bananito River Bridge (Highway)	*File:*	
LOCATION:	Province of Limón	**CODE:**	
BOREHOLE:	**P-2**	**DATE:**	24/04/2010
ELEVATION:	m.s.n.m.	**DEPTH:**	20.25 m
EQUIPMENT:	SPT and Casing	**DIAMETER:**	AWJ
DRILLER:	V. Murillo	**WATER TABLE:**	2.65 m

BORING LOG

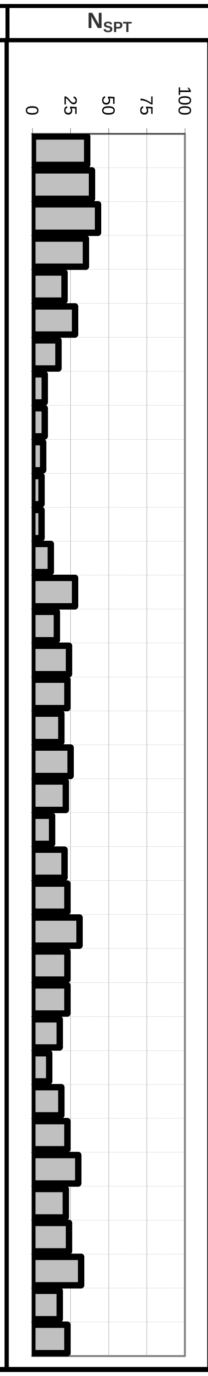

#	DEPTH (m) From	DEPTH (m) To	N_{SPT}	% Recovery	Description	LL	PI	WN (%)	%>#200	SUCS
1	0.00	0.45	**36**	67	Brown poorly graded GRAVEL, mixed with					
2	0.45	0.90	**39**	56	some sand and silt, dense.					
3	0.90	1.35	**43**	78						
4	1.35	1.80	**35**	67	% Pas: 3/4=68; 3/8=62; #4=48; #10=34; #40=20;	NP	NP	9.2	12	GP-G
5	1.80	2.25	**21**	67						
6	2.25	2.70	**28**	56	Very fine gray SAND, poorly graded, mixed					
7	2.70	3.15	**17**	67	with a fraction of silt size particles, fines					
8	3.15	3.60	**8**	67	are not plastic, loose relative density.					
9	3.60	4.05	**8**	56						
10	4.05	4.50	**7**	56	% Passing: #40=100;	NP	NP	21.3	9	SP-SI
11	4.50	4.95	**6**	67	Fine gray SILT, not plastic, mixed with					
12	4.95	5.40	**6**	67	fraction of sand size particles, loose to mediur					
13	5.40	5.85	**12**	67	% Passing: #40=100;	NP	NP	39.1	57	ML
14	5.85	6.30	**28**	33						
15	6.30	6.75	**16**	44						
16	6.75	7.20	**24**	33						
17	7.20	7.65	**23**	33	% Passing: #40=100;	NP	NP	25.2	19	SM
18	7.65	8.10	**19**	44	Very fine gray silty SAND, fines are not					
19	8.10	8.55	**25**	44	plastic, medium relative density,					
20	8.55	9.00	**22**	56	some seashells are observed.					
21	9.00	9.45	**13**	67						
22	9.45	9.90	**21**	44	% Passing: #40=100;	NP	NP	29.0	23	SM
23	9.90	10.35	**23**	44						
24	10.35	10.80	**31**	78	Very fine greenish gray silty SAND, fines					
25	10.80	11.25	**23**	22	are not plastic, some seashells observed,					
26	11.25	11.70	**23**	67	relative density medium.					
27	11.70	12.15	**18**	56						
28	12.15	12.60	**11**	67	% Passing: #40=100;	NP	NP	38.7	32	SM
29	12.60	13.05	**19**	56						
30	13.05	13.50	**23**	56						
31	13.50	13.95	**30**	56						
32	13.95	14.40	**22**	67						
33	14.40	14.85	**24**	67	% Passing: #40=100;	NP	NP	38.6	56	ML
34	14.85	15.30	**32**	56	Greenish gray very sandy SILT, fines are					
35	15.30	15.75	**18**	44	not plastic, medium relative density.					
36	15.75	16.20	**23**	44						

Observations:

Described by:	J.P. Rodríguez	*Revised by:*	J. Rodríguez	*Approved by:*	J. Rodríguez
Date:	15/07/2010	*Date:*	15/07/2010	*Date:*	15/07/2010
Signature:		*Signature:*		*Signature:*	

INGENIERIA SUELOS Y MATERIALES
insuma s.a.
INGENIEROS Y GEOLOGOS CONSULTORES

BORING LOG

PROJECT:	Bananito River Bridge (Highway)	*File:*	
LOCATION:	Province of Limón	**CODE:**	
BOREHOLE:	**P-2 (Continued)**	**DATE:**	24/04/2010
ELEVATION:	m.s.n.m.	**DEPTH:**	20.25 m
EQUIPMENT:	SPT and Casing	**DIAMETER:**	AWJ
DRILLER:	V. Murillo	**WATER TABLE:**	2.65 m

#	DEPTH (m) From	DEPTH (m) To	N_{SPT}	% Recovery (0 25 50 75 100)	N_{SPT} (0 25 50 75 100)	Symbol	Description	LL	PI	WN (%)	%>#200	SUCS
37	16.20	16.65	**23**	44								
38	16.65	17.10	**17**	33								
39	17.10	17.55	**26**	33			% Passing: #10=100; #40=98;	NP	NP	28.9	81	ML
40	17.55	18.00	**14**	44			Greenish gray SILT, mixed with small					
41	18.00	18.45	**16**	44			fraction of sand size particles, medium					
42	18.45	18.90	**16**	44			relative density.					
43	18.90	19.35	**18**	33			% Passing: 3/8=94; #4=92; #10=91; #40=89;	NP	NP	32.6	86	ML
44	19.35	19.80	**22**	56								
45	19.80	20.25	**20**	56								
46							^ ^ ^ End of borehole: 20.25 m ^ ^ ^					
47												
48												
49												
50												
51												
52												
53												
54												
55												
56												
57												
58												
59												
60												
61												
62												
63												
64												
65												
66												
67												
68												
69												
70												
71												
72												

Observations:

Described by:	J.P. Rodríguez	*Revised by:*	J. Rodríguez	*Approved by:*	J. Rodríguez
Date:	15/07/2010	*Date:*	15/07/2010	*Date:*	15/07/2010
Signature:		*Signature:*		*Signature:*	

APPENDIX D

RIO BANANITO RAILROAD BRIDGE BORING LOGS

INGENIERIA SUELOS Y MATERIALES — hsuma s.a. — INGENIEROS Y GEOLOGOS CONSULTORES	PROJECT:	Bananito River Bridge (Railroad)	File:	
	LOCATION:	Province of Limón	CODE:	
	BOREHOLE:	**P-1**	DATE:	19/04/2010
	ELEVATION:	m.s.n.m.	DEPTH:	13.95 m
BORING LOG	EQUIPMENT:	SPT and Casing	DIAMETER:	AWJ
	DRILLER:	V. Murillo	WATER TABLE:	5.65 m

#	DEPTH (m) From	DEPTH (m) To	N_{SPT}	% Recovery	Symbol	Description	LL	PI	WN (%)	%>#200	SUCS
1	0.00	0.45	**26**	44		Fill that consists in a mixture of GRAVEL					
2	0.45	0.90	**11**	22		and silt.					
3	0.90	1.35	**6**	56		Brown clayey SAND, mixed with some					
4	1.35	1.80	**4**	22		gravel, loose.					
5	1.80	2.25	**4**	22		%Pas: 3/4=81; 3/8=77; #4=69; #10=62; #40=52;	43	18	21.3	40	SC
6	2.25	2.70	**4**	22							
7	2.70	3.15	**4**	56							
8	3.15	3.60	**1**	100		%Passing: #4=99; #10=98; #40=96;	62	33	55.2	93	CH
9	3.60	4.05	**0**	22		Brown plastic CLAY, medium to high					
10	4.05	4.50	**0**	100		plasticity, very soft to soft consistency.					
11	4.50	4.95	**1**	78		%Passing: #40=100;	64	36	62.2	97	CH
12	4.95	5.40	**2**	44							
13	5.40	5.85	**3**	44		Greenish gray plastic CLAY, mixed with a					
14	5.85	6.30	**7**	56		fraction of sand size particles, soft.					
15	6.30	6.75	**7**	44		%Passing: #40=100;	76	39	36.6	69	CH
16	6.75	7.20	**7**	44		Gray or brownish gray clayey SAND, mixed					
17	7.20	7.65	**15**	56		with particles of gravel, fines with medium					
18	7.65	8.10	**20**	56		plasticity, loose to dense relative density.					
19	8.10	8.55	**8**	56		%Pas: 3/4=90; 3/8=84; #4=78; #10=69; #40=40;	36	8	23.4	23	SC
20	8.55	9.00	**24**	56							
21	9.00	9.45	**36**	33							
22	9.45	9.90	**20**	22							
23	9.90	10.35	**16**	67							
24	10.35	10.80	**19**	56		%Pas: 3/4=89; 3/8=73; #4=62; #10=50; #40=27;	42	20	18.0	17	SC
25	10.80	11.25	**21**	67		Greenish gray clayey SAND, fines with					
26	11.25	11.70	**25**	67		low to medium plasticity, predominantly					
27	11.70	12.15	**23**	33		medium relative density.					
28	12.15	12.60	**6**	22							
29	12.60	13.05	**17**	89		%Pas: 3/4=79; 3/8=69; #4=56; #10=44; #40=31;	41	19	19.8	22	SC
30	13.05	13.50	**24**	56							
31	13.50	13.95	**18**	56							
32						^ ^ ^ End of borehole: 13.95 m ^ ^ ^					
33											
34											
35											
36											

Observations:

Described by:	J.P. Rodríguez	*Revised by:*	J. Rodríguez	*Approved by:*	J. Rodríguez
Date:	15/07/2010	*Date:*	15/07/2010	*Date:*	15/07/2010
Signature:		*Signature:*		*Signature:*	

INGENIERIA SUELOS Y MATERIALES
hsuma s.a.
INGENIEROS Y GEOLOGOS CONSULTORES

BORING LOG

PROJECT:	Bananito River Bridge (Railroad)	*File:*	
LOCATION:	Province of Limón	**CODE:**	
BOREHOLE:	**P-2**	**DATE:**	20/04/2010
ELEVATION:	m.s.n.m.	**DEPTH:**	13.95 m
EQUIPMENT:	SPT and Casing	**DIAMETER:**	AWJ
DRILLER:	V. Murillo	**WATER TABLE:**	6.65 m

#	DEPTH (m) From	DEPTH (m) To	N_{SPT}	% Recovery	Description	LL	PI	WN (%)	%>#200	SUCS
1	0.00	0.45	**6**	89	Brown plastic CLAY, medium to high					
2	0.45	0.90	**2**	67	plasticity, very soft to soft consistency.					
3	0.90	1.35	**3**	67	%Passing: #40=100;	54	25	50.3	97	CH
4	1.35	1.80	**3**	44						
5	1.80	2.25	**3**	44						
6	2.25	2.70	**3**	33						
7	2.70	3.15	**3**	44	%Passing: #40=100;	55	28	48.2	98	CH
8	3.15	3.60	**4**	44						
9	3.60	4.05	**5**	22						
10	4.05	4.50	**10**	56	Brown clayey SAND, some gravel, loose.					
11	4.50	4.95	**7**	44	%Passing: #4=86; #10=81; #40=61;	39	14	28.7	47	SC
12	4.95	5.40	**9**	22	Brown silty SAND, fines with low plasticity,					
13	5.40	5.85	**8**	67	loose relative density.					
14	5.85	6.30	**13**	56	%Passing: 3/8=97; #4=92; #10=89; #40=48;	32	5	26.8	21	SM
15	6.30	6.75	**19**	44						
16	6.75	7.20	**7**	44	Gray or brownish gray clayey SAND, mixed					
17	7.20	7.65	**8**	44	with particles of gravel, fines with medium					
18	7.65	8.10	**11**		plasticity, loose to dense relative density.					
19	8.10	8.55	**4**	22						
20	8.55	9.00	**23**	67						
21	9.00	9.45	**36**	56	%Passing: 3/8=83; #4=64; #10=49; #40=31;	34	11	16.0	23	SC
22	9.45	9.90	**16**	33						
23	9.90	10.35	**21**	78						
24	10.35	10.80	**9**	33						
25	10.80	11.25	**28**	44	%Passing: 3/8=83; #4=70; #10=52; #40=39;	31	8	13.2	17	SM
26	11.25	11.70	**15**	33	Gray or greenish gray silty SAND, fines					
27	11.70	12.15	**20**	33	have no or very little plasticity, medium					
28	12.15	12.60	**16**	33	relative density.					
29	12.60	13.05	**27**	33						
30	13.05	13.50	**26**	33	%Passing: 3/8=90; #4=61; #10=45; #40=23;	NP	NP	13.9	14	SM
31	13.50	13.95	**22**	44						
32					^ ^ ^ End of borehole: 13.95 m ^ ^ ^ ^					
33										
34										
35										
36										

Observations:

Described by:	J.P. Rodríguez	*Revised by:*	J.P. Rodríguez	*Approved by:*	J.P. Rodríguez
Date:	15/07/2010	*Date:*	15/07/2010	*Date:*	15/07/2010
Signature:		*Signature:*		*Signature:*	

APPENDIX E

RIO ESTRELLA BRIDGE
BORING LOG

PROJECT:	Estrella River Bridge	*File:*	
LOCATION:	Cahuita, province of Limón	**CODE:**	
BOREHOLE:	**P-1**	**DATE:**	26/04/2010
ELEVATION:	m.s.n.m.	**DEPTH:**	20.25 m
EQUIPMENT:	SPT and Casing	**DIAMETER:**	AWJ
DRILLER:	V. Murillo	**WATER TABLE:**	4.9 m

INGENIERIA SUELOS Y MATERIALES
insuma s.a.
INGENIEROS Y GEOLOGOS CONSULTORES

BORING LOG

#	DEPTH (m) From	DEPTH (m) To	N_{SPT}	% Recovery	Description	LL	PI	WN (%)	%>#200	SUCS
1	0.00	0.45	10	44	Grayish brown or brown very sandy SILT					
2	0.45	0.90	7	67	and/or very silty SAND, fines are not plastic					
3	0.90	1.35	6	56	very loose to loose relative density.					
4	1.35	1.80	2	89	% Passing: #4=99; #10=97; #40=90;	NP	NP	24.7	52	ML
5	1.80	2.25	2	89						
6	2.25	2.70	1	67						
7	2.70	3.15	1	67						
8	3.15	3.60	1	67	% Passing: 3/8=81; #4=80; #10=79; #40=76;	52	19	36.6	74	MH
9	3.60	4.05	2	78	Brown clayey SILT, mixed with fraction of					
10	4.05	4.50	2	78	sand size particles, medium plasticity, soft.					
11	4.50	4.95	2	78	Gray well graded sandy GRAVEL and/or					
12	4.95	5.40	14	56	gravelly SAND, no plasticity, medium.					
13	5.40	5.85	10	56	% Pas: 3/4=77; 3/8=64; #4=45; #10=27; #40=8;	NP	NP	14.1	3	GW
14	5.85	6.30	16	56						
15	6.30	6.75	12							
16	6.75	7.20	7	33						
17	7.20	7.65	10	33						
18	7.65	8.10	10	44	% Passing: 3/8=90; #4=72; #10=54; #40=16;	NP	NP	16.3	5	SW-S
19	8.10	8.55	12	22	Gray well graded silty SAND, with some					
20	8.55	9.00	10	44	gravel, fines have no plasticity, medium to					
21	9.00	9.45	28	44	dense relative density.					
22	9.45	9.90	34	44	% Passing: #4=77; #10=56; #40=19;	NP	NP	15.6	8	SW-S
23	9.90	10.35	22	67						
24	10.35	10.80	24	56	Greenish gray very fine silty SAND, fines					
25	10.80	11.25	19	67	have no platicity, medium to dense relative					
26	11.25	11.70	19	56	density.					
27	11.70	12.15	24	56	% Passing: #4=95; #10=93; #40=83;	NP	NP	23.8	30	SM
28	12.15	12.60	17	33						
29	12.60	13.05	26	89						
30	13.05	13.50	27	33						
31	13.50	13.95	35	56	% Passing: #40=100;	NP	NP	31.7	67	ML
32	13.95	14.40	24	33						
33	14.40	14.85	38	67						
34	14.85	15.30	35	44	% Passing: #40 = 100;	NP	NP	22.4	33	SM
35	15.30	15.75	28	33						
36	15.75	16.20	36	44						

Observations:

Described by:	J.P. Rodríguez	*Revised by:*	J.P. Rodríguez	*Approved by:*	J.P. Rodríguez
Date:	15/07/2010	*Date:*	15/07/2010	*Date:*	15/07/2010
Signature:		*Signature:*		*Signature:*	

PROJECT:	Estrella River Bridge	*File:*	
LOCATION:	Cahuita, province of Limón	**CODE:**	
BOREHOLE:	**P-1 (Continued)**	**DATE:**	26/04/2010
ELEVATION:	m.s.n.m.	**DEPTH:**	20.25 m
EQUIPMENT:	SPT and Casing	**DIAMETER:**	AWJ
DRILLER:	V. Murillo	**WATER TABLE:**	No hay

BORING LOG

#	DEPTH (m) From	To	N_{SPT}	% Recovery	Symbol	Description	LL	PI	WN (%)	%>#200	SUCS
37	16.20	16.65	**36**	56		% Passing: #40=100;	NP	NP	22.6	31	SM
38	16.65	17.10	**17**	33							
39	17.10	17.55	**25**	56		Greenish gray very fine silty SAND, fines					
40	17.55	18.00	**21**	22		have no platicity, medium to dense relative					
41	18.00	18.45	**22**	22		density.					
42	18.45	18.90	**33**	44		% Passing: #40=100;	NP	NP	27.8	43	SM
43	18.90	19.35	**32**	56							
44	19.35	19.80	**36**	44							
45	19.80	20.25	**38**	56							
46						^ ^ ^ End of borehole: 20.25 m ^ ^ ^					
47											
48											
49											
50											
51											
52											
53											
54											
55											
56											
57											
58											
59											
60											
61											
62											
63											
64											
65											
66											
67											
68											
69											
70											
71											
72											

Observations:

Described by:	J.P. Rodríguez	*Revised by:*	J.P. Rodríguez	*Approved by:*	J.P. Rodríguez
Date:	15/07/2010	*Date:*	15/07/2010	*Date:*	15/07/2010
Signature:		*Signature:*		*Signature:*	

Appendix B. PSHA Seismic Source Model Documentation

Summary of Central and South America Seismic Sources

The Central and South American seismic source model includes information for both areal source zones for shallow crustal provinces and fault sources that represent the specific tectonic elements of the region. Fault sources include three types: shallow crustal faults, subduction interface zones, and subduction intraplate zones.

Areal Sources

The areal source zones represent parts of the region with similar tectonic and seismologic characteristics. Definition of the areal source zones was based on examination of spatial patterns of topography, fault locations and kinematics, and historical seismicity. The recurrence model for the areal source zones is based on the historical magnitude frequency distribution for events occurring within the volume of crust defined by the areal source zone boundary and extending from the surface to the base of the shallow crust (~40 km). These events are conservatively assumed to occur on structures within an areal source volume that is commonly much shallower (e.g., 0 to 12 km) than the area of sampled seismicity.

Shallow Crustal Faults

The shallow fault sources, included in the model are primarily from the International Lithosphere Project (ILP) Quaternary fault and fold database. This fault database has been published through a series of open-file reports. ILP reports are available for Argentina, Brazil, Chile and Bolivia, Colombia, Ecuador, Peru, Venezuela, Costa Rica, Panama, and the area around Managua, Nicaragua (see References). The ILP faults included in the model are only those that meet the criteria of having a reported slip rate of >0.2 mm/yr. Slip rates attributed to these line sources are based on the ILP reported rate or a rate determined by other published papers or estimated based on published data from regional geodetic networks. Major crustal faults from other countries not included in the ILP reports (e.g., Motagua and Polochic faults in Guatemala) were added based on other published sources.

Subduction Zones

Regional seismological and geodetic studies indicate that the subduction zones beneath South America and Central America have complex geometries that change along the length of the plate boundary. The geometry of the subduction zone used in the source model is based on analysis of our composite seismicity catalog (see Appendix A) and seismological and geodetic analyses presented in scientific literature (see Reference list). The subduction zone is divided into 10 separate structural segments on the interface portion and 19 separate structural segments on the intraplate portion (Figure 1). The subduction zone segments were defined based on occurrence of large magnitude historical earthquakes, differences in the geometry (strike and dip) of the subducted plate, differences in the age of the subducting plates, and presence of physical asperities such as seamount chains and oceanic fracture zones.

Slip rates along the plate interface zones were estimated taking into consideration the overall plate motion rate, plate-normal component of motion, and amount of seismic coupling or seismic efficiency along the plate interface. Plate motion rates were derived from published vectors determined by local GPS geodic networks, global plate motion models (e.g., NUVEL 1-A) or GPS-based global plate motion models (obtained through the UNAVCO web-based plate motion calculator).

The maximum earthquake magnitude distribution for the plate interface events is based on two or three potential fault rupture scenarios (characteristic earthquakes) for each subduction zone segment. Factors considered in the analysis of maximum magnitude include: (a) the minimum size of the rupture area based on the maximum historical rupture area for each segment; (b) uncertainties in rupture length and width; (c) presence of physical features on the subducting plate (i.e. fracture zones) that could act as rupture termination points; and (d) the possibility of ruptures larger than historical maximums could occur.

Earthquake recurrence on intraplate sources is modeled as an exponential magnitude distribution. The maximum earthquake magnitude estimates for the intraplate events are based on recorded seismicity, examples from similar tectonic settings, and the physics behind the earthquake generating mechanisms in these environments. The historical magnitude frequency distribution for the intraplate source zone is determined for those events occurring within the volume of crust defined by the map projection of the intraplate zone and extending from the base of the shallow crust (e.g., 40 km) to the maximum depth of recorded earthquakes inferred to be associated with the subducted slab. These events are conservatively assumed to occur along the plane representing the top of the subducted slab.

Magnitude recurrence model parameters are based on a reduction of a catalog of earthquake events from 1530 to 2006.

References

Subduction Zone:

Barrientos, S. 2005, Giant returns in time: Nature 437, p. 329.

Barrientos, S.E., and Ward, S.N., 1990, The 1960 Chile earthquake: Inversion for slip distribution from surface deformation: Geophysical Journal International, v. 103, p. 589-598.

Beck, S., Barrientos, S., Kausel, E., Reyes, M. 1998. Source characteristics of historic earthquakes along the central Chile subduction zone. Journal of South American Earth Sciences Vol. 11, No. 2, pp. 115-129.

Beck, S.L. and Nishenko, S.P. 1990. Variations in the mode of great earthquake rupture along the central Peru subduction zone. Geophysical Research Letters, 17, 1969-1972.

Bevis, M., et al., 2001, On the strength of interplate coupling and the rate of back arc convergence in the central Andes: An analysis of the interseismic velocity field: Geochemistry Geophysics Geosystems, v. 2, 2001GC000198.

Bradley R. Hackerd, Geoffrey A. Aberse, Robin L. Fergasona, (in press), Thermal structure of the Costa Rica – Nicaragua

Cahill, T., and Isacks, B.L., 1992, Seismicity and shape of the subducted Nazca Plate: Journal of Geophysical Research, v. 97, p. 17,503-17,529.

Cisternas, M., Atwater, B., et al. 2005. Predecessors of the giant 1960 Chile earthquake. Nature 437, pp. 404-407.

CowanCreager, K.C., Chiao, L.Y., et al. 1995. Membrane Strain Rates in the Subducting Plate Beneath South America. Geophysical Research Letters, vol. 22, no. 16, pp. 2321-2324.

DeMets, C. 2001. A new estimate for present-day Cocos-Caribbean plate motion: Implications for slip along the Central American volcanic arc: Geophysical Research Letters, v. 28, DOI 10.1029/2001GL013518.

DeMets, C. 2002. Reply to ``Comment on lsquo: A new estimate for Present-day Cocos-Caribbean plate motion: Implications for slip along the Central American volcanic arc" by Marco Guzmãn-Speziale and Juan Martín Gómez: Geophysical Research Letters, Vol. 29, DOI 10.1029/2002GL015384.

DeMets, C., and Dixon, T.H., 1999, New kinematic models for Pacific-North America motion from 3 Ma to present, I: Evidence for steady motion and biases in the NUVEL-1A model, Geophysical Research Letters, v. 26, p. 1921-1924.

DeMets, C., Gordon, R., et al. 1990. Current plate motions. Geophys, J. Int., Vol. 101, pp. 425-478.

DeMets, C., Jansma, E.J. 2000. GPS Constraints on Caribbean-North America plate motion. Geophysical Research Letters, Vol. 27, No. 3, pp. 437-440.

Dewey, J.F. and Lamb, S.H. 1992. Active tectonics of the Andes. Tectonophysics, Vol. 205, 79-95.

Dorbath, L., Cisternas. A., et al. 1990. Assessment of the size of large and great historical earthquakes in Peru. Bulletin of the Seismological Society of America, Vol. 80, No. 3, pp. 551-556.

Dorbath, L., Dorbath, C., Jiménez, E. and Rivera, L., 1991. Seismicity and tectonic deformation in the eastern Cordillera and Sub Andean zone of Central Perú: Journal of South American Earth Sciences, v. 4, p. 13-24.

Geomatrix Consultants, 2004a, Seismicity Update U.S. Department of State New Embassy at the Cardemas Site, Panama City, Panama, Project No. 8734.002, 16p.

Geomatrix Consultants, 2004b, Seismicity Update U.S. Department of State New Embassy Casa Grande/Casa Chica Compound, Managua, Nicaruagua, Project No. 8734.005, 14p.

Geomatrix Consultants, 2004c, Seismicity Update U.S. Department of State New Embassy Compound, Belmopan, Belize, Project No. 8734.013, 20p.

Geomatrix Consultants, 2004d, Seismicity Update U.S. Department of State New Embassy Site, Quito, Ecuador, Project No. 8734.015, 14p.

Grange, F., Cunningham, P., et al. 1984. The configuration of the seismic zone and the downgoing slab in southern Peru. Geophysical Research Letters, vol. 11, no. 1, pp. 38-41.

GSHAP Piloto Report, http://www.seismo.ethz.ch/gshap/piloto/report.html, 3/3/06

Guzmán-Speziale, M., and Meneses-Rocha, J.J., 2000, The North America—Caribbean plate boundary west of the Motagua-Polochic fault system: a fault jog in Southeastern Mexico: Journal of South American Earth Sciences, v. 13, p. 459-468.

Guzman-Speziale, M., Valdes-González, C., et al. 2005. Seismic activity along the Central America volcanic arc: Is it related to subduction of the Cocos plate? Tectonophisics 400, pp. 241-254.

Hackneym, R., Götze, H.-J., and Meyer, U., 2005, Topographic, bathymetric and gravity characteristics of convergent margins: Geotechnologien Science Report No. 5, Status Seminar, Abstract, p. 30-33.

Hartzell, S. and Langer, C. 1993. Importance of model parameterization in finite fault inversions: application to the 1974 M_w 8.1 Peru Earthquake. J. Geophys. Res., Vol. 98, 22123-22134.

Heubeck, C., and Mann, P., 1991, Geologic evaluation of plate kinematic models for the North American—Caribbean plate boundary zone: Tectonophysics, v. 191, p. 1-26.

Johnston, S.T., Thorkelson, D.J. 1996. Cocos-Nazca slab window beneath Central America. Earth and Planetary Science Letters 146, pp. 465-475.

Kley, J., Monaldi, C.R., Salfity, J.A., 1999, Along-strike segmentation of the Andean foreland: causes and consequences: Tectonophysics, 259, p. 171-184.

Klotz, J., Angermann, D., et al. 1999. GPS-derived deformation of the Central Andes including the 1995 Antofagasta M_W=8.0 Earthquake. Pure and Applied Geophysics 154, 709-730.

Klotz, J., Khazaradze, G., et al. 2001. Earthquake cycle dominates contemporary crustal deformation in Central and Southern Andes. Earth and Planetary Science Letters 193, pp. 437-446.

Langer, C.J. and Spence, W. 1995. The 1974 Peru earthquake series. Bull. Seism. Soc. Am., Vol. 85, No. 3, pp. 665-687.

MMI Engineering, 2003, LNG Pipeline and Facility Geologic and Geotechnical Studies. Camisea, Peru, Unpublished consultant report.

McCaffrey, R. 1997. Short Notes: Statistical Significance of the Seismic Coupling Coefficient. Bulletin of the Seismological Society of America, vol. 87, no. 4, pp. 1069-1073.

Pacheco, J.F., Sykes, L.R., et al. 1993. Nature of Seismic Coupling Along Simple Plate Boundaries of the Subduction Type. Journal of Geophysical Research, vol. 98, pp. 14,133-14,159.

Protti, M., Gündel, F., McNally, K.,1994, The geometry of the Wadati-Benioff zone under southern Central America and its tectonic significance: results from a high-resolution local seismographic network. Physics of the Earth and Planetary Interiors, 84, pp. 271-287.

Quezada, J., Bataille, K., and González, G., 2005, The effect of subduction earthquakes on the coastal configuration of Northern Chile: 6th International Symposium on Andean Geodynamics, Barcelona, Extended Abstracts, p. 578-581.

Ruegg, J.C., et al., 2002, Interseismic strain accumulation in the south central Chile from GPS measurements, 1996-1999: Geophysical Research Letters, v. 29, p. 12-1—12-4.

Tichelaar, B.W., and Ruff, L.J. 1993. Depth of seismic coupling along subduction zones. Journal of Geophysical Research, 98, B2, 2017-2037.

Tichelaar, B.W., and Ruff, L.J., 1991, Seismic coupling along the Chilean subduction Zone: Journal of Geophysical Research, v. 96, p. 11,997-12,022.

Trenkamp., R. Kellogg J.N., Freymueller J.T., Mora P. H., 2002. Wide plate margin deformation, southern Central America and northwestern South America CASA GPS observations. South American Earth icnes 15:157-171.

White, S.M., Trenkamp, R., et al. 2003. Recent crustal deformation and the earthquake cycle along the Ecuador-Columbia subduction zone. Earth and Planetary Science Letters 216, pp. 231-242.

Wiens, Douglas, Chilean Patagonia Seismicity (personal communication, 03/04/06).

Upper plate:

Allmendinger R.W., Jordan Teresa E., Kay S.M., Isacks B.L., 1997. The evolution of the Altiplano-Puna Plateu of the Central Andes. Annu.Rev.Earth Planet Sci. 25:139-174.

Audemard F.A., 1996, Paleosesimicity studies on the Oca-Ancon fault system, northwestern Venezuela. Tectonophysics 259:67-80.

Audemard F.A., Bouquet J.C., Rodriguez J. 1999. Neotectonic and paleosismicity studies of the Uramaco fault northen Falcon basin, northwestern Venezulea. Tectonophysics 308:25-35.

Audemard, F.A., Machette, M.N., Dart, R.L., and Haller, K.M., 2000, Map and Database of Quaternary Faults in Venezuela and its Offshore Regions: U.S. Geological Survey Open-File Report 00-018, 76 p., 1 plate (1:2,000,000 scale).

Bommer, J.J., et al., 2002, The El Salvador earthquakes of January and February 2001: Context, characteristics and implications for seismic risk: Soil Dynamics and Earthquake Engineering, v. 22, p. 389-418.

Burkart, B., 1983, Neogene North American—Caribbean Plate boundary across northern Central America: Offset along the polochic fault: Tectonophysics, v. 99, p. 251-270.

Cáceres, D., Monterroso, D., and Tavakoli, B., Crustal deformation in northern Central America: Tectonophysics, v. 404, p. 119-131.

Cembrano J., Herve F., Lavenu A. 1996, The Liquine Pfqui fault zone: a long-lived intra-arc fault system in southern Chile. Tectonophysics 259:55-66.

Colleta B., Roure F., De Toni B., Loureiro D., Passalacqua H., 1997, Tectonic inheritance, crustal architecture, and contrasting structural styles in the Venezuelan Andes. Tectonics 16(5):777-794.

Colombo F., Busquets P., Ramos E., Verges J., Ragona D. 2000, Quaternary alluvial terraces n an active tectonic region: the San Juan river valley, Andean Ranges, San Juan Province, Argentina. Journal of South America Earth Sciences 13:611-626.

Corredor F., 2003, Seismic strain rates and distributed continental deformation in the northern Andes and three-dimensional seismotectonics of northwestern South America. Tectonophysics 372: 147-166.

Costa C., 2005. The seismogenic potential for large earthquakes at the southernmost Pampeana flat-slab segment (Argentina) from geologic perspective. 6th International Symposium of Andean Geodynamics, Extended Abstracts: 190-193.

Costa C. and Vita-Finzi, 1996. Late Holocene faulting in the southeast Sierras Pampeanas of Argentina. Geology 24(12):112-1130.

Costa, C., Machette, M.N, Dart, R.L., Bastias, H.E., Paredes, J.D., Perucca, L.P., Tello, G.I., and Haller, K.M., 2000, Map and Database of Quaternary Faults and Folds in Argentina: U.S. Geological Survey Open-File Report 00-0108, 76 p., 90 p., 1 plate (1:4,000,000 scale).

Cowan, H., Machette, M.N., Amador, Xavier, Morgan, Karen S., Dart, R.L., and Bradley, Lee-Ann, 2000, Map and Database of Quaternary Faults and Folds in the Vicinity of Managua, Nicaragua: U.S. Geological Survey Open-File Report 00-0437, 61 p., 1 plate (1:750,000 scale).

Cowan, H., Machette, M.N., Haller, K.M., and Dart, R.L., 1998, Map and database of Quaternary faults and folds in in Panama and its offshore regions: U.S. Geological Survey Open-File Report 98-779, 41 p., 1 plate (1:500K scale).

Deaton, B.C., Burkart, B., 1984, Time of sinstral slip along the Polochic fault of Guatemala: Tectonophysics, v. 102, p. 297-313.

Eguez, Arturo, Alvarado, Alexandra, Yepes, Hugo, Machette, Michael N., Costa, Carlos, and Richard L. Dart, 2003 Database and Map of Quaternary Faults and Folds in Ecuador and its offshore regions: U.S. Geological Survey Open-File Report 03-289, 71 p., 1 plate (1:1,250,000 scale).

Fernández, M., and Rojas, W., 2000, Faulting, shallow seismicity and seismic hazard analysis for the Costa Rican Central Valley: Soil Dynamics and Earthquake Engineering, v. 20, p. 59-73.

Finch, R.C., and Ritchie, A.W., 1991, The Guayape fault system, Honduras, Central America: Journal of South American Earth Sciences, v. 4, p. 43-60.

Guillaume Backe, Dhont D., Hevouet Y., Gonzales L. 2005. Active tectonic escape of the northwestern Venezuelan Andes. 6th International Symposium of Andean Geodynamics, Extended Abstracts: 86-89.

Guzmán-Speziale, M., 2001, Active seismic deformation in the grabens of northern Central America and its relationship to the relative motion of the North America—Caribbean plate boundary: Tectonophysics, v. 337, p. 39-51.

Herail G., Oller J., Baby P., Bonhomme M., Soler P., 1996. Strike-slip faulting, thrusting and related basins in the Cenozoic evolution of the southern branch of the Bolivian orocline. Tectonophysics 259:201-212.

Heubeck C. and Man P., 1991, Geologic evaluation of plate kinematic models for the North American- Caribbean plate boundary zone. Tectonophysics, 191:1-26.

Horton, B., 1999, Erosional control on the geometry and kinematics of thrust belt development in the Central Andes. Tectonics 18(6):1292-1304.

Isacks B., 1988. Uplift of the Central Andena Plateau and Bending of the Bolivian Orocline. Journal of Geophysical Research, 93(B4):3211-3231.

Jordan T. and Allemendinger R.W., 1986. The Sierras Pampeanas of Argentina: A modern analog of Rocky Mountain foreland deformation. American Journal of Science 286:737-764.

Kendrick E., Bevis M., Smalley R., Brooks, B. 2001. An integrated crustal velocity field for the central Andes. Geochimestry Geophysics Geosystems, 11p.

Kiremidjian, A.S., Haresh, C.S., and Sutch, P.L., 1982, Seismic Hazard and Uncertainty Analysis of Honduras: Soil Dynamics and Earthquake Engineering, v. 1, p. 83-84.

Kley J., Gangui A., Kruger D., 1996, Basement-involved blind thrusting in the Eastern Cordillera Oriental, Southern Bolivia: evidence from cross-sectional balancing, gravimetric and magnetotelluric data. Tectonophysics, v. 301, p. 75-94.

Klosko E.R., Hindle D., Kley J., Norabuena E., Dixon T., Liu M., 2002, Comparison of GPS, Seismological, and Geological observations of Andean Mountain Building. Palte Boundary zones, P. 123-124.

Lavenu, A., Thiele, R., Machette, M.N., Dart, R.L., and Haller, K.M., 2000, Map and Database of Quaternary Faults and Folds in Bolivia and Chile: U.S. Geological Survey Open-File Report 00-0283, 38 p., 2 plates.

Machare, J., Fenton, C.H., Machette, M.N., Lavenu, A., Costa, C., and Dart, R.L., 2003, Database and Map of Quaternary Faults and Folds in Peru and its Offshore Region: U.S. Geological Survey Open-File Report 03-0451, 54 p., 1 plate.

Mering, C., Huaman-Rodrigo D., Chorowica J., Deffontains, B., Guillande, R., 1996. New Data on the Geodynamics of southern Peru computerized analysis of SPOT and SAR ERS-1 images. Tectonophysics, 259, 153-169.

Montero, W., Denyer, P., Barquero, R., Alvarado, G.E., Cowan, H., Machette, M.N., Haller, K.M., and Dart, R.L., 1998, Map and database of Quaternary faults and folds in Costa Rica and its offshore regions: U.S. Geological Survey Open-File Report 98-481, 63 p., 1 plate (1:750K scale).

Muñoz, A.V., 1988, Tectonic patterns of the Panama Block deduced from seismicity, gravitational data and earthquake mechanisms: implications to the seismic hazard: Tectonophysics, v. 154, p. 253-267.

Norabuena F., Leffler-Griffin L., Mao A., Dizon T., Stein S., Sacks L.O. Ocola L., Ellis M., 1998, Space Geodetic Observations of Nazca-South America Convergence Across the Central Andes. Science 279:358-359.

Paris, G., Machette, M.N., Dart, R.L., and Haller, K.M., 2000, Map and Database of Quaternary Faults and Folds in Colombia and its Offshore Regions: U.S. Geological Survey Open-File Report 00-248, 61 p., 1 plate (1:2,500,000 scale).

Perez J.O., Bilham R., Bendick R., Velandia R.J., Hernandez N., Moncayo C., Hoyer M., Kozuch M., 2001, Velocity field across southern Caribbean plate boundary and estimates of Caribbean/South American plate motion using GPS Geodesy 1994-2000. Geophysical Research Letters, 28(15): 2987-2990.

Pratt, T.L., et al., 2003, High-resolution seismic imaging of faults beneath Limón Bay, northern Panama Canal, Republic of Panama: Tectonophysics, v. 368. p. 211-227.

Ramos V., Cegarra M., Cristallini, 1996, Cenozoic tectonics of the High Andes of west-central Argentina (30-36° S latitude). Tectonophysics, 259:185-200.

Ramos V., 1999, Plate tectonic setting of the Andean Cordillera. Episodes 22(23):183-190.

Ramos V.A., Cristallini E.O., Perez D.J., 2003. The Pampean flat-slab of the Central Andes, Journal of South America Earth Sciences 15: 59-78.

Reutter K.J., Scheuber E., Chong G., 1996. The Precordillera fault system of Chuquimata, Northern Chile: evidence for reversals along arc-parallel strike-slip faults. Tectonophysics, 259:213-228.

Roeder D. and Chamberlain R.L., 1995. Eastern Cordillera of Colmbia: Jurassic-Neogene crustal evolution, in A. Tankard, R. Suarez, and H.J. Welsinski, Petroleum basins of South America: AAPG Memoir 62, 633-645.

Saadi, Allaoua, Machette, M.N., Haller, K.M., Dart, R.L., Bradley, L.-A., de Souza, A.M.P.D., 2002, Map and Database of Quaternary Faults and Lineaments in

Brazil: U.S. Geological Survey Open-File Report 02-230, 58 p., 1 plate (1:6,000,000 scale).

Schwartz, D.P., Lloyd S.C., and Donnelly, T.W., 1979, Quaternary faulting along the Caribbean—North American plate boundary in Central America: Tectonophysics, v. 52, p. 431-445.

Suarez G., Molnar P., Burchfiel B.C., 1983. Seismicity, fault plane solutions, depth of faulting, and active tectonics of the Andes Peru, Ecuador, and Southern Colombia. Journal of Geophysical Research, 88(B12):10403-10428.

Trenkamp R., Mora P. H., Salcedo H. E., Kellog J.N. 2004, Possible rapid strain accumulation rates near Cali, Colombia, determined from GPS measurements (1996-2003). Earth Sciences Research Journal, 8:1, 25-33.

Wells, S.G., et al., 1988, Regional variations in tectonic geomorphology along a segmented convergent plate boundary, Pacific Coast of Costa Rica: Geomorphology, v. 1, p. 239-265.

Wolters, B., 1986, Seismicity and tectonics of southern Central America and adjacent regions with special attention to the surroundings of Panama: Tectonophysics, v. 128, p. 21-46.

Whitman D., Isacks B.L., Kay S.M., 1996. Lithospheric structure and along-strike segmentation of central Andean plateau: seismic Q, magmatism, flexure, topography and tectonics.

Appendix A

The historic earthquake catalog for South and Central America was assembled from a number of sources. Among the agencies and published sources used in the data compilation are (in order of numbers of events):

- GS United States Geological Survey, Denver, Colorado
- ISC International Seismological Centre, Newbury, UK
- GUC Geofísica, Universidad de Chile
- SIS Nicaragua Earthquake Information
- SAT Shepherd and Turner 1992 An earthquakes catalogue for the Caribbean
- RSN Red Sismological Nacional (RSN), ICE-UCR San Jose Costa Rica
- CER CERESIS, Catalog of Earthquakes for South America , 1985
- PDE Preliminary Determination of Epicenter from NEIS/CGS
- GCG Guatemala City, Guatemala
- Department of Defense, U.S.
- OSO OSSO Observatory, Colombia
- SAA Shepherd and Aspinall, 1982
- LAO Large Aperture Seismic Array (LASA), Montana, USA.
- HRV Harvard, Massachusetts, USA
- TRN Trinidad. Trinidad-Tobago
- SAN Santiago, Chile
- HDC Heredia, Cost Rica
- ROT Rothe, J.P. ,The Seismicity of the Earth, 1953-1965, UNESCO, 1969
- HRV Harvard Moment Tensor Solutions
- NAO NORSAR, Norway.
- CGS U.S. Coast and Geodetic Survey, Rockville, MD, USA
- SCB San Calixto, Bolivia
- CAR Caracas, Venezuela.
- BRK Berkeley, California, USA
- AMB Ambrayseys, 1994.
- OAE Observatorio Astronómico de Quito, Ecuador
- MOS Moscow, Russia
- PAS Pasadena, California, USA.
- BJI Beijing, China
- USGS United States Geological Survey
- USCGS United States Coast and Geodetic Survey
- PSA Instituto Nacional de Prevención Sísmica (INPRES), San Juan, Argentina
- QUE Quito, Ecuador (also listed as QUI)
- PAL Palisades, New York, USA
- HFS Hagfors, Sweden.
- STL Santa Lucia, Chile
- NEI Preliminary Determination of Epicentres from NEIS/CGS
- G-R Gutenberg and Richter, 'Seismicity of the Earth'
- TOJ Toral, 1992
- G-M Güendel and McNally, 1986
- FIE Gunther Fiedler, Caracas, Venezuela
- SIG Catalog of Significant Earthquakes (Dunbar, Lockridge, Whiteside, 1993)
- SJR San José, Costa Rica
- BCI Bureau Central International de Seismologie, Strasbourg, France.
- SYK Sykes L.R., Earthquake Catalogue. (1963, 1965, 1966)
- IGP Geophysical Institute of Peru
- TAC Tacubaya, México
- SJS Instituto Costarricense de Electricidad, Costa Rica.
- WMR Montero, 1989
- LIM Lima, Peru

Figure 1